DOE/ID/12708--T1

DE92 014307

ENHANCED TUBES FOR STEAM CONDENSERS

Volume 1
Summary of Condensation and Fouling

Volume 2
Detailed Study of Steam Condensation

February 1992

Work Performed Under Contract No. DE-FC07-88ID12708

Prepared for the
U.S. Department of Energy
Under DOE Idaho Field Office
Sponsored by the Office of the Assistant Secretary
for Conservation and Renewable Energy
Office of Industrial Technologies
Washington, D.C.

Prepared by
The Pennsylvania State University
The Graduate School
Department of Mechanical Engineering

ENHANCED TUBES FOR STEAM CONDENSERS

Volume 1

Summary of Condensation and Fouling

R. L. Webb, L. Chamra, and H. Jaber

February 1992

Prepared for the
U.S. Department of Energy
Assistant Secretary for Conservation and Renewable Energy
Under DOE Idaho Field Office
Contract No. DE-FC07-88ID12708

ABSTRACT

Electric utility steam condensers typically use plain tubes made of titanium, stainless steel, or copper alloys. Approximately two-thirds of the total thermal resistance is on the water side of the plain tube. This program seeks to conceive and develop a tube geometry that has special enhancement geometries on the tube (water) side and the steam (shell) side. This "enhanced" tube geometry, will provide increased heat transfer coefficients.

The enhanced tubes will allow the steam to condense at a lower temperature. The reduced condensing temperature will reduce the turbine heat rate, and increase the plant peak load capability. Water side fouling and fouling control is a very important consideration affecting the choice of the tube side enhancement. Hence, we have consciously considered fouling potential in our selection of the tube side surface geometry. Using appropriate correlations and theoretical models, we have designed condensation and water side surface geometries that will provide high performance and be cleanable using sponge ball cleaning. Commercial tube manufacturers have made the required tube geometries for test purposes. The heat transfer test program includes measurement of the condensation and water side heat transfer coefficients. Fouling tests are being run to measure the waterside fouling resistance, and to test the ability of the sponge ball cleaning system to clean the tubes.

ACKNOWLEDGEMENTS

This program was funded by the Department of Energy and the Electric Power Research Institute. The tube geometries tested were provided, without charge, by three commercial tube manufacturers. Wolverine Tube of Decatur, AL provided the 748 fpm C/N-19, the 3D-SS, 3D-DS, Korodense, and the Corrugated 1 and Corrugated 2 tubes. Wieland-Werke AG of Ulm, Germany provided the 433 fpm copper-nickel and titanium tubes (CU-11, C/N-11, TiA-11 and TiB-11) and the TiA-16 tubes. The attached particle tube (A/P) was provided by UOP Corp. of Tonawanda, New York. We would like to thank Taprogge America Corp., Woodbury, NY, for providing the sponge-balls, and Water Technology of America, Pensacola, FL, for the brushes used in the fouling tests.

Our special thanks go to Mr. Gary Peterson of DOE, Dr. Manohar Sohal of INEL, and Mr. John Tsou of EPRI for providing funding and the project management. Mr. Petur Thors of Wolverine, Klaus Menze of Wieland-Werke, and Dr. Elias Ragi of UOP Corp. provided engineering support on the special tube geometries they provided. Mr. Robert Renfftlen of Taprogge America and Mr. Bill Boesch of Water Technology of America provided valuable counsel on selection of the sponge balls and brushes, respectively. Dr. Peter Stryker, Bucknell University, provided valuable contributions to the condensation test program. Dr. Nae-Hyun Kim also made major contributions to the tube side enhancement and fouling measurements during the first program year, while completing his PhD program.

NOMENCLATURE

A	Reference area, ($= \pi D_o L$), m^2.
A_i	Tube-side surface area ($= \pi D_i L$), m^2.
c_p	Specific heat of water, J/kg-C.
D_i	Maximum tube-side diameter, m.
D_o	Diameter over the fins, m.
d_p	Foulant particle diameter, m.
dR_f/dt_o	Initial fouling rate, m^2-K/W-s.
e	Fin height or internal ridge height for the enhancement, m.
e_i	Fin height for the internal enhancement, m.
E_i	Ratio of the tube inside heat transfer coefficient of the enhanced tube to the plain tube, dimensionless.
E_o	Ratio of the finned tube condensing coefficient to that of a smooth tube of diameter D_o, at the same ΔT, dimensionless.
f	Water side friction factor, dimensionless.
fpi	Fins per in, in^{-1}.
fpm	Fins per meter, m^{-1}.
g	Acceleration of gravity, 9.806 m/s^2.
h	Heat transfer coefficient, W/m^2-K.
j	Colburn j-factor for water side enhancement $(h/u\rho c_p)Pr^{2/3}$, dimensionless.
k_m	Material thermal conductivity, W/m-K.
L	Tube length, m.
LMTD	Log mean temperature difference, K.
m_w	Water mass flow rate, kg/s.
n	Exponent in equation A.4.
p	Internal ridge axial pitch, mm^{-1}.
q	Heat transfer rate, W/m^2.
Q	Tube heat load, W.
Re	Reynolds number, $Re = uD_i/\nu$, dimensionless.
R_f	Fouling resistance, m^2-K/W.

R_f^*	Asymptotic fouling resistance, m^2-K/W.
R_o	Thermal resistance based on the outside area, m^2-K/W.
R_{tot}	Total thermal resistance, m^2-K/W.
St	Stanton number, dimensionless (= $h/\rho c_p u$)
t	Time, sec.
t_b	Fin base thickness, mm.
t_w	Wall thickness, mm.
T_i	Measured wall temperature at top (i = 1), side (i = 2), bottom (i = 3), K
T_{sat}	Steam saturation temperature, K.
ΔT	Temperature difference between the saturation temperature and the average wall temperature, $T_{sat} - T_w$, K.
ΔT_c	Coolant temperature rise, K.
t_t	Fin tip thickness, mm.
T_f	$T_{f,in}$ (test section inlet water temperature), $T_{f,out}$ (test section outlet water temperature), K.
$T_{w,av}$	Average tube wall temperature, K.
u	Tube side water velocity, m/sec.
U	Overall heat transfer coefficient (based on $\pi D_o L$), U_{oe} (for the enhanced tube), U_{op} (for the smooth tube), U_c (clean tube), U_f (fouled tube), W/m^2-K.
UA	Overall heat transfer capacitance, W/K.
u^*	Friction velocity ($=(\tau_w/\rho)^{1/2}$), m/s.

Greek Letters

α	Helix angle, deg.
λ	Latent heat, J/kg.
μ	Dynamic viscosity, kg/m.s.
ν	Absolute viscosity, m/s^2.
ρ	Water density, kg/m^3.
ρ_p	Density of a particle, kg/m^3.
τ_w	Apparent wall shear stress based on pressure drop, Pa.

TABLE OF CONTENTS

1 INTRODUCTION

1.1 Program Objectives

This program developed tube geometries for steam condensers, which have special surface geometries on the inside and outside surfaces. The special surface geometries provide higher heat transfer coefficients than currently used plain tubes. This will improve the steam condenser performance relative to the currently used plain tubes. The program is applicable to industrial and electric utility steam condensers. Used in electric utility steam condensers, the enhanced tubes will increase the thermal efficiency of the plants, and provide higher peak load capability.

The program objectives were to obtain a UA value 50-80% higher than the presently used plain tube. The increased UA value will result in reduced steam condensing temperature. This allows expansion of the steam to a lower turbine exhaust pressure, resulting in increased electricity generation.

It is envisioned that the enhanced tube would initially be used for retubing (tube-for-tube replacement) of existing steam condensers. Greater performance improvements would be obtained by integrating the higher performance of the enhanced condenser tube in the design of a new plant. This would require a turbine specifically designed to operate at the lower back pressure.

A typical water velocity in industrial steam condensers is 6 ft/sec. At 6 ft/sec water velocity, approximately two-thirds of the total thermal resistance is on the water side of the plain tube. Because the dominant thermal resistance is on the water side, little performance improvement would result from use of enhancement on the steam side alone. In order to obtain significant performance improvement, it is necessary to enhance both the water and steam sides.

1.2 Technology Survey

Some prior work has been done to develop enhanced steam condenser tubes. In 1980, the TVA retubed the Gallatin Unit 1 with the 7/8 in O.D. Wolverine LPD Korodense tube. This tube is shown in Fig. 5.10a. The Korodense tube has a spiral corrugation in the outer surface, which provides a "rib roughness" on the inner surface. The corrugations are spaced at 0.4 in, and the inner rib height is 0.020 in. Withers and Young (1971) state that the Korodense LPD tube provides 65% water side enhancement and 37% steam side enhancement. Boyd et al. (1983) describe the plant installation, and Rabas et al. (1990) provide current information on the success of the installation. Since 1980, the TVA has retubed eight additional condensers with the Korodense LPD tube. Rabas et al. (1990) evaluate the success of these installations. They conclude that the Korodense tube "is a viable and cost-effective option for many applications." The cost premium of copper alloy Korodense tubes is 20-25% over that of plain tubes and 15% for titanium tubes. Depending on the installation, the clean tube UA-values were increased 25-to-60% over the plain tube values. None of the installations had on-line tube cleaning systems. However, the performance of the Korodense tube remained superior to plain tubes for about one year, after which cleaning was required.

The Korodense tube provides relatively small steam side enhancement. The present program sought to obtain higher steam side enhancement, along with water side enhancement comparable to that of the Korodense tube. Water side fouling and fouling control was an important element of the present program. Tests were conducted to show that the enhanced tubes were cleanable with on-line sponge ball or brush cleaning systems. As described by Keysselitz (1984), Taprogge has developed a "recirculating sponge ball" cleaning system that has been installed in many electric utility plants having plain tubes. Other fouling research, e.g., Panchal (1989) has shown that intermittent chlorination can effectively control biological fouling in plain tubes.

Nosetani et al. (1989) describe work underway in Japan to evaluate use enhanced tubes in steam condensers. They installed 35 enhanced tubes in the condenser of a 500 MW plant and measured the long term tube performance. Their admiralty tube had 9 fins/in (0.028 in fin height) on the outer surface with a plain tube I.D.

Webb et al. (1984) have simulated the performance of several candidate enhanced tubes in electric utility condensers. Their work shows that the steam condensing temperature may be decreased 5-8 F for Cu-Ni or stainless steel tubes. Used in a 946 MW nuclear plant, the simulation analysis showed that the annual average generation rate would be increased as much as 2.6 MW, and the peak load generation was increased 10.8 MW. These performance improvements assumed no plant alterations other than the tube-for-tube replacement. If it is possible to replace the tube sheets and thus rebundle the condenser, greater performance improvement is possible. Ideally, the turbine should be designed to take advantage of the lower condensing pressure. If this is done, for a new plant design, the full performance of the enhanced condenser tube may be attained.

1.3 Program Methodology

Steam condensers in the U.S. have long used copper alloy such as 90/10 cu/ni, or Admiralty copper alloys. Current trends are toward stainless steel or titanium tubes. The present program consciously focused on enhancements for both copper alloy and titanium tubes.

This program sought to develop new enhanced tube geometries, specifically developed for steam condensers. Water side fouling and cleaning were consciously considered in selection of the tube side surface geometry.

The project work was undertaken in three sub-programs. They are:

1. Water Side Enhancement: This work involves selection of the inside enhancement geometry and evaluation of its heat transfer and fouling characteristics.
2. Steam Side Enhancement: This addresses selection of the steam side enhancement geometry and measurement of the steam condensation coefficient.
3. After completion of the two sub-programs, the final candidate enhanced tubes were manufactured and tested. The test measured the UA-value with 6 ft/sec water side velocity and 108 F steam condensation temperature.

A computer model developed by Jaber (1991) was used to predict the steam condensation performance on "integral fin" tubes, as a function of fin height, fin spacing, fin shape and tube material.

The desired enhanced tube geometries were developed and manufactured by either of the following companies. They are Wolverine Tube Co. (Decatur, AL) and Wieland-Werke AG (Ulm, Germany), and UOP Corp. (Tonawanda, NY).

2 LITERATURE SURVEY

2.1 Condensation Enhancement

Enhanced condenser tubes have been developed, and are routinely used in refrigeration condensers for shell side condensation. Webb (1988) surveyed the advances in this area. Enhanced tubes have not been as widely used for steam condensation. This is because condensate flooding of the interfin region is more severe with water, which has a much higher surface tension than refrigerants or organic fluids. Such condensate flooding substantially reduces the condensation coefficient in the flooded zone, as described by Rudy and Webb (1985).

Some steam condensation research has been done on enhanced tubes. Karkhu and Borovkov (1971), Shekriladze and Rusishvili (1980), Shklover et al. (1981) have tested "threaded tubes" of different materials and geometries with steam and other fluids. Yau, Cooper, and Rose (1984, 1985, 1986) have used several fluids (including steam) to determine the enhancement level of horizontal integral finned copper tubes. They tested rectangular fins for a wide range of fin spacings, 0.5 mm to 20 mm. They have also investigated the effect of vapor velocity, fin spacing and coolant velocity with steam condensing at atmospheric pressure. A maximum enhancement level (the ratio of the condensing coefficient of the enhanced tube to that of a plain tube) of 3.6 (based on root diameter) was obtained for 1.5 mm fin spacing. Wanniarachchi, Marto, and Rose (1984,1985,1986) tested horizontal copper integral finned tubes with steam condensing at atmospheric and vacuum conditions. They measured the effect of fin spacing, fin dimensions, and saturation temperature. The fin height, fin thickness, and fin spacing, ranged from 0.5 mm to 2.0 mm, 0.5 mm to 2.0 mm, 0.5 mm to 9.0 mm, respectively. The maximum enhancement level occurred at 1.5 mm fin spacing, measured at the fin base, (for e = 1.0 mm and 2.0 mm), and at 2.0 mm (for e = 0.5 mm and 1.5 mm). The maximum enhancement level was 3.6 and 5.2 (based on root diameter) for vacuum and atmospheric conditions, respectively.

Marto et al. (1986) studied the effect of fin shape on the condensing coefficient for atmospheric and vacuum conditions. Steam was condensed on four copper tubes with four different fin shapes (rectangular, triangular, trapezoidal, and parabolic). The results show only a small difference in performance among the trapezoidal, rectangular, and triangular fins with the highest enhancement for the rectangular fin. However, the parabolic fin produced approximately 15% higher enhancement than the rectangular fin. On the other hand, Kedzierski and Webb (1987) condensed R-11 on copper tubes with special fin shapes, and reported significant differences for the different fin shapes.

The tube thermal conductivity strongly affects the enhancement levels of finned tubes. Mills et al. (1975) condensed steam on horizontal grooved tubes having 0.71 mm groove pitch and 0.458 mm depth. Three different tube materials were tested: copper, brass, and 70/30 copper-nickel with corresponding thermal conductivities of 381, 100, and 28.5 W/m-K. The tube performance decreased as the thermal conductivity decreased. Mitrou (1986) condensed steam (under vacuum conditions) on tubes of different materials having triangular fins (spirally threaded) of 1.0 mm height, and 2.1 mm base thickness. The materials tested were: copper (350 W/m-K), copper-nickel (52 W/m-K), aluminum (237 W/m-K), and stainless steel (15 W/m-K). These results also show decreasing performance as the thermal conductivity decreases. The maximum enhancement obtained was for copper, while the condensation coefficient on the stainless steel tube was 30% below that of a smooth tube. Enhancement types other than the "standard" integral finned tubes have also been described in the literature and by some tubing manufacturers. The Gregorig (1954), Adamek (1981), and Webb-Kedzierski (1990) profiles are predicted to provide high enhancement levels when R-11 condenses on copper tubes. Trapezoidal fin shapes are produced by manufacturers such as Wolverine (U.S), Wieland (Germany), Hitachi and Sumitomo (Japan), Yorkshire (Great Britain). The fin pitch ranges from 0.5-to-1.3 mm, and some of these have a "saw tooth" fin shape. The tubes are typically used for refrigerants, which have considerably lower surface tension than that of water. Several different copper enhanced tubes with special fin shapes were tested by Webb and Murawski (1990). There is no information about

steam condensation on such high performance surfaces. However, it is likely that condensate retention would yield low performance on closely spaced fins.

2.2 Water-Side Enhancement and Fouling

Particulate fouling with water flow in enhanced tubes have been investigated by Webb and Kim (1989) and Kim and Webb (1989). These two papers report accelerated particulate fouling data for water flow in commercially available enhanced tubes. Those studies showed that most enhanced tubes foul at a higher rate than for a plain tube operated at the same water velocity. The previous two studies investigated use of an on-line brush cleaning system to clean the tubes. Those measurements showed that the on-line brush effectively cleaned the tubes.

When an on-line cleaning system is used, large steam condensers typically use a sponge-ball cleaning system rather than the on-line brush cleaning system. Use of the sponge-ball on-line cleaning system is described by Keysselitz (1984). If only biological fouling is expected, intermittent chlorination may be used, rather than a sponge-ball system. Renfftlen (1991) reports that enhanced tubes can be successfully cleaned using the sponge ball cleaning system.

There has been growing interest in using enhanced tubes in electric utility steam condensers, which typically use plain tubes. Boyd et al. (1983) describes operating experience of the Wolverine Korodense tube in steam condensers. The Korodense tube provides approximately 65% tube side enhancement, but less than 30% steam-side enhancement. Webb et al. (1984) show that approximately two-thirds of the total thermal resistance is on the water side of the plain tube. Rabas et al. (1990) provide an update of operating experience with the Korodense tube, since publication of the Boyd et al. paper. Sommerscales et al. (1991) describes the results of experiments to investigate particulate fouling in enhanced tubes. They conclude that the Korodense tube have the property of providing better heat transfer and it is less susceptible to

fouling than a smooth tube. However, Rabas et al. (1991) describes long term operating experience of twelve TVA condensers, nine of which were retubed with Korodense tubes. Although the results show that the Korodense tube fouls faster than plain tubes, a relatively small fouling resistance occurred within nine months after cleaning.

In order to obtain significant performance improvement, it is necessary to enhance the water side, in addition to the steam side. Successful application of enhanced tubes to steam condensers requires that foulant material be cleanable from the water-side. Very little information has been published on fouling and on-line cleaning of water-side enhanced tubes. Kim and Webb (1989) report fouling and on-line brush cleaning data for water-side enhancements used in the air conditioning industry. Webb and Chamra (1991) extended this research to water side enhancements and on-line cleaning systems applicable to electric utility steam condensers.

It is possible that an enhancement geometry, that is cleanable by on-line brushing, may not be cleanable with the sponge-ball system. Hence, the geometries chosen for steam condensers were carefully selected, with the intent that they would be amenable to sponge-ball cleaning. Webb and Chamra (1991) shows that the enhanced tubes can be cleaned by either cleaning mechanism.

3 EXPERIMENTAL FACILITIES

Three different experimental facilities were used to obtain the data. A brief description of each apparatus is given below. Detailed description of the condensation and fouling apparatuses are given in Appendices A, B, respectively. These appendices also describe the test procedure and the data reduction procedures.

3.1 Condensation Apparatus

Two variants of the test apparatus were used. The first variant was used to measure steam condensation on single horizontal tubes. This was accomplished by measuring the wall temperature at four locations around the tube circumference.

The second variant measured the overa" UA-value of a doubly enhanced tube with 6.0 ft/sec water side velocity. Condensation occurred at 8.1 KPa (1.18 psi) with cooling water entering at approximately 24 C (75 F).

3.2 Fouling Test Apparatus

This apparatus measured the water side fouling resistance in either four 19 mm O.D. (or three 22 mm O.D.) tubes simultaneously. The apparatus was designed to operate and record data 24 hour/day unattended with heat input to the test section. Heat is transferred to the 3.05 m long test sections by condensing R-114 on the annulus side of the test section.

3.2.1 On-Line Cleaning Systems Used

Aluminum oxide particles were used for the foulant material. The foulant particle diameter used in all tests except two was 0.3 μm. The other two tests used 3 μm diameter particles. Both sponge-ball and brush cleaning systems were tested. Figures

3.1 and 3.2 show the brush and ball cleaning techniques, respectively. The apparatus contains brush holders at the ends of the 3.05 m long measuring section. Four solenoid valves, controlled by an electronic signal from the personal computer, are used to actuate the brush operation. When the signal is "on", the solenoid valves reverse the flow direction, causing the brushes to pass through the tubes. When the signal is "off", the solenoid valves return the brushes to their original position. The brushes are chosen such that the brush diameter is 0.5 mm larger than the root diameter of each tube. The brushes were provided by Water Technology of America, Pensacola, FL.

Figure 3.1 Brush cleaning system operation

The sponge-balls are manually injected into the tube, as shown in Figure 3.2, and then they are collected in the downstream water reservoir. The pressure drop across the tube causes the sponge-balls to pass through the tubes. The appropriate sponge-ball diameter is selected by testing the ability of the water flow to drive the ball through the tube. If the ball diameter is too large, it will not be driven through the tube at the design water velocity. The sponge-balls are normally 2-3 mm larger than the tube root diameter. The sponge-balls were selected and provided by Taprogge America Corporation, Woodbury, New York.

balls are collected in the reservoir

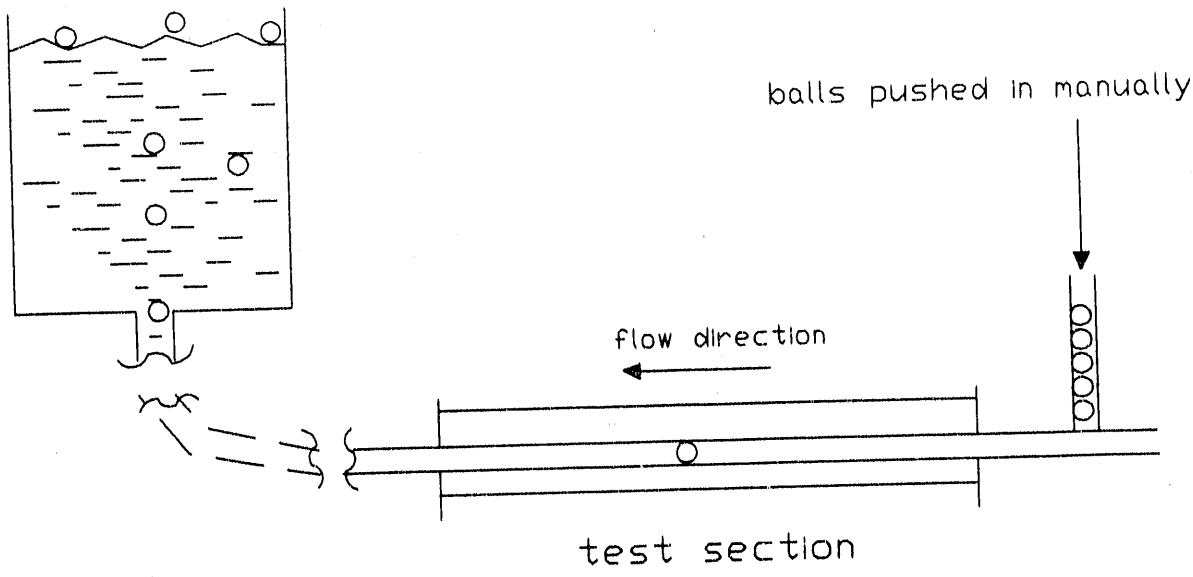

Figure 3.2 Apparatus used to inject sponge-balls into test section

3.3 Measurement of the Water-Side Coefficient

The water-side (inside the tube) heat transfer coefficient was measured either at the Wolverine or Wieland test facilities. It was determined by doing a "Wilson plot" on the tube. The procedure used by Wolverine is described below.

An eight foot long tube is installed in an R-12 evaporator shell. The R-12 boils on the shell side at 75 psia (62 F) and is held at a constant temperature during the test. Water flows inside the tube. The R-12 vapor is condensed against cold aqueous ethylene glycol in a separate condenser.

Data are taken at constant average heat flux for a series of six flow rates, which span 20,000 to 80,000 Reynolds number. The inlet water temperature is adjusted for each test point to obtain 36,000 Btu/hr heat removal. This maintains a constant heat transfer coefficient for the R-12 on the shell-side.

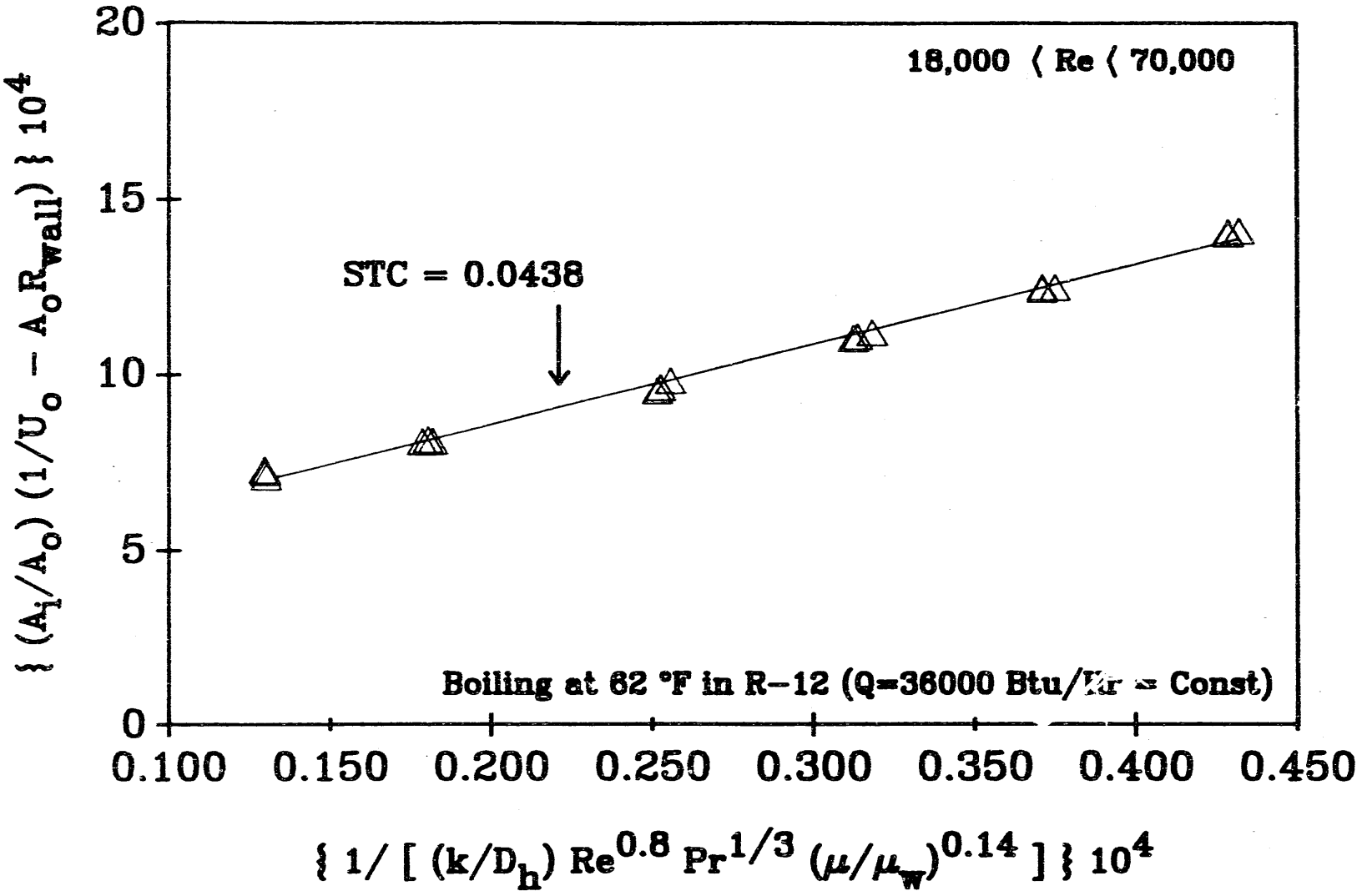

Fig. 3.3 Sample Wilson Plot to determine the water-side heat transfer coefficient.

Figure 3.3 shows a typical Wilson plot. The X-axis is the inverse of the water-side thermal resistance. The Y-axis is the total thermal resistance, less the tube wall conduction resistance. A straight line curve fit (on semi-log coordinates) gives the "Sieder-Tate coefficient," STC, shown on the graph. The shell side R-12 thermal resistance is given by the intercept of the curve fit with the Y-axis at X = 0. The water side heat transfer coefficient (h_i) is then calculated by the equation

$$\frac{h_i D_h}{k} = STC\, Re^{0.8} Pr^{1/3} \left(\frac{\mu}{\mu_w} \right)^{0.14} \qquad (1)$$

The value of STC for Figure 3.3 is 0.0438. The water side heat transfer coefficient is 62% higher than that of a plain tube. The "Sieder Tate coefficient," STC, for the plain and enhanced tubes is given in Table 3.1.

4 ENHANCED TUBE GEOMETRIES TESTED

4.1 Selection of Enhancement Geometries

Table 3.1
THE SIEDER TATE COEFFICIENTS

Tube	STC
Plain	0.029
Korodense	0.0490
Corrugated 2	0.0470
3D-DS	0.0446
SS-16	0.0402
NW	0.044

Our intent was to develop special steam and water side enhancement geometries that would provide the needed steam-side, water-side, and fouling performance. The tubes geometries were chosen based on a theoretical analysis, correlations and suggestions provided by tube manufacturers. The following criteria were established for selection of the enhancement geometries:

1. Adding a steam-side enhancement geometry to the outer surface will reduce the tube inside diameter. Reduced tube I.D. will act to increase the water side pressure drop, independent of the tube-side enhancement. Hence, we sought a tube side enhancement that would provide high steam side enhancement with the maximum possible tube inside diameter.

2. The tube side enhancement must consciously consider cleanability of the water side geometry using the recirculating sponge ball cleaning system. Based on discussions with Taprogge, we concluded that the inside enhancement should have "rounded" internal ridges, as opposed to "sharp" internal ridges.
3. Because the controlling thermal resistance is on the water side, candidate water side enhancements should provide at least 60% water side enhancement.

4.2 Steam Side Enhancement Geometries

The first basic type enhancement geometry used is the integral-fin tube. As previously stated, a computer model developed by Jaber (1991) was used to identify the preferred integral-fin geometry. The computer model predicted that a 7/8" O.D tube having approximately 13 fins/in is preferred. A fin height of 0.5 mm is preferred for titanium and for cu/ni. The titanium fins must have a greater base thickness than that of the cu/ni tubes to compensate for the lower thermal conductivity of titanium.

The second basic enhancement geometry consists of a dense array of spherical particles that are sintered to the outer tube surface (Fig. 4.1b).

Eight steam side enhancement geometries were tested. These are shown in Fig. 4.1 and Fig 4.2 and are listed in Table 4.1. Table 4.2 gives the tube dimensions. The second column of Tables 4.1 and 4.2 list a code descriptor, to which the tubes will be referred to in the future discussion.

Tubes 2-through-6 are "integral fin" tubes, and are illustrated in Fig. 4.1 and Fig 4.2. These tubes have 11, 16, or 19 fins/in. Tubes 2 and 4 (Fig. 4.1a and 4.1d) are identical (except for the tube material) and have 433 fpm (11 fpi) with 1.1 mm fin height. Tube 3 (Fig. 4.1c) has 748 fpm (19 fpi) with 0.5 mm fin height. Tubes 5 and 6 (Fig. 4.2a and

4.2b) are titanium with 433 fpm (11 fpi), and have 0.43 and 0.28 mm fin height, respectively. Tube 7 (Fig. 4.2c) is stainless steel with 630 fpm (16 fpi) and has 0.32 mm fin height. Tube 8 (Fig. 4.1b) tube is a plain copper/nickel tube with 0.5 mm diameter copper particles sintered to the surface, with 50% area coverage.

4.3 Water Side Enhancement Geometries

Selection of the tube side enhancement must consciously consider cleanability of the water side geometry using the recirculating sponge ball cleaning system, in addition to increased heat transfer. We feel that an internal geometry that has "rounded" internal ridges, as opposed to "sharp" internal ridges will be more cleanable. Based on discussions with a manufacturer of the sponge ball cleaning system, we have selected three possible tube side enhancements. They are:

1. A wavy internal roughness, which is illustrated on the inner surface of the Fig. 4.1a and 4.1c tubes.
2. A 3-dimensional roughness, which is illustrated in Fig. 5.9c.
3. A helically corrugated roughness illustrated in Fig. 5.10a.

The inner surface of the Fig. 4.1 or 4.2 finned tubes may use either the wavy or the 3-dimensional roughness. The Fig. 5.10a corrugated tube is envisioned for the inner surface of the Fig. 4.1b attached particle tube.

4.4 Composite Candidate Tube Geometries

The "candidate" tube geometries must have enhancement on the steam and water sides. The candidate geometries are the same as shown in Tables 4.1 and 4.2, except for Tubes 1, 3 and 8. Tube 1 is excluded, because it is a plain tube. Tube 3 is excluded, because copper material is not suitable. The attached particles of Tube 8 would be

replaced by aluminum particles would be attached to a Korodense tube. Although Tube 7 was made of stainless steel, it can also be made of titanium.

Table 4.1

Tubes Tested In Condensation Test Cell

No.	Code	Geometry	Material	Manufacturer
1	Plain	Smooth	copper	-
2	CU-11	Integral-fin	copper	Wieland
3	C/N-19	Integral-fin	90/10 cu/ni	Wolverine
4	C/N-11	Integral-fin	90/10 cu/ni	Wieland
5	TiA-11	Integral-fin	titanium	Wieland
6	TiB-11	Integral-fin	titanium	Wieland
7	SS-16	Integral-fin	stn. stl	Wieland
8	A/P-50	Attached part.	cu particles on cu/ni tube	UOP

Table 4.2

Dimensions of the Tubes Tested in Condensation Test Cell

No.	Code	D_o mm	fpm -	t_w mm	e_o mm	t_b mm	t_t mm
1	Plain	22.23	-	0.9	-	-	-
2	CU-11	19.00	433	0.9	1.12	0.9	0.30
3	C/N-19	22.23	748	0.9	0.50	0.6	0.20
4	C/N-11	22.23	433	0.9	1.12	0.9	0.30

Table 4.2
Dimensions of the Tubes Tested in Condensation Test Cell

No.	Code	D_o mm	fpm -	t_w mm	e_o mm	t_b mm	t_t mm
5	TiA-11	18.29	433	0.46	0.43	1.0	0.64
6	TiB-11	18.29	433	0.46	0.28	1.4	0.93
7	SS-16	18.43	630	0.46	0.32	1.2	0.75
8	A/P-50	22.23	-	0.46	0.43	-	-

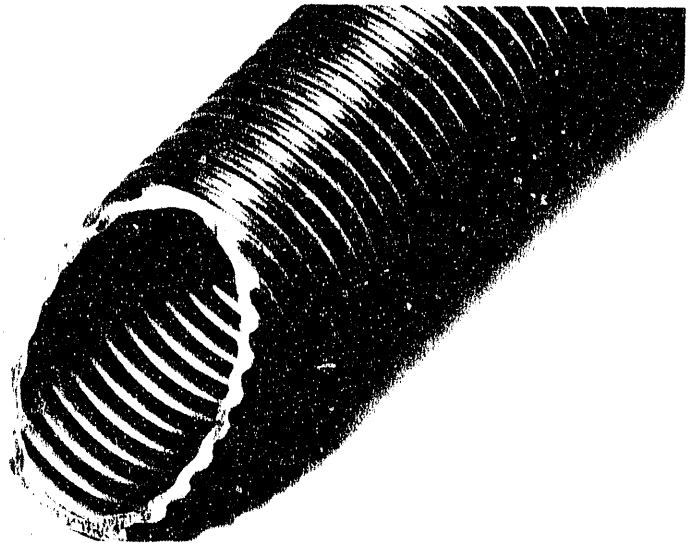

4.1a C/N-11 copper

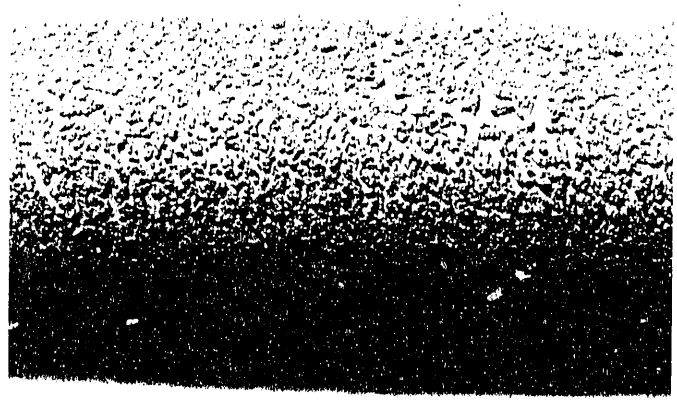

4.1b A/P-50

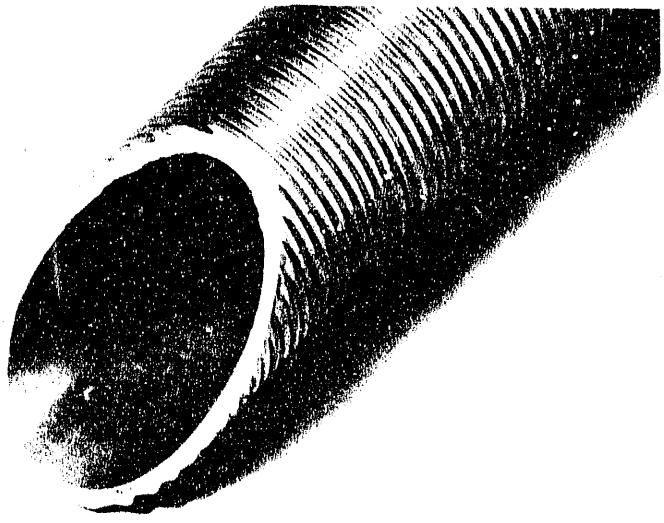

4.1c C/N-19 Cu/Ni

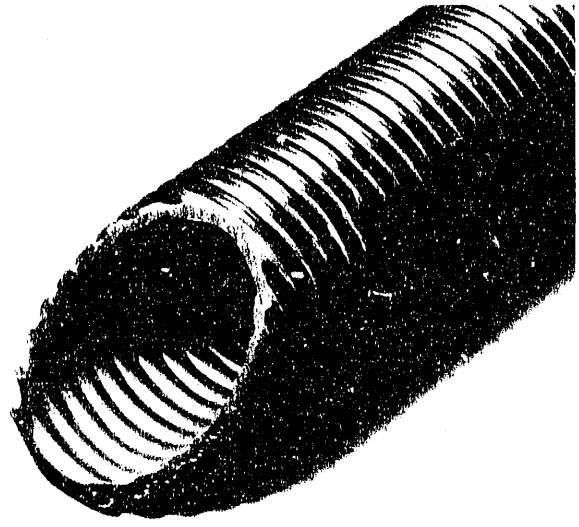

4.1d C/N-11 Cu/Ni

Figure 4.1 Copper and nickel tubes tested in condensation cell

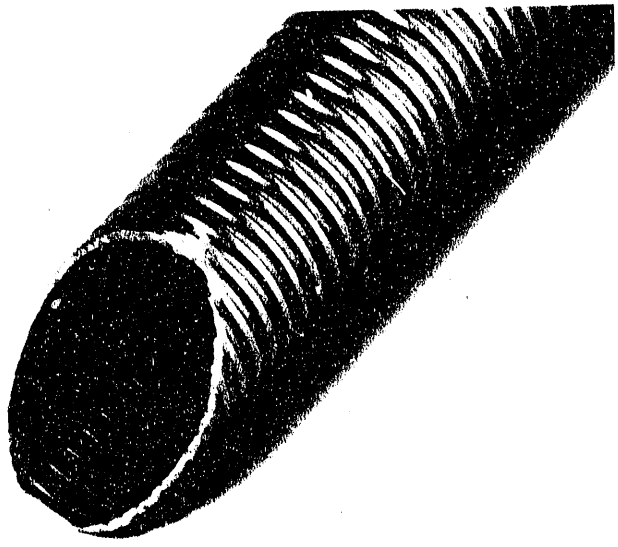

4.2a TiA-11

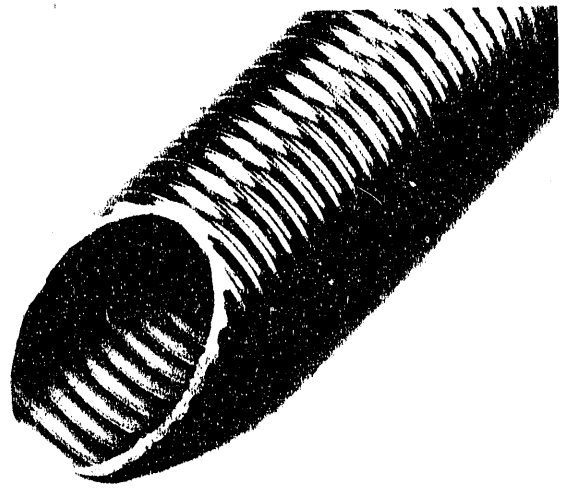

4.2b TiB-11

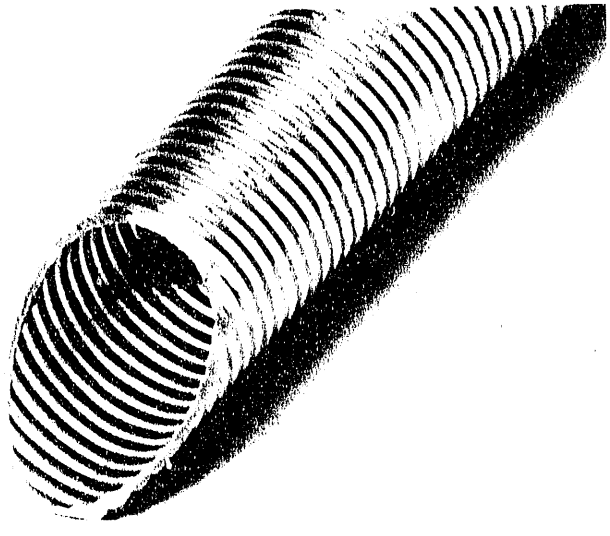

4.2c SS-16

Figure 4.2 Titanium and stainless steel tubes tested in condensation cell

5 TEST RESULTS

5.1 Steam Condensation Results

A 22.23 mm diameter smooth copper tube was tested at two different saturation temperatures, 54 C and 69 C. The purpose of this test was to verify the operation of the apparatus by comparing the data to the theory for a horizontal tube derived by Nusselt (1916). Figure 5.1 shows the data obtained for the plain tube. The experimental values were within -2% and +5% of the Nusselt theory. For condensation on plain, horizontal tubes, the Nusselt equation is

$$h = 0.725 \left(\frac{g k^3 \lambda}{D \nu (T_{sat} - T_w)} \right)^{1/4} \qquad (5.2)$$

Since these data agreed well with the Nusselt theory, the smooth tube performance will be represented from now on by the Nusselt theory.

In presenting the following results for the enhanced tubes, the "enhancement level" is defined as the ratio of the condensing coefficient, based on the envelope area over the fins (diameter D_o), to the condensing coefficient of a smooth tube of diameter D_o. Both coefficients are compared at the same (T_{sat} - T_w). The different symbols that appear in the graphs are for different tests, which were taken on different days.

5.1.1 Copper Alloy Tubes

Figure 5.2 shows the condensing coefficient vs. ΔT (= T_{sat} - $T_{w,av}$) for the 19.0 mm CU-11 copper tube, which has 433 fpm (11 fpi), e = 1.12 mm, and t_b = 0.9 mm. The average enhancement level is 2.85.

Three different 90/10 copper-nickel tubes were tested. The first is a 22.23 mm diameter C/N-11 tube which has the same fin shape, dimensions and fin pitch as the 19 mm diameter CU-11 copper tube. The data are shown in Figure 5.3, where an average enhancement level of 1.75 is obtained. The second cu/ni tube (C/N-19) has the same diameter as the C/N-11 tube, but has a smaller fin pitch, and a smaller fin height. The results for the C/N-19 tube are shown in Figure 5.4, for which an average enhancement level of 1.64 is obtained. Thus, the 742 fpm tube provided only slightly less enhancement than the 433 fpm tube.

The third type, A/P-50, is a smooth copper-nickel tube with copper particles sintered to the surface. Approximately 50% of the tube projected surface is covered with particles. Figure 5.5 shows the data obtained for this tube. The enhancement level was a strong function of ΔT as can be seen from Figure 5.5. The maximum enhancement was 1.89 (at the lowest ΔT) and the minimum of 1.4 (at the highest ΔT).

5.1.2 Titanium and Stainless Steel Tubes

Two titanium tubes, TiA-11 and TiB-11, were tested both having the 18.29 mm diameter over the fins and fin pitch, but different fin shapes. The dimensions of the 'A' and 'B' tubes are described in Table 4.2. The major difference between the two tubes is the fin height and the drainage channel shape. Figure 5.6 shows the results for the 'A' tube which show a modest average enhancement of 1.22. The results for the 'B' tube are shown in Figure 5.7, where the average enhancement level is 1.05. An 18.43 mm O.D. stainless steel tube having 16 fins/in on the inner surface and a wavy inner surface was tested. This tube has a higher internal wave height than the TiA-11 and TiB-11 tubes. Table 5.1 summarizes the enhancement level of each of the tested tubes.

Table 5.1 External Enhancement Levels, E_o for $(T_s - T_w) = 5.1$ K	
Tube Code	**E_o**
CU-11	2.80
C/N-11	1.75
C/N-19	1.64
A/P-50	1.70
TiA-11	1.22
TiB-11	1.05
SS-16	1.70

5.2 Water Side Enhancement

The clean tube heat transfer coefficients were measured by the tube manufacturers, using the Wilson plot method with water on the tube and annulus sides. The Colburn j-factor and the friction factor are plotted in Figure 5.8 for the Table 5.2, 5.3 and 5.4 water side geometries. Two tubes, the 3D-SS and Corrugated 1, are not included in Figure 5.8 because of their inferior thermal performance compared to the other enhanced tubes. The plotted values were obtained from smooth curve fits of the test data.

5.3 Fouling Test Results

5.3.1 Tube Geometries Tested

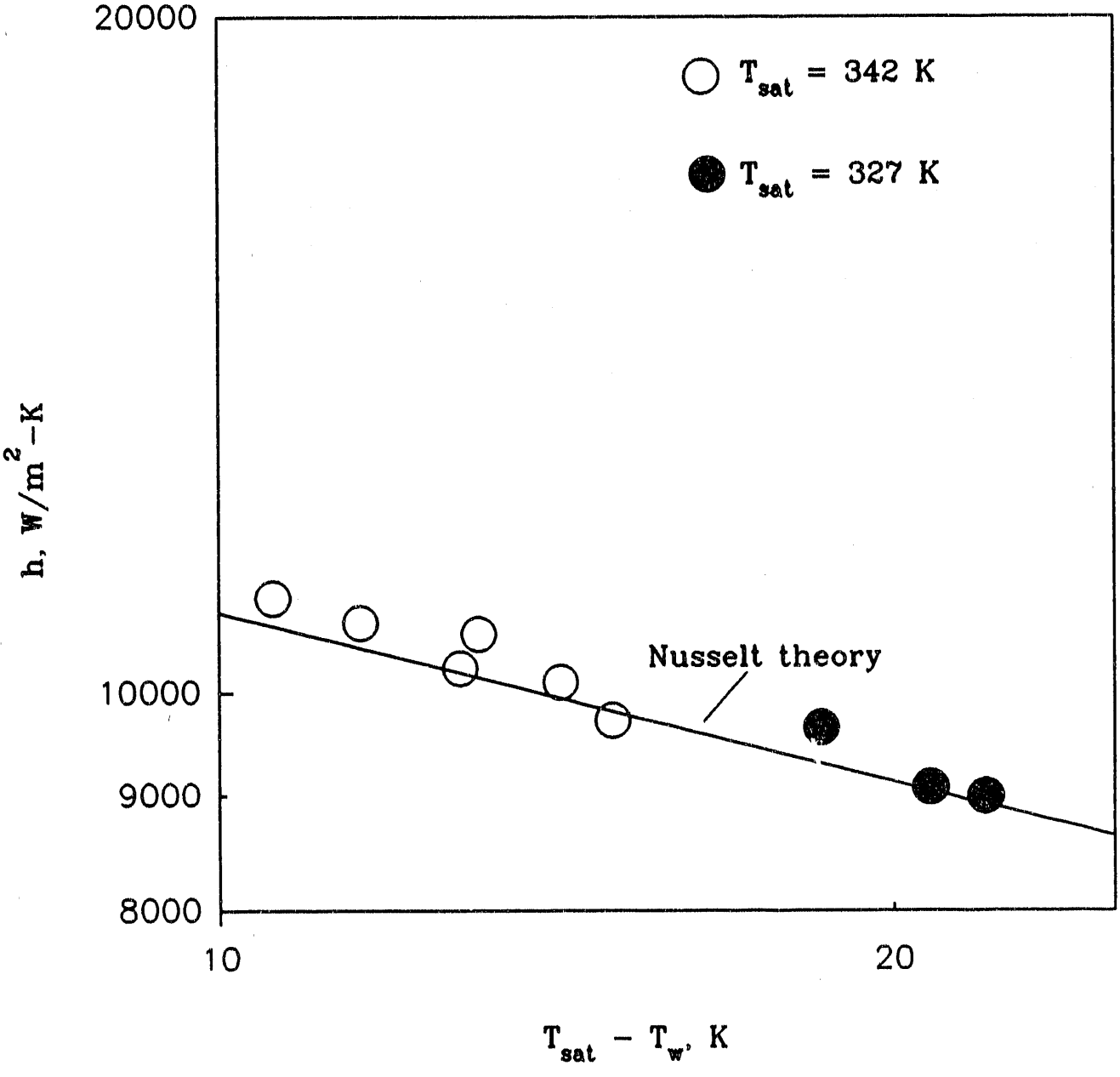

Figure 5.1 Condensation coefficient for the plain copper tube

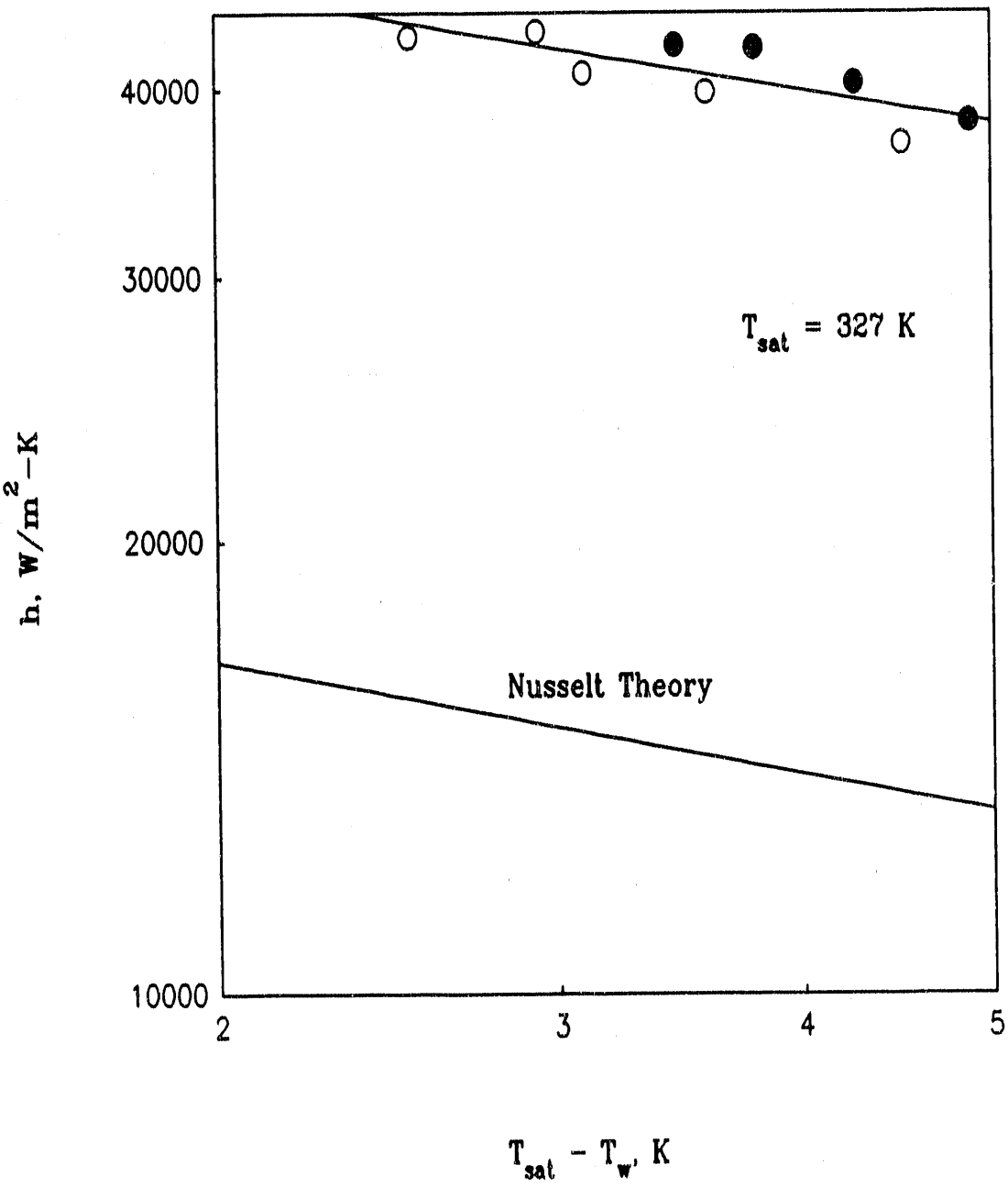

Figure 5.2 Condensation coefficient for the CU-11 copper tube

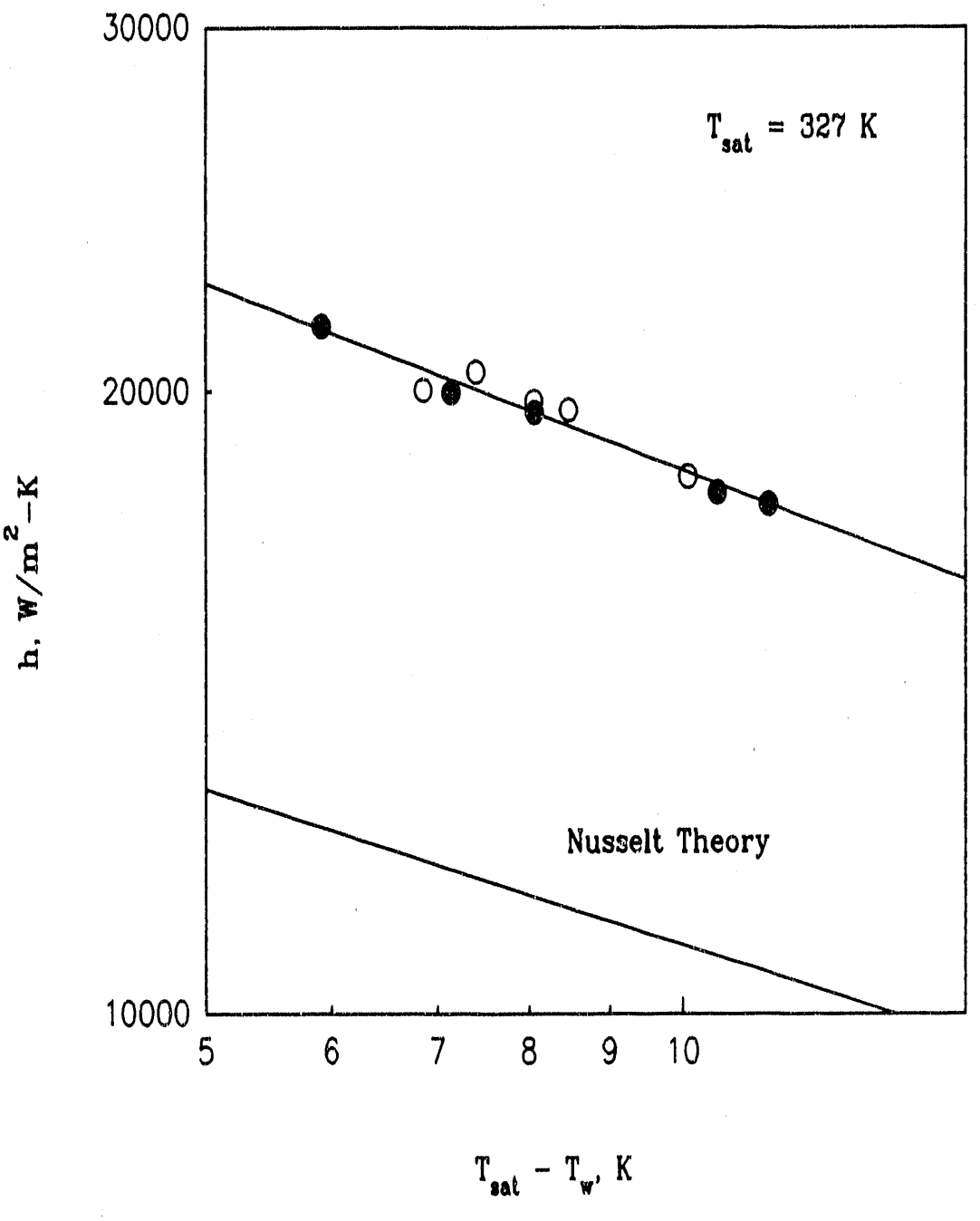

Figure 5.3 Condensation coefficient for the C/N-11 tube

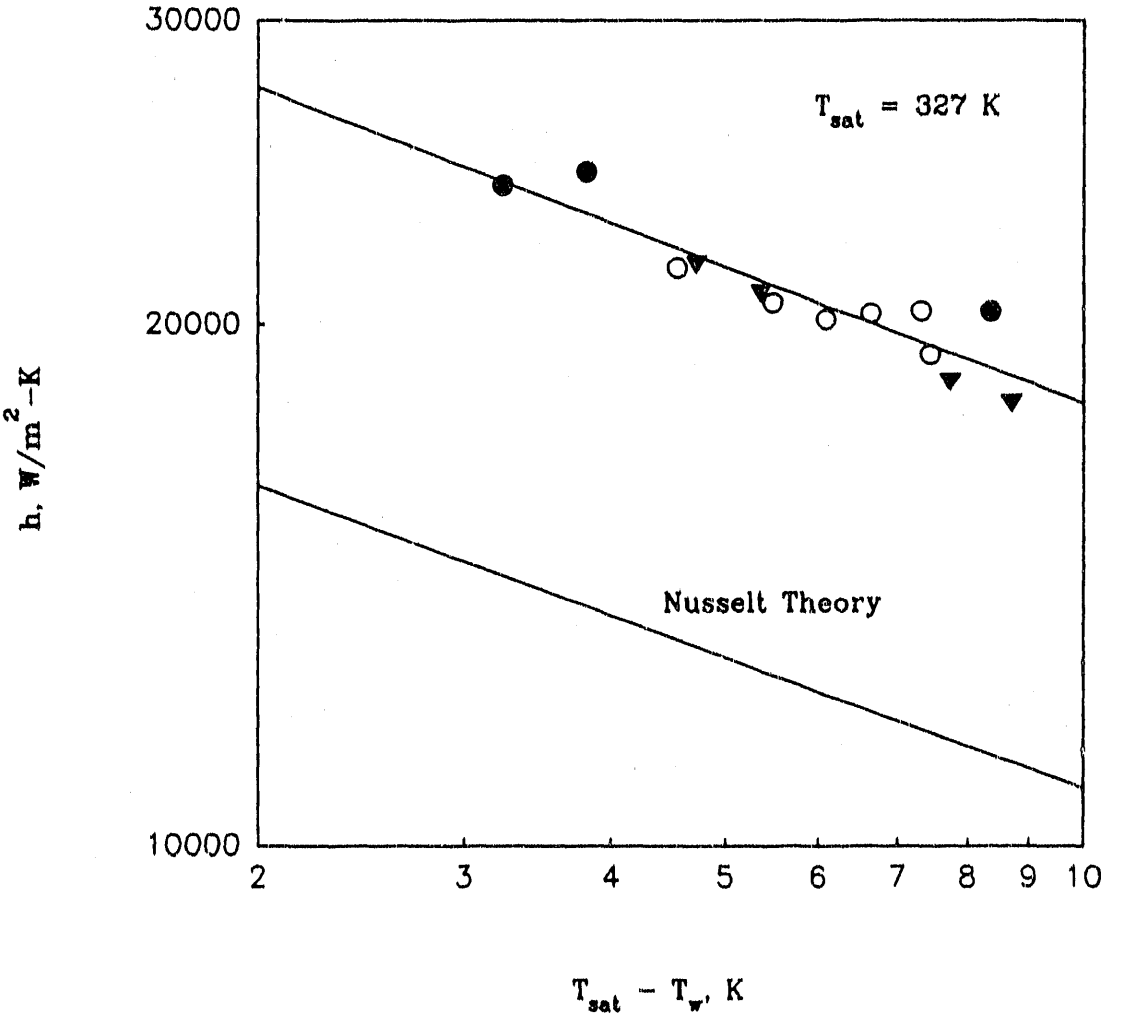

Figure 5.4 Condensation coefficient for the C/N-19 tube

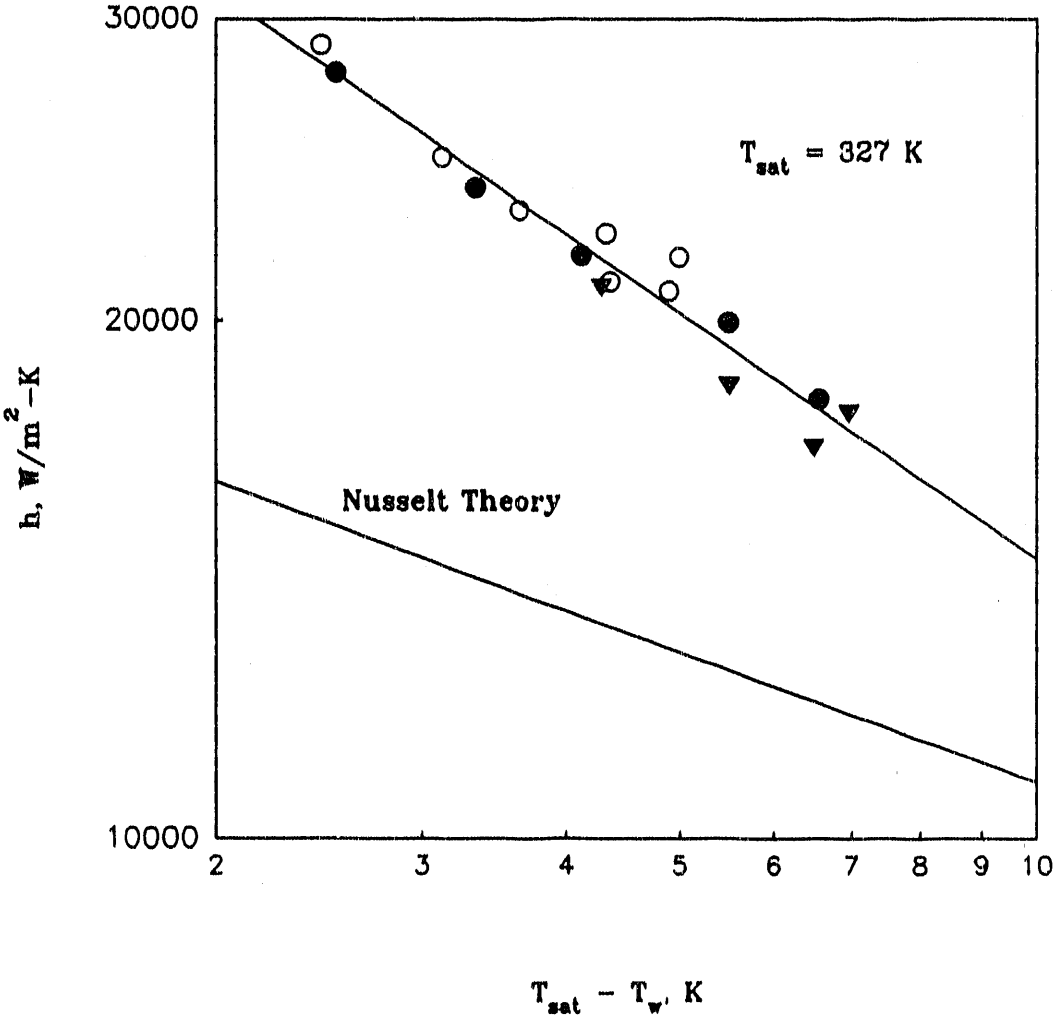

Figure 5.5 Condensation coefficient for the A/P-50 tube

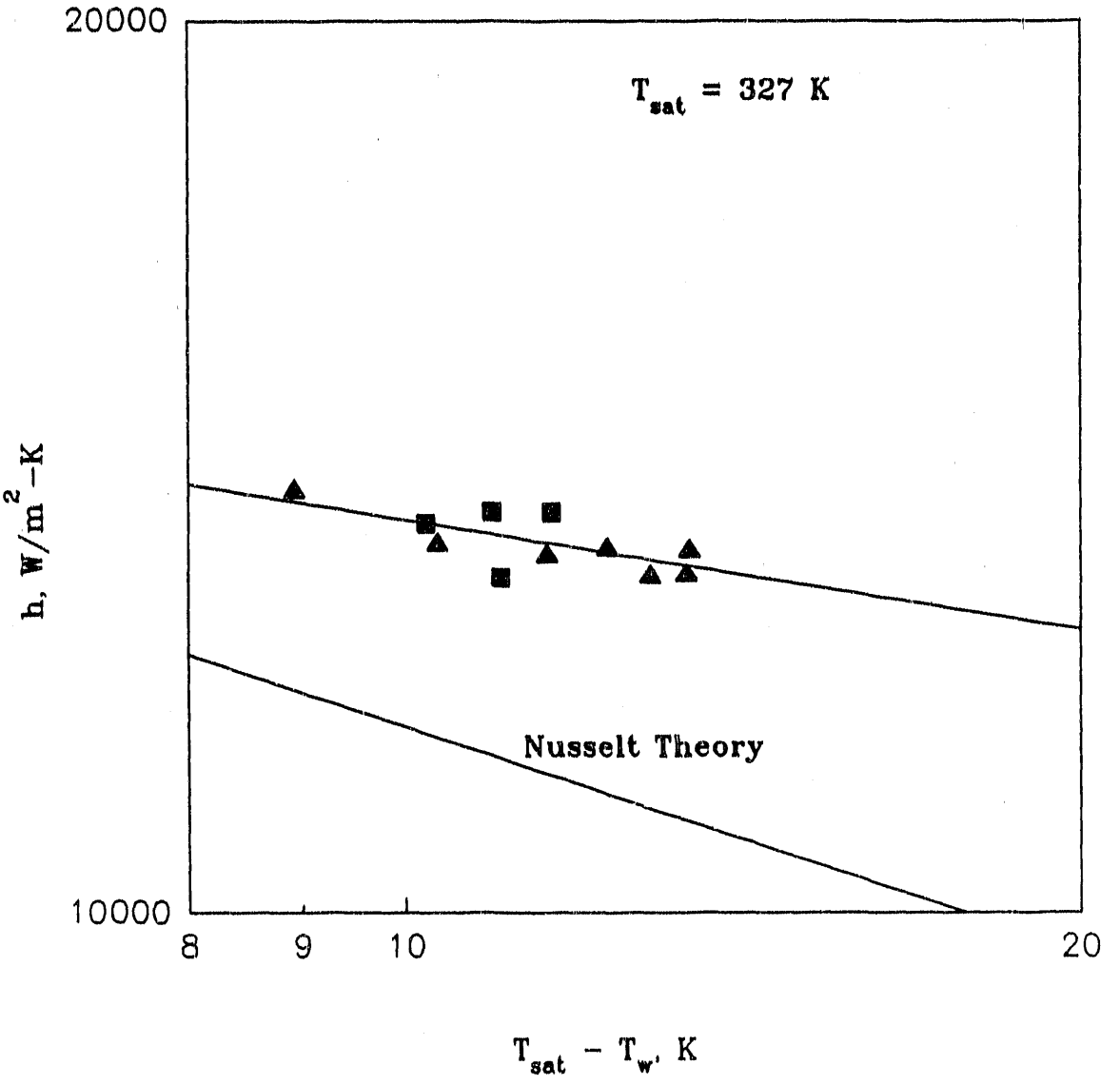

Figure 5.6 Condensation coefficient for the TiA-11 tube

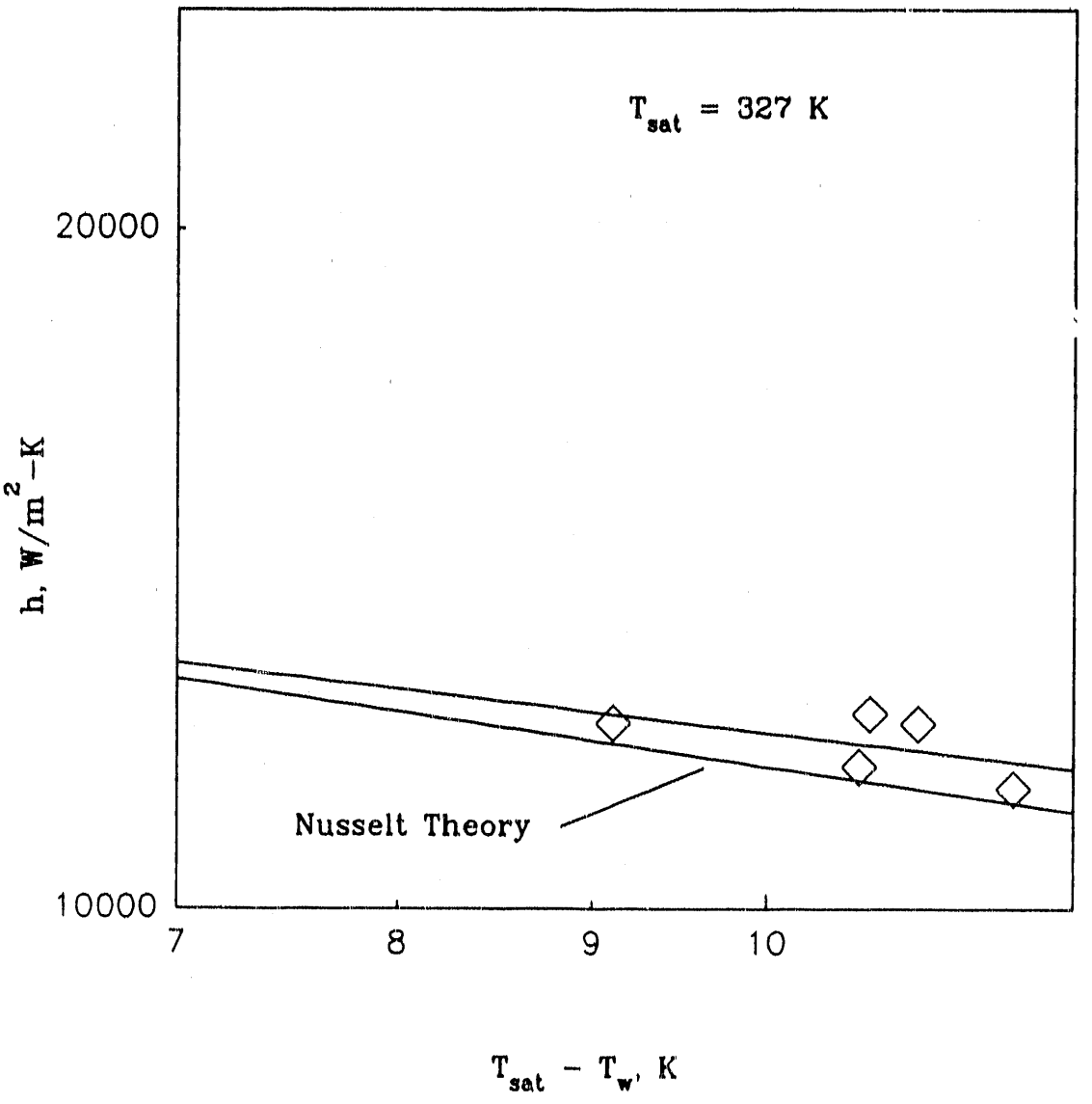

Figure 5.7 Condensation coefficient for the TiB-11 tube

Data were taken on three different sets of tubes. The tubes were made by the manufacturers identified in the Acknowledgement. The internal geometry dimensions of the nominal 19 mm outside diameter set are listed in Table 5.2. Figure 5.9 shows photos of the enhanced tubes described in Table 5.2. Table 5.3 lists the internal dimensions of the nominal 22 mm outside diameter tubes. The I.D. dimension is the minimum inside diameter. Figure 5.10 shows the Table 5.3 tube geometries. Table 5.4 lists the enhanced tubes dimensions for the third set. Figure 5.11 shows the Table 5.4 tube geometries.

Table 5.2
19 mm O.D. Tube Dimensions

Tube	I.D. [mm]	e_i [mm]	p [mm]	α [deg]
Plain	14.3	-	-	-
3D-SS	14.7	0.25	5.50	35
3D-DS	14.7	0.25	5.50	35
NW	14.6	0.35	2.45	90

Table 5.3
22 mm O.D. Tube Dimensions

Tube	I.D. [mm]	e_i [mm]	p [mm]	α [deg]
Plain	17.9	-	-	-
NW	18.0	0.25	2.20	90
Korodense	19.7	0.50	10.0	81

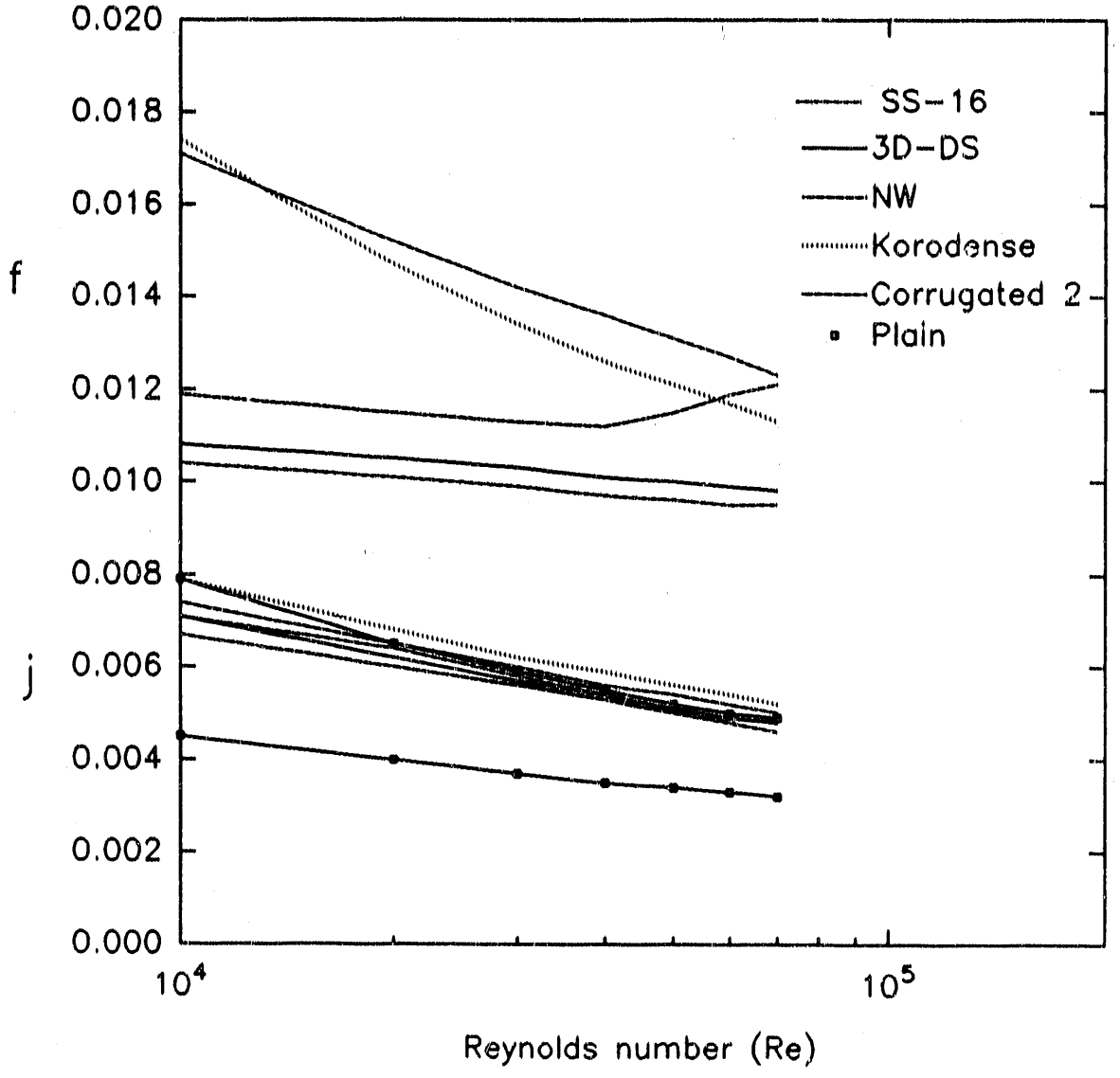

Figure 5.8 Colburn-j and friction factors for the enhanced tubes

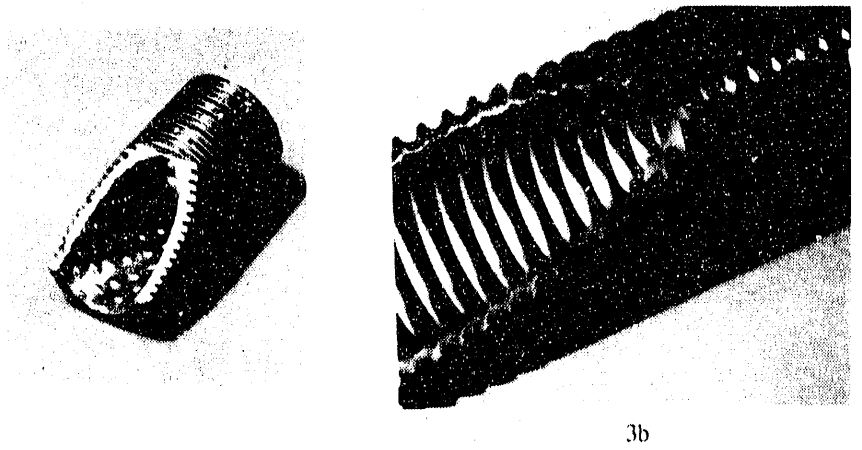

3a

3b

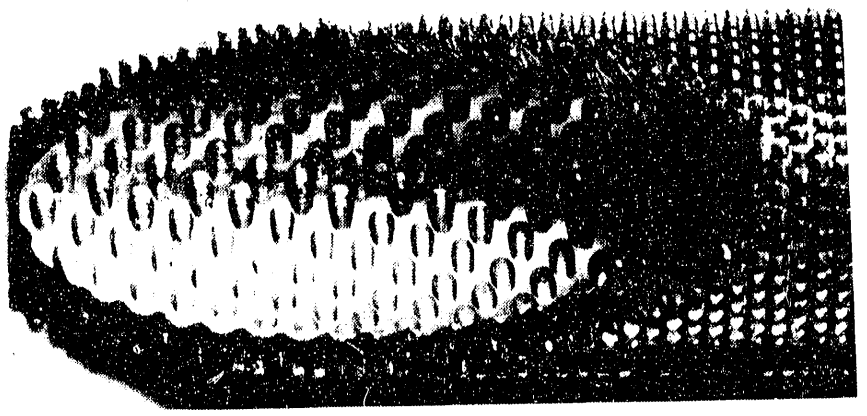

3c

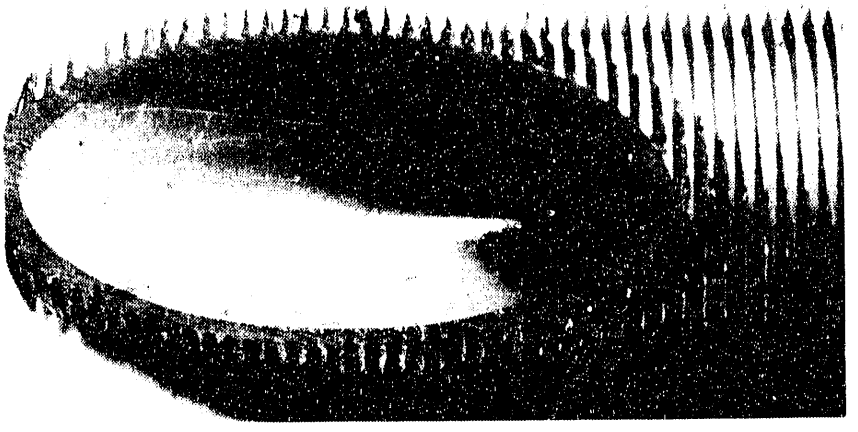

3d

Figure 5.9 (a) 3D-SS, (b) NW, (c) 3D-DS, (d) plain tube geometries

a

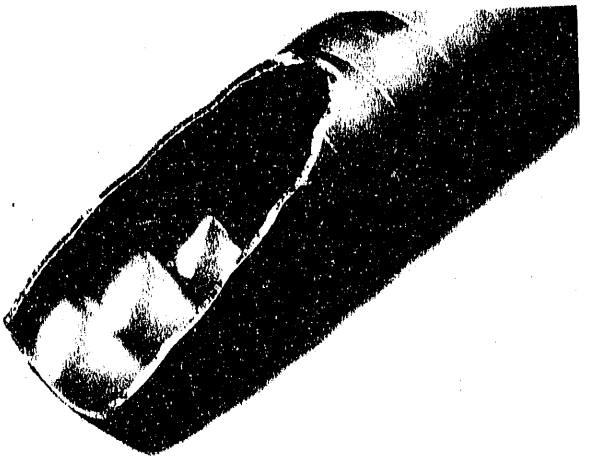

b

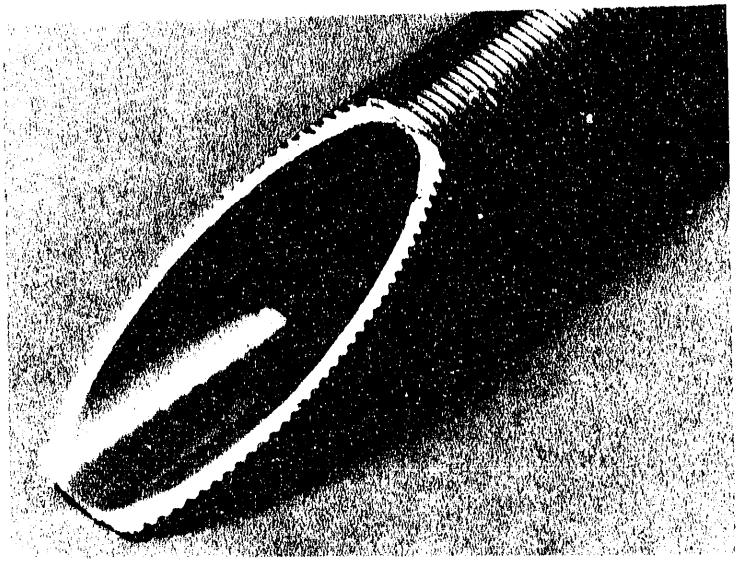

c

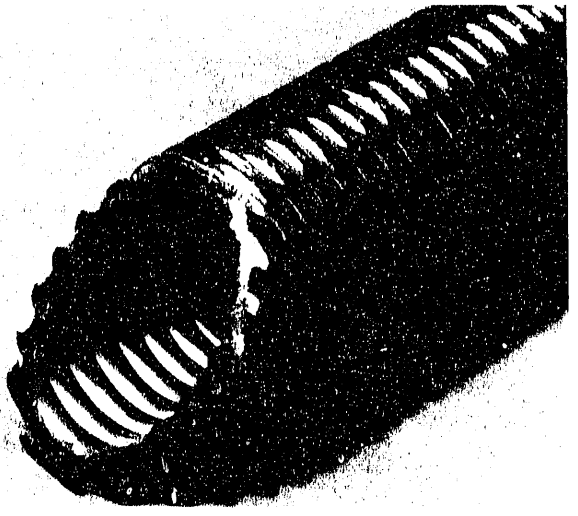

Figure 5.10 (a) Korodense, (b) plain, and (c) NW tube geometries

a

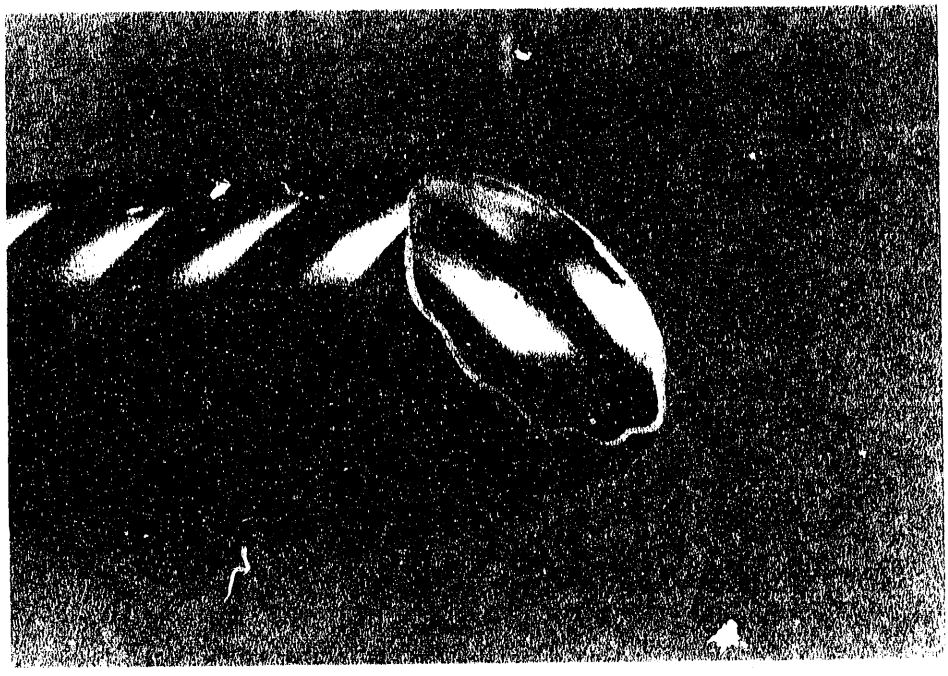

b

Figure 5.11 (a) Corrugated 1 and (b) corrugated 2 tube geometries

Table 5.4 22 mm O.D. Tube Dimensions				
Tube	**I.D. [mm]**	**e_i [mm]**	**p [mm]**	**α [deg]**
Plain	17.9	-	-	-
Corrugated 1	20.3	0.61	12.2	45
Corrugated 2	20.3	0.73	14.6	45

5.3.2 Fouling Data for the Table 5.2 Geometries

Figure 5.12 shows fouling curves for the Table 5.2 geometries. The fouling curves show an asymptotic behavior. The sponge-ball cleaning system was activated at 18 hours as shown on Figure 5.12. The ball activation reduced the R_f in each tube to zero. In this test, three sponge-balls were injected manually, one after another, with a one hour waiting period, followed by another three balls. Figure 5.12 shows that the fouling rates are higher following the ball cleaning than the initial fouling rates. The higher fouling rates are because ball cleaning returns foulant to the water, thereby increasing its foulant concentration. To prevent increasing the foulant concentration, a modified cleaning technique was adopted. This technique was described earlier.

Figure 5.13 shows the results of sponge-ball cleaning for three cleaning cycles. Free fouling was allowed to occur until R_f in one tube reached 5.3×10^{-5} m^2-K/W (3.0×10^{-4} hr-ft^2-F/Btu), then the sponge-balls are applied. Figure 5.13 shows that sponge-ball cleaning reduced the R_f to zero in each tube for each cleaning passage. The figure also shows that the fouling rate following each sponge-ball cleaning cycle is repeatable.

5.3.3 Fouling Data for the Table 5.3 Geometries

Figure 5.14 shows the asymptotic free fouling curves for the Table 5.3 geometries. The asymptotic fouling resistance is reached after 32 hours in all the tubes. The plain tube shows negligible fouling resistance as in the previous tests. Figure 5.15 shows the results of a repeat fouling test to check the repeatability of the fouling curves. The fouling data are very close in both Figures 5.14 and 5.15 runs.

Fouling curves for three sponge-balls cleaning cycles are shown in Figure 5.16. The figure shows that the fouling resistance drops to zero after each cleaning cycle in each tube. The fouling curves are repeatable after each cycle.

Figure 5.17 shows the results of four brush cleaning cycles. The fouling resistance was allowed to reach 5.3×10^{-5} m^2-K/W (3.0×10^{-4} hr-ft^2-F/Btu) before the brushes are passed through each tube. The fouling resistance for the Korodense tube drops to zero after each cleaning cycle. However, the initial fouling factor for the NW tube appears to increase after each cycle. Later inspection showed that improper brush diameter was used for the NW tube. The brush used in the NW tube was 18 mm diameter, as opposed to the desired 18.5 mm diameter. However, the smaller brush did substantially reduce the fouling resistance in the NW tube. Webb and Kim (1989) used the on-line brush cleaning to clean a TWX tube, which is similar to the NW tube geometry. They showed that a correctly sized brush decreased the fouling resistance down to zero after each cycle.

Both cleaning systems, sponge-balls and brushes, are very effective in cleaning the enhanced tubes.

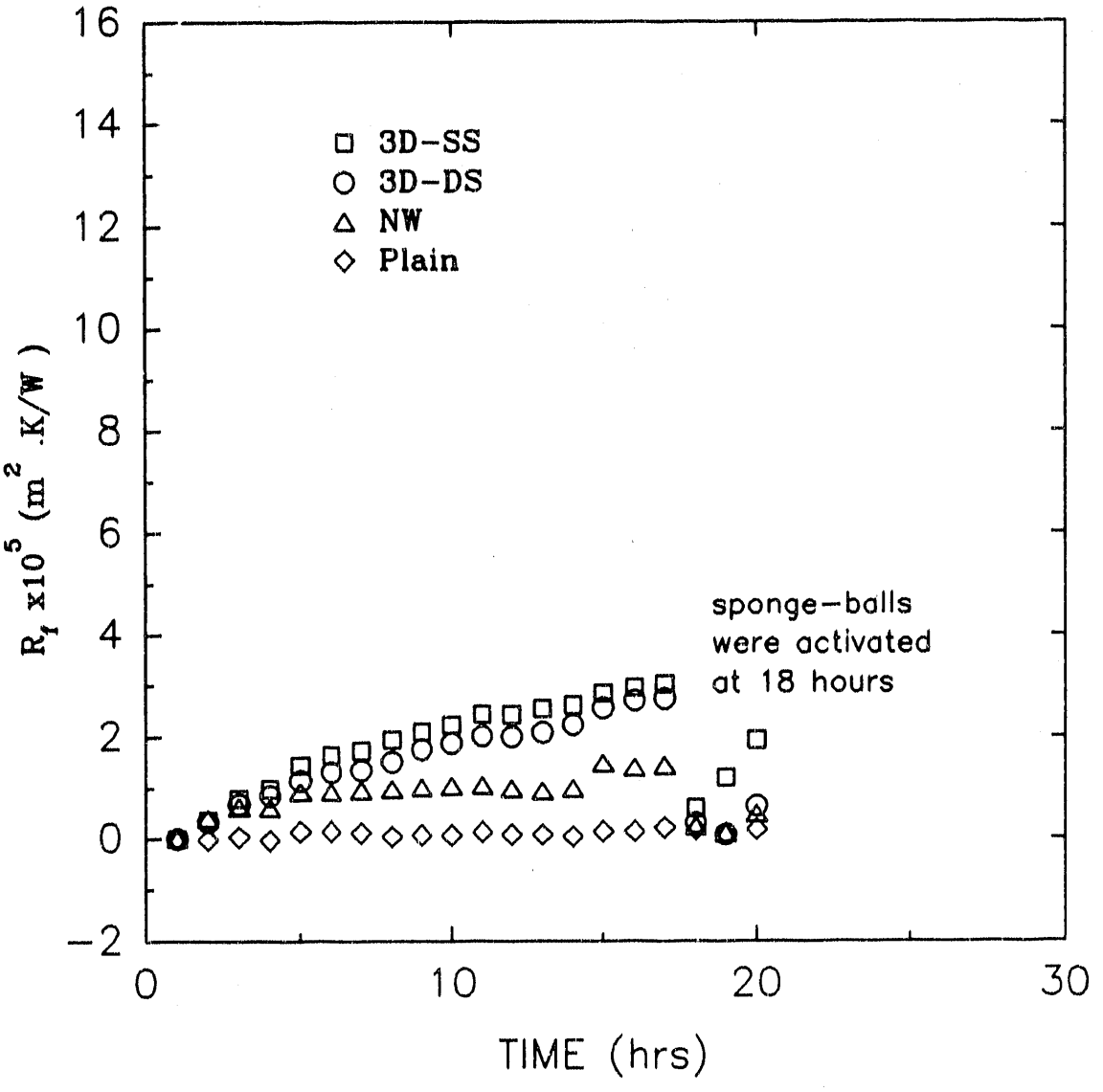

Figure 5.12 Free fouling test curves for 19 mm O.D tubes with one sponge-ball cleaning cycle, 3 μm aluminum oxide

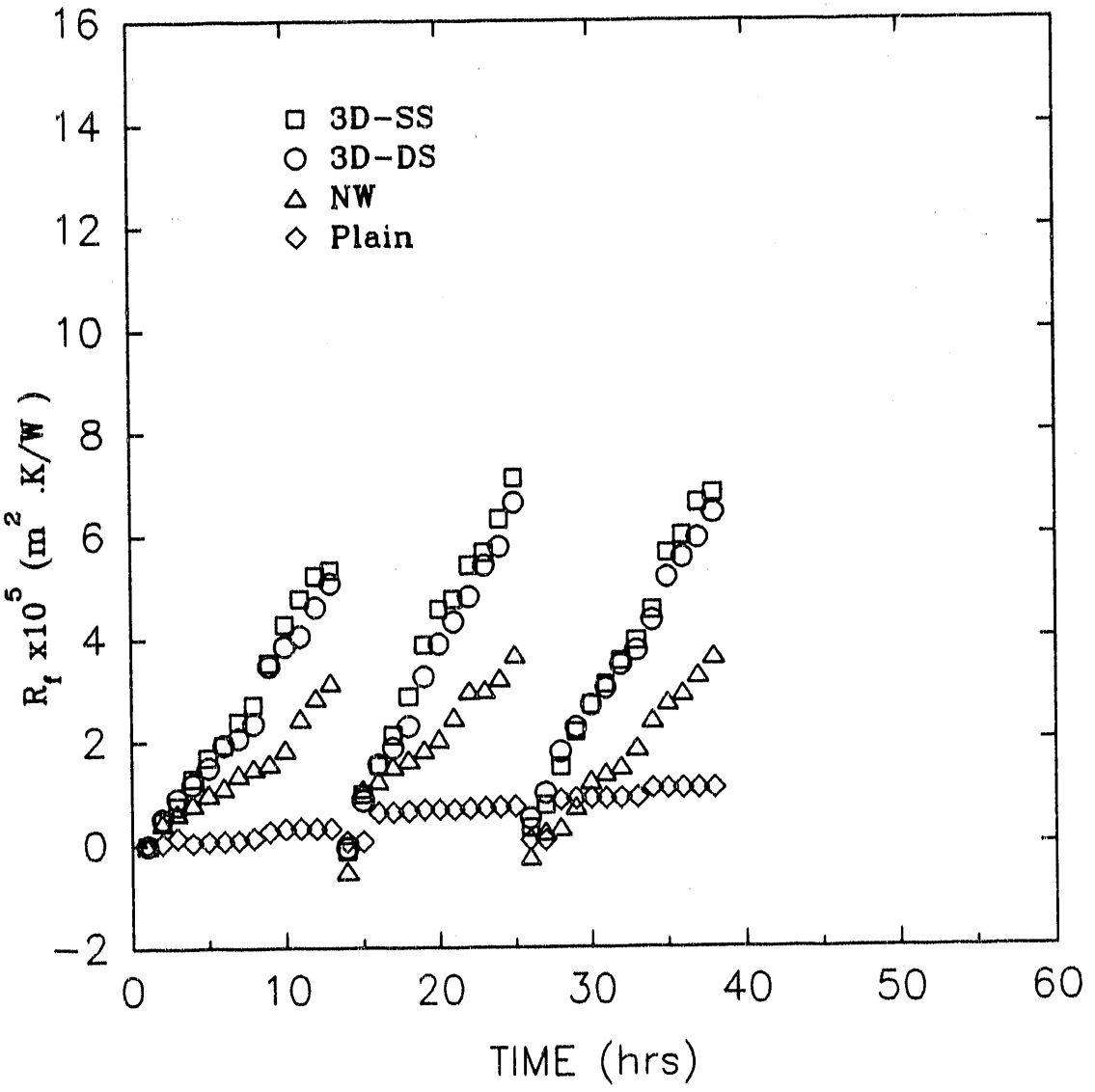

Figure 5.13 Fouling curves for three sponge-ball cleaning cycles for 19 mm O.D. tubes, 3 μm aluminum oxide

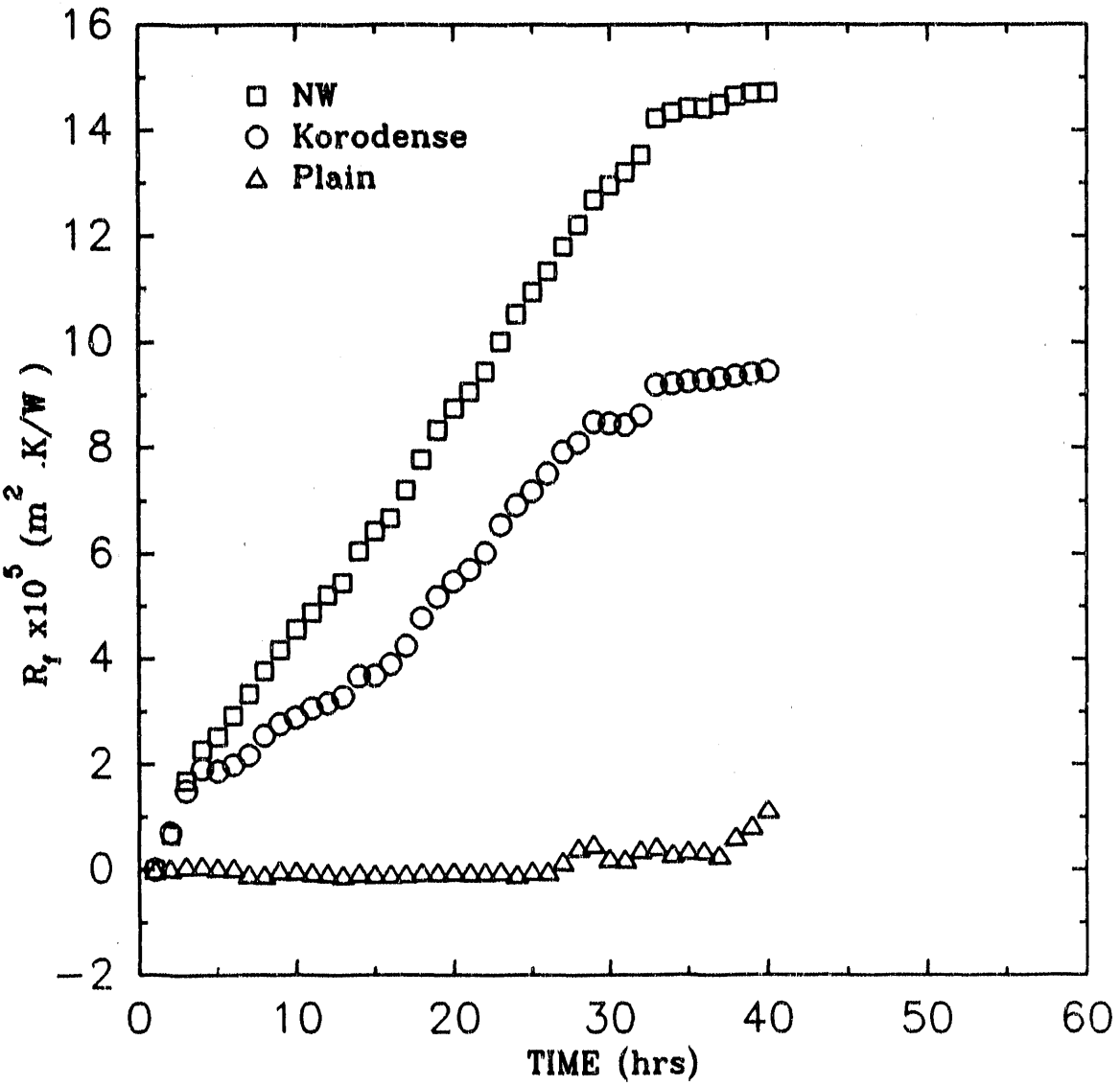

Figure 5.14 Asymptotic fouling curves for 22 mm O.D. tubes, 0.3 μm aluminum oxide

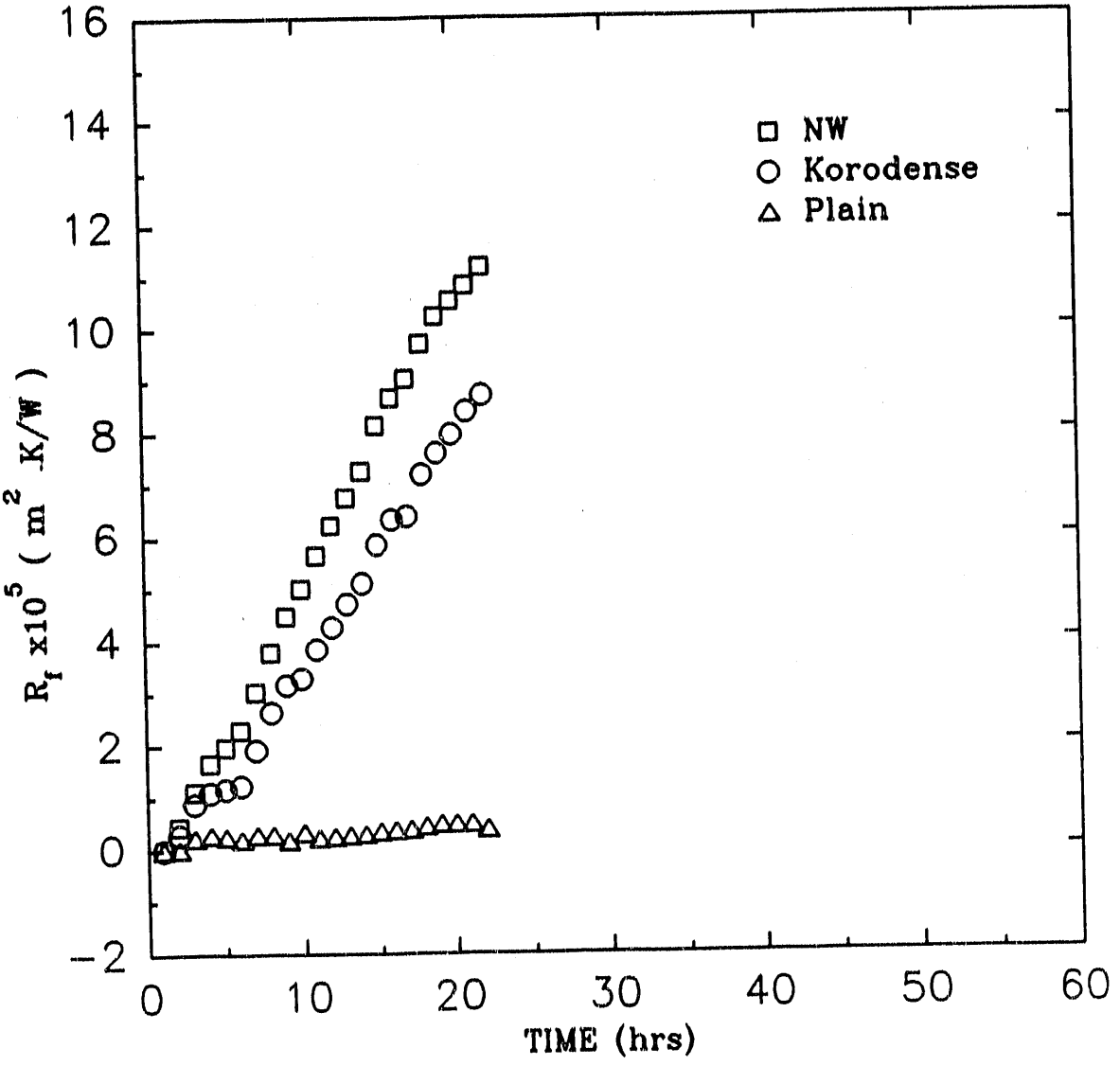

Figure 5.15 Free fouling curves for 22 mm O.D., 0.3 μm aluminum oxide

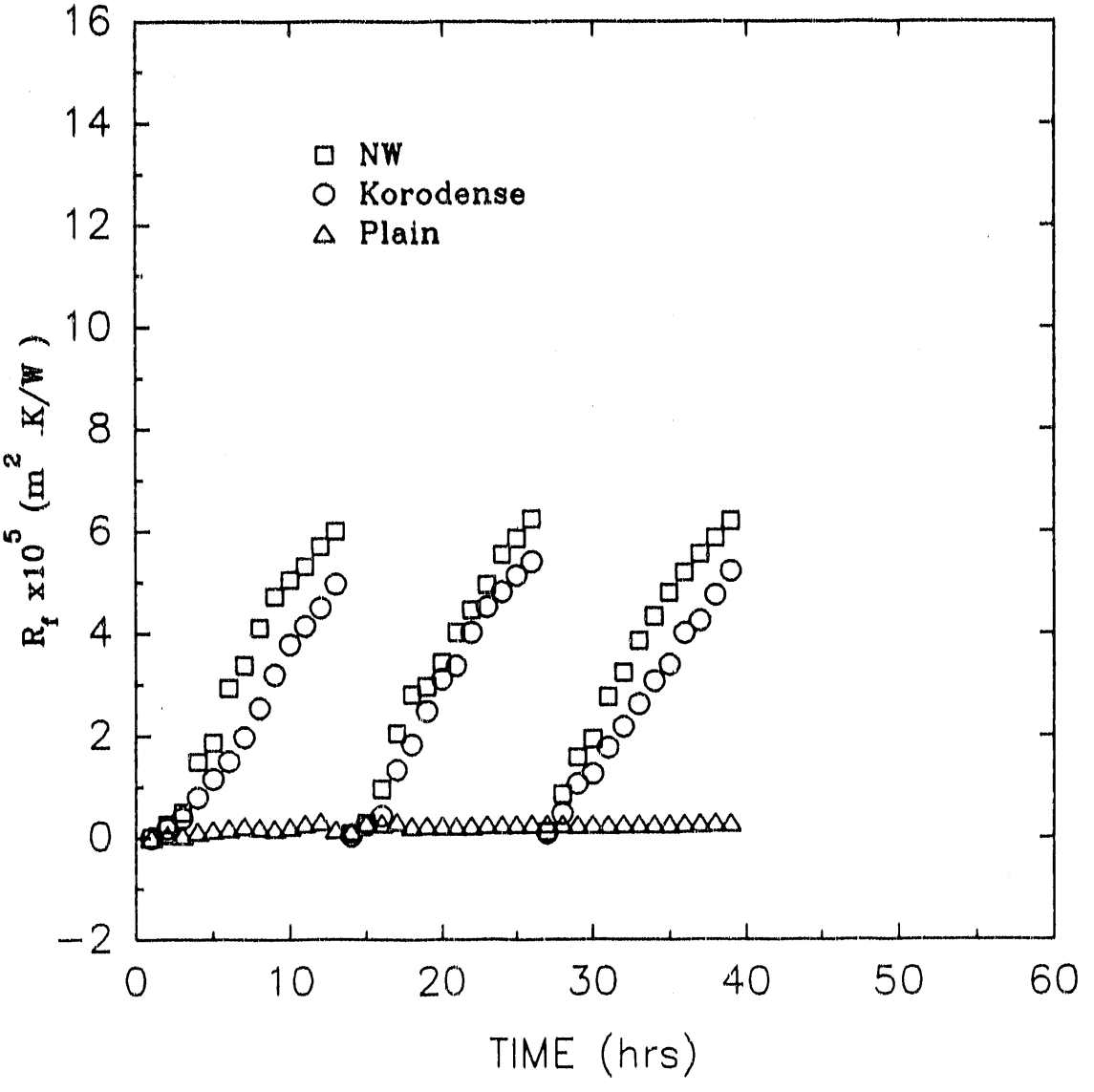

Figure 5.16 Fouling curves for three sponge-ball cleaning cycles for 22 mm O.D. tubes, 0.3 μm aluminum oxide

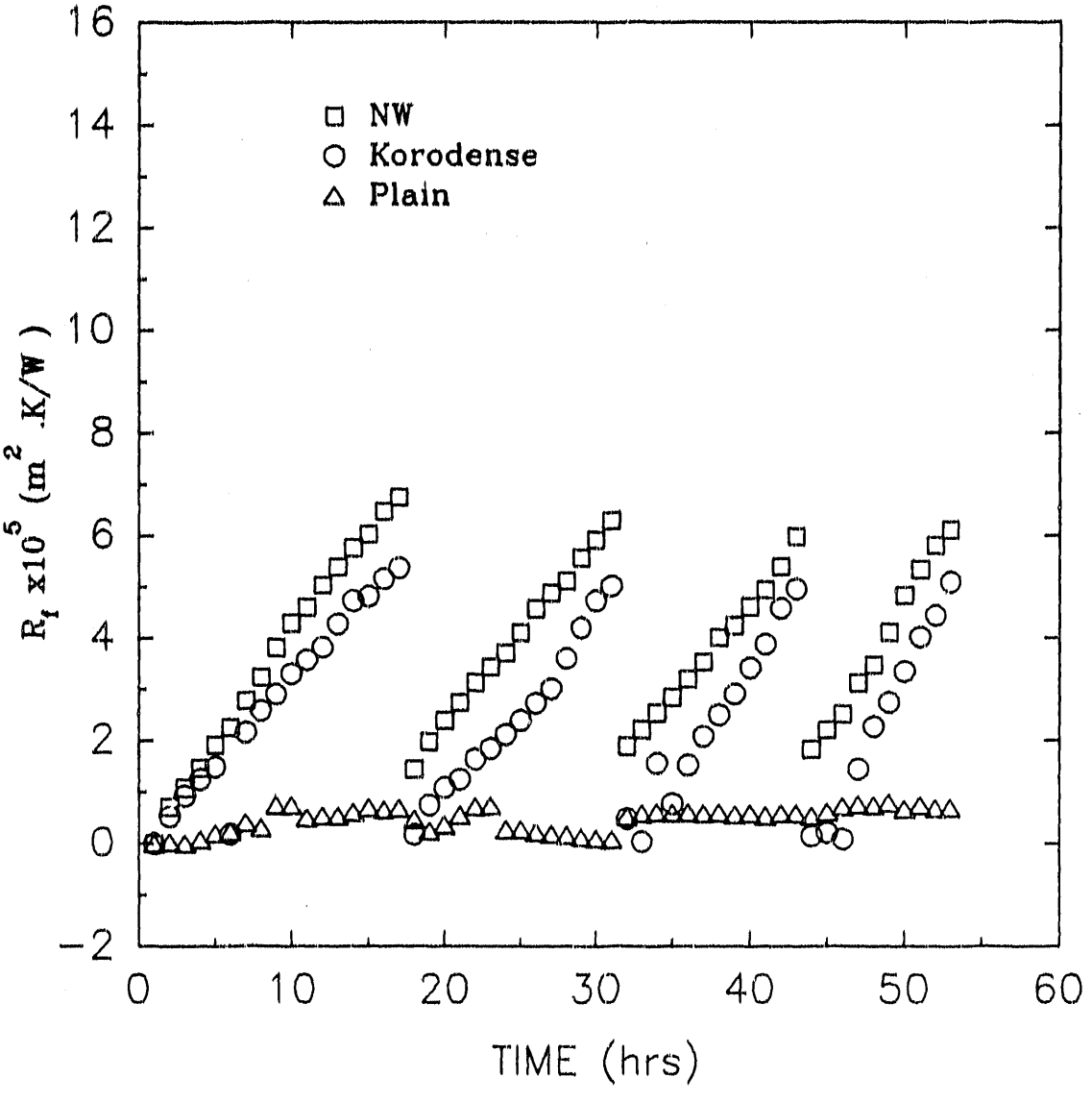

Figure 5.17 Brush cleaning cycles for 22 mm O.D., 0.3 μm aluminum oxide

5.3.4 Fouling Data for the Table 5.4 Geometries

The asymptotic fouling curves for these tubes are shown in Figure 5.18. The 45 degree corrugated tubes foul faster than the plain tube. However, the corrugated tube with 0.73 mm internal ridge height fouls faster than the corrugated tube having a smaller ridge height (0.61 mm). The asymptotic fouling resistance is reached after approximately 36 hours in both corrugated tubes.

Figure 5.19 shows the results of three cleaning cycles using sponge-balls cleaning method. The fouling resistance drops to zero after each cleaning cycle. The fouling data are repeatable after each cycle. This test shows that the sponge-balls cleaning method is very effective in cleaning the corrugated tubes.

The brush cleaning test results are shown in Figure 5.20. As expected, the fouling resistances are brought to zero after six brush passes.

5.3.5 Discussion of Fouling Results

The fouling rate is sensitive both to particle size and enhancement geometry. The NW tube was tested using two different particle sizes. The particle size used for the Figures 5.12 and 5.13 data is 3 μm. Figures 5.14 through 5.20 used 0.3 μm particles. Comparison of these figures shows that the fouling rate of the NW is faster for 0.3 μm particle size than for 3 μm particles. Smaller particles, whose Schmidt numbers are small, yield higher deposition velocities than larger particles. That is because in the diffusion regime, the particle deposition velocity becomes proportional to $Sc^{-2/3}$, as shown by Webb and Kim (1989).

The free fouling tests (Figs. 5.12, 5.14, and 5.18) show asymptotic behavior for all of the tubes tested. The data show that the free fouling rate is sensitive to the tube geometry.

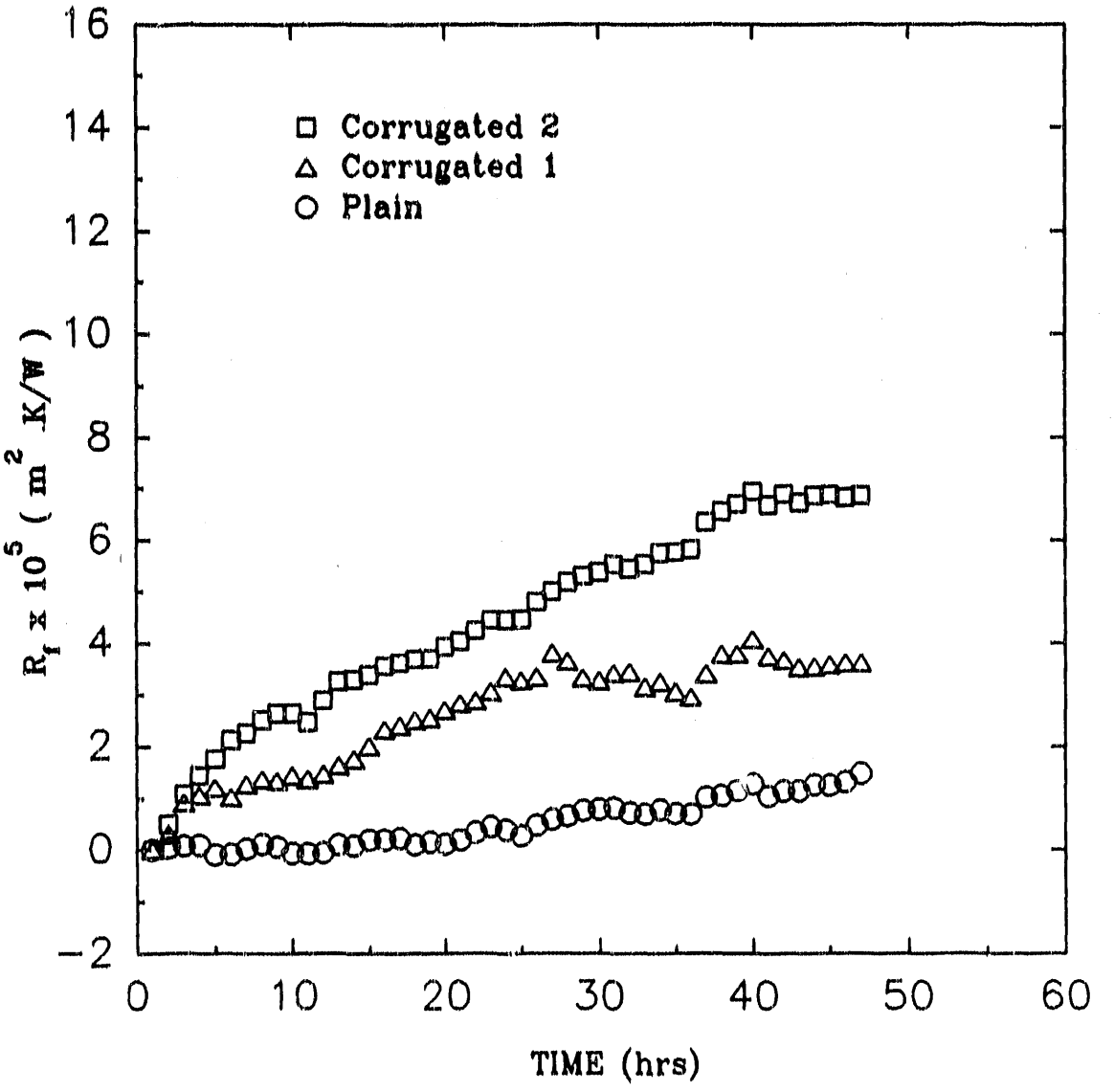

Figure 5.18 Asymptotic fouling curves for 22 mm O.D. corrugated tubes, 0.3 μm aluminum oxide

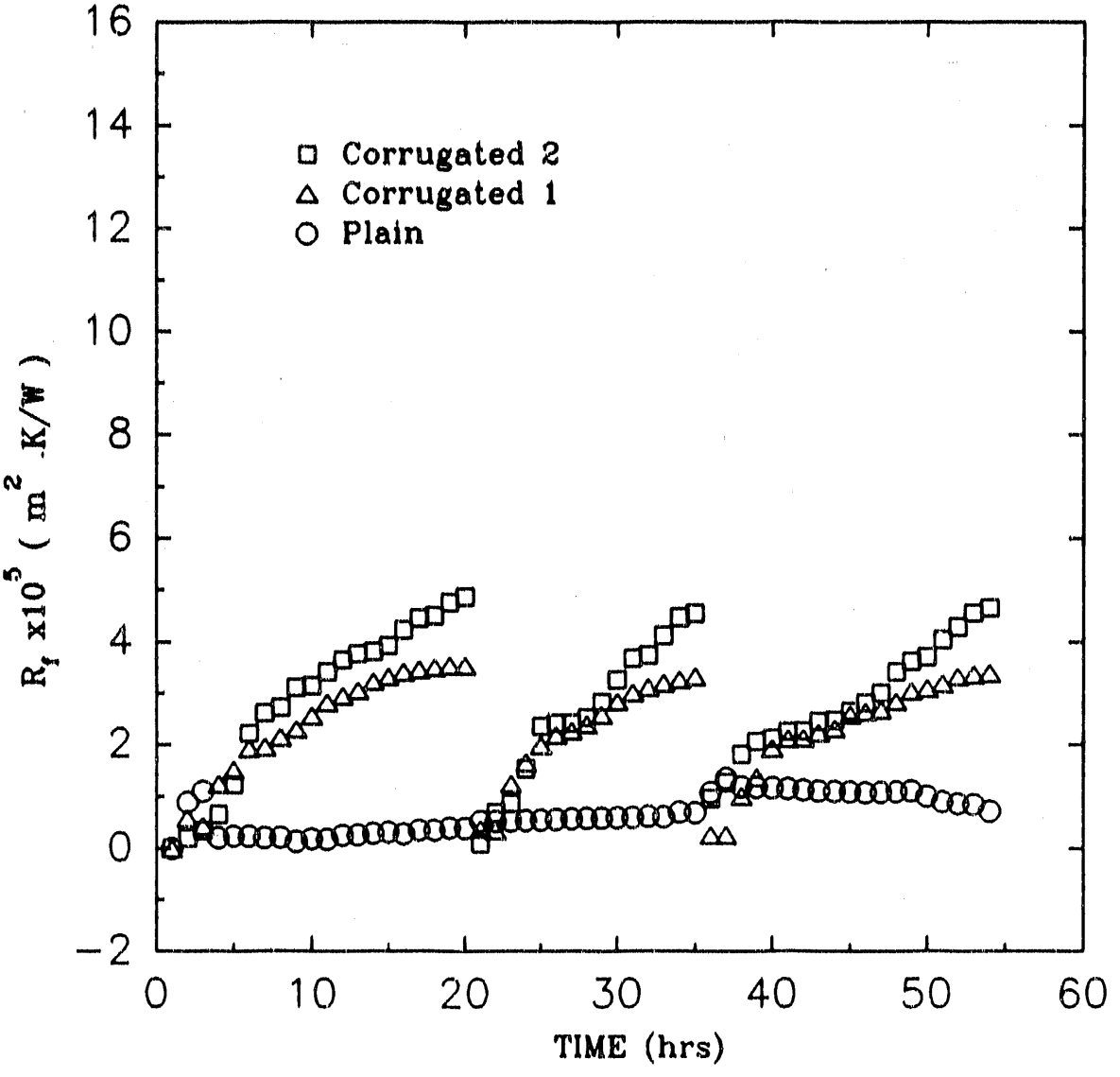

Figure 5.19 Three sponge-ball cleaning cycles for 22 mm O.D. corrugated tubes, o.3 μm aluminum oxide

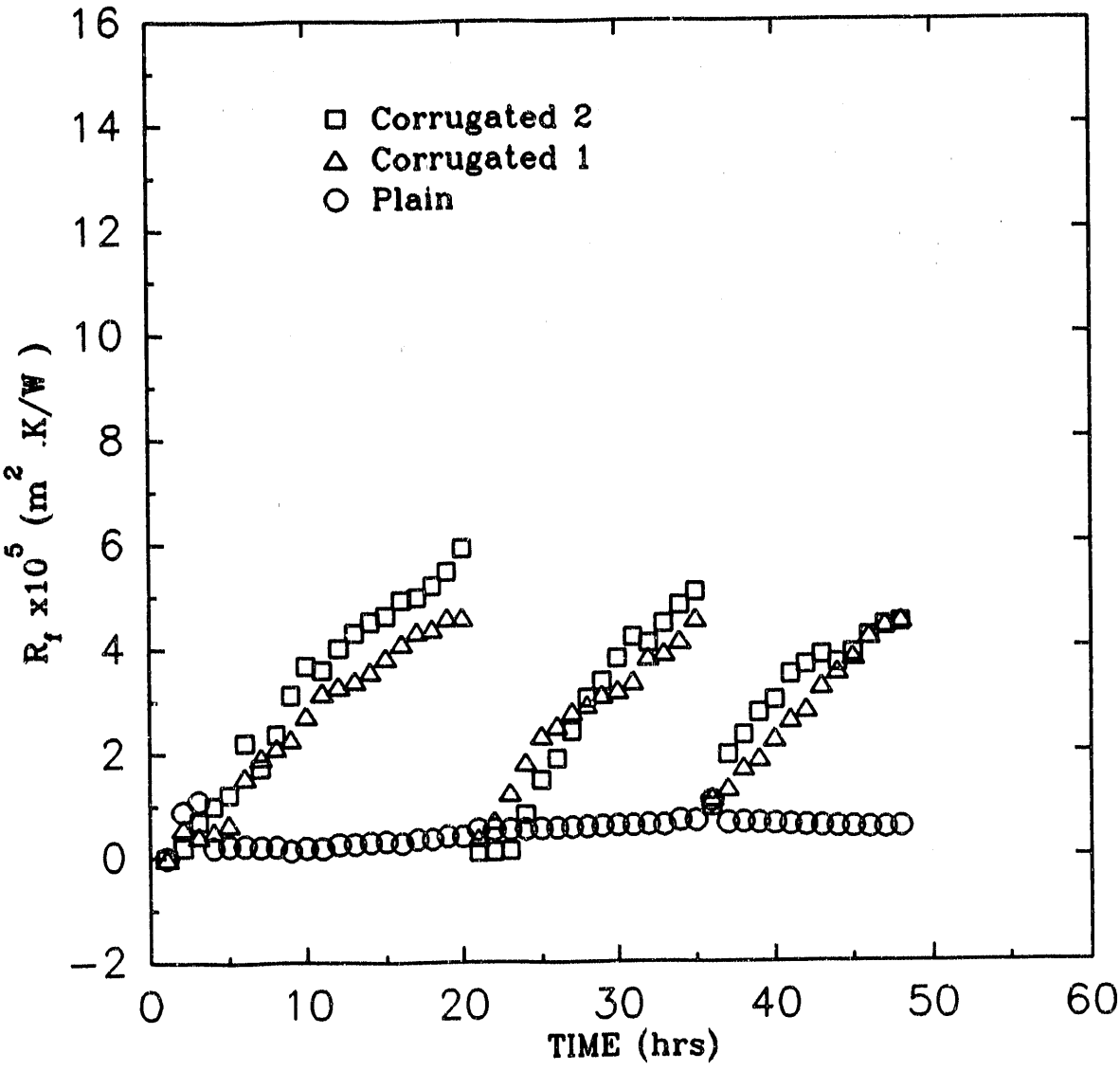

Figure 5.20 Fouling curves for three brush cleaning cycles for 22 mm O.D. corrugated tubes, 0.3 μm aluminum oxide

Table 5.5 lists the fouling resistance after 15 hours for three tube geometries using 3 μm diameter particles. Table 5.5 shows that the NW tube fouls at a lower rate than the 3D-SS and the 3D-DS tubes. The 3D-SS tube shows the highest fouling resistance.

Table 5.5
Fouling Resistance After 15 Hours
(3μm aluminum oxide particles)

Tube	O.D. [mm]	R_f [m^2-K/W]
3D-SS	19.0	$2.8x10^{-5}$
3D-DS	19.0	$2.5x10^{-5}$
NW	19.0	$1.5x10^{-5}$

Table 5.6 lists the fouling resistance for the 22 mm tubes at 15 hours. The table shows that Corrugated-1 (0.61 mm internal ridge height) has the lowest fouling resistance, R_f = $1.6x10^{-5}$ m^2-K/W. Increase of the internal ridge height to 0.73 mm caused R_f to increase to $2.5x10^{-5}$ m^2-K/W. The R_f of the Korodense and NW tubes after 15 hours are 2.3 and 3.5 times higher than that of the Corrugated-2 tube, respectively.

Table 5.6 Fouling Resistance After 15 Hours (0.3μm aluminum oxide particles)		
Tube	**O.D. [mm]**	**R_f [m^2-K/W]**
Korodense	22.0	$5.8x10^{-5}$
NW	22.0	$8.8x10^{-5}$
Corrugated 1	22.0	$1.6x10^{-5}$
Corrugated 2	22.0	$2.5x10^{-5}$

The sponge-ball cleaning system was very effective in cleaning all of the enhanced tubes. Also, the on line brushing brought the fouling resistance to zero in all the tubes except the NW tube, which occurred because of the under size brush. Six brush passes (three brushing cycles) were applied in order to compare with the sponge-balls system, which used six sponge-balls. However, Webb and Kim (1989) showed that two passes (one cycle) is sufficient to clean the enhanced tubes they tested. Both on-line ball and brush cleaning were effective in cleaning the geometries tested here.

5.4 Overall Heat Transfer Coefficient

Three enhanced tubes were selected to measure the overall heat transfer coefficient. These tubes have enhancement on the steam and the water sides. The Ti-A, C/N-11, and SS-16 tubes described in Table 4.1 and 4.2 were tested using the method described in APPENDIX A. The tests were conducted at a saturation temperature of 41.7 C (107 F). Either two or three of the 18 in (405 mm) tube lengths in the test cell were connected in series using U-bends to form the length tested. Three 18 in lengths were used for the C/N-11 and 16-SS tubes, and two 18 in lengths were used for the TiA-11

tube. As shown in Table 4.2, the O.D. of the C/N-11 tube is 22.2 mm, and the TiA-11 and SS-16 tubes are approximately 18.4 mm. The data were taken for 42 C steam saturation temperature with water velocities between 1.0 and 3.0 m/s. The measured UA/L values of all three tubes are shown on Figure 5.21. Figure 5.21 also shows the UA/L value for plain 22.2 diameter, 0.90 mm wall copper/nickel, and 18.4 mm diameter, 0.46 mm wall titanium tubes. The plain tube condensation coefficient was predicted using the Nusselt equation (Equation 5.1) and the Petukhov equation for turbulent flow in smooth tubes. The Petukhov equation is

$$St = \frac{f/2}{1.07 + 12.7\sqrt{f/2}\,(Pr^{2/3} - 1)} \tag{5.3}$$

where

$$f = \left(1.58 \ln (Re) - 3.28\right)^{-2} \tag{5.4}$$

Using Equation (A.6) in Appendix A, the water side and tube wall resistances were subtracted from the total resistance (1/UA) to derive the condensing coefficient for the Ti-A and C/N-11 tubes. These derived condensing coefficients were compared with the condensing coefficients obtained by measurement of the tube wall temperature. These tests were described in Section 5.1 and the data are shown on Figures 5.3 and 5.6. The back-calculated and the directly measured condensing coefficients agreed within ±5%.

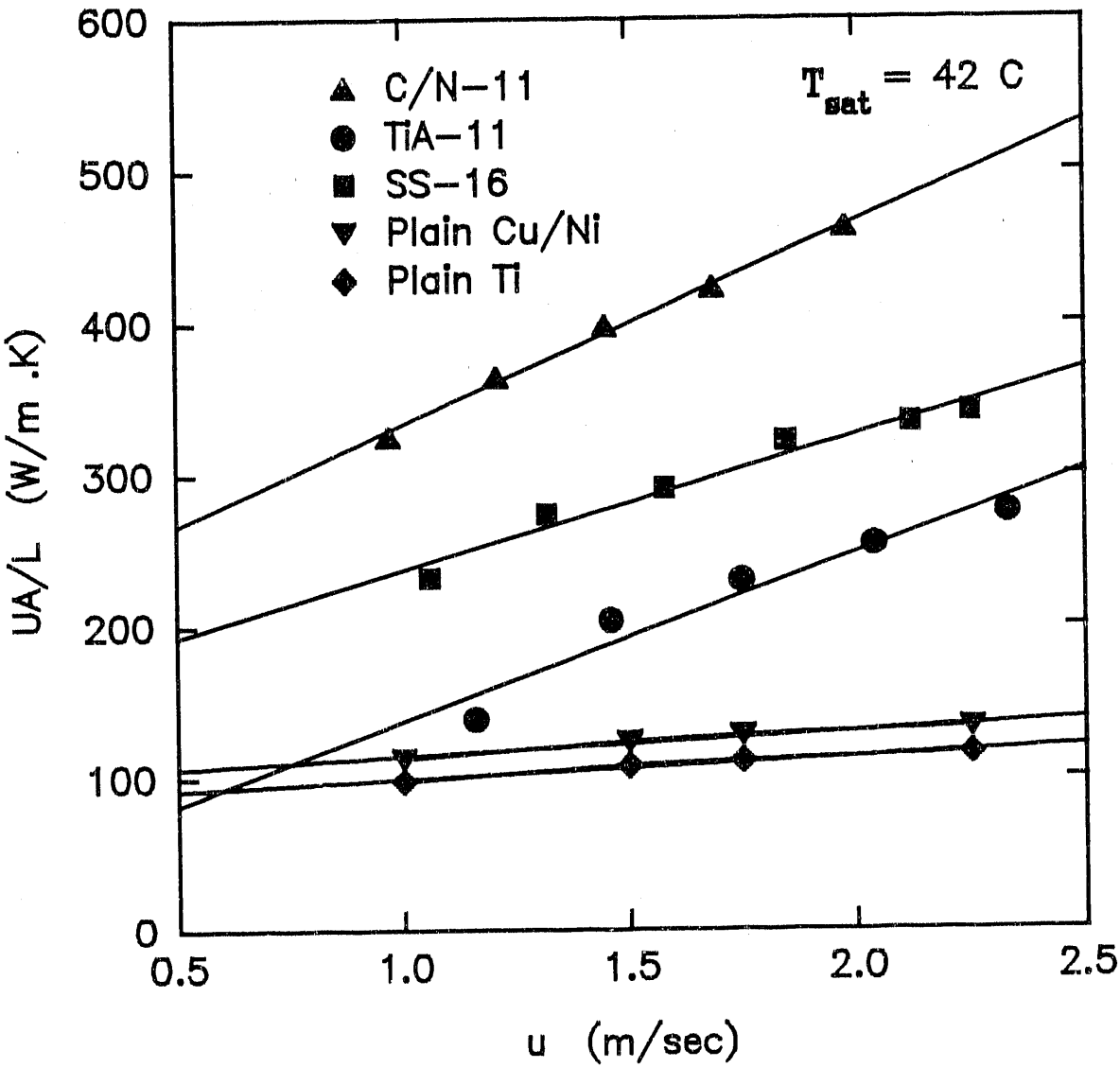

Figure 5.21 UA/L data for the candidate enhanced tubes

6 PERFORMANCE COMPARISON OF CANDIDATE CONDENSER TUBES

6.1 Candidate Tube Geometries

The enhanced tube geometries selected as candidates for installation in electric utility steam condensers are listed in Table 6.1. These tubes selected offer the highest performance potential of those tested in the laboratory tests. The first two tubes are of copper/nickel, and the last three are of titanium (or stainless steel). Although tube 4 (SS-16) was made and tested as a stainless steel tube, we will refer to it as titanium material, since its performance should be the same in titanium or stainless steel materials since the tube thermal conductivities are approximately equal. Tube 4 will provide higher performance than Tube 3, which has very little side enhancement. Tube 3 is included, so that one may see the additional benefit provided by the higher water side enhancement of Tube 4.

Table 6.1
Candidate Tube Geometries

No.	Outside	Inside	Material	Figure
1	C/N-11	Wavy-1	Cu/Ni	4.1a
2	A/P-50	Korodense	Cu/Ni	None
3	TiA-11	Wavy-2	Ti	4.2a
4	SS-16	Wavy-3	Stn St1	4.2c
5	A/P-50	Korodense	Ti	None

6.2 UA Enhancement Levels

Table 6.2 compares the UA-values of the candidate tube geometries listed in Table 6.1. The comparison is shown in Table 6.2 and is for steam condensing with (T_{sat} - T_c) = 2.8 C on 22.23 mm O.D. tubes with 26 C water flowing inside at 2.0 m/sec (6.5 ft/sec). The condensing coefficient of the TiA-11 and SS-16 tubes were scaled up to a 22.23 mm tube diameter. Based on the theoretical model of Jaber (1991) increasing the tube diameter from 18.3 mm to 22.23 mm (with all other dimensions unchanged) will increase the enhancement level of an integral finned tube by approximately 10%. The primary reason for this is the reduction of the condensate flooding angle. The predictive model uses the analytical expression of Rudy and Webb (1985) for the calculation of the flooding angle. The column labeled E_o gives the steam side enhancement ratio, relative to a plain tube of the same outside diameter. The plain tube condensation coefficient was calculated using the Nusselt equation (Equation 5.1). The Column labeled E_i lists the water side enhancement, relative to a plain tube. The E_i value was calculated from the water side heat transfer coefficient correlations based on the Wilson plot data. Figure 5.8 shows the water-side j-factor (= $h/u\rho c_p$) vs. Re.

The last column of the table shows the ratio of the enhanced-to-plain tube UA value. The plain tube UA value was calculated using the Nusselt and the Petukhov equations for the steam and water side coefficients, respectively. The UA-values of AP-50/Korodense tubes (#2 and #5) are based on the measured condensation coefficient (h_o) shown on Figure 5.5, and the Wolverine correlation for Korodense water side coefficient (h_i). The UA-value is calculated using the equation

$$\frac{1}{UA} = \frac{1}{h_o A_o} + \frac{t_w}{k_m A_w} + \frac{1}{h_i A_i} \qquad (5.5)$$

The tube inside diameters (D_i) and wall thickness (t_w) values are shown in Table 6.2. The inside diameters differ, because of the different fin heights and tube wall thicknesses. The calculated steam side (E_o) and water side enhancements (E_i) are shown in Table 6.2.

Table 6.2 shows that the greatest UA enhancement occurs for the copper-nickel tubes. The C/N-11, C/N-19, and A/P-50 tubes give UA enhancement ratios of 1.80, 1.61, and 1.68, respectively. The UA value of the C/N-19 tube is lower than that of C/N-11 primarily because it has a smaller water side heat transfer coefficient. It is not possible to make a wavy inside enhancement for the C/N-19 that will have the same E_i as the wavy inside enhancement used in the C/N-11 tube. This is because the C/N-19 tube has a smaller wave pitch and a lower external fin height than those of the C/N-11 tube.

The SS-16 tube gives a UA enhancement ratio of 1.49, which is substantially higher than the 1.21 value for the TiA-11 tube. The primary reason for the lower UA enhancement ratio of the TiA-11 tube is its lower water side heat transfer coefficient. The greatest UA enhancement ratio of the titanium tubes would occur for tube 5 (A/P-50/Koroden-se). This tube provides approximately the same water side enhancement as the SS-16, but it has a greater condensation coefficient.

Table 6.2

Overall Heat Transfer Coefficient for 2.3 m/s Water Velocity

(D_o = 22.23 mm, ΔT = 2.8 C, T_c = 26 C, R_f = 0.0)

No.	Tube		Material	D_i mm	t_w mm	E_o	E_i	$UA)_e/UA)_p$
	Outside	Inside						
1	C/N-11	Wavy-1	cu/ni	18.18	0.90	1.75	1.54	1.51
2	C/N-19	3D-SS	cu/ni	19.52	0.90	1.64	1.61	1.61
3	A/P-50	Korodense	cu/ni	20.50	0.90	1.70	1.62	1.65
4	TiA-11	Wavy-2	Ti	20.07	0.65	1.34	1.05	1.17
5	SS-16	Wavy-3	Stn Stl	20.40	0.60	1.60	1.48	1.46
6	A/P-50	Korodense	Ti	20.03	0.60	1.70	1.62	1.55

6.3 Simulated Plant Performance

Two condensers in actual power plants, one fossil and the other nuclear are considered in this simulation study. The detailed design and operating conditions are given by Webb et al. (1984). The Webb et al. (1984) paper also gives details on the turbine back pressure curves and the circulating water pump curves. The analysis was performed for two different scenarios:

1. A tube-for-tube replacement. Thus, each plain tube is replaced by an enhanced tube of equal outside diameter. This typically involves reduced condenser water flow rate.
2. A new condenser. In this case, the total length of tubing in the condenser is the same as the plain tube design. But, tube length and the number of tubes may be different from the plain tube design. This approach allows the enhanced tube condenser to operate at the same cooling water flow rate as the plain tube condenser.

The tube wall thickness values are 0.035 inch (0.9 mm) for cu/ni tubes, and 0.018 inch (0.46 mm) for titanium or stainless steel tubes. The calculations are based on constant outside diameter (plain tube diameter is equal to the diameter over the fins) and constant pumping power.

The water velocity is determined from the balance point on the pump and system curve, which accounts for the friction factor of each enhanced tube. The system resistance is the sum of the pressure drop in the condenser tube, and the flow losses external to the condenser tubes. Since the enhanced tubes have a higher pressure drop than the plain tube, the water velocity in the enhanced tubes is reduced. For a new condenser, the total water flow rate is maintained constant by using a greater number of tubes, which are shorter in length than the plain tube design. Details of this calculation are given by Webb et al. (1984).

The present experimental results are used for the condensing coefficient, with the exception of the Korodense tube, which was obtained from Wolverine. This condensation coefficient was multiplied by a 0.80 bundle factor. The water side heat transfer coefficient was calculated (at the balance point water velocity) using correlations obtained from the Wilson plot analysis of experimental data. A typical value for the fouling factor (R_f = 0.00025 hr-ft^2-F/Btu) was also incorporated in the calculations. The overall heat transfer coefficient was then calculated using the steam and water side heat transfer coefficients, and the fouling resistance.

The experimental condensation enhancement level of the 18.3 mm diameter TIA-11 and the SS-16 tubes were scaled up to 22.23 mm tube diameter. Based on a theoretical computer model developed by Jaber (1991), it was determined that increasing the tube diameter from 18.29 mm to 22.23 mm (with all other dimensions unchanged) will increase the steam side enhancement level of an integral finned tube by approximately 5 to 10%. The primary reason for this increase is the reduction in the condensate flooding angle and hence an increase in the active (unflooded) region. The predictive model uses the analytical expression of Rudy and Webb (1981) for the calculation of the flooding angle. Hence, the enhancement level for the TIA-11 and the SS-16 tubes increase from 1.22 and 1.34 (18.29 mm diameter) to 1.34 and 1.45 (for a 22.23 mm tube), respectively. The values for the 28.58 mm O.D. (1.125") tube were obtained in a similar fashion. The last two columns of Tables 6.3 and 6.4 show the steam condensation temperature for the month of July. Notes 1 and 2 at the bottom of Tables 6.3 and 6.4 refer to re-tubed and new condensers, respectively.

Tables 6.3 and 6.4 show the simulation results for the fossil and nuclear plants, respectively. The tables include a plain tube, which presently exists in the plants, and a standard Korodense tube. The inside diameter in Tables 6.3 and 6.4 are in inches. The fossil plant of Table 6.3 presently contains plain copper/nickel tubes. Table 6.3 shows the predicted results for both copper/nickel and titanium tubes. Table 6.4 is a nuclear plant, and only titanium tubes were considered for the tube replacement.

For re-tubing with copper/nickel tubes, Table 6.3 shows that the Korodense tube gives the lowest condensing temperature (89.54 F), as compared to 93.25 F for the plain/plain tube. The T_{sat} in a new condenser with Korodense tubes is 88.43 F. The performance improvement provided by the Korodense tube is better than the other geometries for a re-tubed condenser. This is because of the reduction in the water flow rates, primarily caused by the smaller tube inside diameter. The Korodense tube reduces the water flow rate 11%, whereas Geometry 2 reduces the flow rate 15%, and Geometry 1 reduces the water flow rate by 20%. For a new condenser with cu/ni tubes, tube 2 gives 0.13 F lower T_{sat} than the Korodense tube. Table 6.3 also contains titanium and stainless steel tubes. Both materials provide the same thermal performance. A lower condensing temperature (87.0 F) is provided by Tube 4. This is primarily because the titanium and stainless tubes have a thinner wall thickness (0.45 mm) as compared to the 0.89 mm for the cu/ni tubes. The thinner wall provides a greater cross sectional flow area, so the tube will have a higher water flow rate.

For a titanium tube in the Table 6.3 fossil plant, the best performance was given by Geometry 4, which gives 87.00 F condensing temperature (re-tubed) and 86.20 F (new design) as compared to the 93.25 F value for the plain cu/ni tube, or 89.4 F for the Korodense tube. Note that the titanium Korodense tube provides higher water flow rate than given by a copper/nickel Korodense tube. Because the titanium tube has a thinner wall, it has a greater cross sectional flow area.

Only titanium tubes are compared in Table 6.4 for the nuclear plant. The best performance is given by Geometry 4. Geometry 5 gives marginally higher performance than the standard Korodense tube. Geometry 5 gives 0.20 F lower T_{sat} in a new condenser, as compared to a re-tubed condenser. Here, the enhanced tube operates with the same water flow rate as the reference plain tube design. Use of Geometry 5 in a new condenser drops the condensing temperature from 74.00 F to 67.8 F.

Table 6.3

SIMULATED FOSSIL PLANT CONDENSER PERFORMANCE

[7/8" O.D. tubes, R_f = 0.00025 hr-ft^2-F/Btu, 0.80 Bundle Factor]

No	Outside	Inside	Material	D_i (in)	m_w/m_{wp} Note 1	h_i/h_{ip}	h_o/h_{op}	U_o/U_{op}	R_o/R_{tot}	T_{sat} (F) Note 1	T_{sat} (F) Note 2
	Plain	Plain	Cu/Ni	0.805	1.00	1.00	1.00	1.00	0.43	93.25	93.25
	Korodense	Korodense	Cu/Ni	0.805	0.89	1.48	1.37	1.44	0.35	89.54	88.43
1	C/N-11	Wavy-1	Cu/Ni	0.717	0.80	1.54	1.75	1.34	0.30	90.00	89.20
2	A/P-50	Korodense	Cu/Ni	0.765	0.85	1.55	1.70	1.46	0.28	90.03	88.30
	Korodense	Korodense	Ti	0.839	0.93	1.41	1.37	1.40	0.34	89.40	88.70
3	TiA-11	Wavy-2	Ti	0.805	0.93	1.05	1.34	1.14	0.30	91.70	91.00
4	SS-16	Wavy-3	Stn St	0.827	0.96	1.57	1.60	1.53	0.36	87.00	86.20
5	A/P-50	Korodense	Ti	0.839	0.93	1.41	1.70	1.51	0.29	88.68	87.70

Note 1: Tube-for-tube replacement

Note 2: New condenser (m_w/m_{wp} = 1)

Table 6.4

SIMULATED NUCLEAR PLANT CONDENSER PERFORMANCE

[1.125" O.D. Titanium tubes, R_f = 0.00025 hr-ft^2-F/Btu, 0.80 Bundle Factor]

No	Outside	Inside	D_i (in)	m_w/m_{wp} Note 1	h_i/h_{ip}	h_o/h_{op}	U_o/U_{op}	R_o/R_{tot}	T_{sat} (F) Note 1	T_{sat} (F) Note 2
	Plain	Plain	1.089	1.00	1.00	1.00	1.00	0.44	74.00	74.00
	Korodense	Korodense	1.089	0.89	1.52	1.37	1.32	0.40	69.22	69.00
3	TiA-11	Wavy-2	1.055	0.88	1.05	1.44	1.16	0.33	72.06	71.10
4	SS-16	Wavy-3	1.077	0.90	1.40	1.55	1.34	0.36	68.20	68.00
5	A/P-50	Korodense	1.089	0.89	1.52	1.70	1.44	0.34	68.03	67.80

Note 1: Tube-for-tube replacement

Note 2: New condenser (m_w/m_{wp} = 1)

6.4 Long Term Fouling Performance

The fouling tests done at Penn State were accelerated tests using very dirty water. The purpose of these tests was to compare the relative fouling rates of the enhanced and plain tubes and to establish if sponge balls will clean the enhanced tubes. The Penn State tests cannot be used to predict the long term fouling rates under actual field conditions.

Rabas et al. (1991) assessed the long term fouling rates of twelve TVA steam condensers, some of which were retubed with Korodense tubes. The condensers involved are the Gallatin and Shawnee plants. Table 6.5 compares the fouling resistance of plain and Korodense tubes at the three plant locations ten months after cleaning.

Table 6.5
Fouling Resistance of TVA Condensers 10 Months After Cleaning ($hr\text{-}ft^2\text{-}F/Btu$)

Location	Plain	Korodense
Gallatin	0.00035	0.00048
Shawnee	0.0001-0.0002	0.0003-0.0005

No cleaning was performed during the ten month fouling period. Although Table 6.5 shows that the Korodense tube had a higher fouling rate than the plain tube, large fouling resistances were not attained. The thermal performance of the Korodense tubes remained superior to that of the plain tubes for more than a year without cleaning. In addition, the thermal performance of both the enhanced and plain tubes was restored to the new, clean levels after mechanical brush cleaning. As previously noted, Renfftlen

(1991) reports that enhanced tubes can be successfully cleaned using the sponge ball cleaning system.

7 FUTURE WORK

7.1 Field Test Program

This involves installing 20-50 tubes in an actual electric utility condenser. The tubes should be instrumented to measure the water flow rate, their individual UA-values, and the fouling resistance. A field test program that has been conducted in Japan is described by Nosetani et al. (1989); this study describes how the tubes may be instrumented to obtain the needed test data. It is recommended that the field test condenser contain an on-line sponge ball cleaning system.

The test program will provide data to:

a. Verify that high UA values will be obtained at a variety of tube locations in the condenser tube bundle.
b. Verify that the water side fouling resistance can be maintained at a low value.
c. Obtain long term erosion and corrosion data. This will be verified by removing tubes after different time periods.

Successful commercial implementation of this technology will have a major impact on national energy consumption.

7.2 Stages of Commercial Implementation

This technology is expected to enter the commercial sector in the following three steps:

1. **Retrofit for Existing Condensers**: This involves a "tube for tube" replacement using the existing condenser water pump. Because the tube inside diameter is smaller than that of the replaced plain tube, the water flow rate will be reduced approximately 7 %. If economic-

ally justified, the water pump impeller could be replaced, so that no flow rate reduction would occur.

2. **Retubing and Rebundling of Condenser**: This allows for more than just tube replacement. The entire condenser tube bundle would be replaced, including the tube sheets. This would allow use of a larger tube diameter, so that there would be no reduction of water flow rate.
3. **New Plant Design**: This would involve complete redesign of the condenser, and selection of the condenser water pump, so that the enhanced tubes would operate at the optimum water flow rate. The low pressure stage of the turbine should be designed to allow it to expand to the lower condensing pressure possible with the enhanced tubes.

7.3 Further Improvements in Enhanced Tube Technology

Although electric utility condensers use both copper/nickel and titanium tubes, it appears that copper/nickel is being phased out, and that titanium (or corrosion resistant stainless steel) is the future material of choice. Additional work needs to be done to obtain maximum enhancement potential for titanium. The 16 fins/in titanium tubes (geometry 4) provides a 45% increase of the UA-value for 6 ft/sec water side velocity. This is significantly better than the TiA-11 tube (geometry 3), which provides only 5% water side enhancement.

The "attached particle" tube concept (geometry 5) appears to offer higher potential, than the integral fin geometries (No. 3 and 4) because higher steam and water side enhancements are believed possible than were obtained with the TiA-11 tube. The test results on the attached particle tube were obtained for copper particles on a copper/nickel tube. We believe that an attached particle tube having aluminum particles on a titanium tube should give comparable performance. The manufacturing

process technology to apply aluminum particles to a titanium tube is yet to be developed. We propose to work with UOP Corp. to develop the concept with aluminum particles on a titanium tube. We must also show that the particles will not come off the tube over a long time period.

8 CONCLUSIONS

1. Significant internal and external enhancements can be achieved for both copper/nickel and titanium (or stainless steel) tubes. The attached particle/Korodense tube increases the overall heat transfer coefficient by as much 65% for cu/ni, and 55% for titanium materials, respectively. The external integral fin geometries provide slightly less enhancement.
2. The selected internal geometries can be effectively cleaned with ball or brush cleaning systems.
3. Based on the above two points, it is necessary to conduct a field test by installing several instrumented tubes in an actual condenser.
4. The recommended copper/nickel tubes for the field test are as follows:
   a. Wieland NW tube 433 fpm (11 fpi), 1.0 or 0.6 mm fin height on the outside and 0.25 mm wave height on the inside.
   b. Combined Korodense/attached particle tube with 0.43 mm copper particles sintered over 50% of the area of a copper/nickel tube.
5. The recommended titanium or stainless steel tubes for the field test are as follows:
   a. Combined Korodense/attached particle tube as per the above specification but with aluminum (or copper) particles sintered over the stainless steel (or titanium) tube.
   b. Wieland NW tube with 633 fpm (16 fpi), 0.43 mm fin height on the outside and 0.16 mm wave height on the inside.
6. The full potential of enhanced tubes can be realized in a new condenser and turbine design. A tube-for-tube replacement results in reduced water flow rate, which diminishes the performance potential.

9 REFERENCES

Adamek, T., 1981, "Bestimmung der Kondensation-grossen auf feingewellten oberflachen zur Auslegun aptimaler Wanprofile," Wärme-und-Stoffuberstrangung, Vol. 15, pp. 255-270.

Adamek, T.A. and Webb, R. L., 1990, " Prediction of Film Condensation on Horizontal Integral Fin Tubes, Int'l. Journal of Heat and Mass Transfer, pp. 1737-1749.

Boyd, L. W., Hammon, J. C., Littrel, J. J., Withers, J. G., 1983, "Efficiency Improvement at Gallatin Unit 1 with Corrugated Condenser Tubing," ASME, 83-JPGC-PWR-4.

El-shobokshy, M.S. and Ismail, I.A., 1980. "Deposition of Aerosol Particles from Turbulent Flow onto Rough Pipe Wall," Atmospheric Environment, Vol. 14, pp. 297-304.

Gregorig, R., 1954, "Film Condensation on Finely Rippled Surfaces with Consideration of Surface Tension," Z. Angew. Math. Phys., Vol. 5, pp. 36-49.

Gudmundsson, J.S., 1981, "Particulate Fouling," in Fouling of Heat Transfer Equipment, edited by E.F.C. Somerscales and J.G. Knudsen, pp. 357-387.

Jaber, M. Hassib, "A Theoretical and Experimental Study of Steam Condensation on Horizontal Enhanced Tubes," PhD. Thesis, Pennsylvania State University, August, 1991.

Karkhu, V. A. and Borovkov, V.P., 1971, "Film Condensation of Vapor at Finely Finned Horizontal Tubes," Heat Transfer-Soviet Research,, Vol. 3, No. 2, pp. 183-191.

Keysselitz, J., 1984, "Can Waterside Condenser Fouling be Controlled Operationally?," in Fouling in Heat Exchange Equipment, ed., J. W. Suitor and A. M. Pritchard, ASME Symp. Vol. HTD-Vol. 35, pp. 105-111.

Kedzierski, M. A., and Webb, R.L., 1987, "Experimental Measurements of Condensation on Plates with Enhanced Fins," ASME HTD-Vol. 85, pp. 87-95.

Kern, D.Q. and Seaton, R.E., 1959. "A Theoretical Analysis of Thermal Surface Fouling." Brit. Chem. Eng., Vol. 14, No. 3, pp. 258-262.

Marto, P. J., Mitrou, E., Wanniarachchi, A. S., Rose, J. W., 1986, "Film Condensation of Steam on Horizontal Finned Tubes : Effect of Fin Shape," Proc. IJHT, Vol. 4, pp. 1695-1700.

Mills, A. F., Hubbard, G. L., James, R. K., Tan, C., 1975, "Experimental Study of Film Condensation on Horizontal Grooved Tubes," Desalination, Vol. 16, pp. 121-133.

Mitrou, E., 1986, "Film Condensation Heat Transfer on Horizontal Finned Tubes, " M. S. Thesis, Naval Postgraduate School, Monterey, California.

Nosetani, T. et al, 1989, "In-Situ Evaluation of Enhanced Heat Transfer Tubes for Surface Condenser (SC Tubes)," in Heat Transfer Equipment Fundamentals, Design, Applications, and Operating Problems, ASME Symp. Vol. HTD-Vol. 108, Ed. R.K. Shah, pp. 97-104.

Nusselt, W., 1916, "Die Oberflachen-kondensation des Wasserdampfes," Z. Ver. Deut. Ing., Vol. 60, pp. 541-569.

Panchal, C.B., 1989, "Experimental Investigation of Seawater Biofouling for Enhanced Surfaces," in Heat Transfer Equipment Fundamentals, Design, Applications, and Operating Problems, ASME Symp. Vol. HTD-Vol. 108, Ed. R.K. Shah, pp. 231-238.

Petukhov, B. S., 1970, "Heat Transfer and Friction in Turbulent Pipe Flow with Variable Physical Properties," Advances in Heat Transfer, eds. J.P. Hartnett and T.F. Irvine, Academic Press Inc., New York, pp. 504-564.

Rabas, T., Merring, R., Schaefer, R., Lopez-Gomez, R., Thors, P., 1990, "Heat-Rate Improvements Obtained With The Use Of Enhanced Tubes In Surface Condensers," presented at the EPRI Condenser Technology Conference, Boston, 1990.

Rabas, T.J., Panchal, C.B., Sasscer, D.S., Schaefer, R., 1991, "Comparison of Power-Plant Condenser Cooling-Water Fouling Rates for Spirally- In dented and Plain Tubes," Fouling and Enhancement Interactions, HTD-Vol. 164, pp. 29-37.

Renfftlen, R.G., 1991, "On-line Sponge Ball Cleaning of Enhanced Heat Transfer Tubes," in Fouling and Enhancement Interactions, ASME Symp. Vol. HTD-Vol. 164, Ed. T.J. Rabas and J.M. Chenoweth, pp. 55-60.

Rudy, T. M. and Webb, R. L., 1981, "Condensate Retention on Horizontal Integral-Fin Tubing," Advances in Heat Transfer, ASME HTD, Vol. 18, pp. 35-41.

Rudy, T.M. and Webb, R.L., 1985, "An Analytical Model to Predict Condensate Retention on Horizontal, Integral-Fin Tubes," Journal of Heat Transfer, Vol. 107, pp. 361-368.

Shekriladze, I. G. and Rusishvili, D. G., 1980, "Heat Transfer in Condensation on Capillary Surfaces," Heat Transfer-Soviet Research, Vol. 12, No. 4, pp. 48-49.

Shklover, G. G., Mil'man, O. O., Baskov, V. S., Ankudinov, G. A., 1981, " Heat Transfer in Condensation of Steam on Finely Finned Horizontal Tubes," Heat Transfer-Soviet Research, Vol. 13, No. 2, pp. 108-114.

Somerscales, E.F.C., Ponteduro, A.F, Bergles, A.E., 1991, "Particulate Fouling of eat Transfer Tubes Enhanced on Their Inner Surface," Fouling and Enhancement Interactions, HTD-Vol. 164, pp. 17-28.

Wanniarachchi, A. S., Marto, P. J., Rose, J. W., 1984, "Filmwise Condensation of Steam on Externally Finned Horizontal Tubes," Fundamentals of Phase Change: Boiling and Condensation, ASME HTD, eds. C.T. Avedisian and T.M. Rudy, Vol. 38, pp. 133-141.

Wanniarachchi, A. S., Marto, P. J., Rose, J. W., 1985, "Film Condensation of Steam on Horizontal Finned Tubes: Effect of Fin Spacing, Thickness, and Height," Multiphase Flow and Heat Transfer, ASME HTD, eds. V.K. Dhir, J.C. Chen, and O.C. Jones, Vol. 47, pp. 93-99.

Wanniarachchi, A. S., Marto, P. J., Rose, J. W., 1986, "Film Condensation of Steam on Horizontal Finned Tubes: Effect of Fin Spacing," J. of Heat Transfer, Vol. 108, pp. 960-966.

Webb, R. L., Haman, L. L., Hui, T. S., 1984. "Enhanced Tubes in Electric Utility Steam Condensers," Heat Transfer in Heat Rejection Systems, ASME-HTD, Vol. 37, eds. S. Sengupta and Y. S. Mussalli, pp. 17-25.

Webb, R.L., 1988, "Enhancement of Film Condensation," International Communications in Heat and Mass Transfer, Volume 15, No. 4, pp. 475-508.

Webb, R.L. and Kim, N-H., 1989. "Particulate Fouling in Enhanced Tubes, 1989. " Heat Transfer Equipment Fundamentals, Design, Applications, and Operating Problems, ed., R. K. Shah, ASME HTD-VOL.108, pp. 315-324, ASME HTD-VOL.108, pp. 315-324.

Webb, R. L., Jaber, M. H., Chamra, L. Kim, N. H., 1990, "Enhanced Tubes for Electric Utility Steam Condensers," presented at the EPRI Condenser Technology Conference, Boston, August 1990.

Webb, R. L. and Kedzierski, M. A., 1990, "Practical Fin Shapes for Surface Tension Drained Condensation," Journal of Heat Transfer, Vol. 112, pp. 479-485.

Webb, R. L. and Murawski, C. G., 1990, "Row Effect for R-11 Condensation on Enhanced Tubes," Trans. of the ASME, Vol. 112, pp. 768-776.

Webb, R. L. and Chamra, L., 1991, "On-Line Cleaning of Particulate Fouling in Enhanced Tubes", Fouling and Enhancement Interactions, HTD-Vol. 164, pp. 47-54.

Withers, J.G. and Young, E.H., 1971, "Steam Condensing on Vertical Rows of Horizontal Corrugated and Plain Tubes," I&EC Process Design & Development, Vol. 10, Jan. 1971, p. 19.

Yau, K. K., Cooper, J. R., and Rose, J. W., 1984, "Effects of Drainage Strips and Fin Spacing on Heat Transfer and Condensate Retention for Horizontal Finned and Plain Condenser Tubes," Fundamentals of Phase Change : Boiling and Condensation, ASME HTD, eds. C.T. Avedisian and T.M. Rudy, Vol. 38, pp. 151-156.

Yau, K. K., Cooper, J. R., Rose, J. W., 1985, "Effect of Fin Spacing on the Performance of Horizontal Integral Fin Condenser Tubes," J. of Heat Transfer, Vol. 102, pp. 20-25.

Yau, K. K., Cooper, J. R., Rose, J. W., 1986, "Horizontal Plain and Low-Finned Condenser Tubes-Effect of Fin Spacing and Drainage Strips on Heat Transfer and Condensate Retention," J. of Heat Transfer, Vol. 108, pp. 946-950.

APPENDIX A

THE STEAM CONDENSATION APPARATUS

Steam Side Condensation Coefficient

The apparatus was designed to measure steam condensation on single horizontal tubes, and on a bank of five horizontal tubes. The apparatus will operate at pressures from 0.1-to-1 atm. The following is a description of the apparatus, the instrumentation, and the tube geometries tested.

The major components of the apparatus (Figure A.1) were the test cell, the boiler, the post-condenser, the vacuum system, the cooling water supply system, the data collection system, and the tubes being tested. The test cell was a welded rectangular box constructed from 12.7 mm thick steel plate, with inside dimensions of 457 mm high, 64 mm wide, and 457 mm deep. On the back of the test cell were nine threaded holes, which contain thermocouple vacuum glands. There was a 374 mm high by 76 mm wide glass observation port at the front to aid in mounting the test tubes and, for visual examination of the condensation process. The ends of the cell were sealed with 16 mm thick steel tube sheets fitted a bolted O-ring seal. Five 26.7 mm diameter holes, spaced at 48.3 mm center-to-center were located on the vertical center line of the tube sheets to position and hold the test tubes. A condensate distribution tube is located above the first tube row for row-effect studies. The test tubes were soldered to stainless steel tube ends (26.5 mm diameter, 76.2 mm long), which passed through the cell end walls (the tube sheets). The tube ends were sealed by two O-rings, where they pass through the tube sheet. The tube ends were connected to the water supply and drain lines. A sealed, copper cylinder was placed inside the test tubes to provide turbulent flow in the 3.81 mm wide annulus spacing.

The upstream side of the test cell was connected to the boiler by an insulated 76.2 mm I.D. steam line. The steam boiler was made of a vertical 254 mm X 2000 mm long carbon steel pipe sealed with plates at top and bottom. The bottom plate was fitted with three electric bayonet heater modules, each with three 2.5 KW elements resulting in a maximum available power of 22.5 KW. Fittings exist on the top plate for a pressure tap, thermocouple, and low water cut-offs.

A tee at the bottom (exit) of the test cell provides a connection for the post condenser. A calibrated condensate collection tube was below the test cell exit. The post condenser was a shell-and-tube heat exchanger containing 10 meter (total length) of 1025 fpm integral finned tubes in six water side passes. Any air leakage into the test cell was withdrawn from the cold end of the post condenser by a vacuum tap. The vacuum system (see Figure A.1) was used to set and maintain the desired condensation

pressure. The system included a vacuum pump, control valve, a desiccant, and a cold trap to remove water vapor before the pump.

Cooling water was supplied at the desired temperature to the tubes and to the post condenser by blending city water and reservoir water supplies.

Measurement of the UA-Value

The cooling water circuit, shown in Figure A.1, was slightly modified to perform measurements of the UA value for a set of selected tubes. Either two or three tubes were connected in series by using U-bends to obtain a total length of either 0.91 m or 1.37 m. The U-bends were made of PVC piping and rubber hoses wrapped with a 50 mm layer of insulation. The inlet and outlet cooling water temperatures were measured, together with the flow rate, to determine the cooling water heat load. The LMTD was calculated and the UA value was determined as described in the following Data Reduction section.

Instrumentation

Three copper/constantan thermocouples (0.127 mm wire diameter) were affixed to each tube by attaching the thermocouple beads in small grooves milled in the outer wall of the tube, at the fin root. The thermocouples were soldered (copper alloy tubes) or epoxyed (titanium tubes) into the milled grooves. The thermocouples were positioned near the center of the tubes, at the 0 (top), 90 (side), and 180 (bottom) degree positions. The vapor temperatures in the test cell, boiler and post-condenser were measured with thermocouples made from the same wire roll as the tube thermocouples. There was a vapor thermocouple in the test cell near the top, middle and bottom tube positions.

Thermistors were used to measure the inlet and outlet water temperatures for each tube. Thermocouples measured the inlet and outlet temperature of the post condenser. All the thermocouples were read with a Fluke 2285B data logger, and the thermistors were read with an Omega thermistor thermometer. The water flow rates were measured with calibrated Dwyer rotameters.

Experimental Procedure

The tubes were cleaned prior to installation. Functionality of the apparatus was checked prior to each test session by verifying that the air infiltration rate was less than 0.015% of the total vapor/air mixture volume per hour, and that all the tube wall thermocouples agreed within ±0.05 C, and the thermistors agreed within ±0.03 C.

The establishment of test conditions for a particular data point included: Setting the test cell pressure to the test conditions; setting the boiler to the anticipated heating rate;

and, setting the tube and post condenser cooling water flow rates and inlet water temperatures so that at least sixty percent of the anticipated condensation would occur in the post condenser.

The condensation apparatus was then allowed to reach a steady state condition defined by vapor pressure fluctuations of less than ±0.5 mm Hg, individual tube wall temperature fluctuations of less than ±5 microvolts (0.1 C), and inlet cooling water temperature fluctuations of less than ±0.05 C. When these conditions were met, the following data were collected for each data point: 1) individual vapor pressures in the boiler, test cell, and post condenser, 2) tube and post condenser water flow rates, 3) tube and post condenser inlet and exit water temperatures, 4) input electrical power to the boiler, 5) the condensate flow rate and 6) tube wall and vapor thermocouple readings. All of the thermocouples were read three times at intervals of one minute for each data point.

Data Reduction

The condensation coefficient (h) was determined from the experimental data with the following data reduction. The heat transfer rate (Q) was determined from the cooling water flow rate and temperature rise (ΔT_c).

$$Q = m_w c_p \Delta T_c \tag{A.1}$$

The NBS copper-constantan tables were used to convert the average of the three successive thermocouple readings for the top, side, and bottom tube wall thermocouples to the corresponding temperatures, T_1, T_2, and T_3 respectively. These temperatures were then used to determine the average tube wall temperature ($T_{w,av}$).

$$T_{w,av} = (T_1 + 2T_2 + T_3)/4 \tag{A.2}$$

The steam condensation temperature was taken as the saturation temperature (T_{sat}) corresponding to the measured pressure in the test cell. The heat transfer coefficient was based on the envelope area over the fins $A = (\pi D_o L)$. The heat transfer coefficient was then calculated by

$$h = Q/[A(T_{sat} - T_{w,av})] \tag{A.3}$$

Data were taken for a range of heat fluxes, accomplished by varying the cooling water flow rate. These h values were then fitted to the power law equation:

$$h = C\,(T_{sat} - T_{w,av})^n \tag{A.4}$$

where C and n are constants determined from the best fit straight line drawn through a plot of h versus $(T_{sat} - T_{w,av})$ on a log-log graph.

The data for the overall heat transfer coefficient were reduced using the following expression:

$$UA = Q/LMTD \tag{A.5}$$

where

$$1/UA = 1/(hA)_o + R_w + 1/(hA)_i \tag{A.6}$$

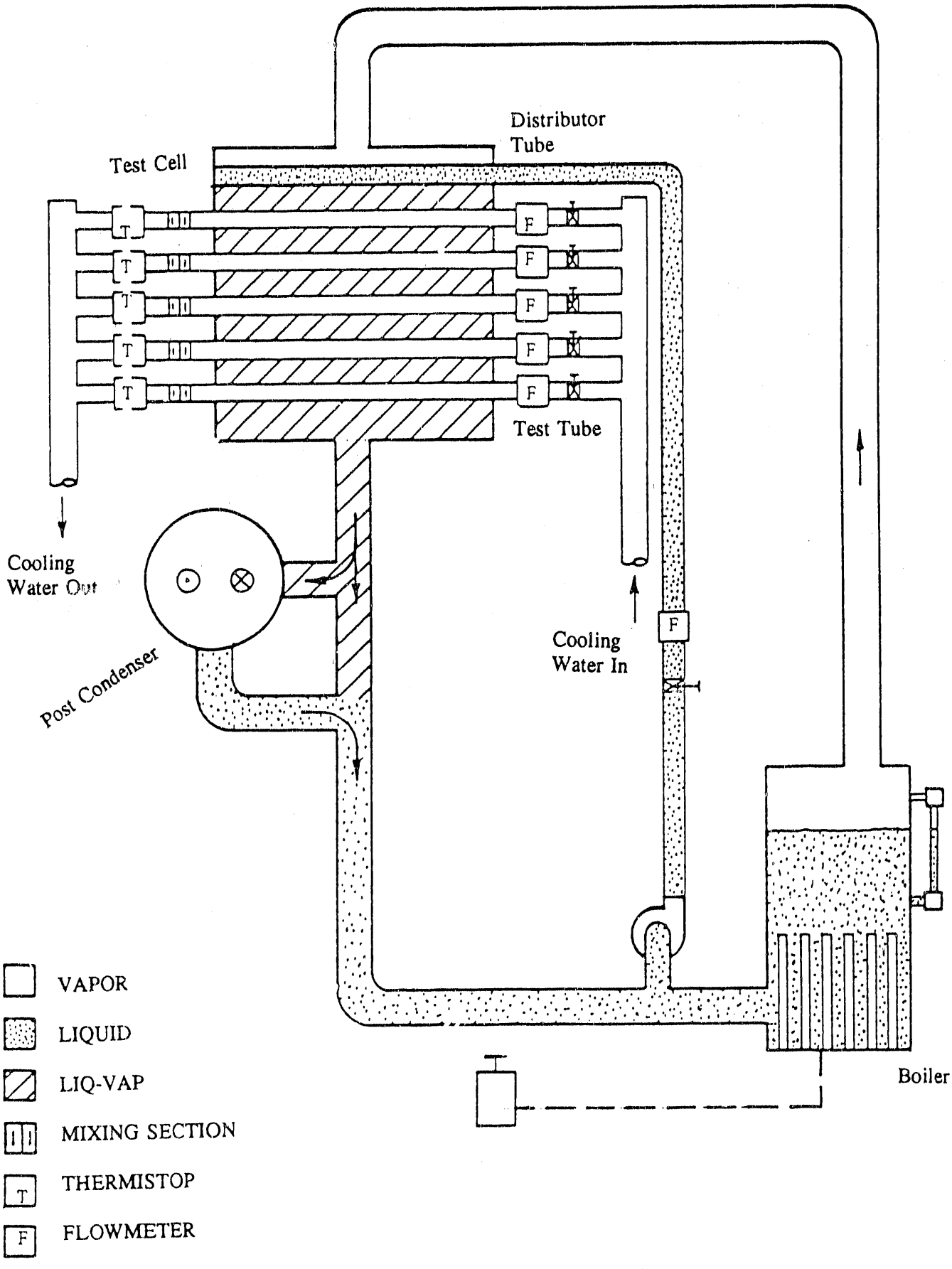

Figure A.1. Schematic of the condensing test cell.

APPENDIX B

THE FOULING APPARATUS

Description of Fouling Apparatus

Figure B.1 is a schematic drawing of the apparatus. The apparatus is capable of testing four 19 mm O.D. (or three 22 mm O.D.) tubes simultaneously. The instrumentation includes an on-line data acquisition system driven by a personal computer, which is used to measure thermistor and pressure transducer outputs. The apparatus was designed to operate and record data 24 hour/day unattended, with heat input to the test section. Heat is transferred to the 3.05 m long test sections by condensing R-114 on the annulus side of the test section. Condensed R-114 is returned to electric heated boilers. Each test section has its own boiler, in which R-114 is heated by three electric band heaters (each of 1200 W capacity). Power to the band heaters is controlled by individual auto-transformers. The heat is removed from the test water in a plate heat exchanger. The tube wall temperatures are measured using thermocouples. They are mounted in pairs (top and bottom of the tube) at two axial locations (one at the center, and the other near the exit). The average wall temperature at each axial location was obtained by averaging the top and bottom wall temperatures.

The water and R-114 saturation temperatures were measured using thermistors, and the condensing pressures were measured with pressure transducers. The refrigerant condensing pressure is compared with the saturation temperature to verify the absence of non-condensibles. R-114 is used because the condenser operates above atmospheric pressure, so non-condensibles cannot enter the system during test operation, or during shut-down periods. The instrumentation capabilities provide a maximum resolution error of 5×10^{-6} m^2-K/W in measurement of the fouling resistance. This is the minimum ability of the instrumentation to sense the change in the fouling resistance.

Figure B.2 shows the detailed design of the fouling test section. It includes means to collect samples of the fouling deposit for physical inspection. This is accomplished using the "deposit sections" shown on Figure B.2. The deposit sections are 0.3 m long, and are installed just downstream from the test section. A more detailed description of the fouling apparatus is given by Webb and Kim (1989).

Test Operation

After each fouling test, once-through city water was run through the apparatus piping for approximately 24 hours to clean the test sections and the apparatus piping. Then, the test section was mechanically cleaned using a hand operated Nylon brush. Before brushing, a weak solution of detergent was added to the test section to aid deposit removal. After brushing, the apparatus was filled with clean city water. The apparatus was run for two hours with clean water to reach steady state. After it reached a steady

state, the amount of particulate required for the desired ppm concentration was added to the system. This was taken as time zero for the next fouling test series, which was approximately 45 hr. During a test, which started at 1500 ppm concentration, the foulant concentration decreased to approximately 1200 ppm. No foulant was added during the test period. This was done to prevent instabilities that could affect the fouling rate, or the retention of the foulant deposit. The flow velocity was nearly constant during the test period.

The sponge-ball cleaning method was initiated after the fouling resistance reached 5.3×10^{-5} m^2-K/W(3.0×10^{-4} hr-ft^2-F/Btu). Six sponge-balls were injected i ~ to each tube at one minute intervals. The sponge-balls were manually introduced using the technique illustrated in Figure 3.2. To prevent an increase in foulant concentration in the circulating water, the dirty water was drained and replaced with clean water. The proper amount of foulant was added to restore the system to the original foulant concentration. This cleaning method was applied to obtain the data of Figures 5.12 through 5.18.

The brush cleaning system was initiated after the fouling resistance reached the limiting value as used in the sponge-ball cleaning system. The brushes were passed six times (three one way and three back) in each tube. The apparatus was run for two hours after applying each cleaning method in order to reach steady state before taking heat transfer fouling data.

Data Reduction

The fouling resistance is calculated as follows: First, the overall heat transfer coefficient (U_c) based on inside surface area (A_i) is measured for the clean tube-side condition. The A_i is defined as $\pi D_i L$. It is intended that the data for U_f and U_c be taken at the same velocity, heat flux and water inlet temperature. Then, the overall heat transfer coefficient is measured for the fouled condition (U_f). The fouling resistance R_f is obtained by

$$R_f = \frac{1}{UA)_f} - \frac{1}{UA)_c} \qquad \text{(B.1)}$$

The overall heat transfer coefficient is obtained as follows:

1. Calculate the heat transfer rate to the test section, q using the water side energy balance equation,

$$q = m_w c_p (T_{f,out} - T_{f,in}) \tag{B.2}$$

2. Calculate the overall heat transfer coefficient, based on inside surface area,

$$UA = \frac{q}{LMTD} \tag{B.3}$$

where

$$LMTD = \frac{T_{f,out} - T_{f,in}}{\ln\left(\frac{T_{sat} - T_{f,in}}{T_{sat} - T_{f,out}}\right)} \tag{B.4}$$

During the test, the fluid velocity reduced a small amount. To account for the reduced water velocity, the clean tube U value (U_c) was adjusted. This adjustment was done as follows:

1. Measure the clean tube U value as a function of water velocity. These data are then curve fitted as a function of water velocity.
2. The U_c is calculated at the actual velocity in the fouled tube using the above described curve fit equation.

The asymptotic fouling resistance (R_f^*) and initial fouling rate (dR_f/dt_o) were calculated by curve-fitting the reduced fouling data into following form.

$$R_f = R_f^*(1-e^{-bt}) \tag{B.5}$$

$$\frac{dR_f}{dt_o} = bR_f^* \tag{B.6}$$

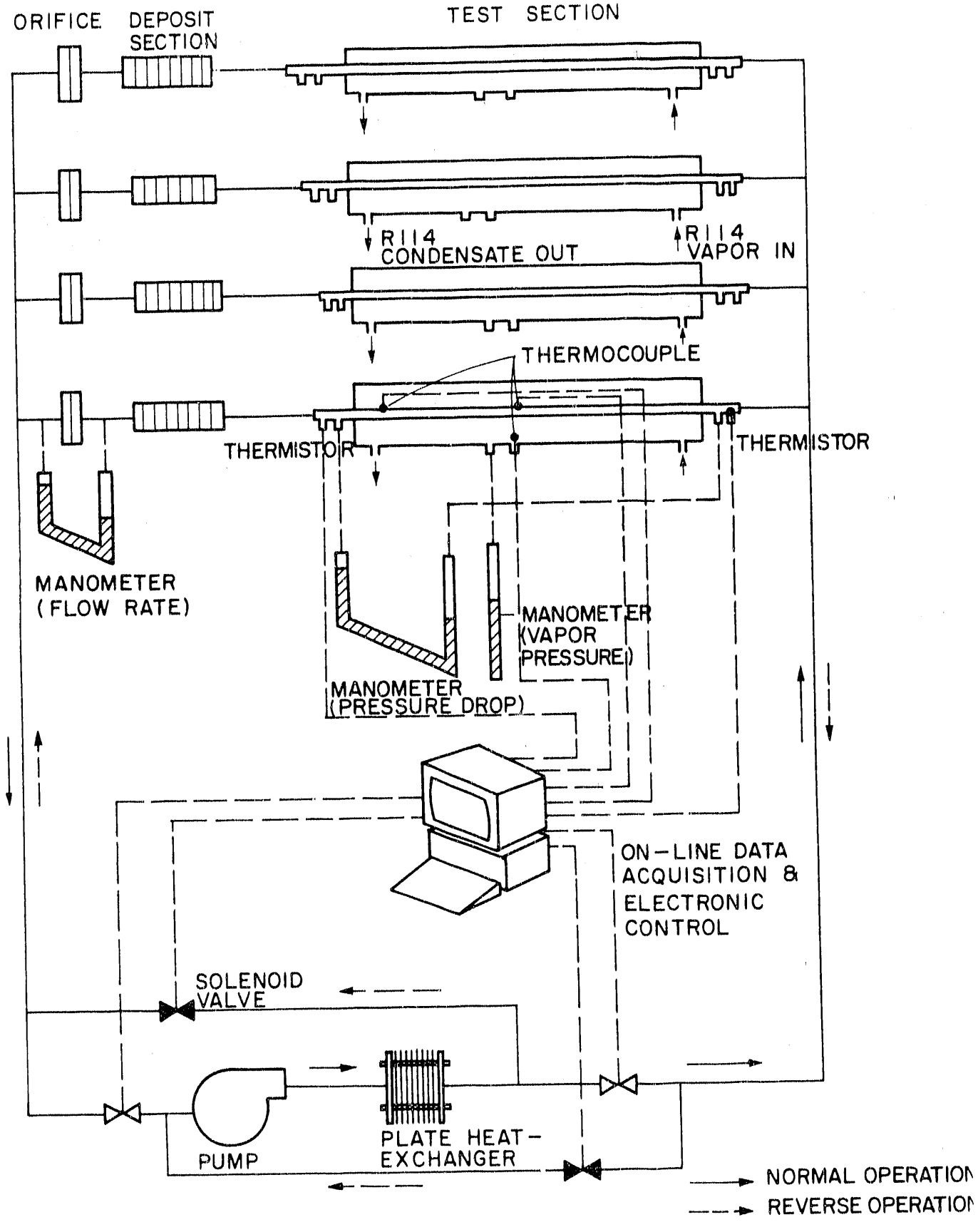

Fig. B.1 Schematic drawing of the fouling apparatus

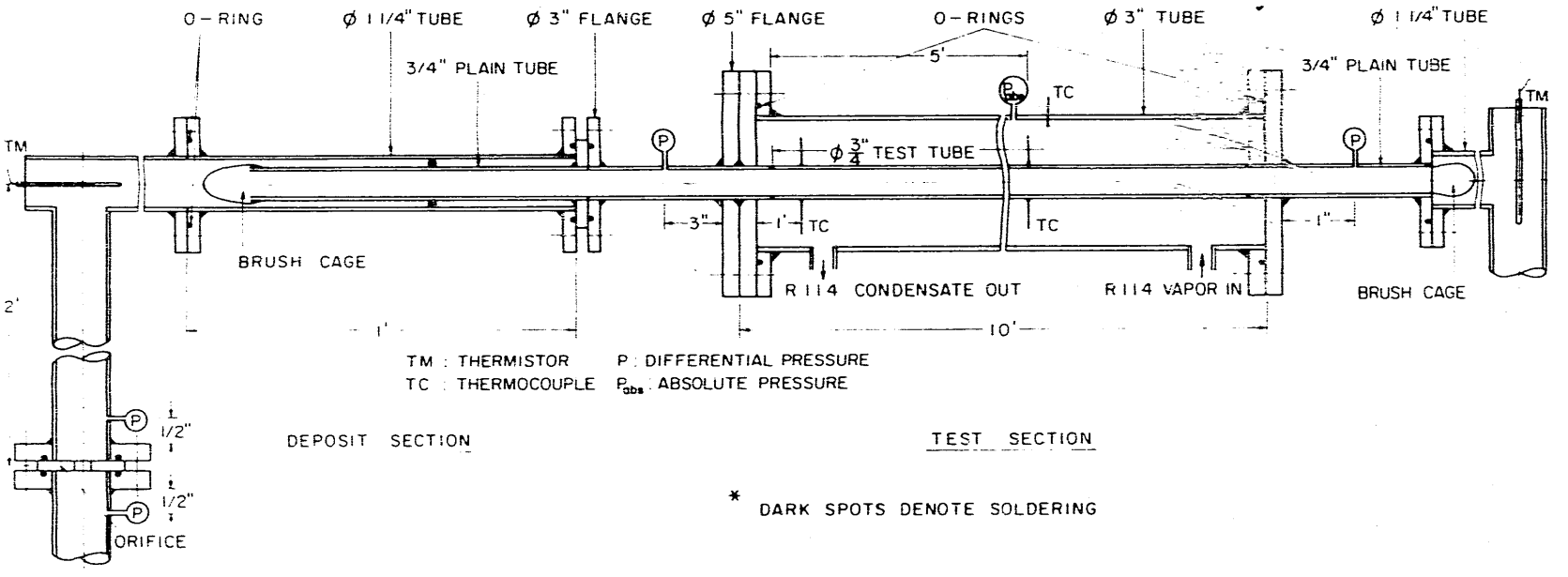

Fig. B.2 Test section of the fouling apparatus

ENHANCED TUBES FOR STEAM CONDENSERS

Volume 2

Detailed Study of Steam Condensation

M. H. Jaber

February 1992

Prepared for the
U.S. Department of Energy
Assistant Secretary for Conservation and Renewable Energy
Under DOE Idaho Field Office
Contract No. DE-FC07-88ID12708

The Pennsylvania State University

The Graduate School

Department of Mechanical Engineering

A THEORETICAL AND EXPERIMENTAL STUDY OF STEAM CONDENSATION ON HORIZONTAL ENHANCED TUBES

A Thesis in

Mechanical Engineering

by

Mohamad Hassib Jaber

Submitted in Partial Fulfillment
of the Requirements
for the Degree of

Doctor of Philosophy

August 1991

We approve the thesis of Mohamad Hassib Jaber.

Date of Signature

Ralph L. Webb — 5 Aug 1991

Ralph L. Webb
Professor of Mechanical Engineering
Thesis Adviser
Chair of Committee

Fan-Bill Cheung — 9 Aug 1991

Fan-Bill Cheung
Professor of Mechanical Engineering

Laura L. Pauley — 5 Aug 1991

Laura L. Pauley
Assistant Professor of Mechanical
Engineering

Gordon Robinson — 9 Aug 1991

Gordon Robinson
Associate Professor of Nuclear
Engineering

Harold R. Jacobs — 6 August 1991

Harold R. Jacobs
Professor of Mechanical Engineering
Head of the Department of
Mechanical Engineering

ABSTRACT

The objective of this research is to identify enhanced surfaces for horizontal steam condensers. Experimental and theoretical approaches were utilized to achieve a solution to the issue. Although the research was directed at electric utility steam condensers, the results are applicable to other industrial sectors that involve steam condensation. Three commercial tube manufacturers provided six specially made enhanced tubes for testing. The measured condensation heat transfer coefficient at 54 C saturation temperature was compared to that of a plain tube to determine the enhancement level. The tubes had different fin size, shape, spacing, and thermal conductivity. The fin height varied between 0.28 mm and 1.12 mm, and the fin distribution varied from 433 fins/meter to 748 fins/meter. The tube outside diameter varied from 18.29 mm to 22.23 mm. The experimental results show that the condensation heat transfer coefficient was enhanced by 34%, 75%, and 280% for titanium, copper nickel, and copper tubes, respectively. A theoretical model was developed to solve the conjugate heat transfer problem between the condensing fluid and the cooling water. The model was justified by predicting data of other investigators for steam and refrigerants. The condensing coefficient was predicted within ±15%. The steam data of the present work were also predicted within -17% and +10%. A numerical parametric study was performed to determine the effect of operating conditions, fin geometry, fin distribution, and tube thermal conductivity on

as the thermal conductivity decreases, (2) the preferred fin height is strongly dependent on the thermal conductivity, (3) the enhancement level increases as the tube diameter increases, and (4) the preferred fin pitch is a function of fin base thickness. However, a fin spacing (measured at the fin base) between 1.1 mm and 1.6 mm will produce the highest enhancement.

One titanium tube and one copper-nickel tube were tested at a saturation temperature of 42 C to determine the overall heat transfer coefficient. At 2.0 m/sec (6.5 ft/sec) water velocity, the overall heat transfer coefficient was enhanced by 21% and 80% for the titanium and copper-nickel tubes, respectively. The estimated water side enhancement was 10% and 80% for the titanium and copper-nickel tubes, respectively.

TABLE OF CONTENTS

LIST OF FIGURES

LIST OF TABLES

NOMENCLATURE

A	Reference area, πD_o, m^2/m.
A_i	Inside heat transfer area, πD_i, m^2/m.
A_{ij}	Sub-regional area ij, m^2/m.
A_f	Surface area of fin, m^2/m.
A_D	Cross sectional area of drainage channel, m^2
A_t	Heat transfer area of fin top, m^2.
A_p	Fin cross sectional area, m^2.
A_o	Total surface area of finned tube, m^2.
B	Property group defined as $3\mu k\Delta T/\rho^2 g\lambda$.
Bo	Bond number, $r^3\rho g/\sigma r'$, dimensionless.
c_b	Fraction of tube flooded.
c_p	Specific heat of water, J/kg-C.
C	Property group defined as $k\Delta T\nu/\sigma\lambda$.
C_f	Friction factor coefficient.
D_o	Diameter over the fins, m.
D_r	Root diameter, m.
D_h	Hydraulic diameter, m.
E_i	Ratio of the tube inside heat transfer coefficient of the enhanced tube to the plain tube.

E_o	Ratio of the finned tube condensing coefficient to that of a smooth tube of diameter D_o, at the same ΔT.
e	Fin height, m.
f	Fanning friction factor, dimensionless.
FPI	Fins per inch, 1/in.
fpm	Fins per meter, 1/m.
g	Gravitational acceleration, m/s^2.
G	Property group defined as $k^3\rho^2 g\lambda/\mu\Delta T$, $J^4/K^4\text{-}sec^4\text{-}m^7$.
H	Film thickness on tube surface, m.
H_s	System head for condenser with plain tubes, m.
H_e	System head for condenser with enhanced tubes, m.
h_j	Condensing coefficient in region j (j = u,f), $W/m^2\text{-}K$.
h_{ij}	Condensing coefficient in sub-region ij, $W/m^2\text{-}K$.
h_c	Coolant heat transfer coefficient, $W/m^2\text{-}K$.
h_{pred}	Predicted heat transfer coefficient, $W/m^2\text{-}K$.
h_{exp}	Experimental heat transfer coefficient, $W/m^2\text{-}K$.
h_f	Heat transfer coefficient of the fin, $W/m^2\text{-}K$.
h_r	Composite heat transfer coefficient of the root region, $W/m^2\text{-}K$.
h_{sid}	Composite heat transfer coefficient of the fin side, $W/m^2\text{-}K$.

h_{top}	Composite heat transfer coefficient of the fin top, W/m^2-K.
h_∞	Heat transfer coefficient of fin top in the flooded region, based on the fin base temperature, W/m^2-K.
h_t	Heat transfer coefficient of fin top in the flooded region, based on the actual fin top temperature, W/m^2-K.
h_{fg}	Latent heat of vaporization, J/kg.
k_m	Material thermal conductivity, W/m-K.
k	Condensate thermal conductivity, W/m-K.
l_{ij}	Length of subregion *ij* along the fin top or tube surface, m.
L	Tube length, m.
L_f	Characteristic length defined by equation [2.7], m.
LMTD	Log-Mean-Temperature-Difference, K.
$\dot{m}_w$	Coolant mass flow rate, kg/s.
$\dot{m}_c$	Condensate mass flow rate, kg/s.
Nu_{di}	Nusselt number of region i, based on D_o, dimensionless.
p	Local pressure of condensate, kPa.
P	Fin perimeter, m.
P_D	Perimeter of drainage channel, m.
P_f	Fin pitch, m^{-1}.
Q	Tube heat load, W.

q_s	Volumetric flow rate of cooling water in a condenser with plain tubes, m^3/sec.
q_e	Volumetric flow rate of cooling water in a condenser with enhanced tubes, m^3/sec.
r	Radius of curvature, m.
r_c	Radius of film interface in the flooded region, m.
r_f	Radius of film at the fin tip in the flooded region, m.
r'	Derivative of r with respect to s, dimensionless.
Re	Tube side Reynolds number, dimensionless.
R_o	Radius over fin, m.
R_r	Radius to fin root, m.
R_t	Fin corner radius, m.
R_B	Radius of circular drainage channel, m.
R_c	Radial thermal resistance through fin in the flooded region, m^2-K/W.
R_D	Radius of condensate drainage channel, m.
Re_{Dh}	Reynolds number based on hydraulic diameter.
R_f	Fouling resistance, m^2-K/W.
s	Coordinate along the fin surface, m; also used as fin spacing measured at fin base, m.
S_m	Total length of condensate film from the fin top corner to base, m.

S	Length of meniscus in the drainage channel as defined by Edwards et al. (1973), m.
S_{ij}	Length of subregion *ij* along the fin side, m.
T^*	Dimensionless temperature defined as $(T - T_c)/(T_{sat} - T_c)$.
T_c	Temperature of coolant, K.
$T_{w,av}$	Average wall temperature, K
T_i	Tube wall temperature at top (i = 1), side (i = 2), and bottom (i = 3), K.
T_{sat}	Steam saturation temperature, K.
$T_{sat,e}$	Steam saturation temperature in condenser with enhanced tubes, K.
ΔT_i	Temperature difference between the saturation temperature and the wall temperature of region i, K.
ΔT_w	Coolant temperature rise, K.
t	Dummy variable in Equation [3.24], m.
t_b	Fin base thickness, mm.
$t_{b,p}$	Base thickness of the film profile, m.
t_t	Fin tip thickness, mm.
t_w	Tube wall thickness, mm.
u	Local film velocity in the z direction, m/s.
U	Overall heat transfer coefficient, W/m^2-K.

w	Local film velocity in the s direction, m/sec.
V	Average film velocity, m/s.
x	Ordinate along the fin side as used by Honda et al (1987,1987a)
x^*	Dummy variable in Equation [3.42], m.
y	Ordinate perpendicular to the fin surface, m.
Z	Parameter in equation [2.2], dimensionless.
z_f	Height of liquid retained by a 3-D spine finned tube (measured from the tube bottom), m.

Greek Letters

ϕ	Angle measured from the tube top, rd.
ϕ_f	Flooding angle, rad.
$\delta(s)$	Local condensate film thickness, m.
Δ	Condensate thickness in the interfin area, m.
κ	Curvature, m^{-1}.
κ'	Derivative of curvature with respect to s, m^{-2}.
κ_o	Curvature at x = 0, m^{-1}.
λ	Angle defined by Equation [3.67].
μ	Dynamic viscosity, N-s/m^2.
η_i	Fin efficiency of region i, i = u or f, dimensionless.

ρ	Condensate density, kg/m^3.
ρ_v	Vapor density, kg/m^3.
θ	Angular coordinate, rad; also, the angle the fin side makes with the vertical.
θ_m	Maximum angular displacement of fin (or film) from fin top corner to base, rad.
ξ	Parameter in Equation [2.6], dimensionless.

ACKNOWLEDGMENTS

I would like to express my sincere gratitude to my adviser, Dr. Ralph L. Webb, for his inspiration and candid perseverance throughout my graduate studies.

I also extend my thanks to the Department of Energy, sponsor of this project. In particular, I would like to thank Mr. Gary Peterson and Mr. Manohar Sohal for their guidance and support.

I also thank Dr. Peter Stryker, of Buckneli University, for his valuable advise and involvement in the experimental program.

I also thank Mr. Klaus Menze of Wieland Werke (Germany), Mr. Elias Ragi of UOP (USA), and Mr. Petur Thors of Wolverine Tube (USA) for providing the enhanced tubes.

I extend my thanks to my doctoral committee members; Professor Fan-Bill Cheung, Professor Gordon Robinson, and Dr. Laura Pauley, for their involvement and help in this project.

Finally, my sincere thanks go to my family and dear friends whose love and understanding have helped me throughout my graduate studies.

CHAPTER 1

OVERVIEW

1.1 Introduction

Integral fins (Figure 1.1), are used extensively in the refrigeration industry and have proven to produce appreciable enhancement on the shell side of a shell and tube condenser. Katz, Beaty, and Foust (1945) were the first to experimentally evaluate the performance of integral finned tubes with a vapor condensing on the outside of the tubes. Results indicated significant enhancement in the heat transfer coefficient and the use of integral fin tubes in condenser application found its way to the refrigeration, power, and process industries. The present research will focus on the enhancement of steam condensation on the shell side of condenser tube bundles, which is of particular interest to the power generation industry.

1.2 General Objective for Using Enhancement in Two-Phase Flow

There are several objectives for using enhancement in two phase flow. Webb (1986) lists three common objectives:

1. Reduced heat transfer area for a constant heat duty.

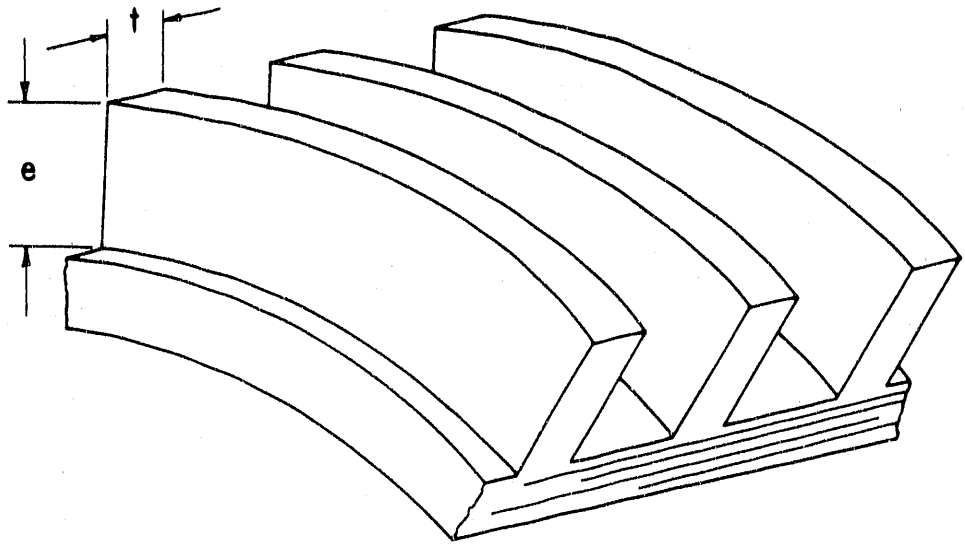

Figure 1.1 Cutaway view of an integral fin tube

2. Increased overall heat transfer coefficient, which results in either one of the following cases:

   a. Increased heat duty

   b. Reduced Log-Mean-Temperature-Difference (LMTD) for a constant heat duty

3. Reduced pumping power for a constant heat duty.

The above objectives are subject to specific constraints of geometry, pumping power, heat duty, and inlet temperature difference between the condensing and cooling fluids. The choice of objective and constraints will depend on the problem at hand, and whether it is a modification of an existing condenser or the design of a new one.

For case 2b, reduction of the LMTD (Log-Mean-Temperature-Difference) is accomplished by lowering the saturation temperature which results in a reduction of the turbine back pressure and hence an increase in the thermodynamic efficiency of the power cycle. Figure 1.2 shows the temperature vs. area for a condensing process. In the case of two phase flow, the pressure drop on the shell side affects the fluid temperature. Hence, Figure 1.2 shows the saturation temperature for two cases when the two phase pressure drop is greater or equal to zero.

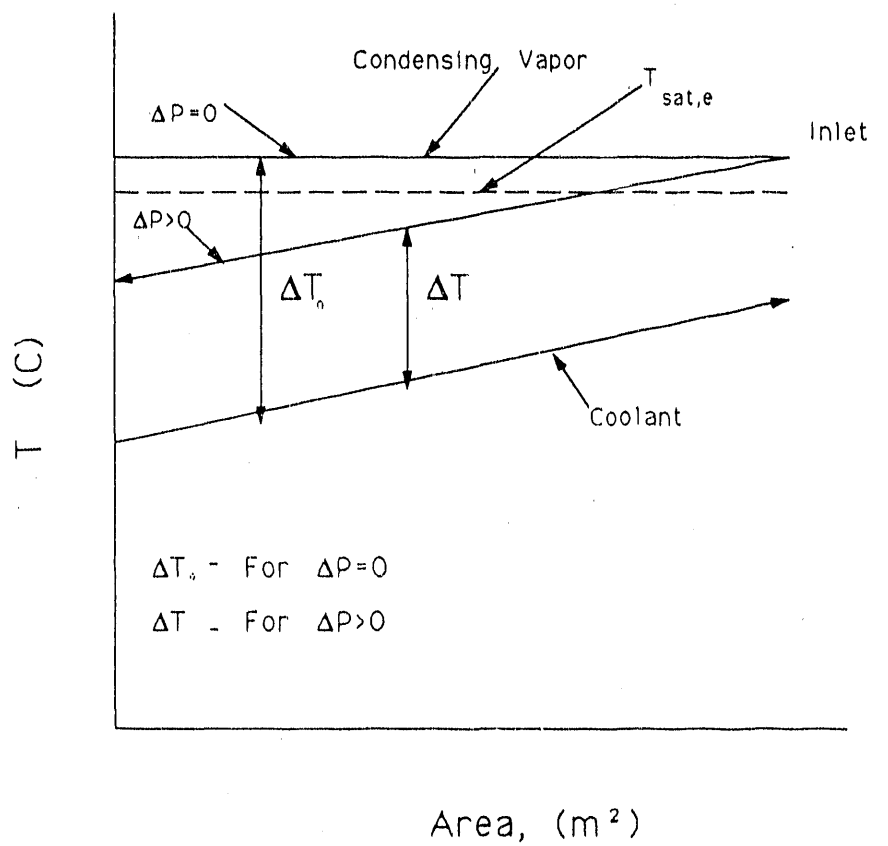

Figure 1.2. Effect of two-phase pressure drop on the LMTD, for a condensing vapor. Webb (1984).

For the case of tube for tube replacement, use of internal enhancement will result in reduction of the cooling water flow rate. The enhancement will have a higher friction head and hence will shift the balance point on the pump curve. Figure 1.3 shows the balance point for the system and pump, with and without internal enhancement. The curves H_s and H_e are the friction characteristics for smooth and enhanced tubes, respectively. The new flow rate will be determined by the balance point between the pump characteristic curve and the new system curve.

1.3 Justification of Research

The interest in enhanced surfaces for single or two-phase flow began some 50 years ago. However, the energy crisis in the early 1970's resulted in an intensified effort to reduce operating costs of existing energy systems by the increase of their efficiencies. Bergles and Webb (1985) show the distribution of the number of publications since 1918 up till 1983 (Figure 1.4). Figure 1.4 shows the large number of papers published between 1970 and 1980 reflecting the magnitude and intensity of research conducted during that period.

In 1984, Webb, Haman, and Hui (1984) presented a simulation study on the economic feasibility of using enhanced surfaces in the condensers of two prototype power plants (one nuclear and the other fossil). The authors considered in their simulation a set of combinations of internal and external enhancements, shown in

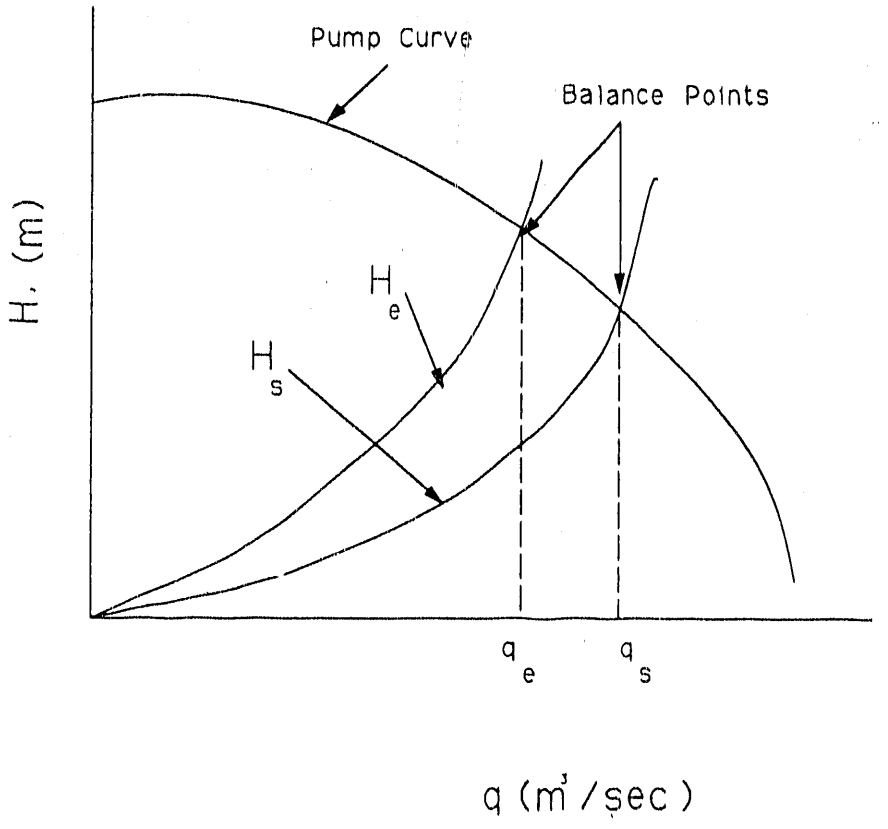

Figure 1.3 Balance points for enhanced and smooth heat exchangers.

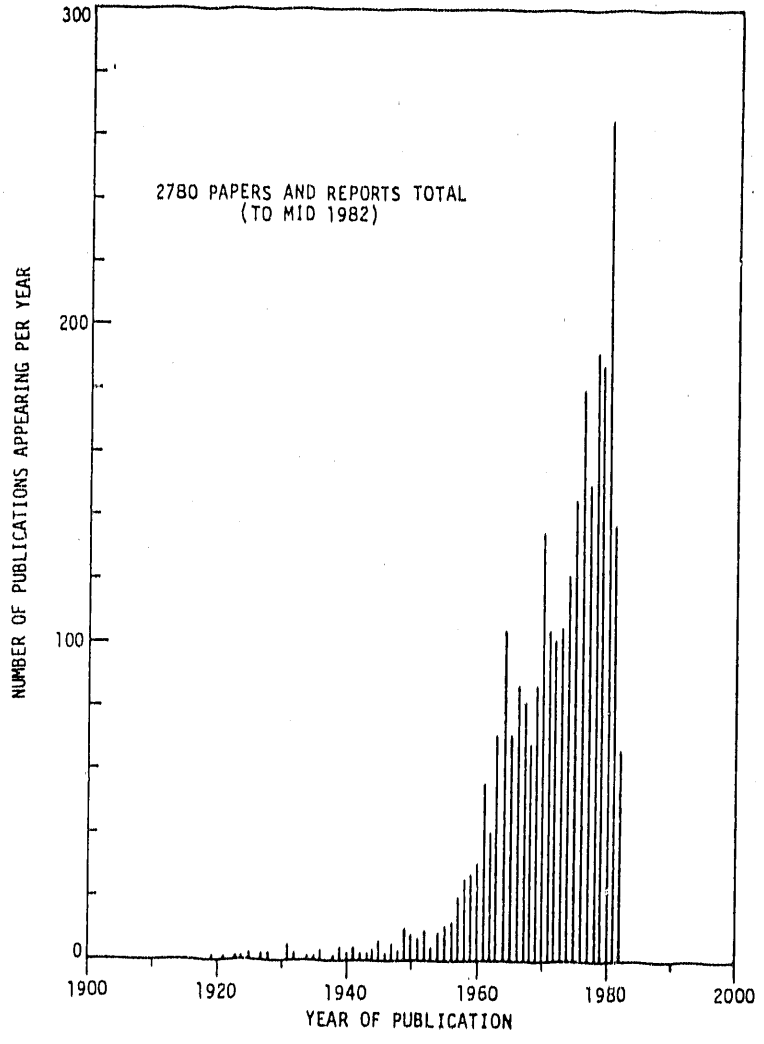

Figure 1.4. Histogram of publications on enhanced surfaces between 1919 and 1983. Bergles et al. (1983).

Figure 1.5. The inside enhancement is used to enhance the heat transfer coefficient of a single phase fluid. The outside enhancement is used to enhance the condensing coefficient. The authors show that the thermal resistance on the inside is larger than that on the outside (for a plain tube,the total thermal resistance is divided approximately 2/3 on the inside and 1/3 on the outside). The simulation results showed that by combining both internal and external enhancements, significant improvements in fuel cost reduction and increase in peak power generation are possible.

Boyd et al. (1983) reported that the Tennessee Valley Authority (TVA) completed, retubing one of its condensers in 1980, with a copper-nickel (cu/ni) corrugated tube; Figure 1.5a. A sample of tubes was instrumented and placed near the top of the condenser. On-site monitoring of tube performance justified the beneficial use of enhanced tubes in condensers. The on-site measurements indicated a 38% to 43% increase in the overall heat transfer coefficient (with no fouling on the tubeside) which resulted in a lower turbine pressure. Translated into economical terms, TVA estimated savings over the plant life to be $900,000.

Although the corrugated tubes tested by Boyd et al. (1983) have approximately 65% enhancement on the inside, the enhancement on the outside is less than 35%. This work will attempt to identify external enhancement geometries for copper-nickel and titanium tubes that will produce appreciable enhancement (more than 35%) on

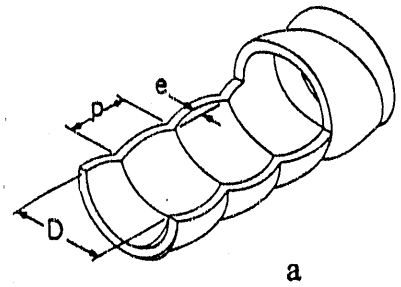

a

b

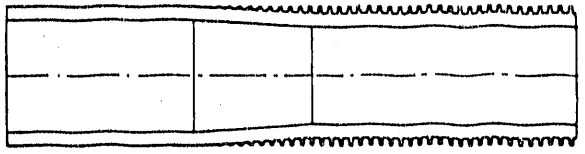

c

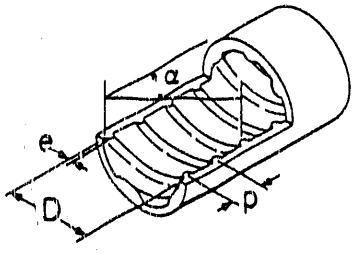

d

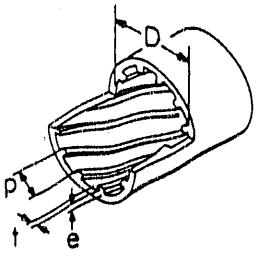

e

Figure 1.5. Geometries of internal and external enhancements considered by Webb et al. (1984).

the steam side (external). It will also identify internal geometries that can produce more than 65% on the inside. The tubes were specially developed by three tube manufacturers.

The promising results of earlier research and the growing interest of various energy sectors prompted the interest in the present project.

1.4 Methodology

The research will be conducted in accordance with the following procedure:

1. Numerical predictions for the performance of integral fin tubes for different operating conditions, fin and tube geometries, and material thermal conductivities. An optimum tube geometry that gives the maximum enhancement will be identified.

2. Manufacture of tubes from copper-nickel and titanium, by several tube manufacturing companies.

3. Consideration of different types of external enhancement (i.e. other than integral fin type).

4. Measurement of the condensing heat transfer coefficient for steam condensing under vacuum conditions.

5. Recommendation for: (i) an enhanced tube, to be used in condensers of electric utility power plants, and (ii) a mathematical model to be used in predicting the performance of enhanced surfaces as part of a condenser design procedure.

CHAPTER 2

LITERATURE SURVEY

2.1 Introduction

A chronological survey of the published literature on steam condensation on externally enhanced horizontal tubes is presented. Experimental data and analytical models are discussed. Although the focus will be on the subject of steam condensing on horizontal integral finned tubes, reference will be made to other fluids and types of enhancements. The data and analytical models will, in general, reflect the effect of fin geometry, fin shape, tube geometry, tube material, and operating conditions on the condensing heat transfer coefficient. The following main topics will be considered:

1. Experimental data
2. Enhancement types
3. Theoretical models

2.2 Experimental Data

2.2.1 Liquid Retention

Although the use of integral fins offers appreciable enhancement levels (as compared to smooth tubes), there are some disadvantages involved - particularly liquid retention in the interfin space. The phenomenon of liquid retention was first investigated by Katz, Hope, and Datsko (1946) who measured the flooded portion of a tube for different fin spacings and several fluids without condensation. They found that there can be significant liquid retention on the tube. However, they erroneously concluded that none of the condensate remains on the tube when condensation occurs. Rudy and Webb (1981) have also investigated liquid retention and were the first to suggest that retention is due to surface tension forces. They conducted static and dynamic tests, for R-11, n-pentane, and steam and concluded that the measured retention is practically the same under both conditions. Hence, they showed that the condensate is retained on the tube during condensation and this retained condensate significantly reduces the tube performance. Combinations of fin geometry, fin distribution, fluids, and condensation rates were used. Figure 2.1 shows the negligible effect of liquid loading on the retention angle. Figure 2.2 shows the effect of surface tension to density ratio on the retention angle for different fin types and fpm. The experimental results led to the conclusion that, for the same fin density, the flooded portion of a tube increases with increasing σ/ρ, and tubes with

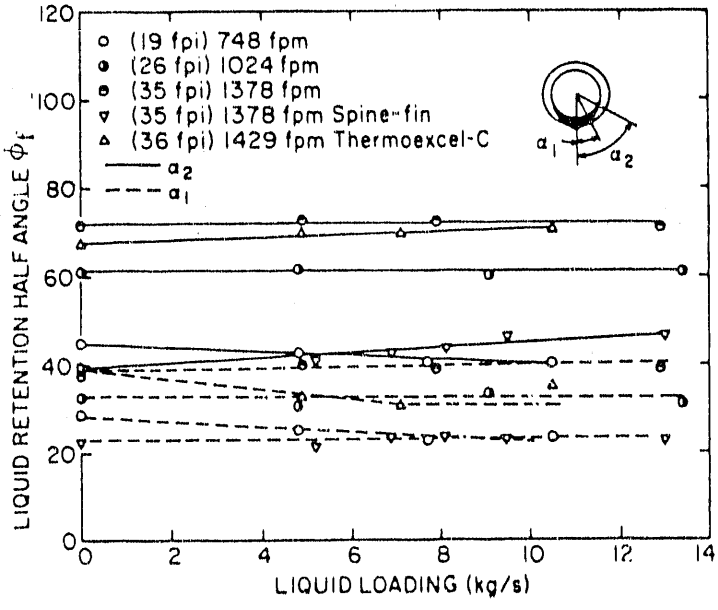

Figure 2.1. Experimental values of retention angles versus liquid loading for R-11. Rudy and Webb (1981).

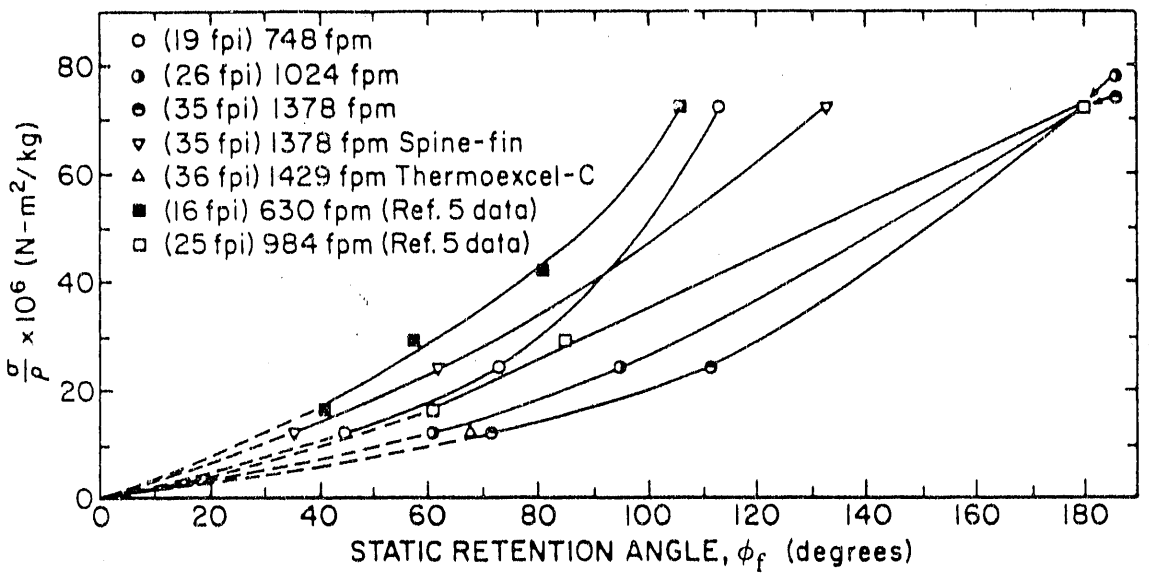

Figure 2.2. Ratio of surface tension to density versus the maximum retention angle. Rudy and Webb (1981).

3-D fins (i.e. spine fins) have a smaller retention angle than 2-D fins. This latter observation is based on the fact that for 3-D fins, a greater space is available for the condensate to spread on the tube surface. Rudy and Webb (1981) analytically derived an equation to predict the retention angle for rectangular fins. In a later publication, Rudy and Webb (1985) presented a generalized formulation for prediction of the retention angle on tubes with fins of rectangular, trapezoidal, and curved (fluted) shapes. For a fluted surface, the fraction of condensate retained is given by:

$$c_b = \frac{1}{\pi}\cos^{-1}\frac{2\sigma(P - t_b)}{\rho g D_o(P_f e - A_p)} \qquad [2.1]$$

Honda et al. (1983) have derived a similar equation to predict the fraction of retained condensate. All of the results indicate that fluids of high σ/ρ (e.g. steam) will flood a larger portion of the tube and vice versa for fluids of low σ/ρ (e.g. R-11). This behavior is shown in Figure 2.2.

2.2.2 Condensing Coefficient

Katz, Beaty, and Foust (1945) tested 12 copper tubes with steam condensing in an annular passage at 1.7 atm. The tubes were 12.7 and 15.875 mm O.D. with fin heights ranging from 1.12 to 9.65 mm and fin density from 157.5 to 945 fpm. Some

of the tubes had internal enhancement and therefore the results were presented in terms of the overall heat transfer coefficient. Those results are perhaps the first experimental verification of the effectiveness of integral fins in condensation processes. Karkhu and Borovkov (1971) condensed steam on 3 brass tubes (D_r = 18 mm) and one commercial copper tube (D_r = 16 mm) with trapezoidal shape integral fins. The operating conditions and geometric parameters of the brass tubes ensured a Bond number less than 0.1 so that the condensate flow along the fin surface is governed by surface tension forces only. The enhancement reported ranges from 50 to 100%. Shekriladze and Rusishvili (1980) condensed steam, R-21, and alcohol (under atmospheric conditions) on threaded surfaces (all tubes had thread pitches of 0.5 or 0.3 mm) of copper, stainless steel, steel-20. The triangular thread pitch had a thread angle of 55 deg. The authors used an analytical model to predict their data and found an agreement of ± 25%. The presentation of their data does not show the effect of tube and fin geometry on the condensing coefficient.

Wanniarachchi, Marto, and Rose (1984) conducted a series of tests on six machined copper tubes, 133 mm long with rectangular fins of 1.0 mm height and thickness. The fin spacing varied from 0.5 to 9.0 mm and the tests were carried out under vacuum (48 C) and atmospheric (100 C) conditions. The outside diameter of the plain tube was equal to the root diameter of the finned tube with a value of 19.0 mm. The maximum vapor side enhancement (based on root diameter) was 3.5 and 5.5 (defined as the ratio of the condensing coefficient based on the root diameter to

that of a plain tube of diameter equal to the root diameter, at the same heat flux) for vacuum and atmospheric conditions, respectively. The maximum value for both pressure levels occurred at a fin spacing of 1.5 mm. Figure 2.3 shows the enhancement ratio vs. fin spacing together with area ratio of finned to plain tube ($A_o/\pi D_r$). The additional enhancement above the area increase was attributed to surface tension effects. The authors propose that the lower enhancement obtained under vacuum conditions is due to a higher condensate viscosity. This paper also studied the effect of the procedure used to determine the experimental condensation heat transfer coefficient. Direct measurement of the wall temperature, of a plain tube, was compared to the indirect method of the Wilson technique. Both methods gave the same trend in the variation of the condensing heat transfer coefficient with fin spacing. But, the Wilson technique resulted in lower magnitudes of the condensing coefficient.

Yau, Cooper, and Rose (1985) studied the effect of fin spacing, vapor velocity, and coolant velocity on the condensing heat transfer coefficient. They used 102 mm long copper tubes with a fixed fin height and width of 1.60 and 0.5 mm, respectively. The fin spacing was varied from 0.5 to 19.5 mm (total of 13 tubes). The smooth tube outside diameter of 12.7 mm is equal to the root diameter of the finned tube. Three vapor velocities 0.5, 0.7, and 1.1 m/sec were considered and coolant velocity ranging from 1.5 to 4.5 m/sec for each of the vapor velocities. All the tests were carried out under atmospheric pressure. The maximum enhancement level (as compared to a

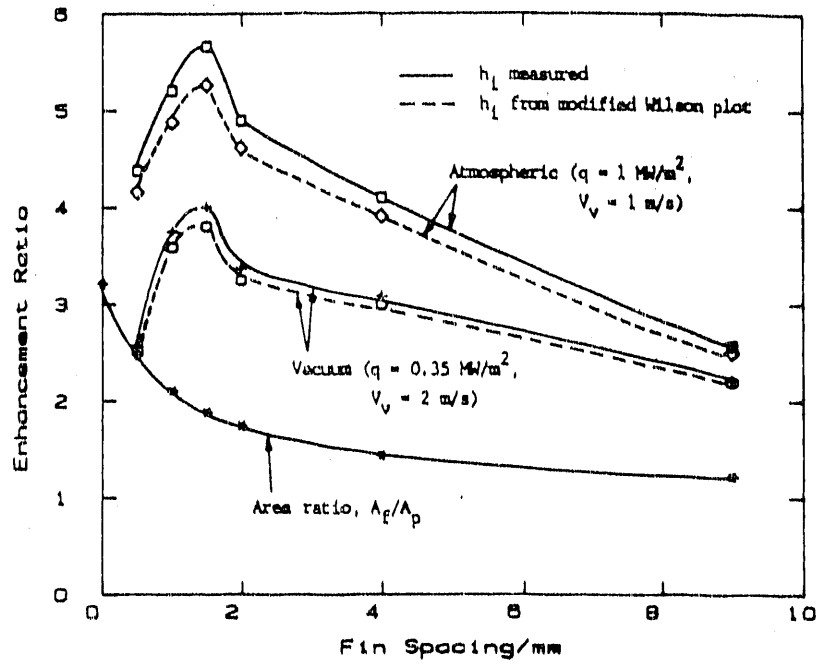

Figure 2.3. Enhancement ratio versus fin spacing for steam condensation under vacuum (48 C) and atmospheric conditions (e = t = 1.0 mm). Wanniarachchi et al. (1984).

smooth tube, based on D_r) was 3.6 (at the same heat flux) at a fin spacing of 1.5 mm. This confirmed earlier findings by Wanniarachchi, Marto, and Rose (1984). Figure 2.4 shows the results of the enhancement ratio vs. fin density. The results also show a non-monotonic behavior of the condensing coefficient as a function of fin density. However, a maximum is achieved at a fin density of 0.5 mm^{-1} (corresponding to a 1.5 mm fin spacing). Figure 2.4 also shows no appreciable influence of the vapor velocity on the enhancement level. It should be noted that such velocities exist in actual condensers only in the air cooling section. Much higher velocities are found in the tube bundle particularly around the periphery. In fact, Fujii (1987) showed that an increase in vapor velocity reduces the enhancement level. The above data are based on near-atmospheric conditions (slightly above 1.0 atm). Practical operating conditions of steam condensers are on the order of 10 - 14 kPa. Hence, this data set does not simulate actual conditions. Moreover, copper tubes are not used in steam condensers.

Wanniarachchi, Marto, and Rose (1985, 1986) measured the condensation coefficient for steam on 24 copper tubes with rectangular fins and root diameter of 19.05 mm (equal to the smooth tube O.D.). The fin spacing, thickness, and height were varied systematically to determine the effect of these parameters on the condensing coefficient. The fin spacing ranged from 0.5 mm to 9.0 mm, the fin height from 0.5 mm to 2.0 mm, and the fin thickness from 0.5 mm to 1.25 mm. Data were taken under atmospheric and vacuum conditions. The maximum enhancement

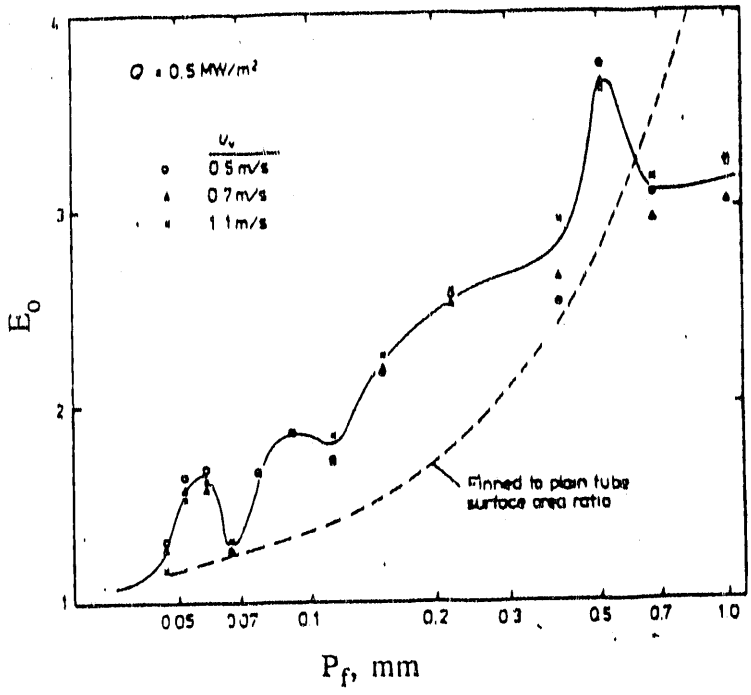

Figure 2.4. Enhancement ratio versus fin density for steam condensation under atmospheric conditions (e = 1.6 mm, t = 0.5 mm) for different vapor velocities. Yau et al. (1985).

level (based on root diameter) was achieved at fin spacings of 1.5 (at e = 1 and 2 mm) and 2.0 mm (for e = 0.5 and 1.5 mm). The enhancement ratio was found to increase with increase in fin height. No optimum fin height was given but rather the data show a monotonic increase in the enhancement level as the fin height is increased from 0.5 to 2.0 mm. The effect of fin thickness on the enhancement ratio does not follow a clearly defined trend. The above authors provide a graph for one particular fin spacing of 1.0 mm that shows a weak optimum fin thickness of 0.75 and 1.0 mm for atmospheric and vacuum conditions, respectively. This trend is not reflected by other fin spacings. It was concluded that the fin spacing is the most important parameter that affects the heat transfer coefficient. Later studies will show that in addition to the fin spacing, the shape of the fin and the drainage channel also play an important role.

Marto et al. (1986) studied the effect of fin shape on the condensing heat transfer coefficient by condensing steam on copper tubes (one smooth tube and four finned tubes) with four different fin shapes. Table 2.1 shows the geometry used and enhancement level (based on root diameter) obtained. The vacuum and atmospheric data are at 0.25MW/m^2 and 0.75 MW/m^2 heat flux, respectively. Table 2.1 shows that the rectangular and trapezoidal shapes gave almost the same enhancement level, with a slightly higher value for the rectangular fin. The authors conclude that the fin shape is not as important a parameter as the fin spacing. This conclusion was based on their results which showed a maximum of 15% higher performance of the parabolic

Table 2.1

Fin geometry and enhancement level for different fin shapes, Marto et al. (1986).

Fin type	t_t	t_b	Enhancement Ratio	
-	mm	mm	Atm	Vac
Smooth	-	"	1.00	1.00
Rectangular	0.5	0.5	3.69	5.5
Triangular	0.00	0.5	3.73	5.49
Trapezoidal	0.17	0.5	3.67	5.41
Parabolic	0.00	0.5	4.09	6.21

profile as compared to the other fin shapes. This conclusion contradicts the findings of Kedzierski and Webb (1987), which show a significant improvement in the condensing coefficient is obtained when the fin shape is of a special form (refer to Figure 2.8).

2.2.3 Tube Material

So far, the discussion focused on the fin geometry and its effect on the enhancement level. Most of the data concerning steam condensation is for copper tubes. The tube thermal conductivity has a significant effect on the condensation process and it is worth presenting in a separate section.

Mills et al. (1975) reported experimental data of steam condensation on horizontal grooved tubes of 19.0 mm O.D and 36 groove per inch (pitch of 0.71 mm). The fins had a trapezoidal shape with a base angle of 60 deg. and a height of 0.458 mm. Three different tube materials were tested: copper, brass, and 70/30 copper-nickel with corresponding thermal conductivities of 381, 100, and 28.5 W/m-K. Steam was condensed at temperatures between 300 K and 327 K with vapor velocities ranging from 0.6 to 2.6 m/sec. Although the data exhibit some scattering, it does however show the trend in the effect of tube material on the condensing heat transfer coefficient. The authors report enhancement levels of the order of 5.5 for brass. This is higher than the enhancement level of 2.0 obtained by Karkhu and

Borovkov (1971) at conditions slightly above atmospheric. This difference might be due to the fact that the Karkhu and Borovkov (1971) brass tubes had fin heights approximately twice the fin height (lower fin efficiency), and smaller fin spacing (more flooding) as compared to Mills et al. (1975). The data clearly showed a drop in performance as the thermal conductivity of the tube decreases.

Shklover et al. (1981) reported data for steam condensation on horizontal integral fin tubes (cut thread fins and rolled thread fins of fin spacings less than 0.3 mm) made of stainless steel (k = 19 W/m-K). The condensing pressure range was from 0.215 to 1.15 bar, heat flux 1.2E05 to 2.8E05 W/m^2, and water velocity 1.7 to 2.3 m/sec. The fin geometries tested were, e = 0.93, 0.7, 0.55 mm, t_b = 1.6, 0.59, 0.43 mm, tube wall thickness of approximately 1.0 mm, and tube O.D of approximately 16.0 mm. The condensation heat transfer coefficients for the finned tubes were within ± 10% of the smooth tube data, indicating a negligible level of improvement. The authors attribute these results to the low thermal conductivity of stainless steel, which results in a low fin efficiency. In addition to the low fin efficiency, the small fin spacing causes a large condensate retention angle, which will reduce the performance of the tube.

Mitrou (1986) conducted an experimental study to determine the effect of material thermal conductivity on the enhancement level. The materials used were copper, copper-nickel, aluminum (D_r = 13.7 mm and D_i = 12.7 mm), and stainless-

steel (D_r = 14.5 mm and D_i = 12.5 mm). The fins had a triangular (spirally threaded) cross section with e = 1.0 mm, t_b = 2.1 mm, t_t = 0.0 mm, and 12 fpi. At a heat flux of 2.5E5 W/m^2 (vacuum conditions), the enhancement level was 3.5, 2.86, 1.81, and 1.0 for copper (k_m = 350 W/m-K), aluminum (k_m = 237 W/m-K), copper-nickel (k_m = 52 W/m-K), and stainless steel (k_m = 15 W/m-K). Figure 2.5 shows the performance of each tube compared to a smooth tube. The trend obtained is similar to that of Mills et al. (1975). Figure 2.5 shows almost no enhancement for a stainless steel tube. The combination of high heat transfer coefficients, low thermal conductivity, and high fins resulted in a low fin efficiency which in turn reduced the performance of the tube. The negligible enhancement reported is also due to a small fin spacing which results in negligible contribution in the root region.

2.2.4 Drainage Strips

Although this section can be included under the topic of "other enhancement types" (since it is a modification introduced to integral fin tubes), it will be discussed here for the sake of continuity in reporting the experimental data.

The negative effects of surface tension is the bridging of condensate in the interfin space over a significant fraction of the tube. The interfin space and fin sides in the flooded region become ineffective for heat transfer. The application of drainage strips (solid or porous) creates a low pressure region due to surface tension

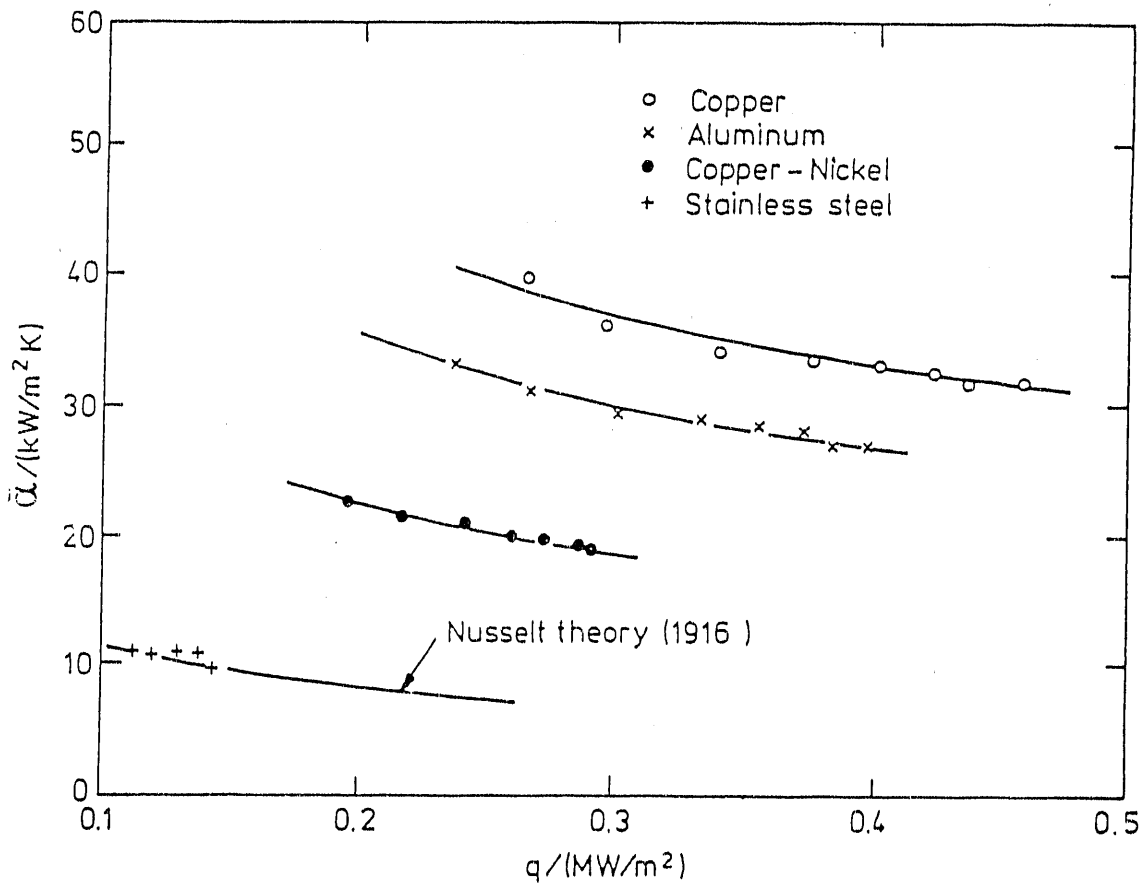

Figure 2.5. Condensing heat transfer coefficient versus heat flux (based on D_r). Effect of material thermal conductivity. Mitrou (1986).

forces. This low pressure region creates a "pull" on the condensate and hence reduces the flooded region on the tube surface. Figure 2.6a shows a flooded integral fin tube. Figure 2.6b shows the same tube with a drainage strip attached at the bottom and the resulting decrease in the flooded area.

Honda, Nozu, and Mitsumori (1983) carried out the first attempt to experimentally study the effect of drainage strips on the performance of integrally finned tubes. They condensed R-113 and methanol on one smooth tube and three integral fin copper tubes with an approximate 19.0 mm O.D and fin height between 0.92 and 1.46 mm. The condensing coefficient was measured with and without the use of drainage strips. The authors use a 1.9 mm thick and 16 mm wide porous nickel strip with a 0.8 mm effective pore diameter and 490 kg/m^3 bulk density. The reported maximum enhancements (over and above the finned tube) were 1.36 and 2.08 for R-113 and methanol, respectively. The enhancement offered by the drainage strip was most effective for small fin spacings and fluids with high σ/ρ (such as steam).

Yau, Cooper, and Rose (1984) used a solid copper drainage strip on one smooth tube and two finned tubes of 1.5 mm and 2.0 mm fin spacing (e = 1.0 mm, t = 0.5 mm, D_r = 12.7 mm). The enhancements achieved by using the strip on the finned tubes were 44% and 19% (over and above the finned tube) for the 1.5 and 2.0 mm spacings, respectively. Measurements of retention angle for water, ethylene

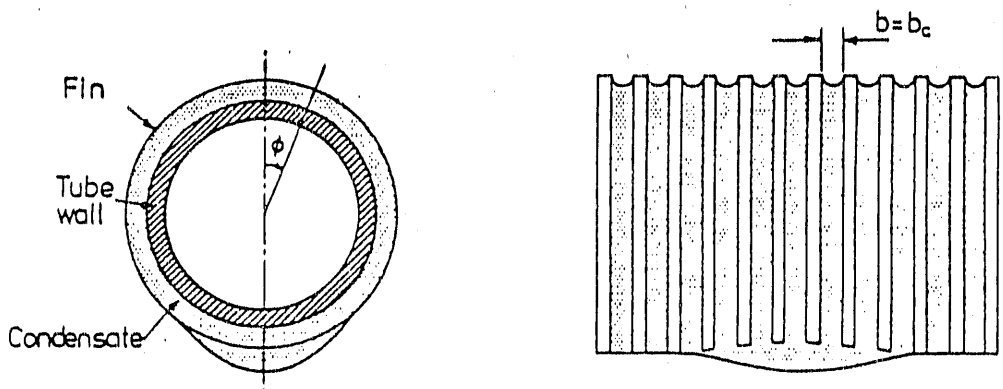

a

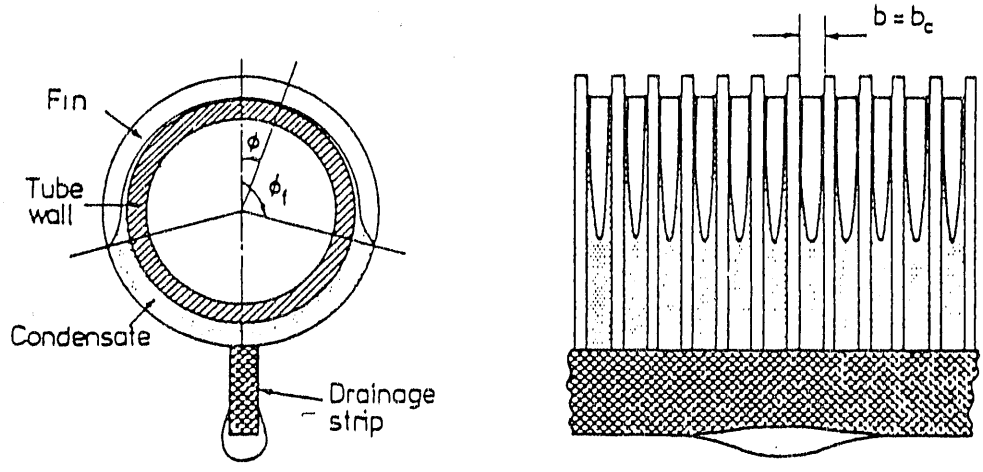

b

Figure 2.6. (a) Fully flooded tube at the critical fin spacing (b)porous drainage strip applied to the fully flooded tube in (a). Marto et al. (1988).

glycol, and R-113 were conducted on the two finned tubes with and without the strip. The results support earlier findings that the effect of drainage strips increases as the dimensionless parameter $\sigma\cos\theta/\rho sgR_o$ increases. Honda and Nozu (1985) reported data on the condensation of methanol (T_s = 343 K) on the same tube and fin geometry as in their 1983 study. However, the 1985 paper studied the effect of strip height and porosity. A 14.0 mm high solid strip of polyvinyl chloride and four nickel porous strips with heights varying from 4 to 19 mm were used. They concluded that porous strips gave higher enhancement than solid strips and that the enhancement increases as the height increases. Yau et al. (1986) reported steam condensation data on two finned tubes and compared the performance of the tubes with and without drainage strips. They used a solid copper strip of 0.5 mm thickness and 8.0 mm high and found a maximum enhancement of 30% (over the finned tube). Marto et al. (1988) conducted extensive experimental research on the use of drainage strips with integral fin tubes for steam condensation. The study included the effect of porous strip height, thickness, porosity, and the effect of solid strip thickness. The materials considered were: bronze, and titanium. The strip height ranged from 3.0 mm to 15.0 mm, the strip thickness ranged from 1.5 mm to 9.0 mm, and pore diameter ranged from 0.0025 mm to 0.13 mm. The finned tube was made of copper with a root diameter of 19.05 mm (same as smooth tube outside diameter). The fin height and thickness were 1.0 mm and a fin spacing of 0.5 mm which resulted in a fully flooded tube. Steam was condensed at atmospheric and vacuum conditions (85 mmHg). Measurements of the flooding angle were also reported. It was observed

that a porous strip of 3.0 mm height did not affect the flooding angle. However, with a porous strip of 8.0 mm or more, the flooded region almost vanished. For the operating conditions and geometric ranges used, the porous strip with a height of approximately 11.0 mm and a pore size between 0.025 and 0.05 mm performed the best. The authors report that, under atmospheric conditions, the best porous strip produced a 65% enhancement (over the finned tube value without a strip) while a solid strip of same width and height produced a 35% enhancement. The authors do not report the enhancement levels for vacuum conditions.

Although the use of drainage strips can offer appreciable enhancement, the issue of practicality still remains to be solved. In retubing existing steam condensers, it is expected that major changes should be done to the tube sheet in order to use strips. Some research is required to determine the feasibility of this application. On the other hand, it is possible that such devices can be used in new condensers, but again a feasibility study is required.

2.2.5 Types of Enhancements

Although the integral fin has been the earliest type of enhancement used, several other types have been introduced and actually installed in existing power plants (e.g. corrugated tubes). Bergles and Webb (1985) presented a data bank of up-to-date enhancement techniques and U.S. patents. More than 300 patents for use

in single and two-phase flow were listed. Only 81 of them are applicable to condensation processes. Webb, Haman, and Hui (1984) performed a simulation retrofit for a fossil and a nuclear plant. They used combinations of internal and external enhancement to show appreciable increase in performance and hence economic savings.

Gregorig (1954) introduced and analyzed fluted surfaces as a means to increase surface tension effects on vertical surfaces. It is known that surface tension effects exist on integral fins of rectangular shapes as verified by Webb and Keswani (1982). However, the fluted surface magnifies this effect leading to a higher condensation coefficient. The profile suggested by Gregorig (1954) was later modified by Zener and Lavi (1974). Adamek (1981) presented a family of profiles and determined an optimum profile that gives the highest condensation coefficient. Figure 2.7 shows the data of Kedzierski and Webb (1987) for R-11 as the condensing fluid. This data shows that the Adamek (1981) profile gives the highest performance. Fluted surfaces are actually used in vertical condensers and evaporators. Most of the published literature, for fluted surfaces, report data on vertical tubes. Michel (1981) reports experimental results for condensation on vertical fluted tubes, where 20 aluminum tubes (O.D = 25.4 mm) and eight different fluids were used. Some of the tubes were tested in the horizontal position and a comparison with a smooth tube shows an enhancement of the order of 1.75 (based on total surface area) when R-11 is used as the condensing fluid. Reilly (1978) condensed steam on the General

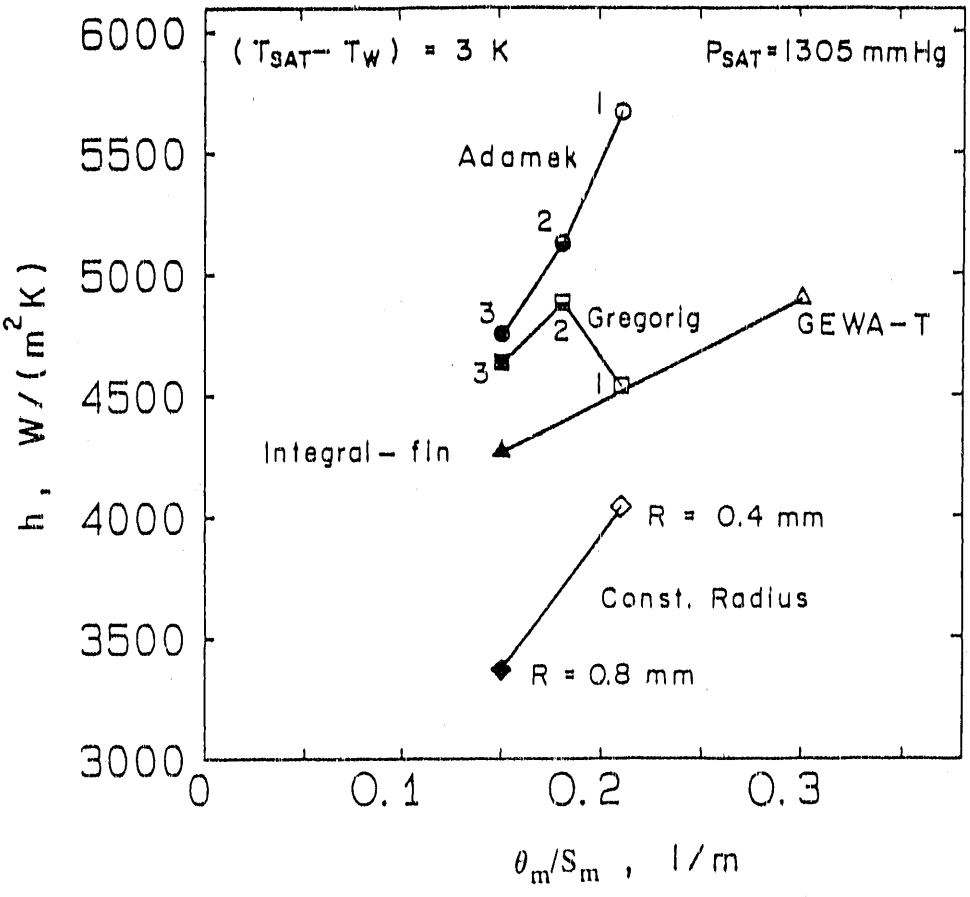

Figure 2.7. Condensing heat transfer coefficient versus θ_m/S_m for different fin profiles, for R-11 as the condensing fluid. Kedzierski and Webb (1987).

Atomic aluminum fluted tube with an outer diameter of 15.875 mm. The experimental data show that the overall heat transfer coefficient can be improved by a factor of 1.5 to 1.7 (compared to a smooth tube of same O.D and operating at the same cooling water flow rate). However, the condensing heat transfer coefficient (based on total surface area) was 10 to 20% less than the corresponding value of a smooth tube of the same O.D. The reason for the differences between the Michel (1981) and Reilly (1978) results may be due to different fin geometry, tube O.D, and condensing fluid.

Kedzeirski and Webb (1989) proposed a new practical fin shape that gives high performance by inducing a surface tension pressure gradient along the fin length. The major advantage of this new profile is that it is based on a practical set of parameters that lead to feasible manufacturing. The parameters, e, t_b, and R_t can be independently specified to construct the fin. This is not possible with the Adamek (1981) profiles. The profile of the fin is given by:

$$r = C_1 + C_2 \exp(Z\theta) + C_3\theta \qquad [2.2]$$

where C_1, C_2, and C_3 are constants determined by the geometric boundary conditions. Expressions for these constants are presented by Kedzierski and Webb (1989). The parameter Z defines the "fatness" of the profile.

Figure 2.8 shows the cross section and profile of this fin, for different values of the parameter Z.

The performance of this profile is compared to that of the Adamek (1981) and Gregorig (1954) profiles. Table 2.2 shows the values of the parameter hS_m based on predictions of R-11 condensing at 40 C and ΔT = 5 C. These predictions were for copper surfaces with an assumed fin efficiency of 100%. It is seen that the new profile offers a 60% higher performance when compared to a Gregorig (1951) profile having the same aspect ratio e/t_b. However, it gives an hS_m 12% lower than the Adamek (1981) profile (also based on the same aspect ratio).

One type of 2-D enhancement is the corrugated (or roped) tube, Figure 1.5a. Tests conducted by Withers and Young (1971) showed enhancement on the steam side in the range of 35 to 50%. Mehta and Rao (1979) reported a maximum enhancement in the condensing coefficient of 38% . This type of enhancement has already been used in an existing power plant (Boyd et al. (1983)). Rabas (1987) published a review of several data sets for steam condensation on roped tubes. The data sets reflected an appreciable enhancement in the condensation coefficient for a groove pitch of about 2.0 mm. Rabas (1987) refers to a report by Tapprogge (1986) who recommended a groove pitch of at least 4.0 mm for effective ball cleaning. However, at a groove pitch of 4.0 mm, roped tubes offer a small enhancement on the steam side. This led Rabas (1987) to propose the design of

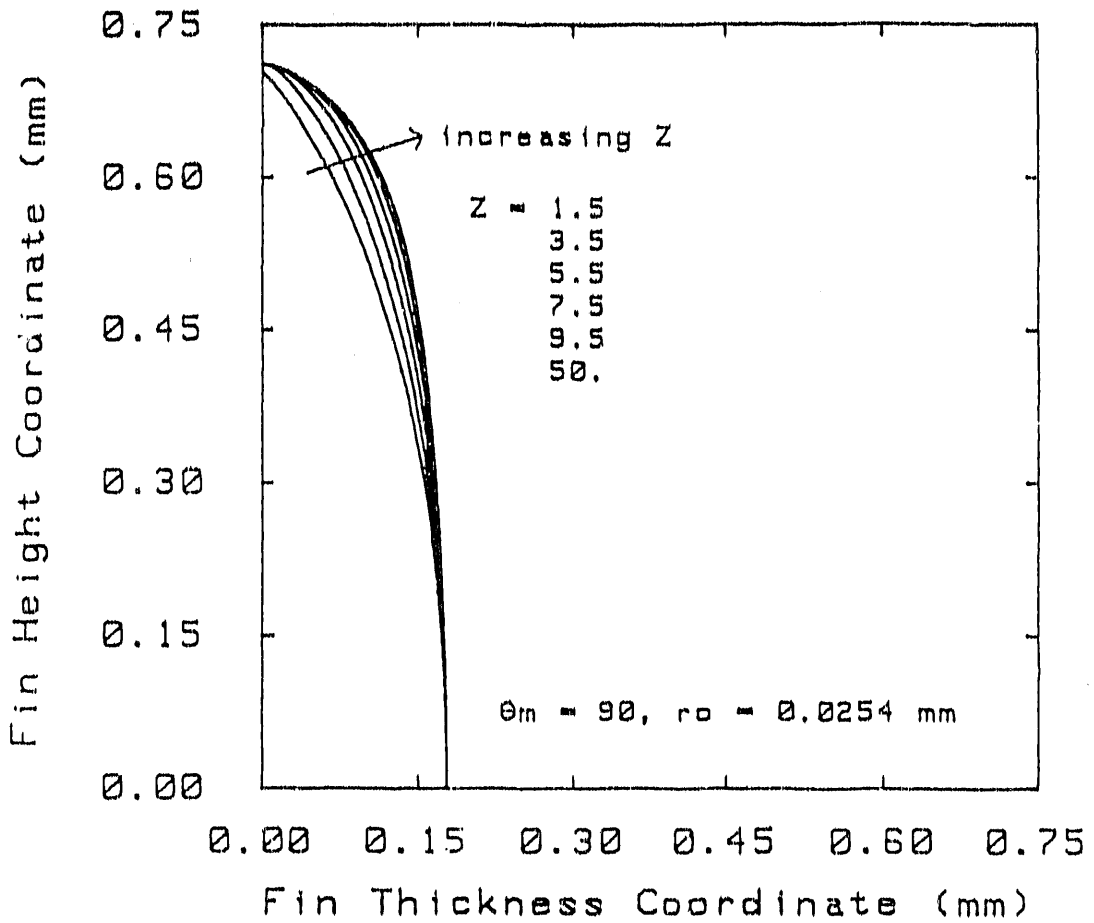

Figure 2.8. Cross section of Kedzierski-Webb profile for different values of the parameter Z. Kedzierski and Webb (1988).

Table 2.2

Comparison of the hS_m value for the Gregorig, Adamek, and K-W profiles.

Profile	Parameter	e	t_b	hS_m
-	-	mm	mm	W/m-s
Gregorig	ξ = 2	0.28	0.356	5.31
Adamek	ξ = -0.78	1.45	0.356	9.45
K-W	Z = 10	1.45	0.356	8.45

(Tip Radius = 0.025 mm)

condensers (with roped tubes, p ≥ 4.0 mm) assuming no enhancement on the steam side. In 1980, the Tennessee Valley Authority (TVA) retubed the Gallatin unit 1 main condenser with corrugated tubes. A sample of tubes were instrumented and the testing period ran for more than one year. Boyd et al. (1983) reported a maximum increase of the overall heat transfer coefficient of 43% (when no fouling was on the tubeside). The enhancement decreased as the fouling increased during the one year test period. However, substantial economic savings were achieved.

A modified version of the corrugated tube was introduced by Yorkshire (1973) known as MERT (Multi-Enhanced-Roped-Tube). The tube is made by creating fine grooves on the corrugation. Rabas (1987) report an enhancement on the steam side of as much as 100%; however, there are no data available in the literature to support this claim. The demand for such a tube was very low and one of the reasons is because of the high cost of manufacturing (10 to 15% higher than corrugated tube) as reported by Yorkshire (1988). A more rigorous analysis is required to determine the feasibility of this type of tube enhancement.

Notaro (1979) described a new enhancement technique in a U.S. patent. It constitutes of a coating of spherical particles that are uniformly distributed over the tube surface. The particle size range was 0.25 to 1.0 mm. A 6.0 m long vertical tube and 50% density of 0.5 mm diameter spheres yielded an enhancement level of 17 times the Nusselt prediction for a smooth tube. Fenner and Ragi (1979) reported

results for condensing R-12 in a vertical tube with "sand-grain" type roughness. Enhancement levels of 2.4 and 4.0 were obtained for low and high exit qualities, respectively. There is apparently no published data available in the literature, for which the coated surface technology has been tested for condensation on horizontal tubes.

2.3 Prediction of Condensation on Integral Fin Tubes

2.3.1 Survey of Models

In 1948, Beatty and Katz (1948) published the first analytical investigation to model film condensation on horizontal integral fin tubes. Their model is basically a combination of vertical flat plate and horizontal tube Nusselt analysis. The condensate film on the fin was modelled using the Nusselt equation for a gravity drained film on a vertical plate. The condensation in the interfin space was modelled using the Nusselt equation for gravity drained film on a horizontal smooth tube of diameter D_r. The weighted average heat transfer coefficient is expressed as:

$$h_{BK} = \eta_f h_f \frac{A_f}{A} + h_r \frac{A_r}{A} \qquad [2.3]$$

where h_r and h_f are the Nusselt condensation heat transfer coefficient for a

horizontal tube and vertical plate, respectively. The authors used a coefficient of 0.689 instead of 0.725 for the constant term in the expression for condensation on horizontal tubes. With the modified coefficient they predicted their experimental data, consisting of six low surface tension fluids and high fin spacings (433 to 630 fpm) within ±10%. The model did not take into account condensation on the fin tips, neglected surface tension forces on the fin, and did not take into account condensation on the flooded part of the tube. According to Rudy and Webb (1985), the last two effects produced compensating error which is why the model gave good predictions.

The first theoretical study of condensation on surface tension drained convex surfaces was carried out by Gregorig (1954). The analysis assumes a pure surface tension flow of the condensate (i.e no gravity effects). Using a Nusselt type analysis, he derived an expression for the local film curvature and by specifying a constant film thickness. A closed form expression for the film thickness was obtained from which the heat transfer coefficient is obtained from $h = k/\delta$. The specification of a constant film thickness was arbitrary. Kedzierski (1987) has experimentally verified the Gregorig (1954) analytical solution. Zener and Lavi (1974) specified a constant pressure gradient, which resulted in a convex surface that produced 15% higher heat transfer coefficient than the convex profile of Gregorig (1954). Kedzierski (1987) provides a survey of convex profiles that were proposed by other authors.

Surface tension effects on horizontal integral fin tubes were studied by Karkhu and Borovkov (1971). In their analysis, they assumed a surface tension induced constant pressure gradient acting along the fin side down to the condensate level in the interfin space where no condensation occurs. This gradient, per unit length, is given by:

$$\Delta p = \frac{\sigma \cos \theta}{R_t (e - \Delta)} \qquad [2.4]$$

where Δ is the condensate thickness in the interfin space and θ is the angle between the fin side and the vertical. The effect of surface tension on condensation heat transfer was analyzed by selecting three tubes with fin geometries that will ensure a surface tension controlled flow for steam and R-113 condensation. By solving the momentum and energy equations, an expression for the local film thickness on the fin side was obtained. Variation of the condensate thickness, Δ, was derived from the momentum equation taking into account the condensate flow from the fin side. The numerical results agreed with the experimental data to within ±5%. The model is limited to the geometry used and conditions present. That is, it was not tested for the case of large fin spacings where the interfin space in the unflooded region offers an appreciable contribution to the heat transfer process.

Edwards et al. (1973) presented an analytical model for the condensation on

grooved tubes. They divided the finned area into two parts, the fin tips and trough. By assuming laminar flow in the trough, momentum and energy balances resulted in a differential equation that was solved numerically to obtain an average heat transfer coefficient for the trough. For condensation on the tip, Edwards et al. (1974) assumed negligible condensation on the fin side and treated the heat transfer process as a one dimensional conduction through the film. This assumption will lead to underestimating the heat transfer on the fin since a surface tension region exists at the fin tip which provides an appreciable contribution to the heat transfer. Their model does not take into account condensation in the flooded region. The model was used to study steam condensation on a 1.0 in O.D. copper tube with a range of 24 to 96 grooves per inch and a titanium tube of the same O.D. with 96 grooves per inch. The predictions for the tube performance took into account the row effect. The numerical results show a strong dependence on tube thermal conductivity. The copper tube produced an enhancement level four times that of the titanium tube. For the copper tubes, the authors propose a fine groove pitch (48 groove per inch) for low overhead drip rates in actual condensers and a coarser pitch (e.g. 24 groove per inch) for high overhead drip rates. They also claimed that a threaded titanium tube produces a better performance than a smooth tube but do not show any quantitative comparison.

Zozulya, Karkhu, and Borovkov (1977) introduced a slight modification to the Karkhu and Borovkov (1977) model and applied it to a larger data set. The data

were predicted within ±15%. It should be noted that both the original and modified models apply only for the cases of surface tension controlled flow on the fin (e.g. Bo < 0.1) and small fin spacings where the interfin space is ineffective.

Rifert et al. (1977) proposed a model to predict the performance of fluted surfaces, and wires fastened to the tube surface. The authors propose a model for the attached wires by postulating that the condensate flows, under surface tension forces, from the tube surface (interwire space) towards the bottom of the wires and then drained by gravity. They derived an expression for the film thickness variation from the mid point of the interwire region to the edge of the drainage channel taking into account a finite film thickness at the midpoint. However, they do not give a method to determine this length or the boundary between the two regions (refer to Figure 2.9). Using their theoretical analysis and a data set for steam, the authors showed that by neglecting the existence of the flooded region and condensation in the thick film region (drainage channel at wire base), the heat transfer coefficient will be overestimated by as much as a factor of 2. Study of the flooding characteristics of fluted fins and attached wires show that the fluted surfaces had a larger flooded area than attached wires. This implies that one can expect to have a higher heat transfer coefficient with wires for the same S_m as a fluted surface.

Rifert (1980) presented an analytical model to solve the conjugate heat transfer problem between a condensing vapor and cooling liquid. The basis of the

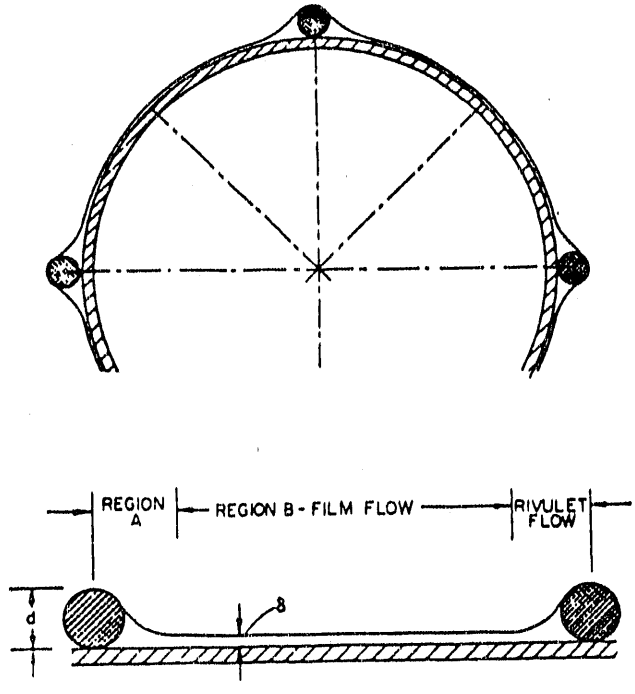

Figure 2.9. Wires fastened to tube surface showing the resulting thin film region in the interwire space. Zozulya et al. (1977).

model is solving the conduction equation with non-linear boundary conditions for condensate flow over the fin surface. A 2-D and a 3-D model were suggested for vertical and horizontal tubes, respectively. No comparison was made between numerical predictions and experimental data.

Rudy and Webb (1981) presented a detailed study of liquid retention encountered on integral fin tubes. They modified the Beaty and Katz theory (1948) to account for the flooded area as given by Equation [2.5]:

$$h = h_{BK}(1 - c_b) \qquad [2.5]$$

where h_{BK} is given by Equation [2.3]. The authors found that even with this modification the experimental data (for R-11) was underpredicted by as much as 30%. Therefore, they proposed that surface tension plays an important role in the condensation process on the fin.

Adamek (1981) defined a family of condensate film profiles. The radius of curvature was given as:

$$\kappa(x) = \begin{cases} \kappa_o - ax^{\xi} & 0 < \xi < \infty \\ ax^{\xi} - \kappa_o & -1 < \xi < 0 \end{cases} \qquad [2.6]$$

Figure 2.10 shows the family of profiles generated by Equation [2.6]. The surface tension induced pressure gradient can be expressed in terms of the condensate curvature as:

$$\frac{dp}{ds} = -\sigma \frac{d\kappa}{ds} \qquad [2.7]$$

Using Equations [2.6] and [2.7], the momentum equation, and a Nusselt type analysis, Adamek (1981) derived the expression for the local film thickness as:

$$\delta(s) = 1.86 \frac{C S_m^{\xi+1} s^{2-\xi}}{\theta_m (\xi + 1)(\xi + 2)} \qquad [2.8]$$

If $\theta_m = \pi/2$, then for $\xi = 2$ and $\xi = 1$, the Gregorig (1954) and Zener and Lavi (1974) condensate profiles are established, respectively. An optimal ξ that gives the maximum heat transfer coefficient was found to be $\xi = -0.5$. Webb (1988) presents a critical evaluation of the practical significance of the Adamek (1981) profiles.

Webb, Keswani, and Rudy (1982) performed an experimental investigation of surface tension forces by condensing R-12 on the face of a 51.0 mm O.D. cylinder with fins on one face. Table 2.3 shows the orientation and fin characteristic lengths used in the experiment. The tilt angle, θ, was defined as the angle the cylinder axis

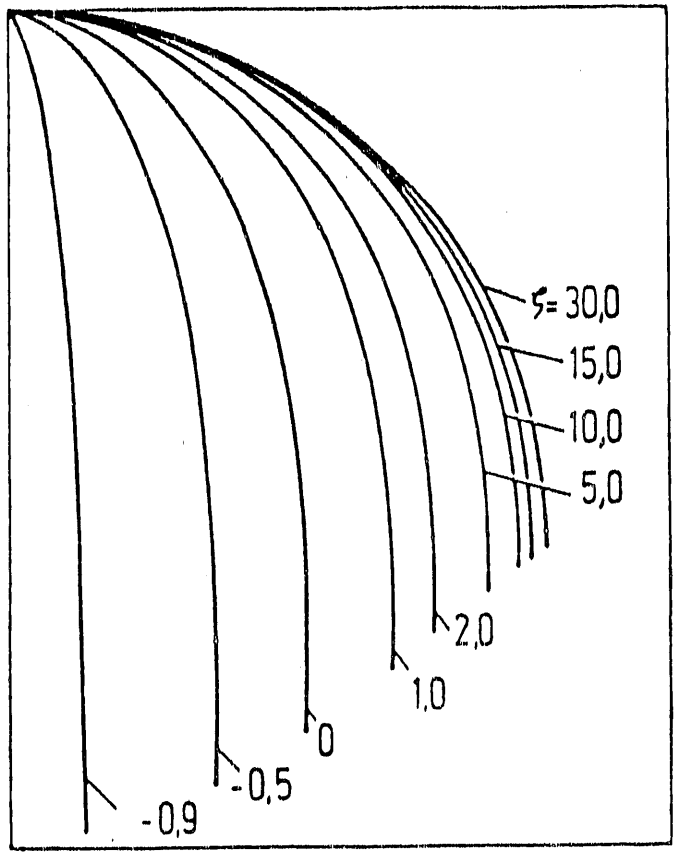

Figure 2.10. Cross section of the Adamek profiles for different values of ξ. Adamek (1981).

Table 2.3

Orientation of fins as tested by Webb, Keswani and Rudy (1982)

θ, deg	β, deg	L_c, mm
90	0	25.4
90	45	25.4
50	0	1.58
60	0	1.60

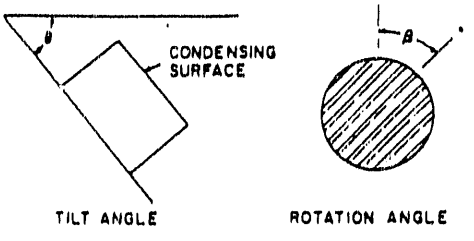

makes with the horizontal. The rotation angle, β, was defined as the angle the cylinder face makes with the vertical. Webb, Keswani, and Rudy (1982) found that the fin condensing coefficient is almost independent of orientation and that the data were under predicted by 70% when the Beaty and Katz (1948) model was used. The experimental study confirmed that film flow over the fins is not governed by gravity alone. Based on this confirmation, Webb, Keswani, and Rudy (1982) assumed a linear surface tension model similar to that used by Karkhu and Borovkov (1971). This model underpredicted their R-12 data by 10%.

Rudy and Webb (1983) derived a modified Beaty and Katz (1948) model and used it to predict the performance of horizontal commercial integral fin tubes with R-11 as the condensing fluid. They assumed a linear surface tension force acting along the fin height, similar to the analysis of Karkhu and Borovkov (1971). The mathematical form of the model is given by:

$$h = (1 - c_b)h_u + c_b h_f \qquad [2.9]$$

where h_u and h_f are the condensing coefficients in the unflooded and flooded regions, respectively. However, the authors assumed that h_f was negligible.

The model was found to best apply for fpm > 1200 and fin height e < 0.9 mm. For fpm < 1200 and e > 0.9 mm their model overpredicted the experimental

values by up to 60%. The overprediction for high fins was attributed to strong gravity forces comparable to the surface tension forces.

Owen et al. (1983) used a modified Beaty and Katz (1948) model to predict existing experimental data for several fluids including R-11 and R-12. They took into account condensation in the flooded region on the fin tips and interfin space. The form of their predictive equation is the same as that of Equation [2.9]. However, the condensing coefficient, h_u, was based on the Nusselt analysis for condensation on a vertical plate. The model predicted all of the considered data within ±30%.

Rifert et al. (1985) studied the effect of surface tension on the heat transfer coefficient of threaded fins and attached wires on vertical tubes. An analytical expression for the condensate thickness was obtained assuming a surface tension controlled flow. The authors found that the assumption of zero film thickness at the tip of the fin ($\delta_{s=0} = 0$) leads to underestimating the film thickness near the fin tip hence overestimating the heat transfer coefficient in that area. Based on their calculations, the authors concluded that the film thickness, along the fin side, is governed by fin curvature at s = 0 and the radius of transition between the thin and thick film regions on the fin side. They therefore sought a particular form of the solution as:

$$\delta(s) = a(b - s)^c \qquad [2.10]$$

where a, b, and c are constants determined from the differential equation and boundary conditions (that describe the local film thickness). Comparing Equation [2.10] with the numerical solution of the differential equation that describes the condensation process on the fin side, they found good agreement. However, no comparison was made between numerical predictions and experimental data.

Webb et al. (1985) proposed a model to predict the condensing coefficient on integral fin tubes. The mathematical form is given as:

$$\eta h = (1 - c_b)(h_r \frac{A_r}{A} + \eta_f h_f \frac{A_f}{A}) + c_b h_b \frac{A_r}{A} \qquad [2.11]$$

The fins were trapezoidal in shape, typical of commercially available tubes. This model uses Adamek (1981) profiles to model the condensate film shape, as opposed to the linear surface tension force assumption. The fraction of the tube flooded, c_b, was obtained from the analytical expression of Rudy and Webb (1985) (Equation [2.1]). An iterative scheme was used to determine the appropriate ξ profile for the given fin geometries and operating conditions. Hence, h_f is calculated by Equation [2.8]. The condensing coefficient in the interfin space in the unflooded region, h_r, is calculated by the Nusselt equation for condensation on a smooth surface of diameter D_r. The calculation of h_r takes into account the amount of condensate flowing from

the fin down to the interfin region. An iterative solution is required, the details of which are given by Webb et al. (1985). The parameter h_b accounts for condensation on the interfin region in the flooded region. By using a 2-D conduction model, Webb et al. (1985) concluded that h_b can be neglected. The tubes tested were made of copper with 19.0 mm diameter (over the fins), 748 fpm to 1378 fpm, fin height from 0.85 mm to 1.53 mm, tip thickness between 0.20 and 0.28 mm, and base thickness between 0.29 mm and 0.42 mm. Table 2.4 shows the predictions for R-11 as the condensing fluid. The model predicted the data within ±20%. Note that condensation on the fin top, in the flooded region, was not accounted for. Hence, the model is not applicable to fully flooded conditions.

It is important to realize that the assumption of surface tension controlled flow is based on the condition that Bo << 1, i.e., surface tension forces are much greater than gravity forces. If this condition is not met, then assuming a surface tension controlled flow will lead to overestimating the condensing coefficient.

There have been recent publications of comprehensive models describing the flow and heat transfer process on integral fin tubes. The Honda and Nozu (1987a,1987) and Adamek and Webb (1990) models are of particular interest and therefore will be discussed in separate sections.

Table 2.4

Predictions of average condensation coefficient as reported by Webb, Rudy, Kedzierski (1985).

fpm	748	1024	1378
ξ	-0.857	-0.771	-0.843
c_b	0.223	0.287	0.338
$h(W/m^2)$	9197	11963	13552
h_{pred}/h_{exp}	1.14	1.00	0.84

2.3.2 Honda and Nozu Model

The basis of the model involves the division of the tube circumference into two regions (i) unflooded - u, and (ii) flooded - f. The model accounts for different wall temperatures in the 'u' and 'f' regions. The objective of the problem is to determine the condensing coefficient of the enhanced tube by the following equation:

$$h = \frac{h_u \eta_u (1 - c_b)\Delta T_u + h_f \eta_f \Delta T_f c_b}{(1 - c_b)\Delta T_u + c_b \Delta T_f} \qquad [2.12]$$

where h_i is the Nusselt number in region i (i = u, f), c_b is the fraction of tube flooded, ΔT_i is the vapor to wall temperature difference at the fin root in region i (i = u, f), η_i is the fin efficiency in region i. The problem becomes one of calculating the different parameters that appear in this equation.

Analytical expressions for the fin efficiency, in the unflooded and flooded regions, were presented for rectangular fins only. The average wall temperature in the unflooded and flooded regions is obtained by solving the 2-D conduction equation in the circumferential direction. The analytical solution is given by Honda et al. (1987a).

The shape of the film, in the unflooded region, has been divided into three possible cases, A,B, and C as shown in Figure 2.11. The film itself can have up to four regions starting from $x = 0$ to $x = x_b$. The root surface is also divided into two regions. All or some of the regions may exist depending on fin geometry and condensate flow rate. Each one of these regions is governed either by surface tension or gravity forces.

Honda et al. (1987a) numerically solved the differential equation that describes the film behavior along the fin from $x = 0$ and $x = x_b$. Results of the numerical solution have shown that there may exist two regions of surface tension controlled flow between $x = 0$ and $x = x_b$. The first region is at the fin corner and the second just before $x = x_b$. The existence of this second region depends on the fin geometry and condensation rate. In the same publication, the authors presented an approximate method based on the results of the numerical solution. This approximate method was later modified in their 1987 paper. The authors use a constant pressure gradient in the surface tension controlled region(s). Moreover they differentiate between fin radius (or length) and the film radius (or length). This is a unique feature of the model although it leads to more complexity.

In their 1987a paper, Honda and Nozu assumed that the film behavior in the root region is identical to that on the fin side. Honda, Nozu, and Uchima (1987) provide a separate solution for condensation in the interfin space in the unflooded

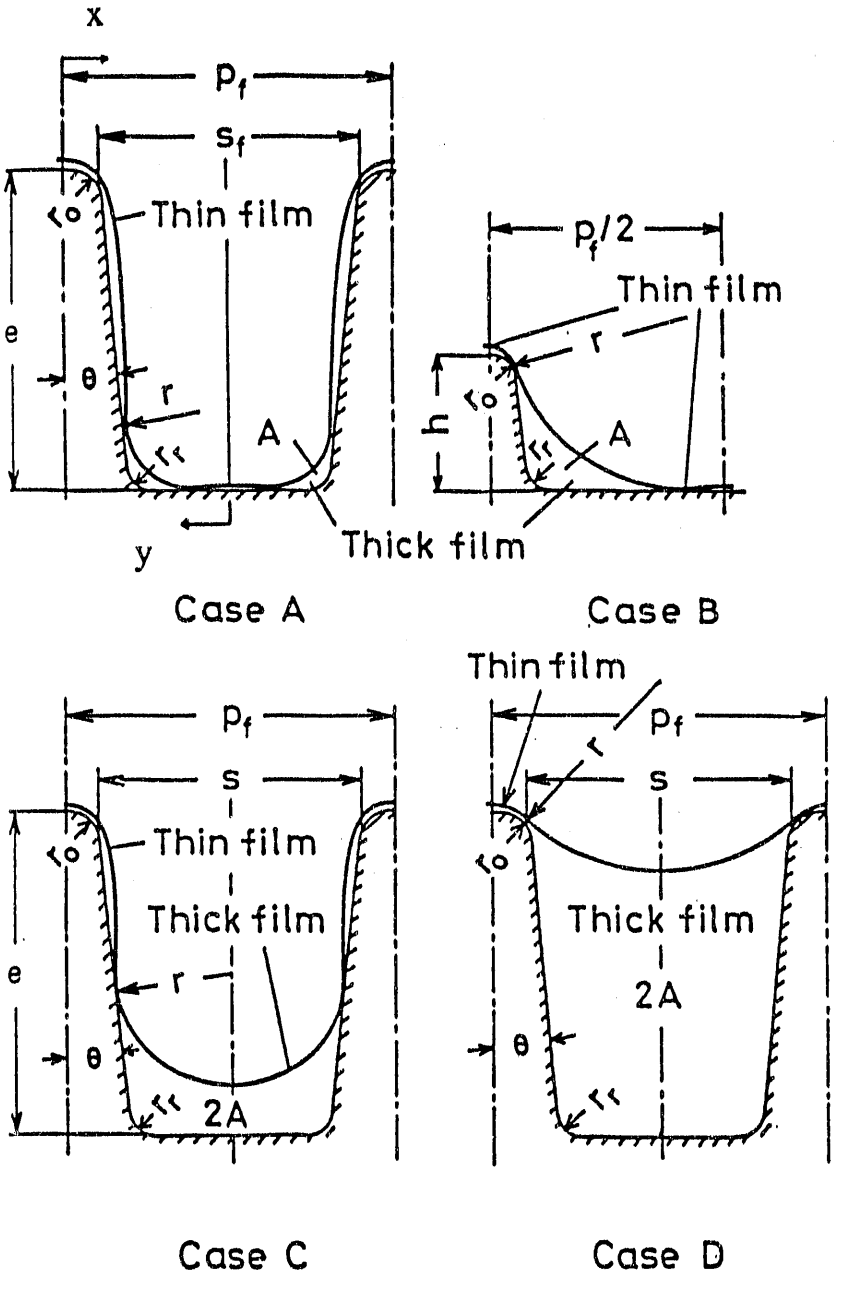

Figure 2.11. Physical representation of the Honda and Nozu model. Honda and Nozu (1987).

region by solving the differential equation for laminar film condensation on a horizontal smooth tube. This modified version divides the interfin space into two subregions, the thick film subregion (governed by gravity forces), and the thin film subregion (governed by surface tension forces). The Nusselt number in each subregion is calculated by an approximate equation based on the numerical solution of the differential equation. The existence of a thin film in the interfin region has already been justified experimentally by Hirasawa et al. (1980). They postulated that the pulling force (induced by surface tension) in the direction of the fin root is responsible for this thin film subregion.

For the flooded region, the model neglects condensation on the interfin space but assumes that condensation does occur on the fin tip. The authors proposed the use of the two region model, Figure 2.12 case D, and neglected gravity forces.

The model was used to predict the steam condensation data, for vacuum and atmospheric conditions, that were obtained by Wanniarachchi et al. (1985). The model predicted the vacuum data well within ±20% but underpredicted the atmospheric data by 10 to 30%.

For tubes with porous drainage strips, Honda and Nozu (1985) used Equation [2.12] to calculate the average heat transfer coefficient of the tube, but derived a modified equation for the flooding angle, ϕ_f. The authors used Darcy's law to

express the pressure gradient within the porous drainage strip. A balance between gravity and surface tension forces resulted in a modified form of the equation for the flooding angle (or c_b).

2.3.3 Adamek and Webb (1990) Model

In this model, the tube is divided into two regions, the flooded and unflooded. It is based on dividing the fin surface and interfin space into regions, where either surface tension or gravity is the controlling driving force. The model does not differentiate between fin length and film length except at the corner of the fin tip. Moreover, it does not account for circumferential wall temperature variation. Figure 2.12 shows the details of the physical model for the unflooded region.

The model uses the Nusselt analysis for gravity drained condensation in the regions where gravity is the controlling force, and a constant pressure gradient (induced by surface tension forces) in the regions where surface tension is the controlling force. The local film thickness in region ij can be written in a general form as:

$$\delta_{ij}(t) = (a_{i-1} + bf_i t)^{1/4} \qquad [2.13]$$

where a_{i-1} accounts for condensate flow from region i-1 to region i (a_{i-1} can be zero),

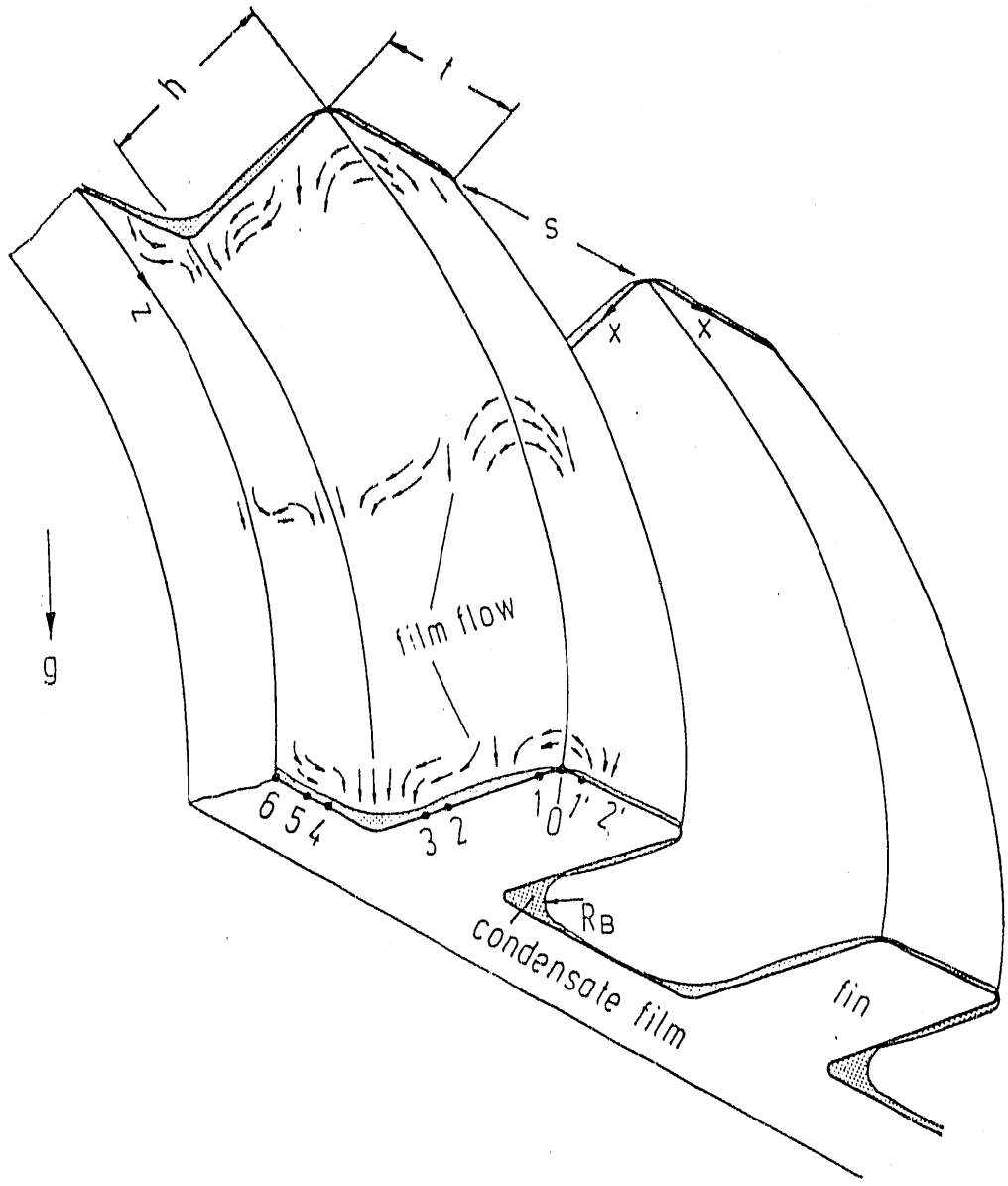

Figure 2.12. Physical representation of the Adamek and Webb model. Adamek and Webb (1990).

b is a property group, f_i is the driving force per unit volume in region i, and t is the direction of condensate flow (t = s or z). Once δ_{ij} is determined, the condensate flow rate can be determined by an energy balance.

The determination of the length of each region on the fin side and interfin space depends on the radius of the drainage channel at the fin base, R_D. This radius is a function of the circumferential coordinate z, and the condensate mass flow rates into the drainage area. Hence an iterative solution is required to calculate the length of each region along the circumference. The fin efficiency is different for each region due to the different heat transfer coefficients. At each position s, along the fin, $\Delta T = T_{sat} - T_w$ is calculated and the corresponding fin efficiency is evaluated using the force acting on the region. This implies a second iteration in the calculation procedure to determine the total mass flow rate on the fin.

A final observation on this model concerns the existence of the different regions. Depending on the fin geometry, fin distribution, and rate of condensation, the different regions may or may not exist. Adamek and Webb (1990) describe several modes that may exist on the fin side and interfin space.

The above discussion is for the unflooded region. For the flooded region, Adamek and Webb (1990) assume no condensation in the interfin region and along the fin side, but appreciable condensation on the fin tip. The same equations that

were derived for the fin top in the unflooded region are applicable to the fin top in the flooded region. Moreover, a 10% reduction in the effective heat transfer area in the flooded region is contributed to the dripping sites.

The model predicts the atmospheric steam data of Wanniarachchi et al. (1986), well within ±15% but overpredicts the vacuum data by as much as 22%. The overprediction at low fin spacings (large flooded area) could be caused by the fact that the model assumes that, in the flooded area, at the fin corner, a surface tension controlled flow exists all along the circumferential direction up to the dripping point.

2.3.4 Comparison of Honda/Nozu and Adamek/Webb Models

It is evident that the Honda and Nozu (1987) model is the most complete and rigorous, especially since it includes circumferential wall temperature variation and distinguishes between the film and fin lengths, but it is rather complex and cumbersome. Honda and Nozu (1987) presented two types of solutions. The first is a numerical one which solves the differential equations of the film shape and wall temperature by a numerical procedure for the top of the tube only. The second is a discretization method which divides the film shape into different regions where either a gravity or surface tension controlled flow is assumed. The expressions that determine the heat transfer in each region were based on the results of the numerical solution of the differential equation that describes the variation of the condensate

thickness. Honda and Nozu (1987) compared the two types and found that the results differ by no more than 5%.

The Adamek and Webb (1990) model is also based on discretizing the film shape into regions of gravity or surface tension controlled flow. The lengths of the regions and the corresponding condensation rates are derived from a purely analytical basis. As was shown above, the condensation rates are dependent on the drainage radius at the fin base. Once the converged value of this radius is established, the regional lengths and condensation rates are directly evaluated which makes this model simple to use. However, the Adamek and Webb (1990) model does not account for circumferential wall temperature variation.

CHAPTER 3

MATHEMATICAL MODELLING

This chapter is concerned with the development of a model to describe the condensation process on horizontal integral finned tubes. Different fin/channel shape combinations are considered. A computer code was developed, based on this model, to predict existing data and perform a parametric study to predict the influence of geometric variables, operating conditions, and tube material on the condensing heat transfer coefficient. The predictions and parametric results are presented in Chapter 5. The unique characteristics of this model, as compared to other models in the literature, is described in Chapter 9.

3.1 Introduction

There are several fin/channel combinations that have been introduced in the literature together with corresponding mathematical models. The present study considers six types of fin/channel combinations as illustrated in Figure 3.1. The profiled fins can be sinusoidal, Gregorig (1954), Adamek (1981), or Kedzierski-Webb (1989). The drainage channel can be either sinusoidal, circular, or flat. Commercial enhanced tubes usually have trapezoidal fins with circular drainage channels.

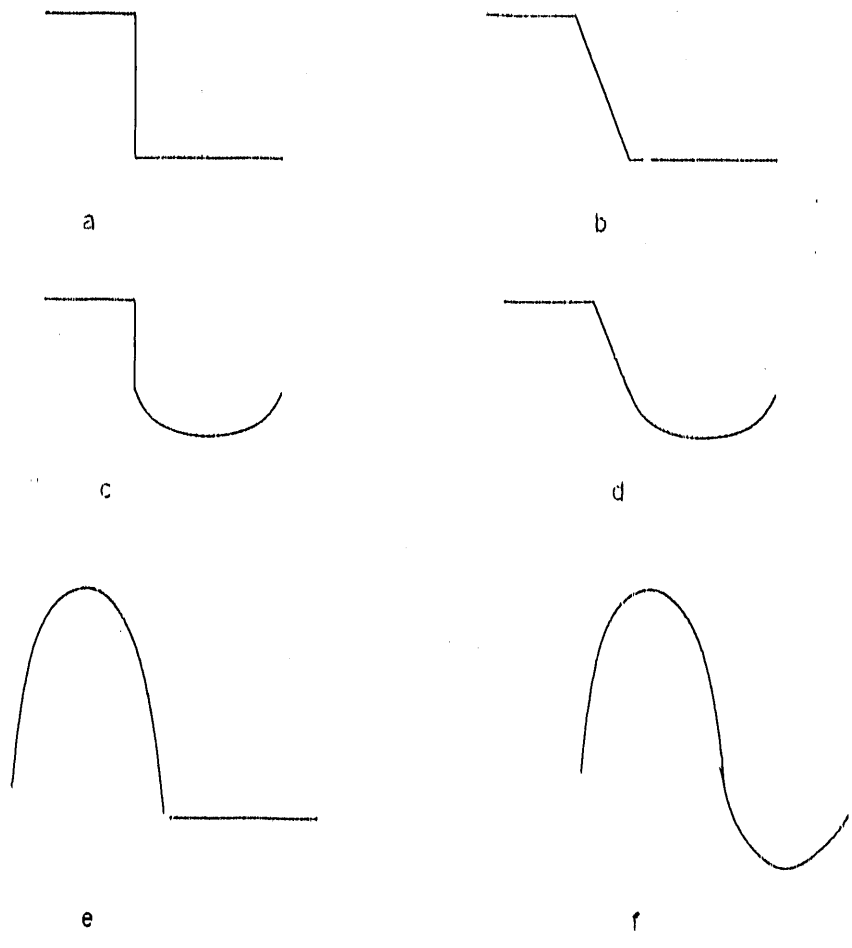

Figure 3.1. Possible fin/channel combinations.

The condensation process on the profiled fins, fin top and side of trapezoidal and rectangular fins can, in general, be described by solving the Navier-Stokes and energy equations. The condensate flow on the fin is assumed to be the same as that shown in Figure 2.12. The equations for the fin side will be described in the coordinate system defined in Figure 3.2. By invoking the boundary layer conditions it can be shown that the momentum and energy equations will reduce to the following:

$$\mu\frac{d^2u}{dy^2} + \rho g = 0 \qquad [3.1]$$

$$\mu\frac{d^2w}{dy^2} - \frac{dp_l}{dy} = 0 \qquad [3.2]$$

$$k\frac{d^2T}{dy^2} = 0 \qquad [3.3]$$

The pressure p_s is that due to surface tension and is given by Batchelor (1967), as:

$$p_l = \frac{-\sigma\left(\frac{\partial^2\delta}{\partial s^2}\right)}{\left[1 + \left(\frac{\partial\delta}{\partial s}\right)^2\right]^{3/2}} + p_{sat} \qquad [3.4]$$

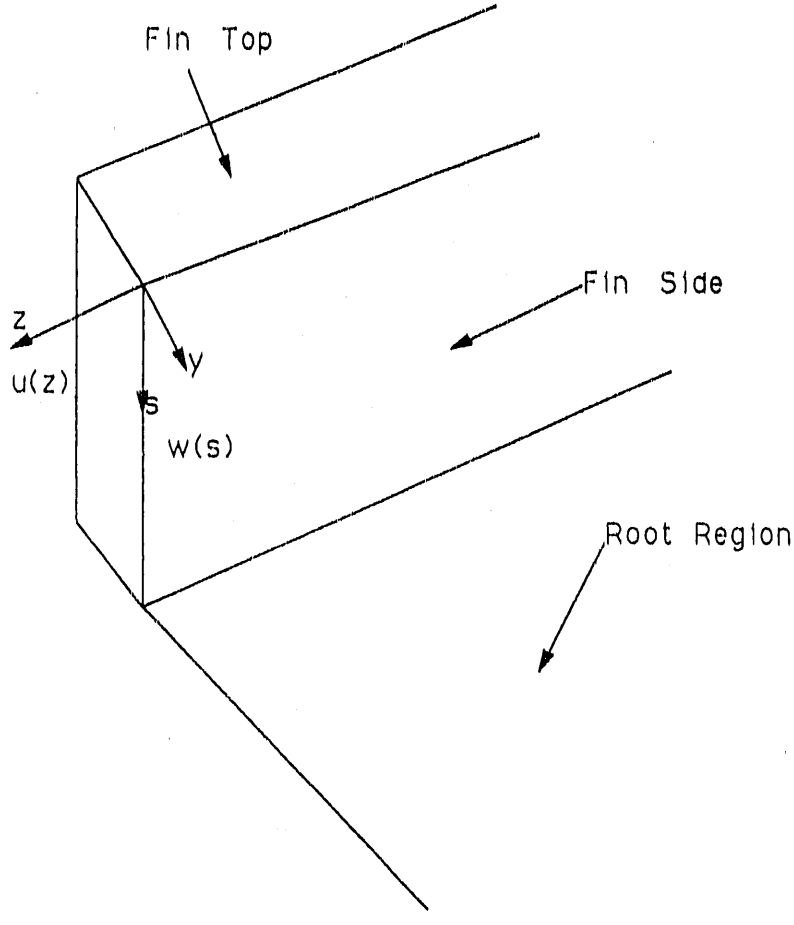

Figure 3.2. Coordinate system

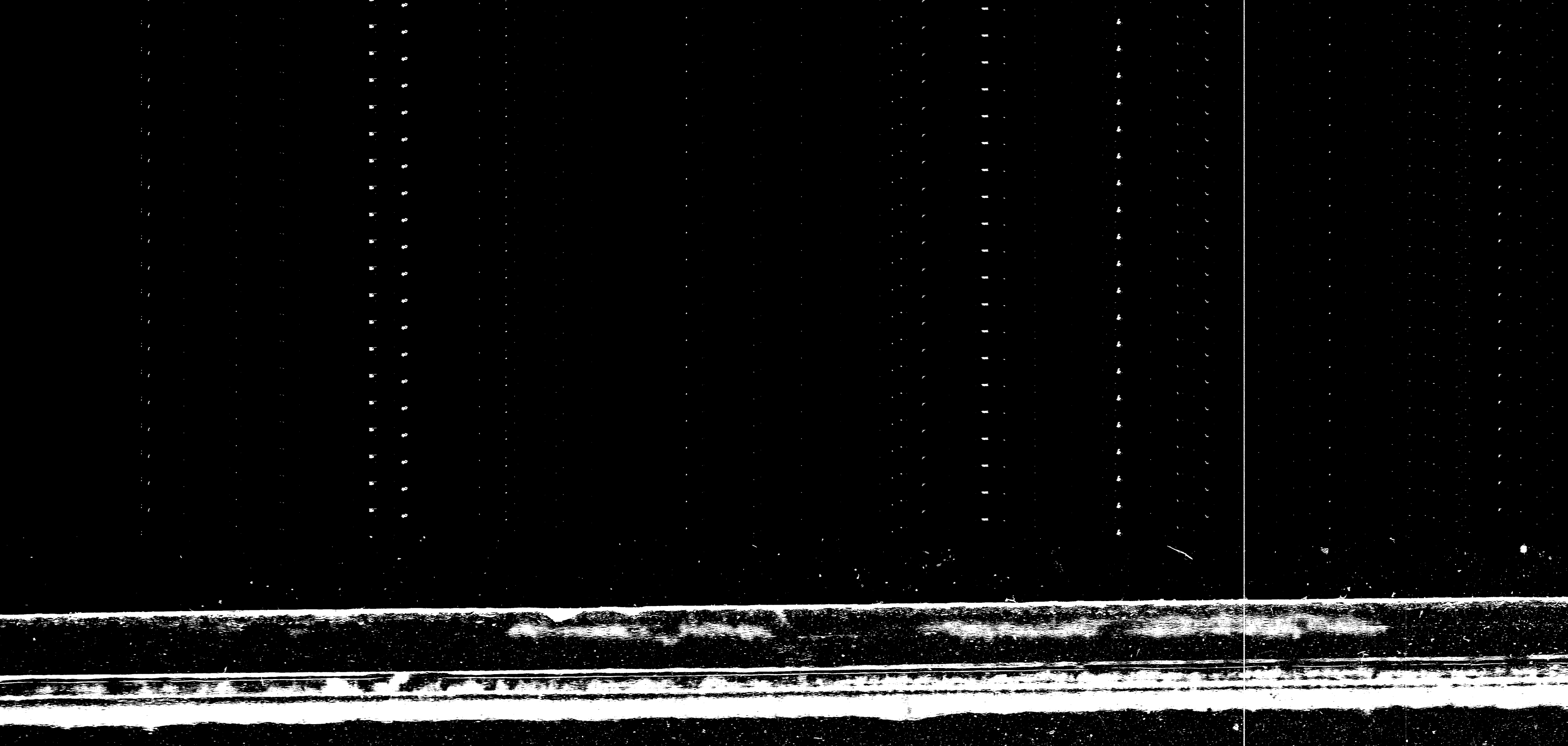

where ∂ is the local film thickness.

A fourth equation can be written for the interface which relates the heat transfer across the film to the rate of condensation. This heat balance is represented by:

$$\frac{\partial}{\partial z}\int_0^{\delta} u\,dy + \frac{\partial}{\partial x}\int_0^{\delta} w\,dy = \frac{k}{h_{fg}\,\rho}\left[\frac{\partial T}{\partial y}\right]_{y=\delta} \qquad [3.5]$$

The boundary conditions are:

$$y = 0, \quad u = 0 \qquad w = 0, \quad T = T_w \qquad [3.6]$$

and at y = δ,

$$\frac{\partial u}{\partial y} = 0, \quad \frac{\partial w}{\partial y} = 0, \quad T = T_{sat} \qquad [3.7]$$

By integrating the momentum and energy equations and applying the above boundary conditions, the following equation results:

$$\frac{\rho g}{3\mu}\frac{\partial \delta^3}{\partial z} + \frac{\sigma}{3\mu}\frac{\partial}{\partial x}\left[\delta^3\frac{\partial p}{\partial x}\right] = \frac{k\Delta T}{\rho h_{fg}\delta} \qquad [3.8]$$

Several authors such as Hirasawa et al. (1980) and Honda and Nozu (1987a) have solved the above set of equations, to determine the film thickness along the fin side, using finite difference techniques. The authors, however, have used different boundary conditions depending on their assumptions regarding the structure of the film and the number of subregions that exist on the fin side.

For flat drainage channels, it is possible to use a similar set of differential equations to describe the condensation process in that region.

3.2 Qualitative Description of the Model

As shown by Rudy and Webb (1981), the existence of fins on a horizontal tube creates a flooded region due to surface tension forces acting along the fin sides and the tube surface. This phenomenon results in two distinct regions, in the circumferential direction, each characterized by different (T_s - T_w) and active area available for condensation. Therefore, the tube was divided into the unflooded (u-region) and, flooded (f-region) regions, with the boundary between them defined by c_b, the fraction of tube flooded. The equation for c_b will be presented later. The unflooded region consists of three subregions namely, the fin top, fin side, and interfin space. These three subregions form the active heat transfer area in the unflooded region. There is however, a drainage channel at the fin root which is inactive due to the thick liquid film. In the flooded region, only the fin top is

assumed to be active while the interfin space is flooded with condensate and hence heat transfer occurs by conduction through the film. Figure 3.3 shows the unflooded and flooded regions and the boundary between them defined by ϕ_f, the flooding angle. Note that c_b is defined as ϕ_f/π. Figure 3.4 shows the active area in the unflooded region with the drainage channel at the fin root. Figure 3.5 shows the film structure in the flooded part of the tube.

Because of the different heat transfer mechanisms in both regions, the tube wall temperature is expected to be different in the unflooded and flooded regions. This has already been demonstrated by wall temperature measurements taken by some authors, such as Rudy (1982) who condensed R-11 on copper integral fin tubes.

3.3 Assumptions

The model will be based on the following assumptions:

1. The condensing vapor is saturated and pure (no non-condensible gases).

2. Zero interfacial shear.

3. Constant vapor and film thermodynamic and transport properties in the

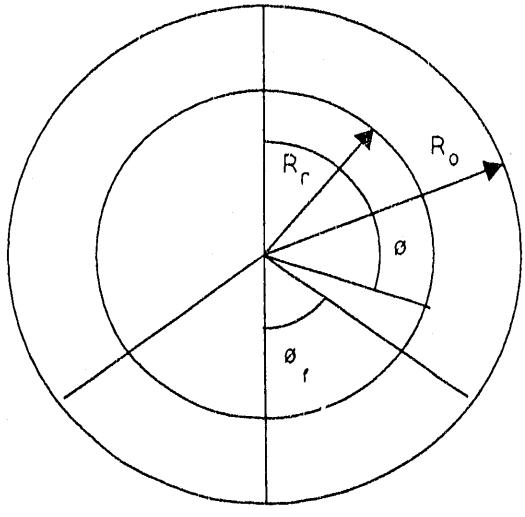

Figure 3.3. The unflooded and flooded regions

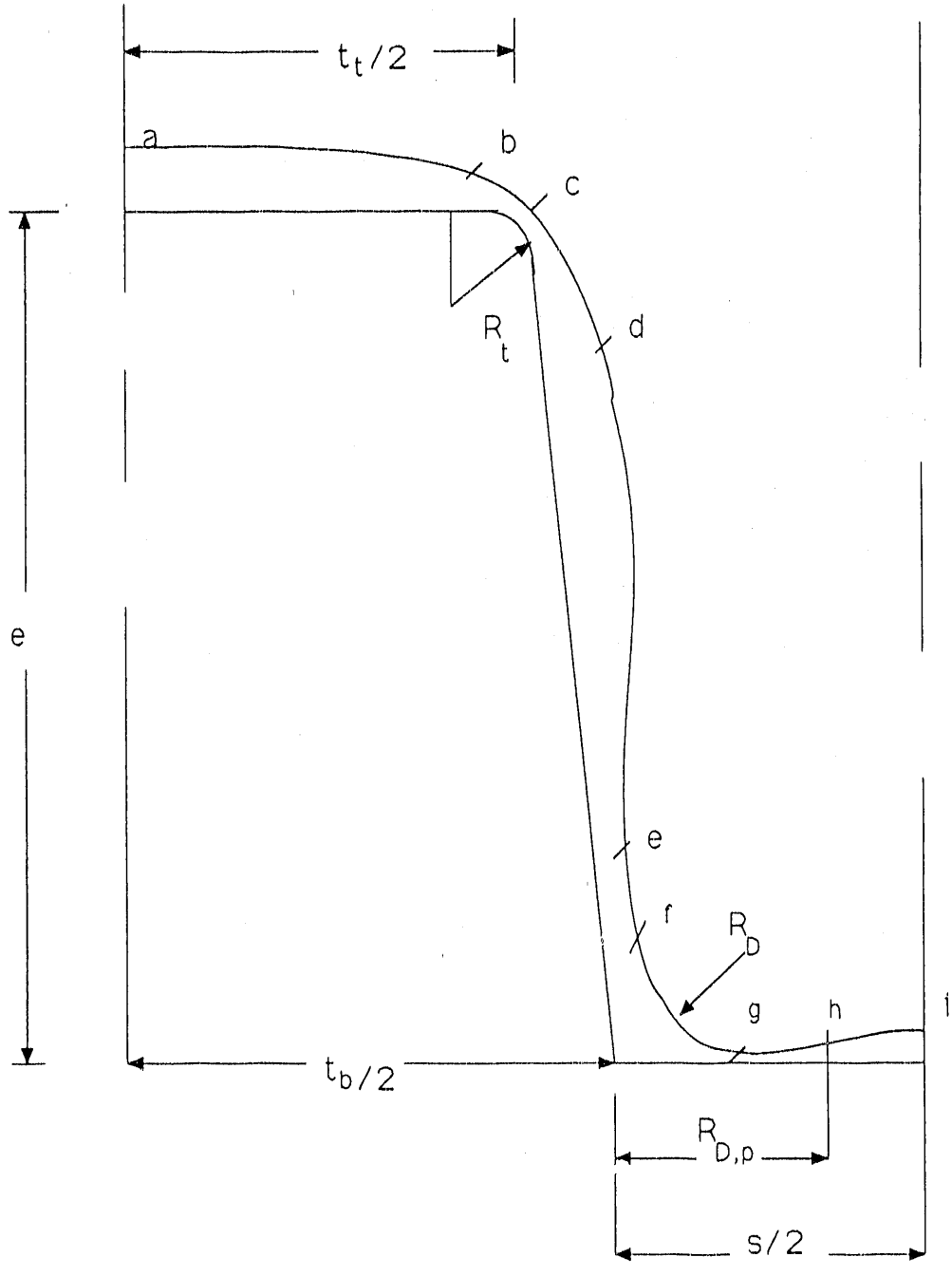

Figure 3.4. The film structure in the unflooded region

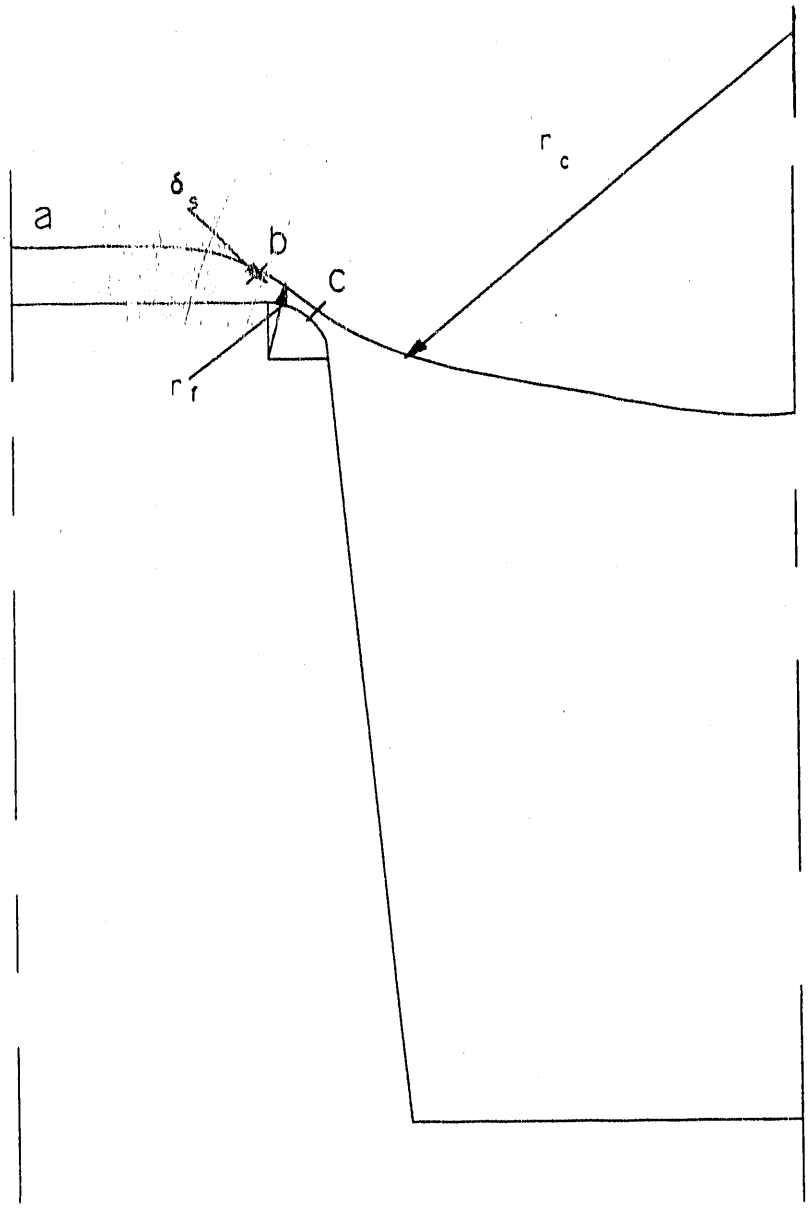

Figure 3.5. The film structure in the flooded region

unflooded and flooded regions.

4. The liquid film on the fin and tube surface is in the laminar regime.

5. The temperature gradient across the film is linear.

6. The fin height is very small compared to the tube radius.

7. Metallic surfaces are assumed to be smooth.

8. One dimensional heat conduction through the fin.

3.4 Theoretical Basis

To obtain a composite heat transfer coefficient for the tube, an energy balance between the condensing vapor and the tube wall, yields the following expression:

$$h = \frac{\eta_u h_u (1 - c_b)\Delta T_u + \eta_f h_f c_b \Delta T_f}{(1 - c_b)\Delta T_u + c_b \Delta T_f} \qquad [3.9]$$

which is identical to that used by Honda and Nozu (1987) (Equation [2.12]). Using

the index, i = u or f, the parameters in Equation [3.9] can be defined as follows: η_i is the fin efficiency, h_i is the condensing heat transfer coefficient, ΔT_i is the vapor to wall temperature difference, c_b is the fraction of tube flooded with condensate. This equation is general and holds for any tube diameter, fin shape, and operating conditions on the tube and shell side. The problem now is to determine the different parameters that appear on the right hand side of the above expression.

3.5 The Flooding Angle for 2-D Fins

A general expression for c_b, that holds for any 2-D fin shape was derived by Rudy and Webb (1985) and is given by:

$$c_b = \frac{1}{\pi}\cos^{-1}\left[1 - \frac{2\sigma(P - t_b)}{\rho g D_o (P_f e - A_p)}\right] \qquad [3.10]$$

where P is the wetted perimeter of fin cross section. For the case of a rectangular fin, Equation [3.10] reduces to:

$$c_b = \frac{1}{\pi}\cos^{-1}\left[1 - \frac{4\sigma}{(D_o s \rho g)}\right] \qquad [3.11]$$

3.5.1 The Flooding Angle for 3-D (Spine) Fins

Using an analysis similar to Rudy and Webb (1985), the flooding angle for 3-D (spine) fins can be obtained by the following equation:

$$c_b = \frac{1}{\pi}\cos^{-1}\left(1 - \frac{z_f}{R_o}\right) \qquad [3.12]$$

where

$$z_f = \frac{\sigma(P - P_f)}{\rho g(P_f' e - A_p)} \qquad [3.13]$$

and

$$P_L = 2e + s_b \qquad [3.14a]$$

$$P_f = t_t + s_b \qquad [3.14b]$$

$$P_f' = t_b + s_b + s_r \qquad [3.14c]$$

$$A_p = e(t_t + e\tan\theta) \qquad [3.14d]$$

The basic difference between the analysis of Rudy (1982) and the above expression is in the term P_f' that takes into account the additional space available for retaining liquid. The parameter z_f is the height of liquid retained by the 3D (spine) finned tube (measured from the tube bottom). The geometric parameters appearing in equations [3.14a] to [3.14d] are shown in Figure 3.6. Equation [3.12] was used to predict c_b for a 1378 fpm spine fin that was tested by Rudy (1985) for R-11, n-pentane, and water. Table 3.1 shows the geometry of the fin and the ratio of predicted to experimental values for the above three fluids. It is seen that Equation [3.12] predicts the data within +6% and -13%.

3.6 The Condensing Coefficient in the Unflooded Region.

The condensing coefficient in the unflooded region, h_u, is composed of three components:

1. The fin top component, h_{top}.

2. The fin side component, h_{sid}.

3. The interfin (or root) component, h_r.

The following analysis focuses on rectangular or trapezoidal fin shapes with a flat (no

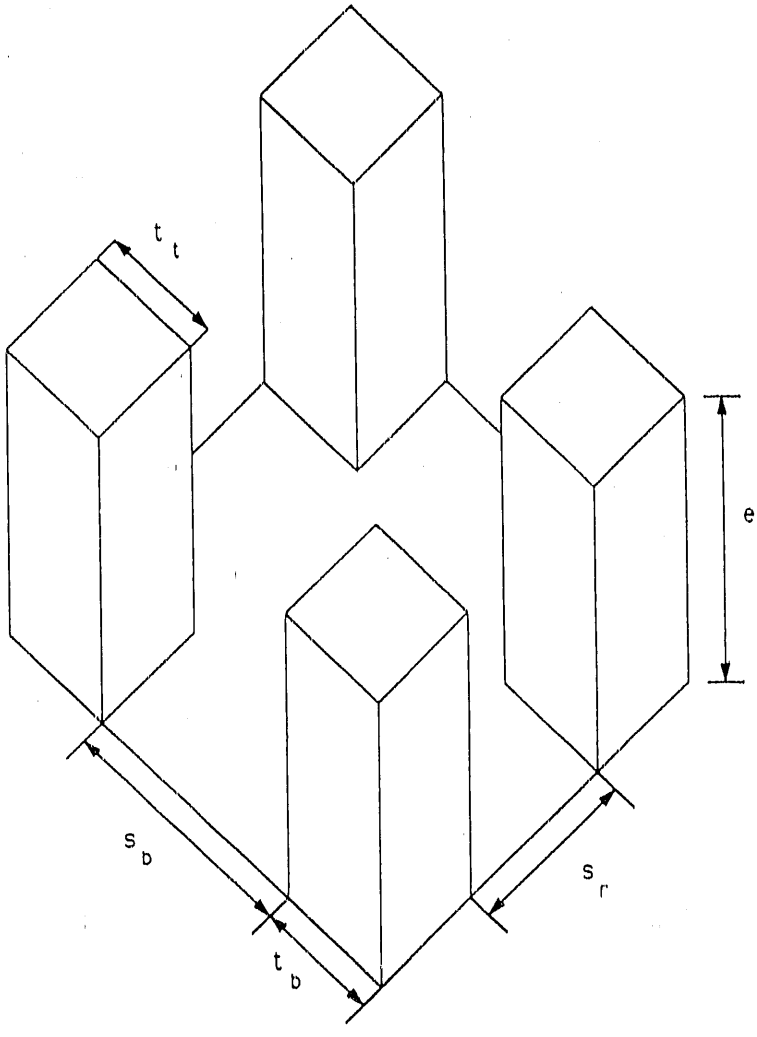

Figure 3.6. Schematic of spine fins

Table 3.1

Prediction of the flooding angle for the 1378 fpm spine finned tube

($t_t = t_b = 0.305$ mm, $s_t = 0.51$ mm, $s_b = 0.46$ mm, $e = 0.89$ mm)

Fluid	$\sigma/\rho \times 10^6$	$c_{b,pred}/c_{b,exp}$
R-11	10.0	1.06
n-pentane	20.0	0.87
water	73.8	1.01

curvature) in the root region, as shown in Figure 3.4.

3.6.1 Condensing Coefficient on the Fin Top, h_{top}

On the fin top, the film is assumed to be divided into two sub-regions, *ab* and *bc*, as shown in Figure 3.4. By making use of the symmetry of the fin, the sum of the lengths of these two sub-regions is equal to one-half the length of the fin tip. The condensate in sub-region *ab* is assumed to be driven by gravity forces and flows in the circumferential direction. The condensate in sub-region *bc* is assumed to be driven by surface tension forces and flows in the axial direction into sub-region *ab*. There are two alternatives to model the condensation process in sub-region *bc* and they are discussed below. The condensation coefficient on the fin top is determined as an area weighted average of the coefficients of both subregions.

3.6.1.1 Sub-region *ab*

The flow in this region is governed by gravity forces and the length of the gravity dominated film flow can be written as:

$$l_{ab} = t_t/2 - l_{bc} \qquad [3.17]$$

where l_{bc} is the length of subregion *bc* and is given in the following section. The

condensation coefficient in subregion *ab* is based on the Nusselt analysis for laminar film condensation on a horizontal tube of diameter D_o. In terms of the local angular coordinate, ϕ, the expression is given, according to Jacob (1949), as:

$$h_{ab}(\phi) = k/\delta_{ab}(\phi) \qquad [3.18]$$

where

$$\delta(\phi) = B(D_o/2)\psi(\phi) \qquad [3.19]$$

where B is a property group and $\psi(\phi)$ is defined as:

$$\psi(\phi) = \left[\frac{4}{3\sin^{4/3}\phi}\int \sin^{1/3}\phi\, d\phi\right]^{0.25} \qquad [3.20]$$

3.6.1.2 Subregion *bc*

The flow in this sub-region is governed by surface tension forces and can be modelled by two different methods.

(a) Alternative I

The surface tension induced pressure gradient is assumed to be constant with the film curvature varying linearly from $1/R_t$ to ∞ and the length of this sub-region is given by Adamek and Webb (1990) as:

$$l_{bc} = 2\omega R_t \qquad [3.15]$$

where ω is the angle swept by this subregion. Based on the assumption that the curvature in subregion *bc* varies linearly from $1/R_t$ to ∞, the area of the triangle shown in Figure 3.7 is equal to $l_{bc}/2R_t$. This area is equal to ω. The corresponding average heat transfer coefficient is obtained by averaging (over the length of sub-region *bc*) the expression for the local coefficient given by Adamek and Webb (1990). It is expressed as:

$$h_{bc} = 0.667\left[\frac{C}{\omega^2 R_t^3}\right]^{0.25} \qquad [3.16]$$

(b) Alternative II.

The condensation process on the fin top can also be modelled using a Kedzierski-Webb (1989) profile. By using this profile, the variation of the curvature of the film will be non-linear and hence closer to the real curvature of the film. This profile is defined by Equation [2.2] and is rewritten here as Equation [3.21]:

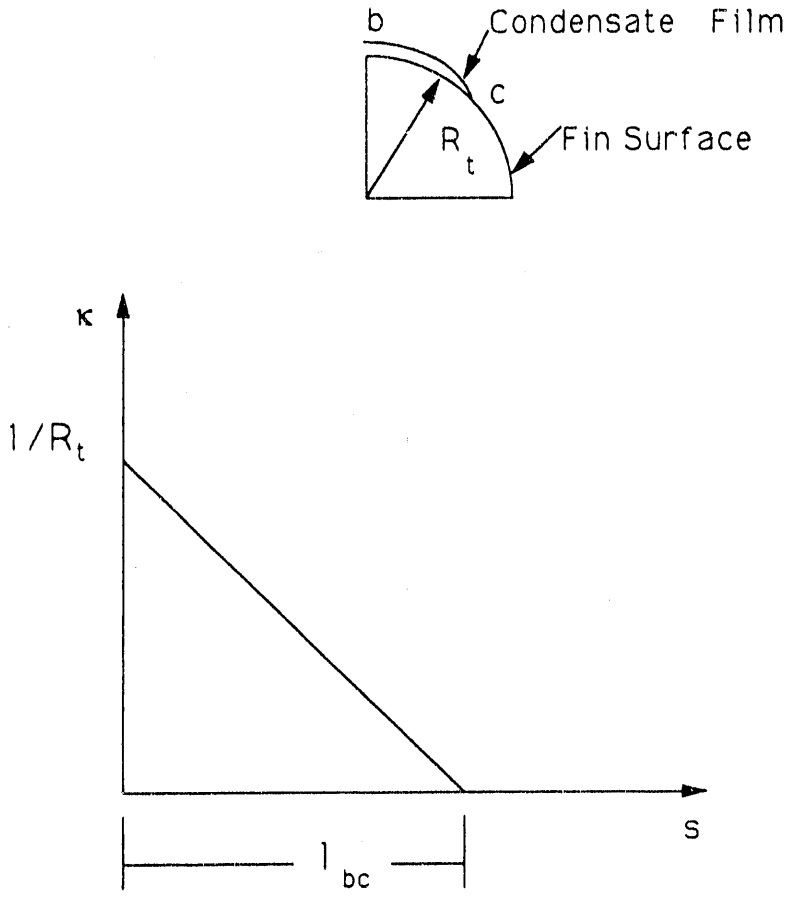

Figure 3.7. Variation of the curvature on the fin tip.

$$r = C_1 + C_2 e^{Z\theta} + C_3\theta \qquad [3.21]$$

A family of K-W (Kedzierski-Webb) profiles is shown in Figure 2.8. The constants C_1, C_2, and C_3 are determined by the geometry boundary conditions and are given by the following expressions:

$$\theta = 0 \qquad r = R_t \qquad [3.22a]$$

$$\delta(\phi) = \int_0^{\pi/2} r\sin(\theta)\,d\theta \qquad [3.22b]$$

and

$$t_t = \int_0^{\pi/2} r\cos(\theta)\,d\theta \qquad [3.22c]$$

The parameter 'Z', that appears in Equation [3.21], defines the "fatness" of the profile. It is recommended to use the minimum possible value for 'Z'. This will minimize the difference between the actual profile and the assumed profile of the film. The film thickness, $\delta(\phi)$, is obtained from Equation [3.19]. The total length of the condensate film, from the fin tip to the center of the fin top is given by:

$$S_m = \int_0^{(\frac{\pi}{2})} r d\theta \qquad [3.23]$$

The condensate film thickness can be determined from the following equation, derived by Adamek (1981):

$$\delta(s) = (\kappa')^{-4/3}\left[4C \int_0^s \kappa(t)^{(1/3)} dt\right]^{(1/4)} \qquad [3.24]$$

The condensing coefficient can then be determined from $k/\delta(s)$.

Depending on the operating conditions and fin geometry, a point of transition is reached on the fin top where gravity forces become important as compared to the surface tension forces. To determine this point of transition, the Bond number is used. The Bond number is defined as the ratio of gravity to surface tension forces and it is expressed as:

$$Bo = \frac{r^3 \rho g}{\sigma r'} \qquad [3.25]$$

The point of transition is assumed to occur at a critical Bond number, $Bo_c = 0.1$.

Hence, the length of the film from the fin tip to the point of transition is defined as l_{cb} which is equal to the value of the ordinate $s = r\theta$ at which the local Bond number reaches the critical value.

3.6.2 Condensing Coefficient on the Fin Side, h_{sid}

The condensate film on the fin side is governed by surface tension and gravity forces. The film is divided into three sub-regions, *cd*, *de*, and *ef* as shown in Figure 3.4. For sub-region *cd*, the flow is assumed to be governed by surface tension and the flow direction is along the s direction only. For sub-region *de*, the flow is assumed to be governed by gravity forces and the flow direction is assumed to be along the s direction only. In reality, the condensate in this region will have two velocity components, one along the s direction and the other along z, the circumferential direction. However, the circumferential component is much smaller than the s-component, as shown by Adamek (1981), that by neglecting the z-component, little error will be incurred. For region *ef*, the flow is assumed to be governed by surface tension forces. Since a drainage channel exists at the fin base then the film will have to undergo a change in curvature from ∞ to $-1/R_D$ which in turn will induce a strong pressure gradient. The condensate flow in this sub-region will be in the direction of the s-component. The condensate from all three regions flows into the drainage channel as shown in Figure 3.4.

The condensing coefficient on the fin side is expressed as an area weighted average of the condensing coefficients of the sub-regions and is expressed as:

$$h_{sid} = \frac{S_{cd}}{S_m} h_{cd} + \frac{S_{de}}{S_m} h_{de} + \frac{S_{ef}}{S_m} h_{ef} \qquad [3.30]$$

Because of the mathematical form of the profile equation, an analytical solution for h_{sid} cannot be obtained, so a numerical integration is required. Depending on the operating conditions, and fin geometry, it is possible that some or all of these sub-regions will disappear starting with sub-region *de*, followed by *ef* and then *cd*.

3.6.2.1 Subregion *cd*

The condensate film in this sub-region is modeled using a K-W profile as defined by Equation [3.21]. Again, the non-linearity of the profile curvature will be closer to the actual profile of the film. However, the geometry boundary conditions are defined as follows:

$$\theta = 0 \qquad r = R_t \qquad [3.27a]$$

$$t_{b,p} = \int_0^{\theta_m} r\cos\theta\, d\theta \qquad [3.27b]$$

and

$$e = \int_0^{\theta_m} r\sin\theta\, d\theta \qquad [3.27c]$$

As is the case for the fin top, a critical Bond number of 0.1 is considered to be the criteria by which gravity and surface tension forces become comparable to each other. The length of the surface tension dominated sub-region is defined as S_{cd} which is equal to the ordinate $s = r\theta$ at which the local Bond number reaches the critical value.

3.6.2.2 Subregion *de*

At the point of transition, a gravity dominated force subregion follows where the condensing coefficient is given by the Nusselt theory for condensation on a vertical or inclined plate. However, the Nusselt theory should be modified to take into account the condensate flow from sub-region *cd*. The modification is presented by Adamek and Webb (1990). The length of this sub-region is denoted by S_{de} and is expressed as:

$$S_{de} = S_m - R_{D,p} - S_{ef} - S_{cd} - H \qquad [3.28]$$

where $R_{D,p}$ is the projection of the drainage channel radius onto the fin side, and H is the film thickness on the tube surface between the fins after the drainage radii from facing fin sides connect at the center of the root region. The following section will discuss both the drainage channel and the conditions for which H is greater or equal to zero.

3.6.2.3 Subregion *ef*

Since a drainage channel with a concave curvature exists at the fin root, the condensate film undergoes a change in curvature from ∞ to $-1/R_D$. Hence, a surface tension dominated sub-region will exist and its length denoted by S_{ef}.

The length of sub-region *ef* is derived by Adamek and Webb (1990) and is given by the following expression:

$$S_{ef} = 4\left[\frac{CR_D^5}{\sigma}\right]^{\frac{1}{6}} \qquad [3.29]$$

where C is a property group and R_D is the drainage channel radius (discussed later).

It should be noted that in calculating the heat transfer in sub-region *ef*, the effect

of condensate flowing from sub-regions *cd* and *de* should be taken into account. A detailed analysis is given by Adamek and Webb (1990).

3.6.2.4 Rectangular Versus Trapezoidal Fins

a) Trapezoidal Fin

If the fin has a rectangular or trapezoidal shape, as shown in Figure 3.1a and 3.1b, then to use the K-W profile to model the film, the tip radius (at the fin top corner) and the base thickness must be known. However, if this radius is not known a tip radius can be estimated by:

$$R_T = \xi t_t \qquad [3.31]$$

where ξ is considered to be 0.05 (i.e. the tip radius is assumed to be 5% of the fin top thickness). The base thickness, for the K-W profile, is defined as:

$$t_{b,p} = (t_b - t_t)/2 \qquad [3.32]$$

Figure 3.8 shows a trapezoidal fin with a K-W profile defined to model the condensate along the fin side.

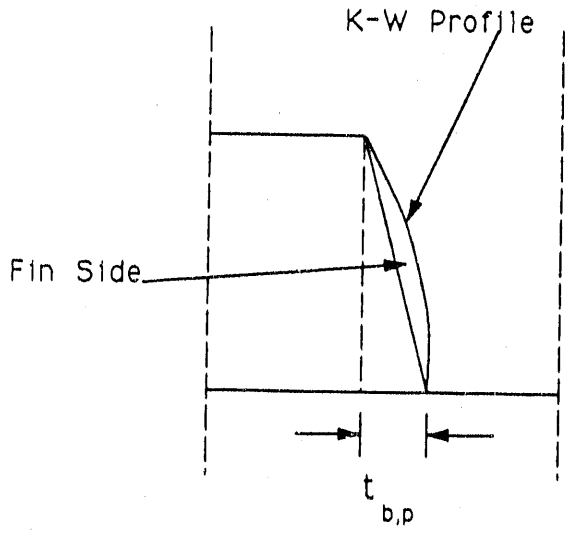

Figure 3.8. Trapezoidal fin with a K-W profile.

(b) Rectangular fin ($t_b = t_t$)

For this case, Equation [3.32] will result in a zero value for $t_{b,p}$ and hence a K-W profile cannot be defined. To circumvent this problem, a profile is selected to fit a fin with a top thickness of $0.95t_t$. This approximation is expected to influence the heat transfer coefficient in this region by less than 1%. In fact, Marto et al. (1986) have studied experimentally the performance of rectangular and trapezoidal fins of the same base thickness and height. The trapezoidal fin with a tip thickness 34% that of the rectangular fin had a condensing coefficient approximately equal to that of the rectangular fin (refer to Table 2.1).

3.6.3 Condensing Coefficient in the Root Region

Two subregions exist. The first is surface tension controlled, while the other is gravity controlled. The existence of two sub regions in the interfin space has been proven experimentally by Hirasawa et al. (1980). The modelling of the root region is an adaptation from the Adamek and Webb (1990) model.

3.6.3.1 Subregion *gh*

The flow in this subregion is governed by surface tension forces and the condensate flows in the axial direction towards the drainage channel. The length of

the subregion, *gh*, is given by:

$$l_{gh} = 4\left[\frac{CR_D^5}{\sigma}\right]^{1/6} \qquad [3.33]$$

The derivation of Equation [3.33] is based on the assumption of a constant surface tension induced pressure gradient. The local film thickness is then given by:

$$\delta_{gh}(s) = \left[\frac{CR_D l_{gh} s}{\sigma}\right]^{1/4} \qquad [3.34]$$

from which, an average condensing coefficient can be obtained.

3.6.3.2 Subregion, *hi*

In this subregion, the flow is governed by gravity forces and the condensate flows in the circumferential direction. The length of subregion, *hi*, is given by:

$$l_{hi} = s/2 - l_{gh} - R_{D,p} \qquad [3.35]$$

where $R_{D,p}$ is the projection of the drainage radius on the tube surface and is given in section 3.7. It is assumed that the projections of the drainage channel on the fin side and on the root region are equal. The local film thickness is given by Equation [3.18] with D_o replaced by D_r.

3.7 Drainage Channel

This channel, region *fg* in Figure 3.4, renders part of the fin side and root region ineffective for heat transfer. That is, the fin side and root region are both reduced by a length of $R_{D,p}$.

The mass flow rate in the drainage channel is given by:

$$M(z) = \rho V(z) A_D(z) \qquad [3.36]$$

where V(z) is the average flow velocity and A_D is the flow cross section area. The gravity and shear forces balance each other. Using the definition of the Fanning friction factor, this force balance can be written as:

$$f\frac{\rho V^2}{2} = \frac{A_D}{P_D}\rho g, \qquad [3.37]$$

where P_D is the wetted perimeter and g' is the component of gravity in the circumferential direction (g sinϕ). The Fanning friction factor can be expressed, in general, as:

$$f = \frac{C_f}{Re_{D_h}} \qquad [3.38]$$

where C_f is the friction factor coefficient and is a function of the channel geometry. The Reynolds number is defined as:

$$Re_{D_h} = \frac{VD_h}{\nu} \qquad [3.39]$$

Using the definition of the hydraulic diameter and conservation of mass, a final expression can be written as:

$$\frac{2C_f \nu M}{\rho g'} = A_D D_h^2 \qquad [3.40]$$

The above equation can be solved for any drainage channel shape. The mass flow rate consists of condensate from the fin side, and from the surface tension sub-region of the drainage channel. This second contribution would occur only for a flat drainage channel.

For the case of flat channels, and when the drainage radius is less than half the fin spacing (measured at the base of the fin), as depicted in Figure 3.4, the flow area is obtained by subtracting the area of a semi-circle of radius R_D from the area of the square of side length R_D which results in a net flow area of $0.215R_D^2$. The friction factor coefficient, C_f, has the value of 12 as determined by Thomas (1968). The average velocity can be expressed as:

$$V(z) = \frac{\left[gD_h^2 \sin\phi\right]}{24\nu} \qquad [3.41]$$

The drainage radius can then be expressed as:

$$R_D(z) = \left[\frac{\nu \int_0^z M(x^*)dx^*}{0.0017\rho g \sin(2z/D_r)}\right]^{1/4} \qquad [3.42]$$

where M(z) is given by:

$$M(z) = M_{cd}(z) + M_{de}(z) + M_{ef}(z) + M_{gh}(z) \qquad [3.43]$$

An iterative routine is used to solve for the drainage channel.

The projection of the drainage radius on the tube surface is given by Adamek and Webb (1990) as:

$$R_{D,p} = R_D \cos(l_{gh}/(2R_D)) \qquad [3.44]$$

Depending on the fin spacing and operating conditions, it is possible that at a certain location in the circumferential direction, the radii from facing fin sides will connect at the center of the root region thereby resulting in a thick film, as shown in Figure 3.9. The film is assumed to have a circular shape of radius equal to half the fin spacing. This film thickness will increases along the circumferential direction. For the case of rectangular fins with vertical sides the drainage channel is assumed to have a rectangular cross section and the flow area is given by:

$$A_D = sH \qquad [3.45]$$

and the perimeter as:

$$P_D = 2H + s \qquad [3.46]$$

Substituting into Equation [3.40] results in the following third degree polynomial:

$$16(se\Gamma)^3 - 4K_\Gamma(e\Gamma)^2 - 4K_\Gamma se\Gamma - s^2K_\Gamma = 0 \qquad [3.47]$$

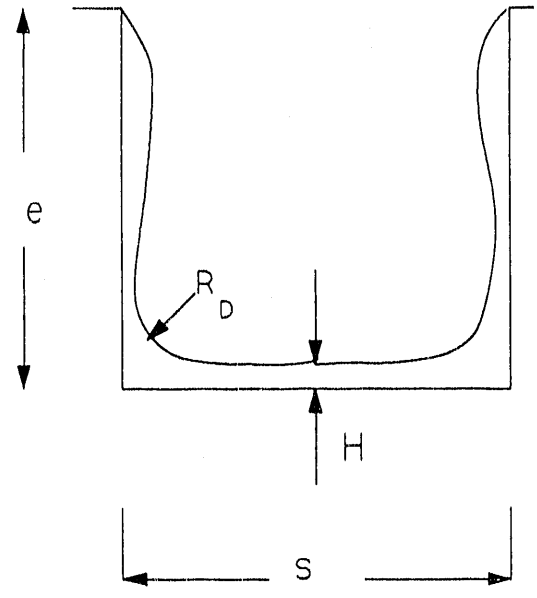

Figure 3.9. Condensate flow in the drainage channel after radii connect.

where

$$r = H/e \qquad [3.48]$$

and

$$K_r = \frac{2C_f \nu M}{\rho g'} \qquad [3.49]$$

Equation [3.49] can be solved iteratively for H once C_f is known. To avoid the iteration, an analytical expression given by Straub et al. (1958) can be used and is expressed as:

$$H = \frac{1}{2}\left[\frac{3C_\alpha M\mu}{2s\rho^2 g'}\right]^{1/3} \qquad [3.50]$$

where C_α is a factor which is a function of the aspect ratio of the drainage channel, H/s. The friction factor coefficient, C_f, is incorporated in this factor. Equation [3.52] is based on a series solution of the 2-D momentum equation that describes the flow in a rectangular channel. A curve fit of the C_α vs. H/s tabulated values results in the following expression:

$$C_\alpha = 9.882164 + \frac{17.96098}{s/2H} \qquad [3.51]$$

Equations [3.47] and [3.50] are basically the same. In fact, sample calculations resulted in almost the same answer for H (approximately 1% difference).

For the case of a trapezoidal drainage channel, the depth of the liquid film, H, is calculated based on an equivalent rectangular cross section whose dimensions are given by:

$$P_D = 2H + (s + H\tan\theta) \qquad [3.52]$$

and

$$A_D = (s + H\tan\theta)H \qquad [3.53]$$

The circular film shape is assumed to have a radius approximated by:

$$R_D = s/2 + H\tan\theta \qquad [3.54]$$

3.8 Condensing Coefficient in the Flooded Region

In the flooded region, it is assumed that heat transfer occurs on the top of the

fin, and through the thick condensate film that covers the root region and fin side. The condensing coefficient on the fin top is determined by the same expressions used for the fin top in the unflooded region. However, it is evaluated at a different vapor to wall temperature difference and fin efficiency. The curvature of the film, in sub-region *bc*, is treated differently here to take into account the fact that the curvature of the thick film changes in the circumferential direction and hence the change in the film curvature is not from $1/R_t$ to ∞, but from $1/R_{eff}$ to ∞. The effective curvature of the film is then defined as:

$$1/R_{eff} = 1/r_c + 1/r_f \qquad [3.55]$$

where r_c and r_f are shown in Figure 3.5. The film radius, r_f is approximated as:

$$r_f = R_t + \delta_s/2 \qquad [3.56]$$

where δ_s is shown on Figure 3.4 and can be evaluated using either of the alternatives presented earlier for the modelling of the film in sub-region *bc*. It is the film thickness at the end of subregion *bc*. The radius of the thick film region is obtained from a balance between gravity and surface tension forces, and it is given by:

$$r_c = \sigma/(\rho g z_c) \qquad [3.57]$$

where z_c is the distance from the bottom of the tube to the boundary between the flooded and unflooded regions. Note that r_c has a negative value since the film surface is concave. Hence, the condensing coefficient in sub-region *bc* is calculated by either Equation [3.16] or Equation [3.24] with R_{eff} substituted for R_t. Both r_c and r_f are a function of z, however, one can use an average δ_s for the whole flooded region and approximate r_c by s'/2 where s' is the fin spacing at the top of the fin.

In the thick film region, i.e. between the fins, the heat transfer is assumed to occur by conduction through the thick liquid film. The heat transfer coefficient for this region is then written as:

$$h_{r,f} = k/H \qquad [3.58]$$

where k is the liquid thermal conductivity and H is the height of the liquid film. The film height is approximately equal to the fin height. The condensing coefficient in the flooded region will then be an area weighted average of the above two components. It should be noted that for high thermal conductivity materials, such as copper, the heat transfer contribution of the thick film region is negligible compared to the total heat transfer in the flooded region. However, for low thermal conductivity materials this contribution can be appreciable.

Due to the condensate drops/columns formed on the bottom of the tube, the

active area is assumed to be 85% of the total heat transfer area in the flooded region.

3.9 Fin Efficiency

The fin efficiency, for a trapezoidal fin, in the unflooded region is calculated using an analytical expression derived by Kern and Kraus (1972). The equation takes into account variation of the fin cross sectional area, assumes adiabatic conditions at the fin top. An area weighted average heat transfer coefficient was used in the present analysis. The equation is expressed as:

$$\eta_u = \frac{\mu_o}{2K^2 e_c}\left[\frac{K_1(\mu_t)I_1(\mu_o) - I_1(\mu_t)K_1(\mu_o)}{I_o(\mu_o)K_1(\mu_t) + I_1(\mu_t)K_o(\mu_o)}\right] \qquad [3.59]$$

where I_i and K_i are modified Bessel functions of the first and second kind of ith order, respectively. The parameters μ and K are given by the following expressions:

$$\mu^2 = 4K^2\left[x + \frac{t_t(1 - \tan(\theta))}{2\tan(\theta)}\right] \qquad [3.60]$$

and

$$K^2 = \frac{h}{k \sin\theta} \qquad [3.61]$$

The values of μ_o and μ_t are obtained at x = 0 and x = e_c, respectively. Equation [3.59] was originally derived for a fin with an insulated tip. To account for convection from the tip, the Harper-Brown approximation is used which is basically correcting the fin height by adding half the fin tip. Therefore, $e_c = e + t_t/2$.

If the fin has a K-W shape, then the fin efficiency is approximated by that of a parabolic fin of the same height and base thickness. The analytical solution is given by Rohsenow and Hartnett (1973):

$$\eta_f = \frac{1}{me_c} \frac{I_{2/3}(4me_c/3)}{I_{-1/3}(4me_c/3)} \qquad [3.62]$$

Values for the modified Bessel functions were obtained by curve fitting of the tabulated values given by Kern and Kraus (1972).

For the flooded region, a heat balance on a fin with adiabatic boundary conditions on the fin sides yields:

$$\eta_f = \frac{1}{R_c h_\infty A_t + \frac{h_\infty}{h_t}} \qquad [3.63]$$

The derivation of η_f is given in Appendix A. The conduction resistance, R_c, is a function of the fin shape. Expressions are derived in Appendix B for different fin shapes relevant to the present analysis.

3.10 Wall Temperature in the Unflooded and Flooded Regions

The radial and circumferential wall temperature distributions are determined numerically by a 2-D conduction code. The computational domain is taken as a rectangle of length $\pi D_r/2$ and thickness equal to the thickness of the tube wall. Figure 3.10 shows the domain together with the boundary conditions. Symmetry of the problem results in adiabatic conditions at both ends. The boundary between the u and f regions is determined by c_b. Ten and five nodes were used for the longitudinal (circumferential) and transverse (radial) directions, respectively. Since the condensation coefficients are a function of the wall temperature, an iterative routine was used. Figure 3.11 shows a block diagram of the computer program.

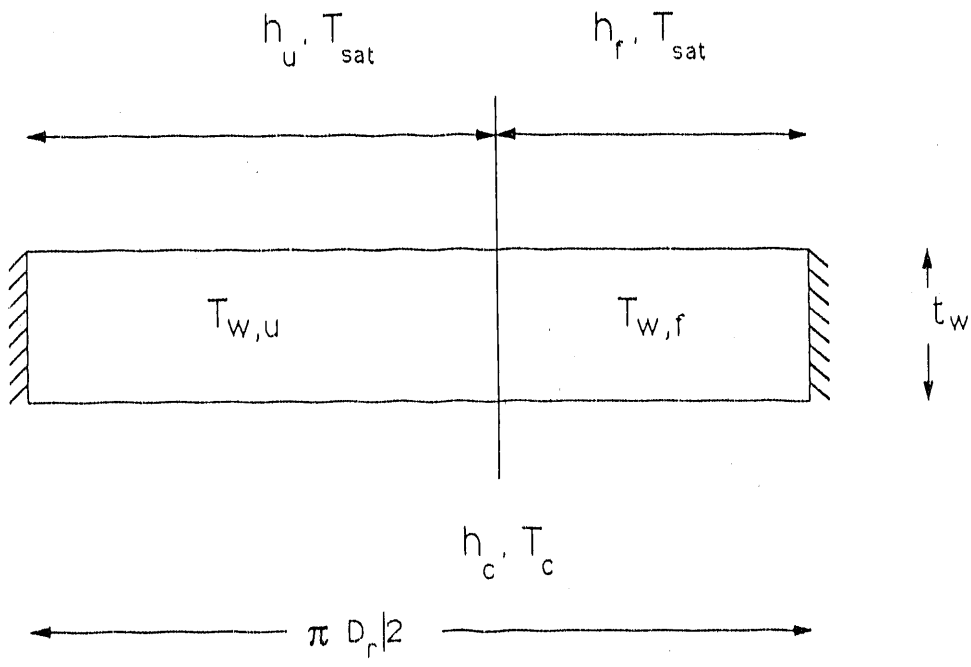

Figure 3.10. Computational domain and boundary conditions.

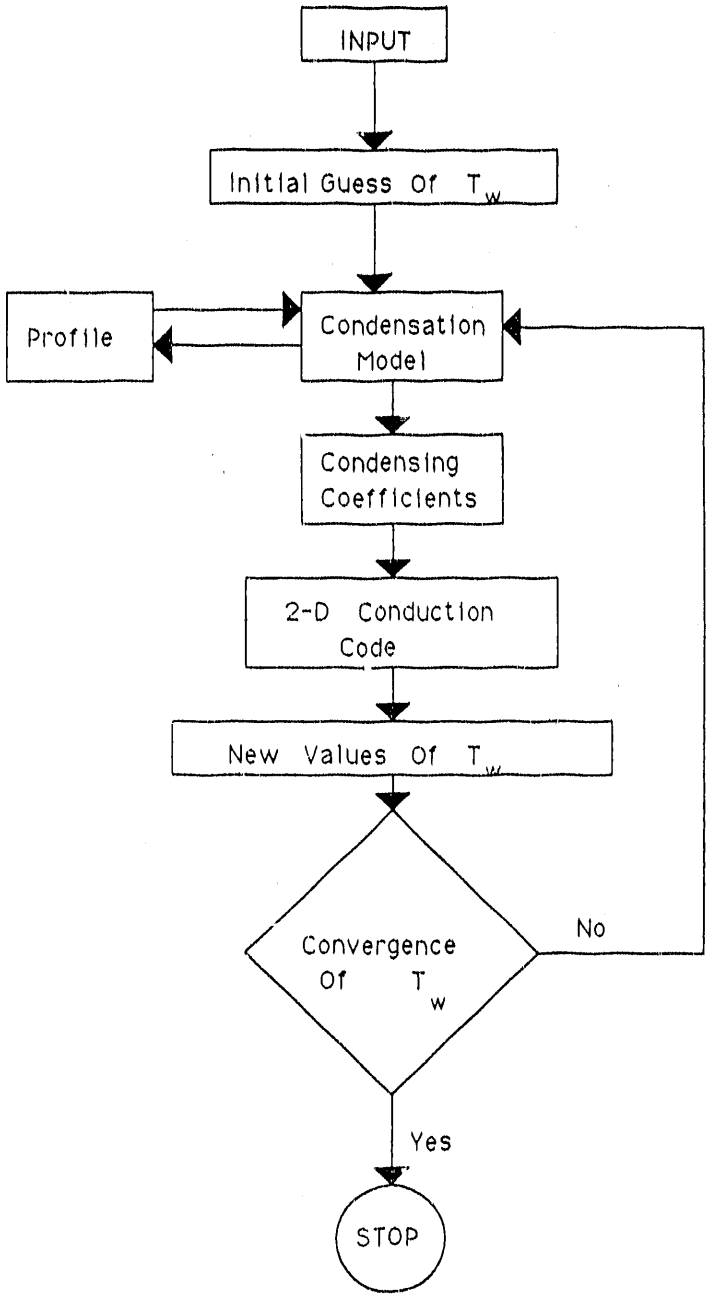

Figure 3.11. Block diagram of the computer code.

3.11 Extension of the Model to other Fin/Drainage Combinations

In this section, the model described above will be modified to accommodate fin/drainage combinations such as those shown in Figure 3.1c and 3.1d. Figure 3.12 shows the proposed structure of the condensate film on the top and side of the fin and also in the circular drainage channel.

3.11.1 Condensing Coefficient on the Fin Top, h_{top}

The fin top region is modelled in the same manner as described earlier for rectangular and trapezoidal fins with the choice of either alternative.

3.11.2 Condensing Coefficient on the Fin Side, h_{sid}

The fin side is divided into three sub-regions. Sub-region *cd* is controlled by surface tension forces and the curvature of the film is assumed to follow that of a K-W profile. To define a K-W profile, a base thickness is defined as $t_{b,p} = (P_f - 2R_B)/2$. The film is assumed to undergo transition into a gravity dominated flow, denoted by subregion *de*. Equations [3.21] together with Equations [3.22a] to [3.22c] apply. The length of sub-region *de* is determined as:

$$S_{de} = S_f - S_{cd} - S_{ef} - S_a \qquad [3.64]$$

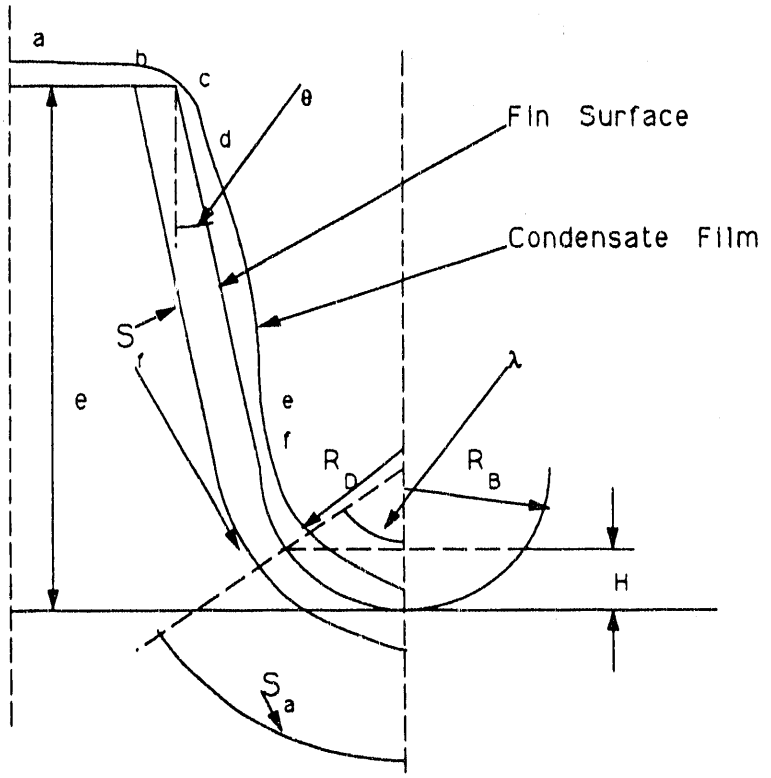

Figure 3.12. Film structure for straight sided fin and circular drainage channel.

where,

$$S_f = (e - R_B)/\cos\theta + \pi R_B/2 \qquad [3.65]$$

and

$$H \leq R_B, \qquad S_a = \lambda R_B \qquad [3.66]$$

$$H > R_B, \qquad S_a = \pi R_B/2 + (H - R_B)/\cos\theta \qquad [3.67]$$

The angle λ is expressed as:

$$\lambda = \cos^{-1}(1 - H/R_B) \qquad [3.68]$$

where H is the film thickness in the root region, which will be defined below. The lengths S_{cd} and S_{ef} are calculated in the same manner as discussed for rectangular and trapezoidal fins with flat drainage channels. However, in calculating the length of region S_{ef}, the radius of the drainage channel must be known. Two cases are identified:

(i) Case I $\qquad H \leq R_B \qquad R_D = R_B \qquad [3.69a]$

(ii) Case II $H > R_B \qquad R_D = s'/2$ [3.69b]

where

$$s' = R_B + (H - R_B)\tan\theta \qquad [3.70]$$

3.11.3 Condensing Coefficient in the Root Region, h_r

Heat transfer across the condensate film in the root region is assumed to occur through conduction only. The heat transfer coefficient is given by:

$$h_r = k/H \qquad [3.71]$$

To calculate the film thickness, H, in the root region, Equation [3.40] can be used. The flow area and perimeter will depend on whether, H, is smaller or larger than R_B hence two cases are defined.

3.11.3.1 Case I ($H \leq R_B$)

The flow area and hydraulic diameter are assumed to be those of a circular segment duct and are given by:

$$A_D = \frac{R_B^2}{2}(2\lambda - \sin 2\lambda) \qquad [3.72]$$

and

$$D_h = \frac{2R_B(2\lambda - \sin 2\lambda)}{2\lambda + 2\sin(\lambda)} \qquad [3.73]$$

Substituting into Equation [3.40] results in the following expression:

$$2R_B^4(2\lambda - \sin 2\lambda)^3 = K_T(2\lambda + 2\sin(\lambda)) \qquad [3.74]$$

Once λ is determined through an iterative scheme, H can be determined by Equation [3.68]. The friction factor coefficient, C_f, is assumed to have a constant value equal to that of laminar flow in a pipe (i.e. 16). Van Dromme and Hellinckx (1973) showed that C_f varies by approximately 13 % over the range $0 < 2H/R_B < 1$.

3.11.3.2 Case II ($H > R_B$)

The flow area and hydraulic diameter are given by the following expressions:

$$A_D = \frac{\pi}{2}R_B^2 + (H - R_B)2R_B \qquad [3.75]$$

and

$$D_h = \frac{2\pi R_B^2 + (H - R_B)8R_B}{\pi R_B + (H - R_B)\cos\theta} \qquad [3.76]$$

Substituting into Equation [3.40] results in the following third degree polynomial:

$$128(R_B X_B)^3 + (96\pi R_B^4 - K_r\cos^2\theta)X_B^2 + (24\pi^2 R_B^5 - 2\pi R_B K_r\cos\theta)X_B = K_r(\pi R_B)^2 + 2\pi^3 R_B^6 \qquad [3.77]$$

where $X_B = H - R_B$. An iterative scheme is used to find H once C_f is known.

There are no expressions for the friction factor of a channel with the sides partly circular and partly straight. Hence, Such a channel will be approximated by a trapezoidal shape with a fin spacing at the base equal to the diameter of the circular channel. Therefore, Equations [3.47] to [3.54] apply. To avoid the iteration involved in Equations [3.74] and [3.77], Equations [3.52] and [3.53] are used as an approximation.

For the case when the fin has a flat top with a circular channel that starts from

the fin tip to the fin base, the analysis is similar to that described above. The fin height is equal to the drainage radius, R_B, and the base thickness is approximated by a line starting from the fin top and tangent to the circular channel and ending at the bottom of the channel. These two dimensions are necessary to define the appropriate K-W profile. To determine the condensate thickness in the channel, Case I as defined by Equation [3.69a] can be applied.

However, for the gravity dominated region, an expression for gravity drained condensation on concave surfaces must be derived. By dividing the concave surface into several differential elements and treating each segment as an inclined surface, the average condensation coefficient in the concave subregion *de* is determined by integration over the length of this sub-region. The final expression is given by:

$$h_{de} = \int_{\alpha_1}^{\alpha_2} B\left[\sin\left(\tan^{-1}\left(-\frac{\cos\alpha}{\sin\alpha}\right)\right)\right]^{1/4} (r\alpha)^{3/4} d\alpha \qquad [3.78]$$

where α_1 and α_2 are defined in Figure 3.13. The angles α_1 and α_2 are determined as follows:

$$\alpha_1 = \frac{S_{cd}}{r_B} \qquad [3.79]$$

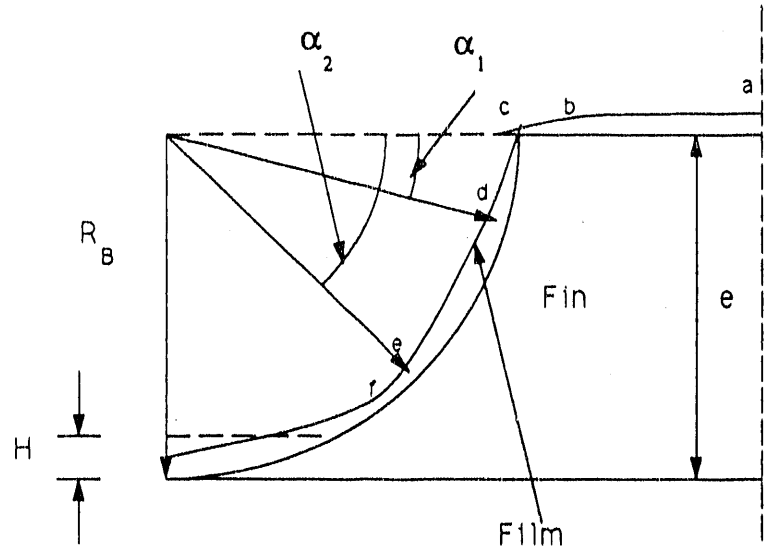

Figure 3.13. Gravity drained condensation on a concave surface

and

$$\alpha_2 = \frac{l_{cd} + l_{de}}{R_B} \qquad [3.80]$$

However, to avoid the complexity in integration, the sub-region *de* is modelled by assuming a straight inclined surface. The angle of inclination is assumed to be equal to that subtended by the tangent line that starts from the fin tip and ends at the base.

3.12 Profiled Fins

For profiled fins, as shown in Figure 3.1e and 3.1f, the fin shape can be defined, in general, as follows:

$$\kappa = f(R_t, e, t_b, \theta_m) \qquad [3.81]$$

Once R_t, e, and t_b are defined, the fin curvature will be expressed in terms of θ only. The angle θ_m usually varies from 0 to $\pi/2$. Some profiles have already been discussed in Chapter 2. Once the function f is known, then the local film thickness (and hence the condensing coefficient) can be obtained from Equation [3.24]. For example, the functional form of f for a K-W profile is given by Equation [3.21].

Once the tip radius, base thickness, height, and θ_m are defined, the fin can be generated by Equation [3.21]. The film thickness can then be determined from Equation [3.24].

It is believed that the effect of gravity on high performance fins will be negligible. Hence, the fin side will consist of two subregions such as cd and de. The analysis of the drainage channel can be done along the same guidelines set above. For drainage channels other than flat and circular, such as sinusoidal, the flow area and hydraulic diameter can be defined and substituted into Equation [3.40] to determine the condensate thickness in the channel.

CHAPTER 4

EXPERIMENTAL PROGRAM

4.1 Introduction

This chapter describes the apparatus and experimental procedure. Data for steam condensation on a selected set of enhanced tubes is presented. The data will show single tube performance and enhancement level.

4.2 Apparatus

Figure 4.1 shows a schematic representation of the apparatus. The apparatus constitutes of four main components: boiler, test cell, post condenser, and air ejection system.

The boiler is a 2 meter long of 254 mm diameter carbon steel pipe. There are three heater modules each consisting of three elements, with each element rated at 2.5 kW at 220 V. This produces a total maximum power of 22.5 kW. The post condenser is a shell and tube heat exchanger with 10 meters of 1024 fpm integral finned tubes in six water side passes. The purpose of the post condenser, is to with-

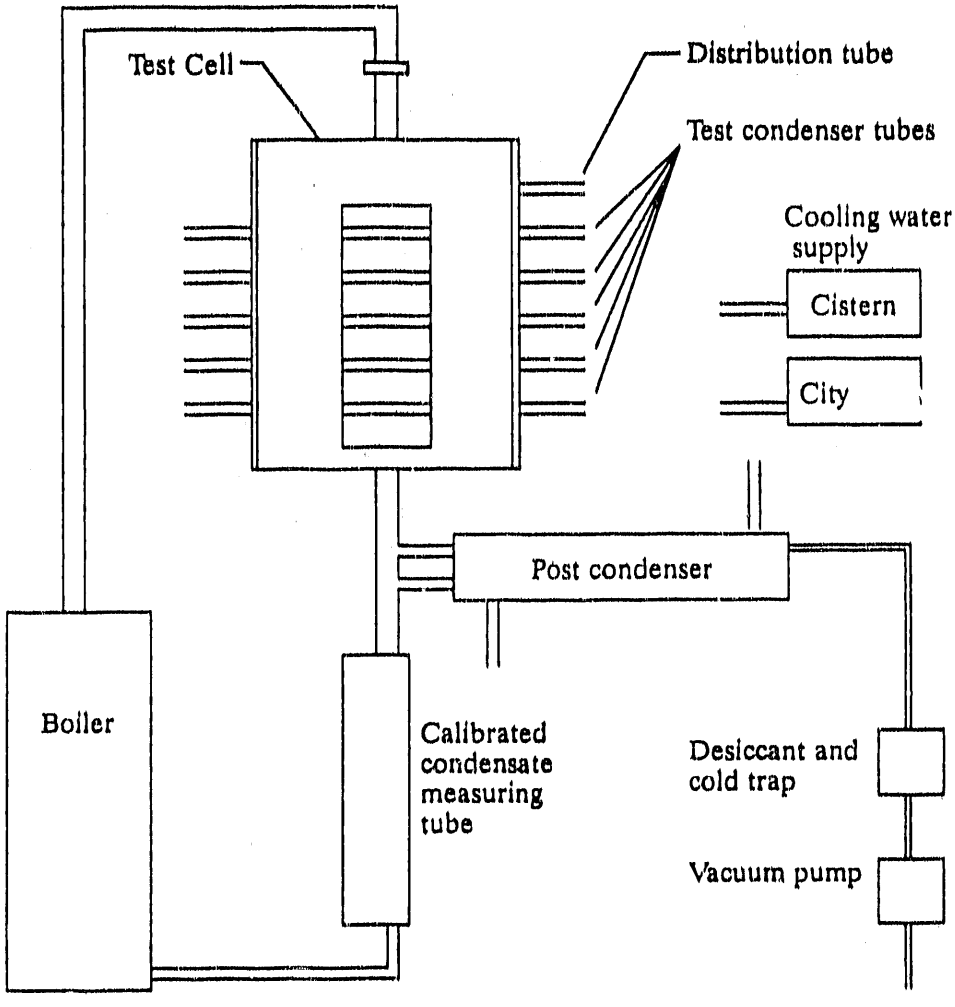

Figure 4.1. Schematic diagram of the condensation test stand.

draw any air leaked into the system. If air leaks into the system, it will migrate to the coldest point which is at the cooling water inlet to the post condenser.

Two test cells were used. One for 3/4" tubes, made of stainless steel, and the other for the 7/8" tubes, made of carbon steel. Tubes with a diameter up to 1.25 " can be tested in the second test cell. A flanged 3" carbon steel pipe allows the passage of steam into the test cell while another flanged pipe accommodates exit of the vapor-liquid mixture from the test cell. The design allows measurement of single tube and row effect performance. However, in the present study only single tube performance was evaluated. Five experimental tubes and one distributor tube are installed. On one side of the test cell, a 374 mm x 76.2 mm opening provides a window for observation of condensate flow patterns and to ensure the existence of filmwise condensation. On the opposite side, 1/8" NPT holes provide access for temperature and pressure measurements. The front and back faces of the test cell are covered by removable tube sheets which are designed in a unique fashion to ensure a leak proof cell. Figure 4.2 shows the tube sheet design. The groove acts as suction manifold connected to the circular gap of each bore. The groove is then connected to a vacuum pump through the threaded hole. The purpose of this design is to establish a pressure in the circular gaps that is lower than the testing pressure so that if there any leaks present, the air will be sucked to the region of lower pressure and exits to the vacuum pump. It is possible to use the same tube sheets for tube diameters between 3/4" and 1 1/4" with proper design of the tube ends.

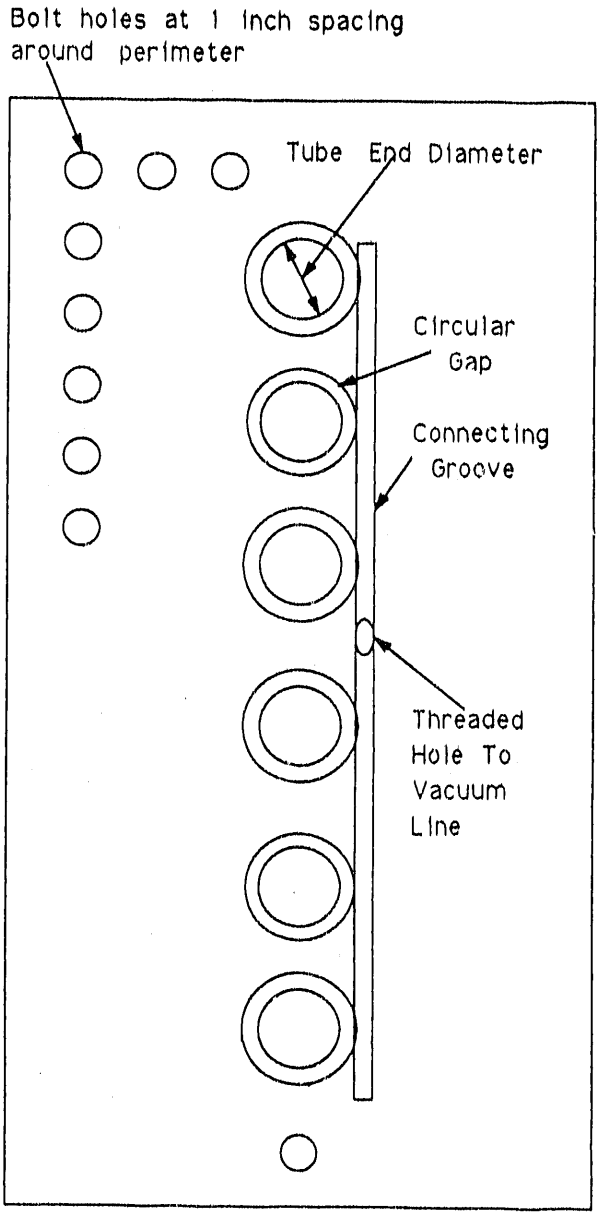

Figure 4.2. Illustration of the inner tube sheet design

Figure 4.3 illustrates the design of a tube end. Each of the test cells has a capacity of testing five tubes and hence the row effect up to the fifth tube. However, by using a distributor tube the row effect of a higher number of tubes can be studied. In the present apparatus, up to twenty rows can be tested. The distributor tube is made of a 7/8" tube with holes of constant diameter and equal spacing. To simulate more than five tubes, the condensate from the fifth tube is recirculated through a pump back to the test cell. The condensate then flows down from the distributor tube to the top tube which would simulate the sixth tube and so forth. The distributor tube was made of a 3/4" copper tube with 0.04" holes at 1/2" spacing. The tube is positioned in such a way so that the holes are facing upwards. A brass screen of length 6.25" long was wrapped around the tube all along the tube length and held in place by O-rings. Before the tube was placed in the test cell, it was connected to a water source and operated at various flow rates covering the desirable range to simulate 20 rows. For the range tested the drainage pattern was observed to be uniformly distributed along the tube producing a similar pattern as would be expected from the tested tubes. However, this pump/distributor tube arrangement was not used in the present work.

The air ejection system, schematic shown in Figure 4.4, consists of a desiccant, cold trap, and vacuum pump. The purpose of this system is to continuously purge the system of the non-condensible air (if present). The non-condensible gas will migrate to the coldest point in the system which is located near the cooling water

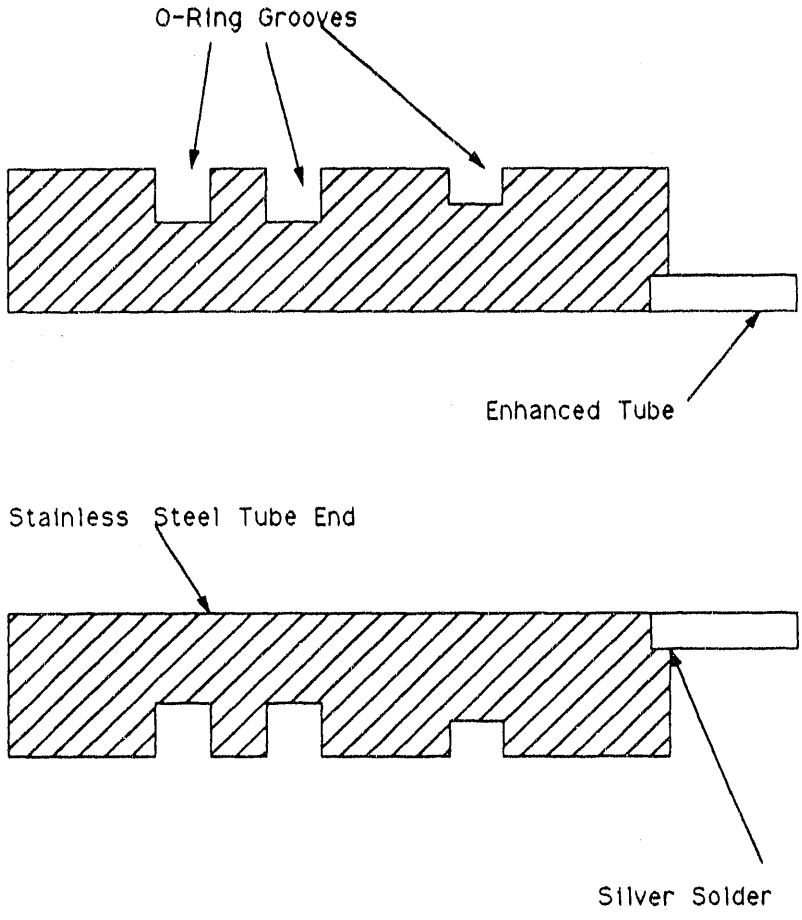

Figure 4.3. Illustration of the tube end design.

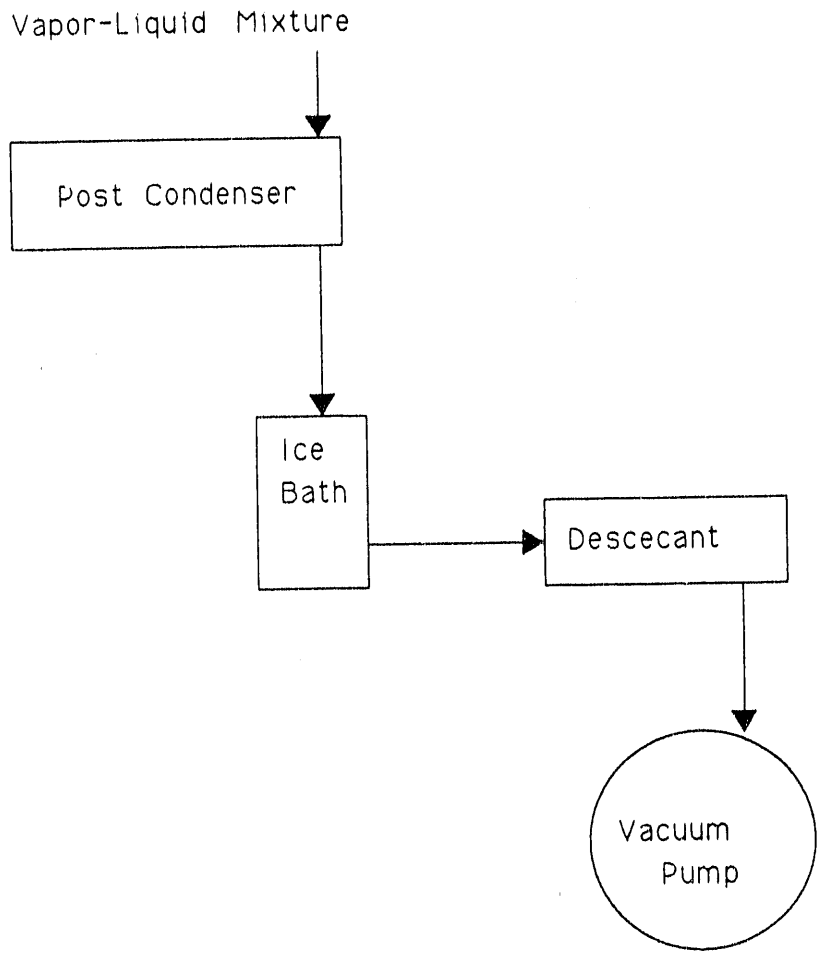

Figure 4.4. Block diagram of air ejection system

inlet in the post condenser. The air ejection system is connected to the post condenser at that point. However, it is still possible that some steam vapor is still present. To ensure that no water vapor reaches the vacuum pump, a descecant and a cold trap are installed on the line connecting the post condenser and the vacuum pump. If any water vapor is present, it will condense in the cold trap and as a further precaution the desiccant will absorb any vapor left.

4.3 Instrumentation

A total of 19 copper/constantan thermocouples of 5 μm diameter are connected to a Fluke 2285B datalogger. They measure the temperatures of the tube wall, inlet and outlet cooling water to post condenser, vapor in boiler, vapor in test cell, and test cell outside temperature. Three of the five experimental tubes are instrumented: the first, third and fifth rows. The wall temperature is measured in three circumferential positions, the top, side, and bottom of the tube. For the copper and copper/nickel tubes, the thermocouples measuring the tube wall temperature were placed between the fins and then peened down by bending the adjacent fin walls. The vapor temperature in the test cell is measured in five locations along the horizontal and vertical directions. An absolute mercury manometer was used to measure the vapor pressure in the boiler, test section, and post condenser.

The cooling water temperature rise in the tubes was measured by five thermistors, while the cooling water flow rate was measured by five Dwyer flow meters. The condensate volumetric flow rates in the test section and post condenser were measured by using calibrated liquid level indicators.

4.4 Test Procedure

4.4.1 Tube Cleaning Procedure

The purpose of cleaning the tubes is to degrease and deoxidize the surfaces to ensure filmwise condensation and eliminate possible thermal resistances between condensing vapor and tube surface. The procedure is as follows:

1. Degrease: The tube is immersed in an acetone bath and scrubbed with a soft tooth brush. Remove and shake the tube to remove any retained acetone and place on an aluminum foil to be dried by a stream of hot air.

2. Deoxidize: The tube is immersed in a bath of Tarn-X (commercial de-oxidizer for copper alloys - contains acidified thiourea, detergent and corrosion inhibitors) and scrubbed with a soft tooth brush. It is then rinsed thoroughly with water. Any weak acid may be used to deoxidize the surface. A 5% solution of acidified dichromate ($Na_2 Cr_2 O_7$) and a 5% solution of H_2SO_4 mixed together

can be used as an alternative to Tarn-X. Another possibility is a 5% solution of acetic acid in warm (120 F) water.

3. Washing: The tube is washed with one gallon of warm water and 0.5 cc of dishwashing detergent using a sponge. It is then thoroughly flushed with water.

4. Neutralization: When a surface is treated with an acid solution, it is necessary to remove the solution trapped in the pores of the surface. Rinsing with water is not enough. Hence to neutralize the surface, a weak base should be used. This is accomplished by washing the surface with a 5% solution of sodium hydroxide (soda ash). Care should be taken in preparing this solution since the reaction is exothermic.

5. Pacification: The deoxidized surface is now highly susceptible to rapid oxidation. The oxidation process can be reduced by pacification of the surface. This is done with a 0.2% solution of sodium nitrite. The tube is then dried as in step 1.

6. Storage: The tube should be wrapped with aluminum foil and then with plastic wrap. This will prevent oxidation and contamination of the surface with grease and other particles suspended in air.

The above procedure was carried out in a well ventilated area. It is necessary to use rubber gloves and eye protection.

When the copper-nickel and titanium were first installed and condensation started, it was noticed that dropwise condensation occurred on some parts of the tubes. It was necessary to oxidize the tubes. The copper-nickel tubes were oxidized with a 50% solution of sodium hydroxide and ethanol (equal volumes). The titanium tubes were pickled with a solution of 15% nitric acid and 2% fluorine. The oxidizing procedure was successful in eliminating the dropwise condensation.

4.4.2 Set-up Procedure

This procedure constitutes the set of steps necessary to prepare for data acquisition which are outlined below:

1. Prepare thermocouple junctions.

2. Mount thermocouples on the walls of three "cleaned tubes" and then install all tubes in the test cell. An annulus of approximately 1.5 mm gap was created by using cylindrical copper rods and inserting them in the tubes. This will reduce the thermal resistance on the tube side and hence lower the axial variation of the wall temperature.

3. Install thermocouples that measure vapor temperature in the test cell and then connect all thermocouples to the data logger then seal and insulate the system.

4. Reduce system pressure to approximately 15 mmHg absolute and then fill the boiler with **soft** water. The water level in the boiler should be 10 inches above the top of the heating elements.

5. Check function of thermistors and thermocouples. This is accomplished by running the cooling water through the experimental tubes without steam generation. Ideally, all the thermocouples should read the same temperature as the cooling water temperature. The function of the thermocouples is accepted if the readings are within ±0.002 mV. For the thermistors, the inlet and outlet temperatures should be the same, however, a 0.03 C difference was accepted.

6. Reduce system pressure down to 6 cmHg absolute and record the pressure and ambient temperature. Leave the system for 24 hours and then record the pressure to determine the leak rate per hour. The second pressure reading should be recorded at the temperature of the first reading or scale the pressure reading using the perfect gas equation. A system leak rate of 1.5mm Hg per hour was achieved.

This will be acceptable since the system is continuously purged during data acquisition. Actually, an estimate of the air leak rate was determined to be approximately 0.0021 kg/hr which amounts to a concentration of 0.015% in the steam air mixture. This low concentration will not affect the condensing process, as shown by Minkowycz and Sparrow (1966), and hence the assumption of a pure vapor is justified.

4.4.3 Setting Operating Conditions

Once the set-up procedure is accomplished, the operating conditions are set as follows:

1. Set the water flow rate through the experimental tubes.

2. Set inlet water temperatures to the experimental tubes and the post condenser. Two sources of cooling water are available. One at a temperature between 78 F and 84 F and the other between 55 F and 60 F. Combinations from both sources are used to set the desired inlet temperatures. Since it is desired to have most of the heat load in the

post condenser (at least 60%), the inlet water to the post condenser is usually set at a few degrees below that to the test tubes.

3. Set cooling water flow rate through the post condenser to ensure, together with the inlet water temperature, at least 60% of the total heat load is carried by the post condenser.

4. Set input electric power to boiler.

5. Pump down system to the desired pressure. The inlet water temperature and water flow rate to the post condenser are varied to achieve test pressure. An auto transformer is also used to adjust the input power as a means to regulate system pressure.

6. Set total test period and time interval for data acquisition.

4.4.4 Data Acquisition

Steady state conditions at which data acquisition begins is assumed to occur when the following criteria are met:

1. System pressure fluctuations are less than ±0.5 mmHg.

2. Fluctuations in the thermocouple readings are not more than ±5 microvolts.

3. Fluctuations in the cooling water temperature rise are not more than 0.15 C.

4. Maximum difference between any two measured vapor temperatures readings should be within ±0.7 C. Moreover, the saturation temperature obtained from the pressure reading should be within ±0.5 C of that measured by the thermocouples. Satisfying this condition will ensure that no air is present in the test cell.

Once the above four conditions are met, then the first data point is ready to be read. The following steps are performed:

1. Read individual pressures of boiler, test cell, and post condenser.

2. Read cooling water flow rate and inlet water temperature in the test cell.

3. Read all 19 thermocouples.

4. Read cooling water flow rate to the post condenser.

5. Measure condensate flow rate of test cell and post condenser by timing the liquid rise in two separate calibrated liquid level indicators.

6. Repeat steps 1 through 5 at each time interval for the total test period.

4.5 Data Reduction

The goal for the data acquisition, is to determine the heat transfer coefficient for the enhanced tubes, and to compare it to that of a smooth tube. From the measurement of the cooling water temperature rise and flow rate, the heat load per tube can be determined as:

$$Q = \dot{m}_w \, c_p \, \Delta T_w \qquad [4.1]$$

The heat transfer coefficient is then determined from Equation [4.2]:

$$h = \frac{Q}{A(T_{sat} - T_{w,av})} \qquad [4.2]$$

where A is the area of a smooth tube of diameter D_o, T_{sat} is the saturation temperature corresponding to the pressure in the test cell (obtained from the steam tables), and $T_{w,av}$ is the average wall temperature determined by Equation [4.3]:

$$T_{w,av} = \frac{1}{4}(T_1 + 2T_2 + T_3) \qquad [4.3]$$

where the subscripts T_1, T_2, and T_3 refer to the top, side and bottom measured wall temperatures of the tube. The set of data points for each tube is taken at different values of (T_{sat} - $T_{w,av}$) by varying the cooling water flow rate. The data for each tube is then fitted to an equation of the form:

$$h = C\Delta T^n \qquad [4.4]$$

where C and n are constants determined from the experimental values. For a smooth tube, the exponent n is determined from the Nusselt theory to be -0.25. However, it was determined experimentally by Wanniarachchi, Marto, and Rose (1984) that for integral finned tubes this exponent is a function of the fin spacing.

The heat balance calculations are conducted by two different methods. The first is to compare the electrical input to the total heat carried by the cooling water in the test cell and the post condenser. The heat losses from the boiler to the ambient air

were estimated to be approximately 2% of total electrical input power. A 2 inch layer of insulation was wrapped around the boiler to offset this loss. The second is to compare the heat load of the cooling water of each, the test cell and the post condenser, to the corresponding condensate heat load. As an example of this second method, the heat balance for the test cell should satisfy the following relation:

$$\dot{m}_w \, c_p \, \Delta T_w = \dot{m}_c \, \lambda \qquad [4.5]$$

where $\dot{m}_c$ is the condensate flow rate. A typical heat balance between the cooling water heat load and condensate load was 3%.

4.6 Operational Problems

At the beginning of the first phase of testing, small black particles were detected in the condensate flow. These particles ultimately clogged the calibrated liquid level indicators attached to the test cell and post condenser. The liquid level indicator attached to the boiler was also clogged. It was necessary to clean the entire apparatus before any data could be taken. The apparatus was dismantled piece by piece. A thick black layer was noticed on all the carbon steel surfaces while the copper tubing and stainless steel test section were clean. A sample of this layer was chemically analyzed to determine its nature. The sample was treated with a 30%

solution of hydraulic acid and placed on a heater. The solution turned into a yellowish green transparent solution and exhibited magnetic behavior. The black layer was determined to be FeO and decomposed R-11. When the heater elements were removed, a very hard black crust was observed. This crust was identified as decomposed R-11 which was the result of exceeding the critical heat flux for R-11 when it was used by previous students.

The hard crust on the heater elements was removed completely by filing the surfaces, then flushing with a 36% solution of HCL, and finally flushing with high pressure hot water. The boiler and the steam supply line were flushed several times with 36% HCL solution and flushed repetitively with high pressure steam. This resulted in cleaning the surfaces almost completely (at least 90%). The same procedure was followed for cleaning the piping which was still attached to the apparatus structure.

At the end of cleaning, all the components were re-installed and a few pipe sections were changed. The system was then ready for testing.

4.7 Experimental Tube Geometries for the Condensing Coefficient

The enhanced surfaces selected for the condensation tests are listed in Table 4.1 with corresponding photographs shown in Figure 4.5. The fin geometry dimensions

Table 4.1

Tubes Tested in Condensation Test Cell

Geometry	Material	Manufacturer	Code
Smooth	copper	-	Plain
Integral-fin	copper	Wieland	CU-11
Integral-fin	90/10 cu/ni	Wolverine	C/N-19
Integral-fin	90/10 cu/ni	Wieland	C/N-11
Integral-fin	titanium	Wieland	TiA-11
Integral-fin	titanium	Wieland	TiB-11
Attached part.	cu particles on 90/10 cu/ni tube	UOP	A/P-50

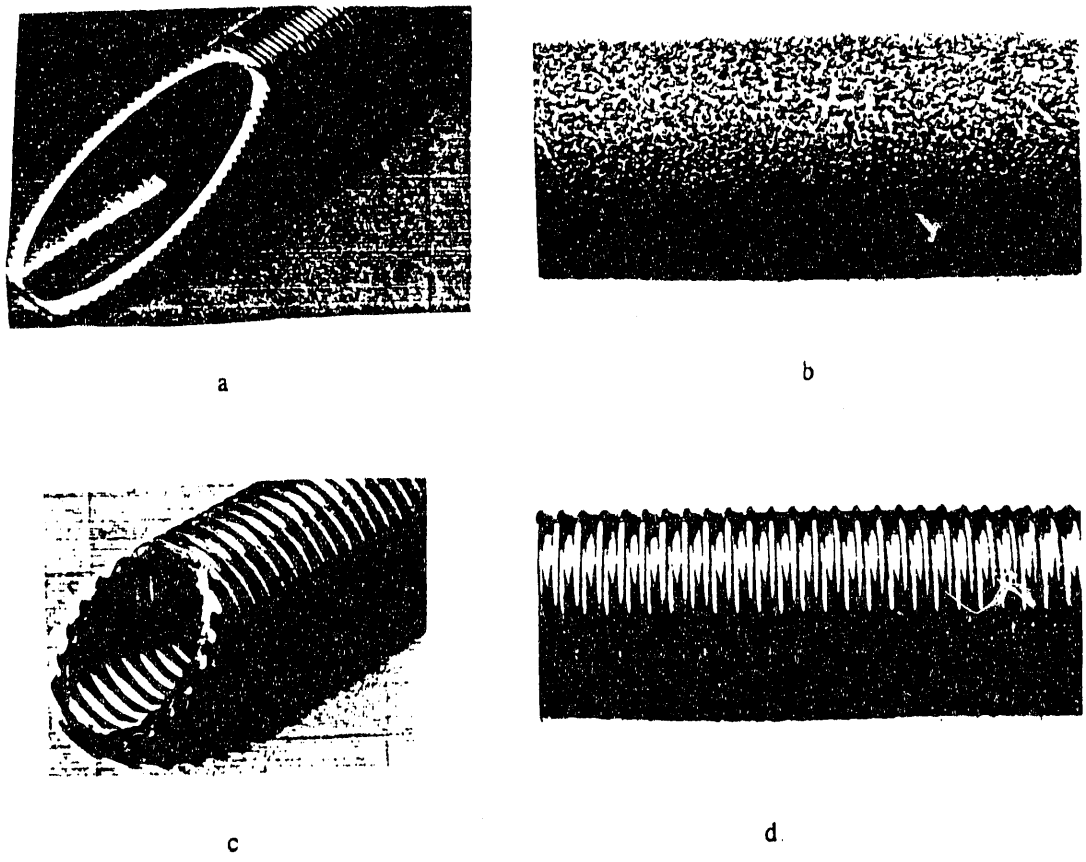

Figure 4.5. Photographs of the tubes (a)748 fpm, C/N-19 (b)Attached particle, A/P-50 (c)433 fpm, C/N-11 (d)433 fpm, TiA-11.

are listed in Table 4.2. The tests were conducted at a condensing temperature of 54 C. A total of six different enhanced tubes and one smooth tube were tested. Five of these tubes are of the integral fin type, while the last type is made of copper particles (0.43 mm diameter) sintered to the surface of a cu/ni tube and covering 50% of its surface area. The copper nickel tubes had a wall thickness of approximately 0.9 mm (0.035") while the titanium tubes had a thickness of approximately 0.46 mm (0.018").

4.8 Experimental Results for the Condensing Coefficient

A 22.23 mm diameter smooth copper tube was tested at two different saturation temperatures, 54 C and 69 C. The purpose of this test was to verify the operation of the apparatus by comparing the data to the theory for a horizontal tube derived by Nusselt (1916). Figure 4.6 shows the data obtained for the plain tube. The experimental values were within -2% and +5% of the Nusselt theory. Since these data agreed well with the Nusselt theory, the smooth tube performance will be represented from now on by the Nusselt theory.

In presenting the following results for the enhanced tubes, the "enhancement level" is defined as the ratio of the condensing coefficient, based on the envelope area over the fins (diameter D_o), to the condensing coefficient of a smooth tube of diameter D_o. Both coefficients are compared at the same (T_{sat} - T_w). The different

Table 4.2

Dimensions of the Tested tubes

Code	D_o	fpm	e	t_b	t_t
	mm	-	mm	mm	mm
Plain	22.23	-	-	-	-
CU-11	19.00	433	1.12	0.9	0.30
C/N-19	22.23	748	0.50	0.6	0.20
C/N-11	22.23	433	1.12	0.9	0.30
TiA-11	18.29	433	0.43	1.0	0.64
TiB-11	18.29	433	0.28	1.4	0.93
A/P-50	22.23	-	0.43	-	-

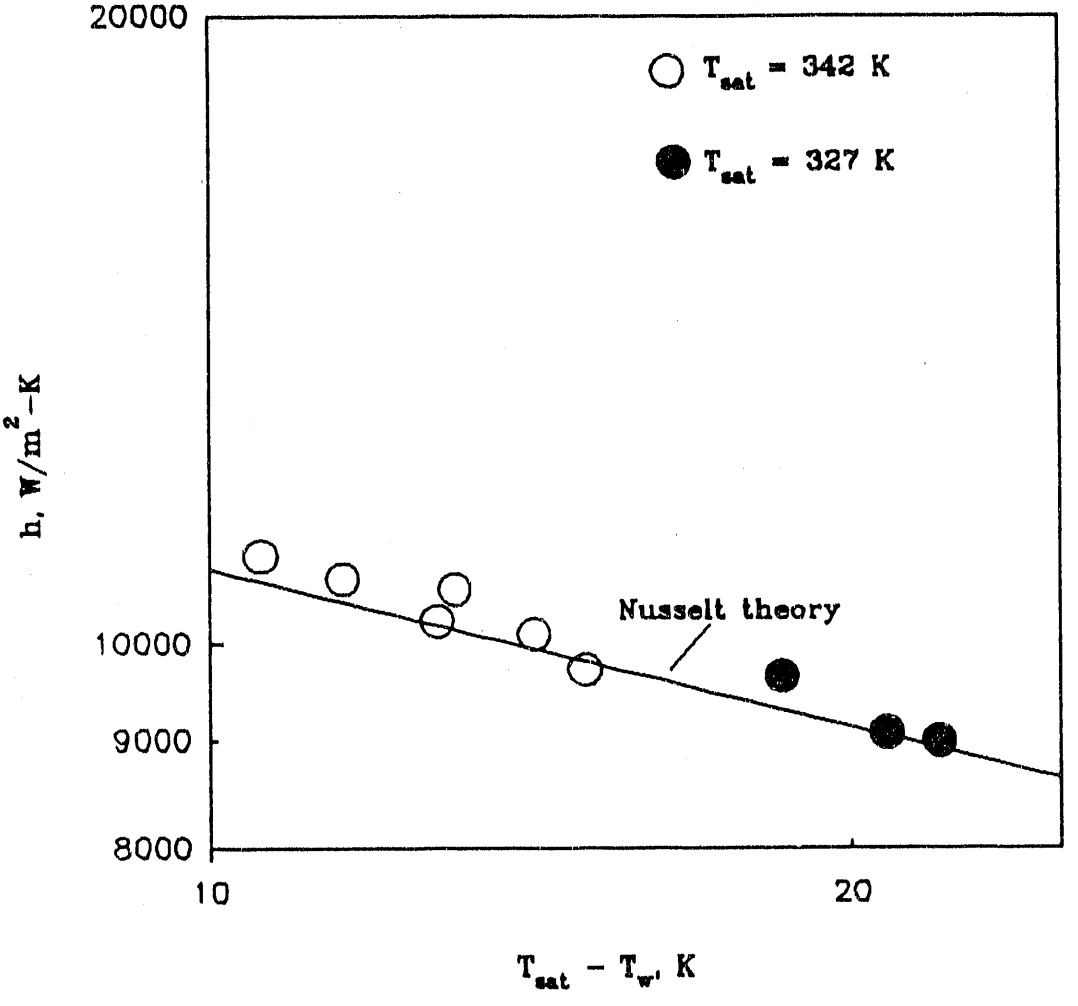

Figure 4.6. Plain copper tube data.

symbols that appear in the graphs are for different tests, which were taken on different days to justify the repeatability of the data. The coefficient n that appears in Equation [4.4] is listed in Table 4.3 for each tube.

Copper Alloy Tubes

Figure 4.7 shows the condensing coefficient vs. ΔT ($= T_{sat} - T_{w,av}$) for the 19.0 mm CU-11 copper tube, which has 433 fpm (11 fpi), e = 1.12 mm, and t_b = 0.9 mm. The average enhancement level is 2.85.

Three different 90/10 copper-nickel tubes were tested. The first is a 22.23 mm diameter C/N-11 tube which has the same fin shape, dimensions and fin pitch as the 19 mm diameter CU-11 copper tube. The data are shown in Figure 4.8, where an average enhancement level of 1.75 is obtained. The second cu/ni tube (C/N-19) has the same diameter as the C/N-11 tube, but has a smaller fin pitch, and a smaller fin height. The results for the C/N-11 tube are shown in Figure 4.9, for which an average enhancement level of 1.64 is obtained. Thus, 742 fpm tube provided only slightly less enhancement as the 433 fpm tube.

The third type, A/P-50, is a smooth copper-nickel tube with copper particles sintered to the surface. Approximately 50% of the tube projected surface is covered with particles. Figure 4.10 shows the data obtained for this tube. The enhancement

Table 4.3

Values of the Exponent n in Equation 4.4

(T_{sat} = 54 C)

Tube Code	C	n
Plain	20828.31	-0.27
CU-11	54345.05	-0.22
C/N-11	36513.21	-0.30
C/N-19	32906.37	-0.26
TiA-11	18033.08	-0.12
TiB-11	18931.72	-0.20
A/P	43219.53	-0.47

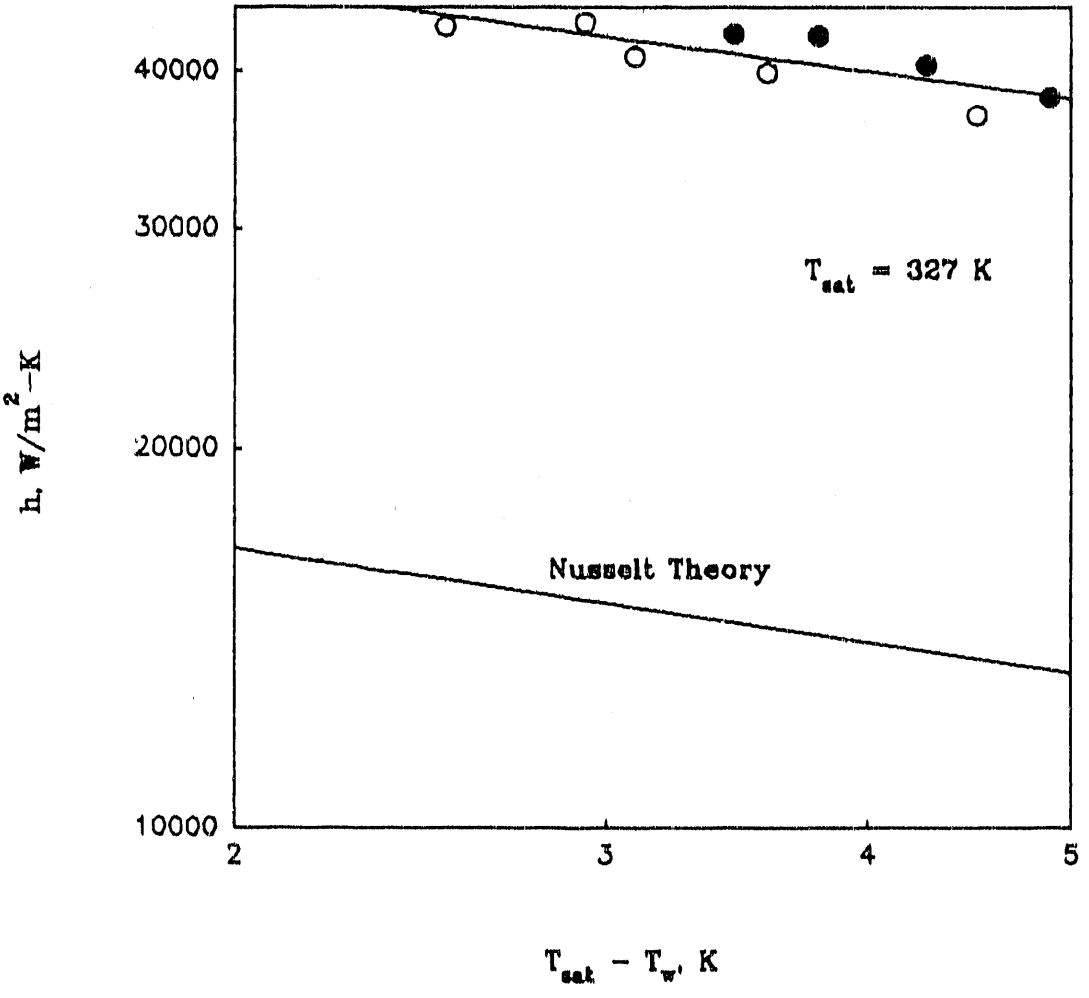

Figure 4.7. Data for the CU-11 tube.

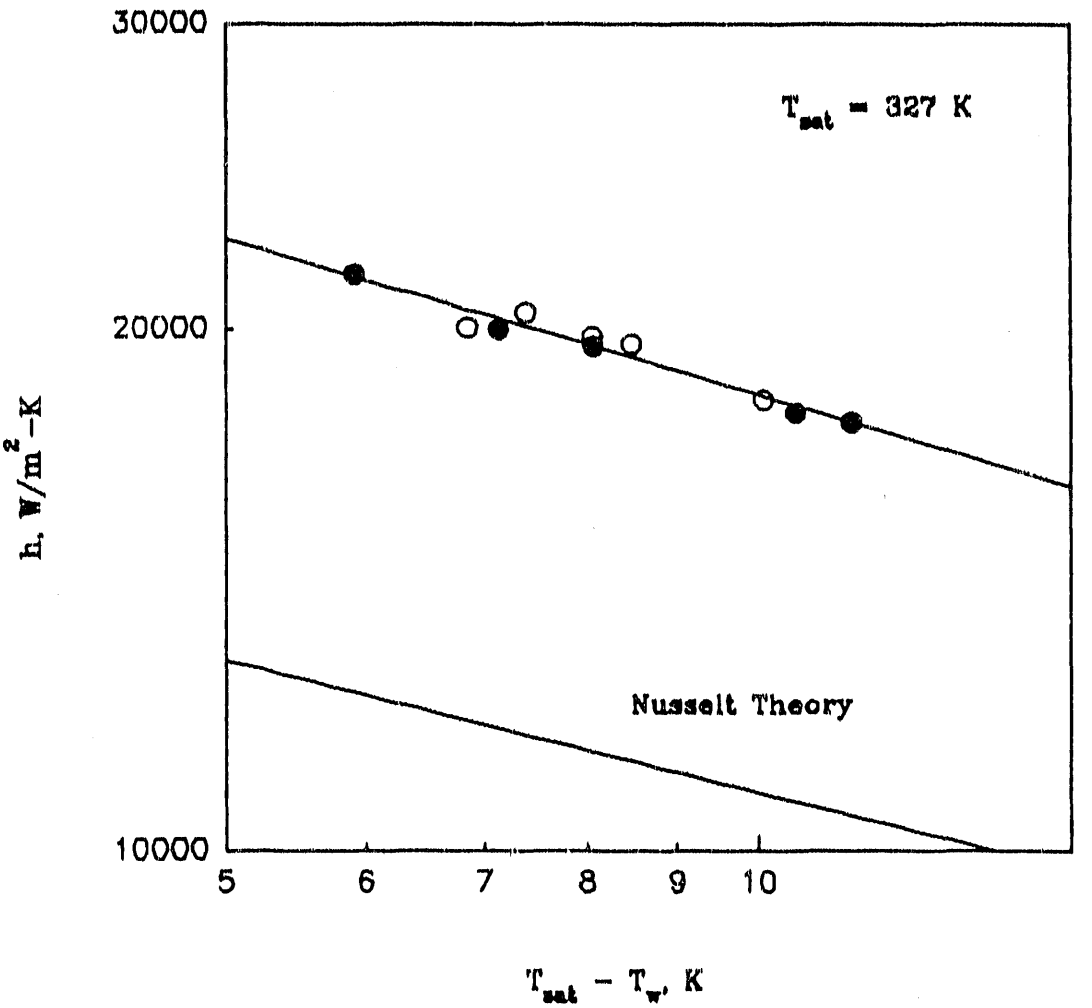

Figure 4.8. Data for the copper–nickel C/N–11 tube

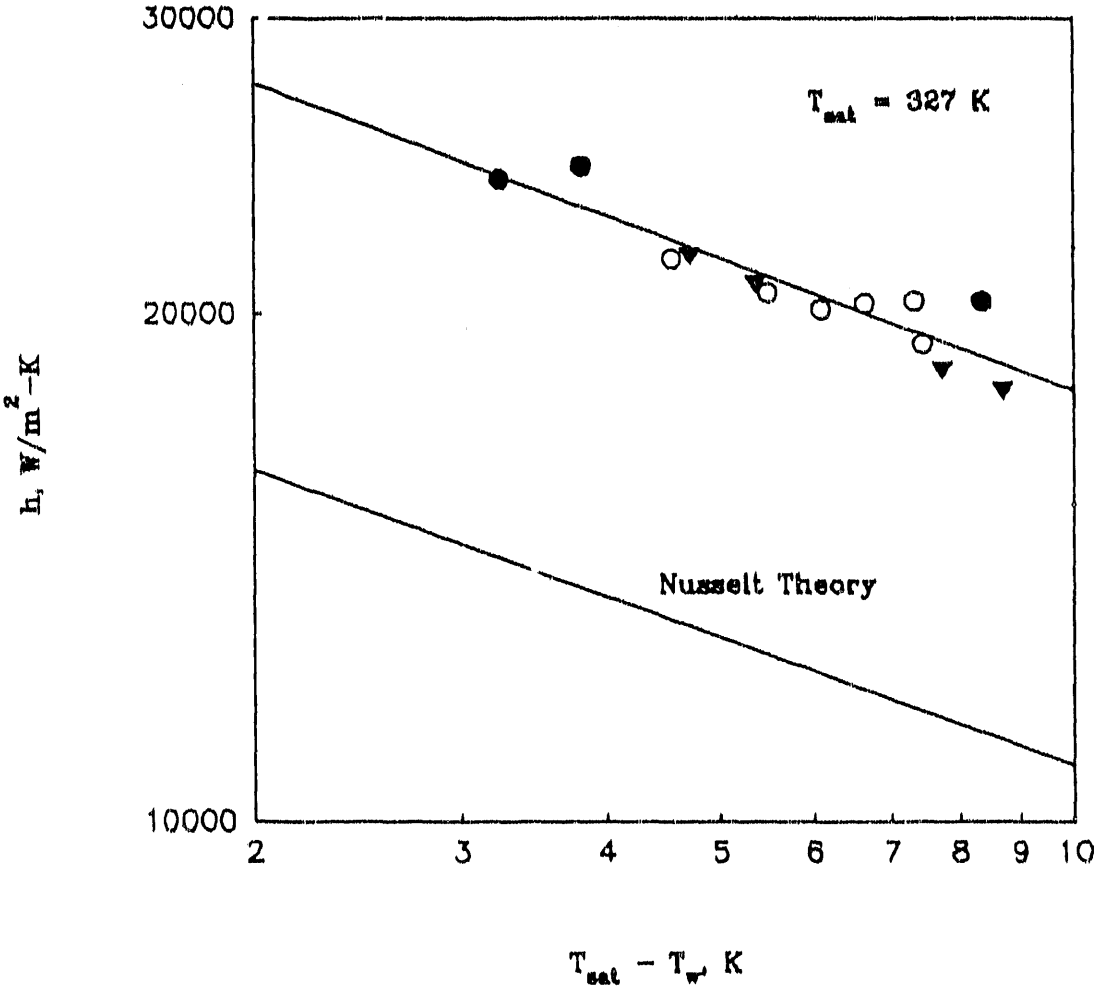

Figure 4.9. Data for the copper–nickel C/N–19 tube.

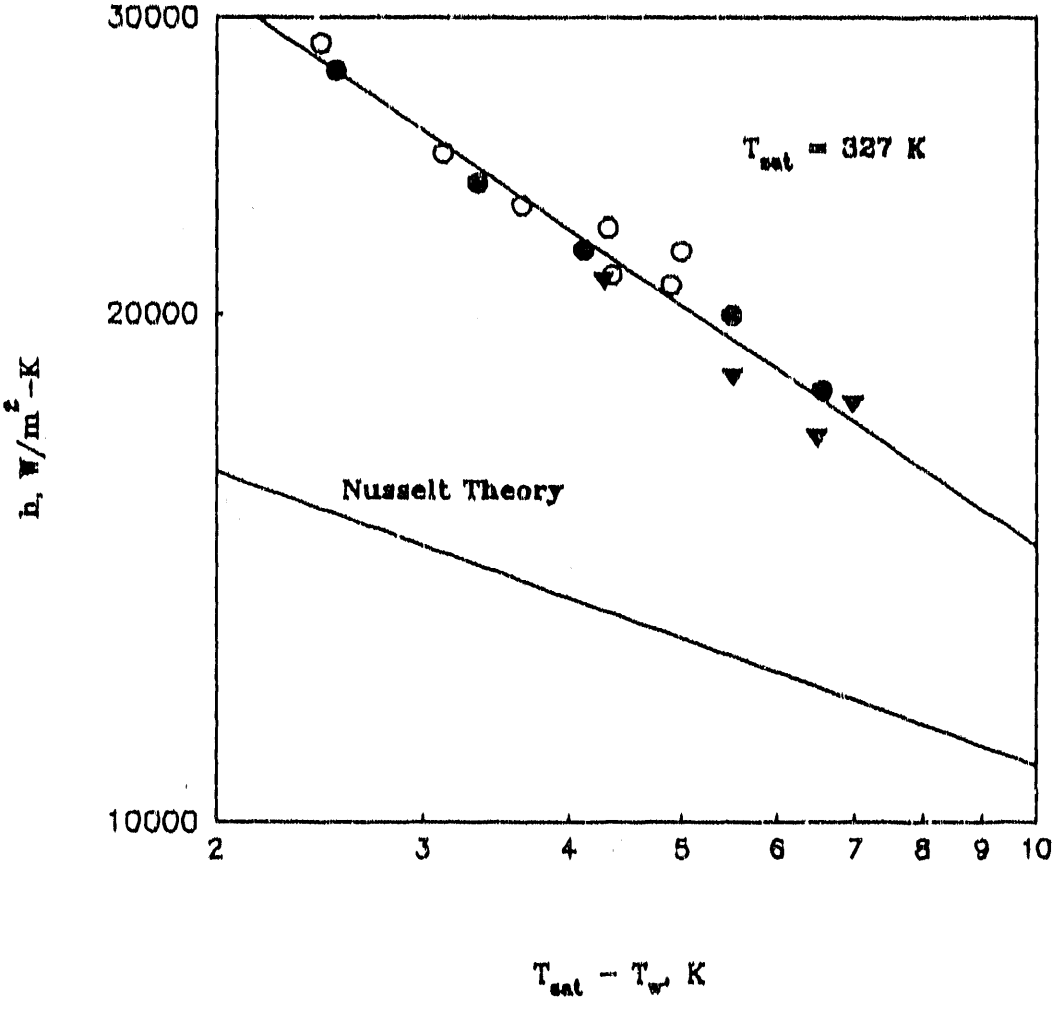

Figure 4.10. Data for the A/P--50 tube

level is a strong function of ΔT as can be seen from the exponent n = -0.47 in Table 4.3. The maximum enhancement was 1.89 (at the lowest ΔT) and the minimum of 1.4 (at the highest ΔT).

Titanium Tubes

Two titanium tubes, TiA-11 and TiB-11, were tested both having the 18.29 mm diameter over the fins and fin pitch, but different fin shapes. The dimensions of the 'A' and 'B' tubes are described in Table 4.2. The major difference between the two tubes is the fin height and the drainage channel shape. Figure 4.11 shows the results for the 'A' tube which show a modest average enhancement of 1.22. The results for the 'B' tube are shown in Figure 4.12 where the average enhancement level is 1.05.

Table 4.4 summarizes the enhancement level of each of the tested tubes and Appendix C presents tabulated values of the data and Appendix D discusses the uncertainty in the condensing heat transfer coefficient.

4.9 Experimental Results for the Overall Heat Transfer Coefficient

Two tubes were selected to measure the overall heat transfer coefficient. The C/N-11 copper nickel and TiA-11 titanium tubes gave the maximum enhancement

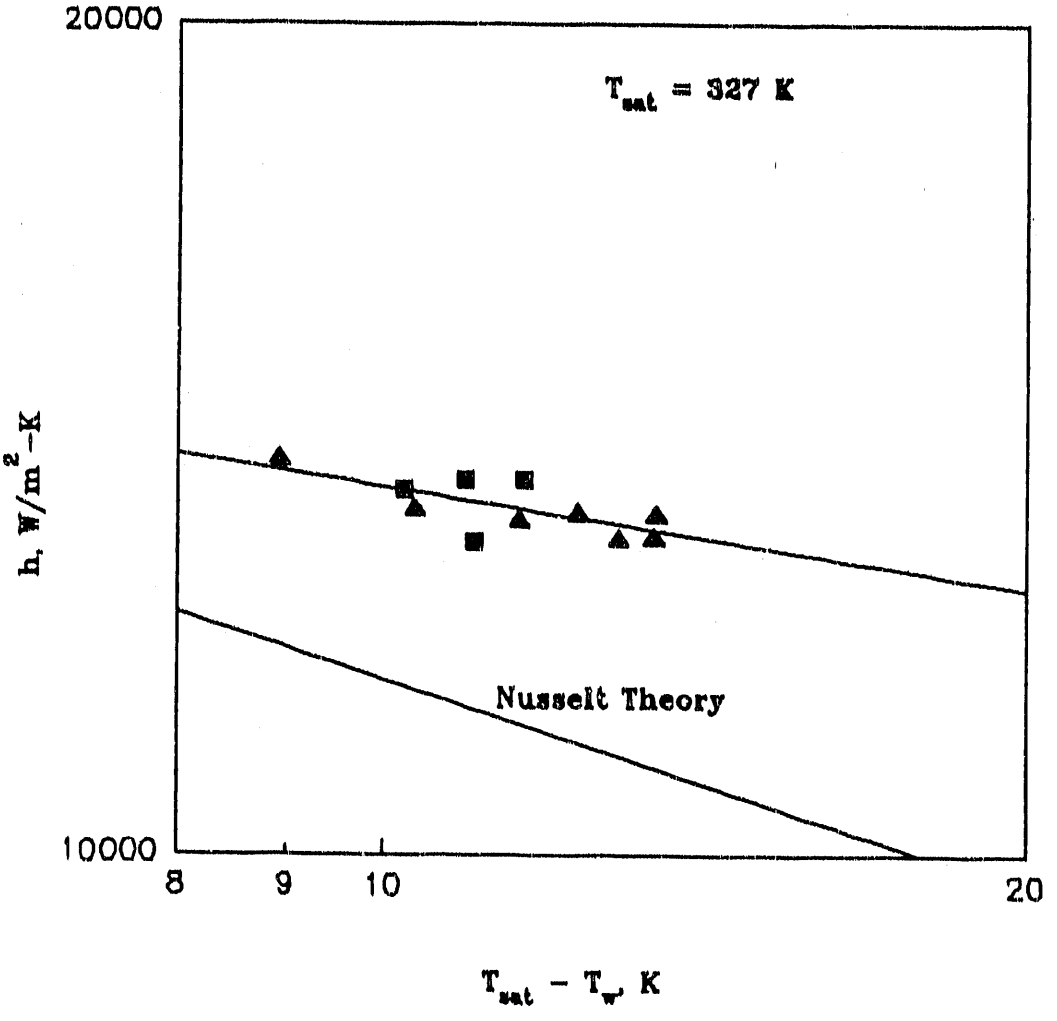

Figure 4.11. Data for the TIA-11 tube

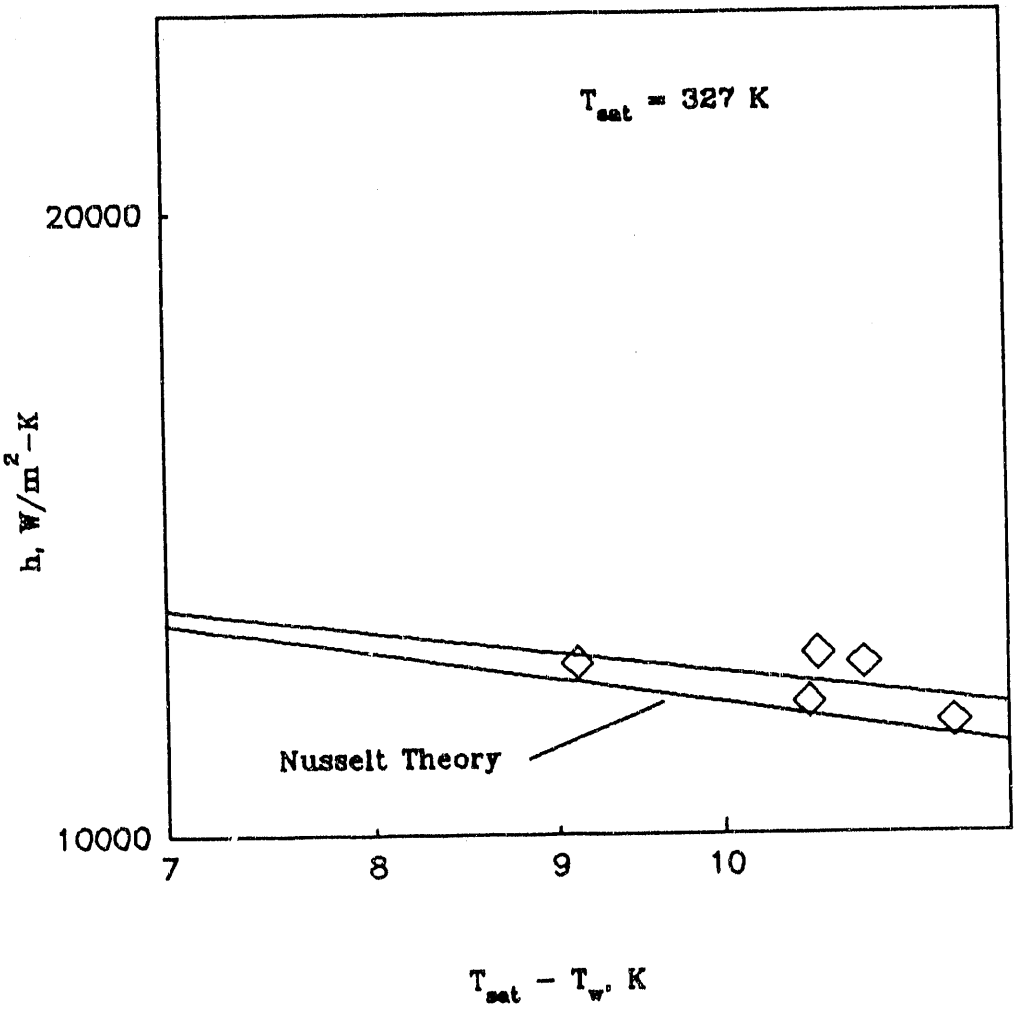

Figure 4.12. Data for the TiB-11' tube

Table 4.4

External Enhancement Levels, E_o

(ΔT = 4.4 C, T_{sat} = 54 C)

Tube Code	E_o
CU-11	2.80
C/N-11	1.75
C/N-19	1.64
A/P-50	1.70
TiA-11	1.22
TiB-11	1.05

enhancement on the steam side. The tests were carried out at a temperature of 41.7 C (107 F). Electric utility steam condensers typically operate at approximately 38 C (100 F). Three tubes were connected in series producing a total length of 1.37 m (4.5 ft).

Figure 4.13 shows the UA value for the C/N-11 tube as a function of water velocity. A typical operating water velocity for electric utility steam condensers is around 1.98 m/sec (6.5 ft/sec). The overall heat transfer coefficient of a plain tube was determined by using the Nusselt theory for the steam side and the Petukhov (1970) equation for the water side. The enhancement in the UA value was determined to be 1.8. Another test was carried out on the C/N-11 tube with steam condensing at 130 F. The measured UA value for the C/N-11 tube was used to calculate the condensing coefficient and hence the enhancement level and then compare it to the measured condensing coefficient. The inside heat transfer coefficient can be calculated using the correlation provide by the tube manufacturers, and the wall resistance was calculated with the knowledge of the wall thickness. Hence, the condensing coefficient can be calculated as follows:

$$\frac{1}{hA} = \frac{1}{UA} - R_w - \frac{1}{h_i A_i} \qquad [4.6]$$

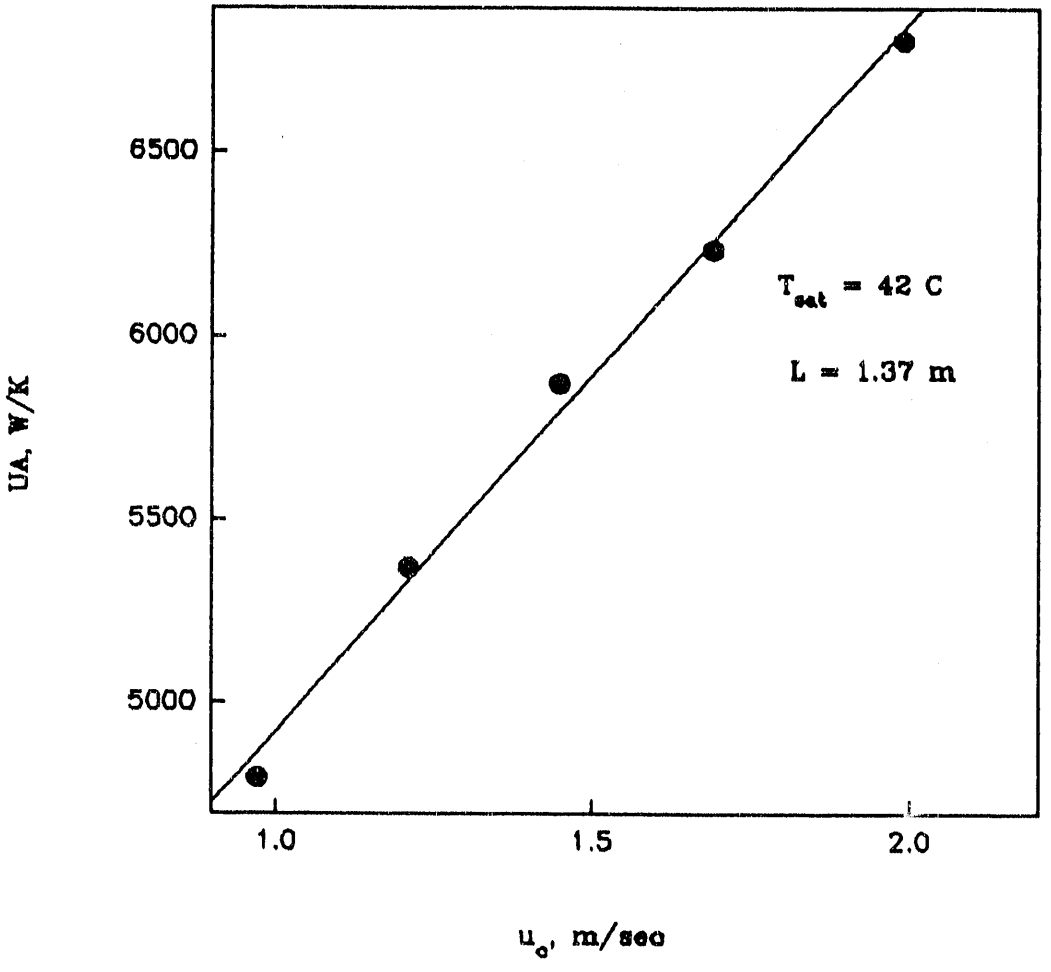

Figure 4.13. Overall thermal performance of C/N-11 tube.

where R_w is the wall resistance, h_i is the heat transfer coefficient, $A_i = \pi D_i L$, and $A = \pi D_o L$. The enhancement level, on the condensing side, was found to be 1.76. This compares to 1.75 as determined by direct measurements of the condensing coefficient as shown in Table 4.4. This result produces more confidence in the instrumentation and experimental procedure.

For the titanium TiA-11 tube, two tubes were connected in series producing a total length of 0.91 m (3 ft). The results for the UA values are shown in Figure 4.14. The UA value for the plain tube was calculated in the same manner as described above. The enhancement level in the UA value is found to be 1.21. Again, another test was carried out at 54.4 C (130 F) to determine the condensing coefficient by subtracting the wall and tubeside thermal resistances as shown by Equation [4.6]. However, the inside heat transfer coefficient for the enhanced tube was estimated from pressure drop estimates provided by the tube manufacturer, since no direct measurements were taken for the heat transfer coefficient. The measured pressure drop was 9% higher than that of a plain tube. Hence, an optimistic estimate of the inside heat transfer coefficient is a value of 10% higher than that of a plain tube. The resulting condensing coefficient is found to be 1.20 compared to a value of 1.22 that was obtained from direct measurements of the wall temperature, as shown in Table 4.4. This result also gives more confidence in the data obtained for the condensing coefficient.

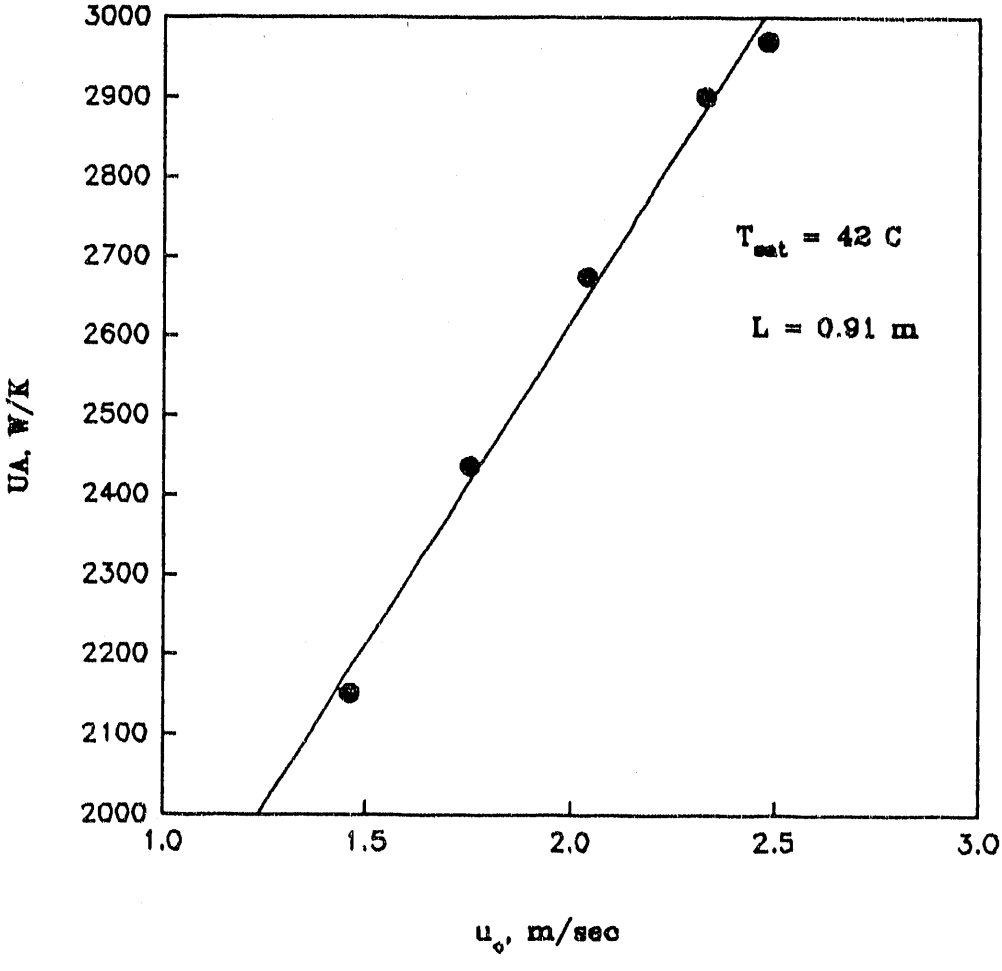

Figure 4.14. Overall thermal performance of the TIA-11 tube.

CHAPTER 5

JUSTIFICATION AND APPLICATION OF MATHEMATICAL MODEL

5.1 Introduction

The model developed in Chapter 3 was used to predict some of the existing data in the literature, for steam and refrigerants. It was also used to predict the data obtained in this project. Once the model was justified, a parametric study was conducted to determine the effect of fin and tube geometry, and operating conditions on the condensing heat transfer coefficient.

In modelling the surface tension induced flow on the fin top (subregion *bc)*, alternative I in section 3.6.1.2 was used because of its simplicity. Moreover, the minimum value of the parameter Z (refer to section 3.6.1.2), that appears in the equation for the K-W profile, was determined iteratively to be between 10.0 and 50.0 depending on the fin geometry.

5.2 Justification of Model

5.2.1 Prediction of Data in the Literature

Table 5.1 presents the fin geometry, saturation temperature, and type of condensing fluid for the data. By predicting data for steam and refrigerants, the use of the model will be justified for fluids with high (steam) and low (refrigerants) surface tension. All the data shown are for copper tubes. Figure 5.1 shows the ratio of predicted to experimental condensing coefficient as a function of fin spacing. All of the data points (except those of Rudy and Webb (1983) and the Honda et al. (1987)) presented in Table 5.1, were obtained by the Wilson technique. This technique is based on measuring the tubeside heat transfer coefficient. By subtracting the tubeside and wall thermal resistances from the overall heat transfer coefficient, the condensing coefficient is obtained. Hence, this method does not require the measurement of the wall temperature. Therefore, the condensing coefficient cannot be predicted by providing the program with the wall temperatures in the flooded and unflooded regions. For the sake of consistency, all the data were predicted by the same procedure. The procedure is based on an iterative scheme to determine the average vapor to wall temperature difference of the tube from the knowledge of the heat flux provided by the references that appear in Table 5.1. This average temperature difference is the denominator of Equation [3.9]. The results show that except for two points, the model predicts the data for steam and refrigerants

Table 5.1

Geometry And Operating Conditions Of

Some Data Presented In The Literature

s mm	e mm	t_b mm	t_t mm
Wanniarachchi et al. (1986), Steam @ 48 C			
0.5,1.0,1.5,2.0,4.0,9.0	1.0	1.0	1.0
Wanniarachchi et al. (1986), Steam @ 100 C			
0.5,1.0,1.5,2.0,4.0,9.0	1.0	1.0	1.0
Yau et al. (1985), Steam @ 100 C			
0.5,1.0,1.5,2.0,4.0,6.0,10.0	1.6	0.5	0.5
Rudy & Webb (1983), R-11 @ 35 C			
1.34	1.53	0.42	0.2
0.98	1.53	0.52	0.2
0.73	0.89	0.29	0.2

Table 5.1 (Continued)

s mm	e mm	t_b mm	t_t mm
	Marto et al. (1988), R-113 @ 48 C		
0.25,0.5,1.0,2.0,4.0	1.0	1.0	1.0
0.25,0.5,1.0,1.5,2.0	1.0	0.5	0.5
0.5,1.0,1.5,2.0	1.0	0.75	0.75
1.0,1.5,2.0	2.0	1.0	1.0
1.0,1.5,2.0	0.5	1.0	1.0
1.0,1.5,2.0	1.5	1.0	1.0
	Masuda et al. (1987), R-113 @ 48 C		
0.25,0.5,1.0,1.5,,2.0	1.59	0.5	0.5
	Honda et al. (1987), R-113 @ 55 C		
0.5	1.46	0.4	0.28
0.34	0.92	0.3	0.18
0.4	1.13	0.1	0.10

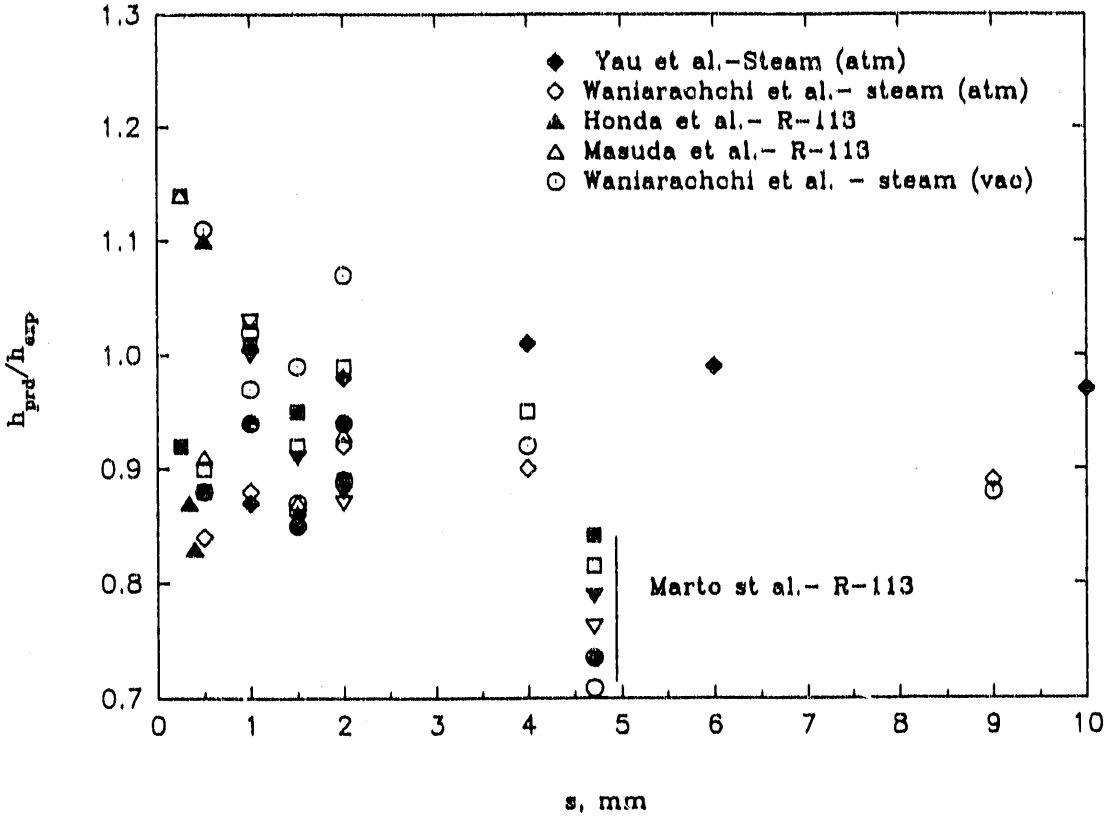

Figure 5.1. Predictions of data for steam and R–113

R-11 and R-113 within ±15%.

5.2.2 Prediction of Data in the Present Project

All of the integral fin tubes tested in this program had trapezoidal fins and a circular channel. The theory presented in section 3.11 (Extension of the Model to Other Fin/Channel Combinations) was used. The tubes considered are the CU-11, C/N-11, C/N-19, TiA-11, and TiB-11. The tubes are defined in Tables 4.1 and 4.2. In predicting the condensing coefficient of these tubes, the measured wall temperatures of the unflooded and flooded regions were used.

Figure 5.2 shows the ratio of predicted to experimental condensing coefficient as a function of (T_{sat} - T_w). The results show that, except for one point, the copper, copper-nickel, and titanium TiA-11 tubes are predicted within -14% and +8%. One data point for the C/N-11 tube was underpredicted by -17%. The data for the titanium TiB-11 tube was over predicted by 22% to 30%. This tube has a fin height of 0.28 mm and a "shallow" circular drainage channel. Hence, it is possible that the condensate in the drainage channel not only covered the entire fin side but also affected the surface tension induced pressure gradient on the fin top, subregion *bc*, in both the unflooded and flooded regions. Hence, by using Equation [3.16], it is possible that the condensing coefficient in subregion *bc* was overpredicted. The possibility of large inaccuracies in the data also exists.

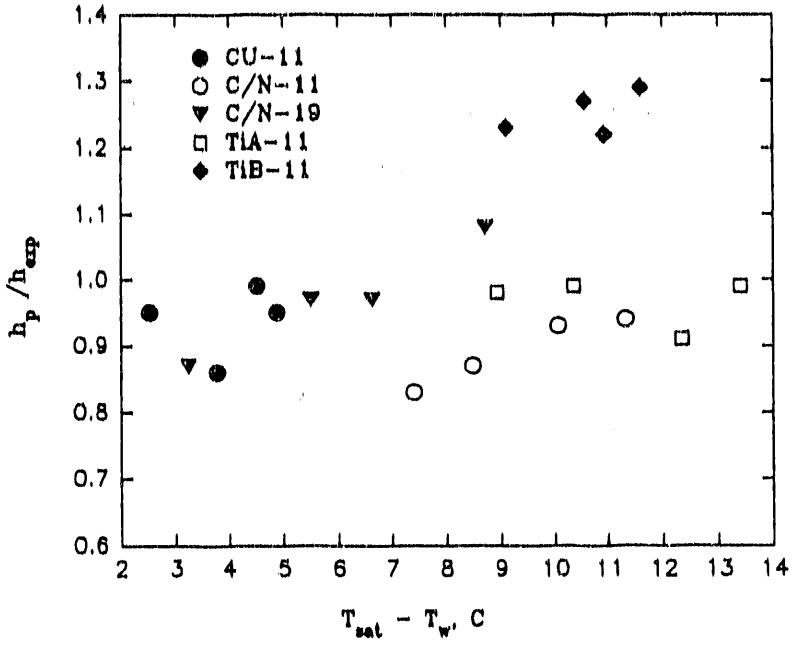

Figure 5.2. Ratio of predicted to experimental condensation coefficient versus ($T_{sat} - T_w$) for the five integral finned tubes tested in the present project..

5.3 Parametric Study

The model was used to predict the performance of integral fin tubes, for different tube and fin geometries, tube thermal conductivity, and fin spacing. The parametric study was basically directed at low thermal conductivity materials with flat drainage channels.

5.3.1 Effect of Fin/Tube Geometry on the Fraction of Tube Flooded, c_b.

The amount of flooding that occurs on an integral fin tube greatly affects the heat transfer performance of that tube. Equation [3.10] was used to determine the effect of tube diameter and fin geometry on the flooding characteristics of steam. The fluid properties are evaluated at a film temperature of 48 C. At this film temperature, the property group, $\sigma/\rho g$ is equal to 7.5E-06 m^2. Figure 5.3 shows c_b vs. the fin spacing for a rectangular fin with $e = t_b = t_t = 1.0$ mm, for different tube diameters. The results show that for the same fin geometry and spacing, the flooding angle decreases as the tube diameter increases. For example, at a fin spacing of 1.5 mm, c_b decreases by 9% when the tube diameter increases from 19.0 mm (3/4") to 22.23 mm (7/8"). This decrease in the flooding angle implies an increase in the active heat transfer area in the unflooded region. This active area consists of all the sub-regions on the fin side, top, and root region excluding the drainage channel.

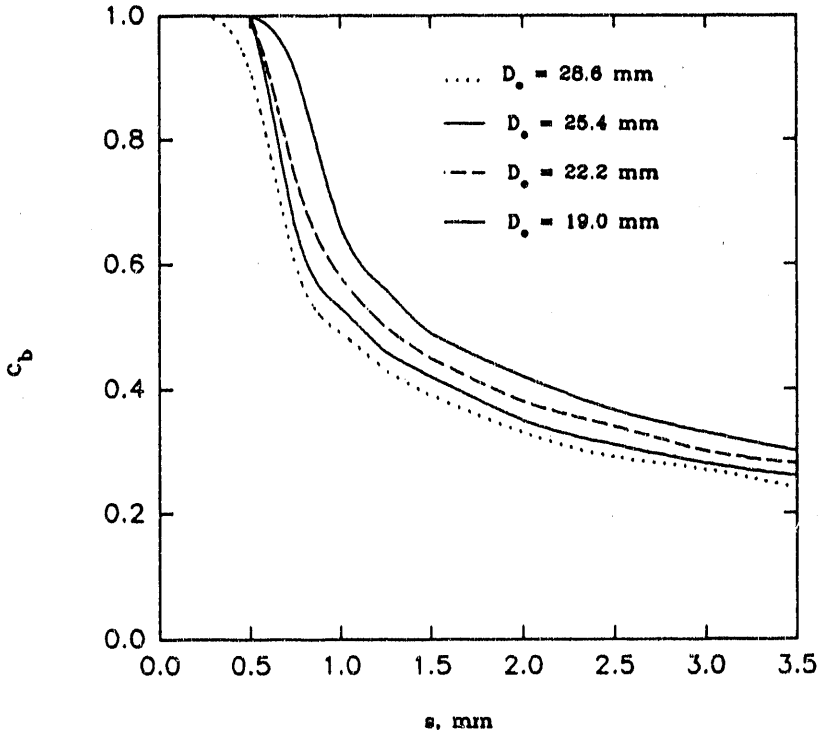

Figure 5.3. Effect of tube diameter on the fraction of tube flooded. $e = t_t = t_b = 1.0$ mm.

Figure 5.4 shows c_b vs. s for a trapezoidal fin with t_b = 1.0 mm, and t_t = 0.2 mm. The tube diameter is fixed at 22.23 mm but the fin height is varied from 0.5 mm to 1.0 mm. The results show that c_b decreases as the fin height decreases. For example at a fin spacing of 1.5 mm, c_b decreases by 20% when the fin height decreases from 0.5 mm to 1.0 mm. At a fin spacing of 1.5 mm, t_b = 1.0 mm, e = 1.0 mm, and 22.23 mm diameter, the comparison between Figures 5.4 and 5.3 show that by reducing the fin tip thickness from 1.0 mm to 0.2 mm, c_b is reduced by 27%.

The implication of these results is that c_b decreases with reduced tip thickness and fin height. As will be shown in section 5.3.3, a lower fin height will also lead to a higher fin efficiency for the low thermal conductivity tubes.

5.3.2 Effect of Fin Spacing and Tube Thermal Conductivity on the Enhancement Level

The predictions in this section were based on a saturation temperature of T_{sat} = 34 C (93 F) and cooling water velocity and temperature of 2.0 m/sec (6.5 ft/sec) and 21 C (70 F), respectively. These conditions correspond to typical operating conditions of electric utility steam condensers. The water side is assumed to have an enhancement level of E_i = 1.8. As will be shown in Chapter 6, this enhancement can be achieved with selection of the internal enhancement geometry. The tube wall thickness was fixed at 0.89 mm (0.035").

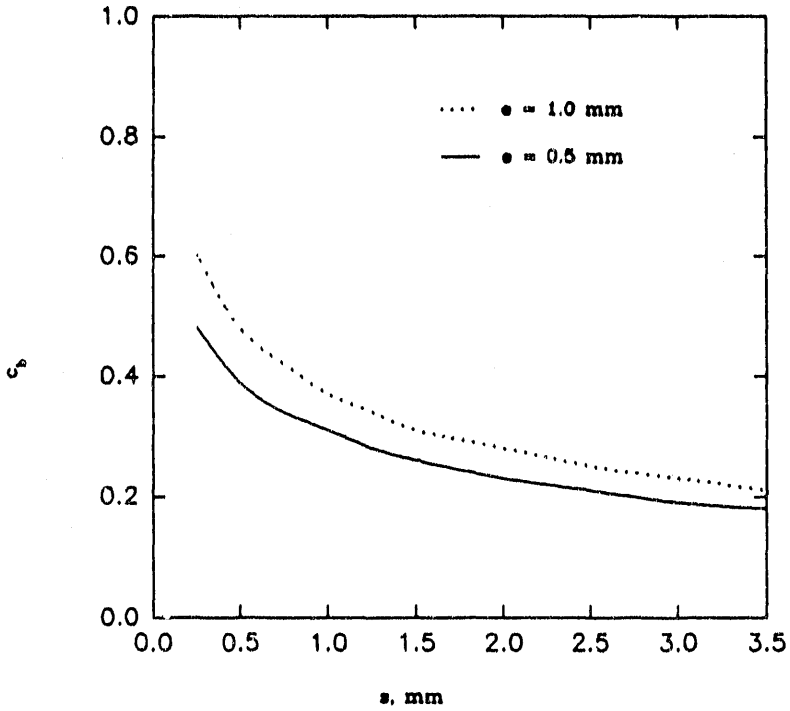

Figure 5.4. Effect of fin height on the fraction of tube flooded. D_o = 22.23 mm, t_b = 1.0 mm, t_t = 0.2 mm.

Figure 5.5 shows the variation of the enhancement level with fins per meter (fpm). The fin geometry is fixed at e = 1.0 mm, t_t = 0.2 mm, and t_b = 0.9 mm. Titanium tubes usually have a lower fin height. However, to show the effect of fin height on the tube performance, a titanium tube with a fin height of 1.0 mm was also included. Hence, the tube materials considered in Figure 5.5 are copper, copper-nickel, admiralty, and titanium. Figure 5.5 shows that the enhancement level decreases as the thermal conductivity decreases with the copper tube having the highest level. These results support previous experimental studies of Mitrou (1986) and Mills et al. (1975). The highest enhancement level is obtained at 492 fpm, 512 fpm, 472 fpm, and 394 fpm, for the copper, admiralty, copper-nickel, and titanium tubes respectively. The maximum enhancement levels are 3.05, 2.96, 1.87, and 1.26 for copper, admiralty, copper-nickel, and titanium, respectively. The predictions of the titanium tube follow an almost flat curve with a dip at 512 fpm (1.05 mm fin spacing). The reason for such a behavior is due to the drainage channel. At fin spacings higher than 1.05 mm, a surface tension induced pressure gradient exists on the tube surface which is primarily responsible for the average 25% enhancement. Once the drainage channel radius becomes equal to half the fin spacing, which is the case for the 512 fpm tube, the surface tension induced pressure gradient on the root surface disappears. Even though there are surface tension induced pressure gradients on the fin top and side, the low thermal conductivity of titanium results in a very low fin efficiency, as will be shown in the following tables.

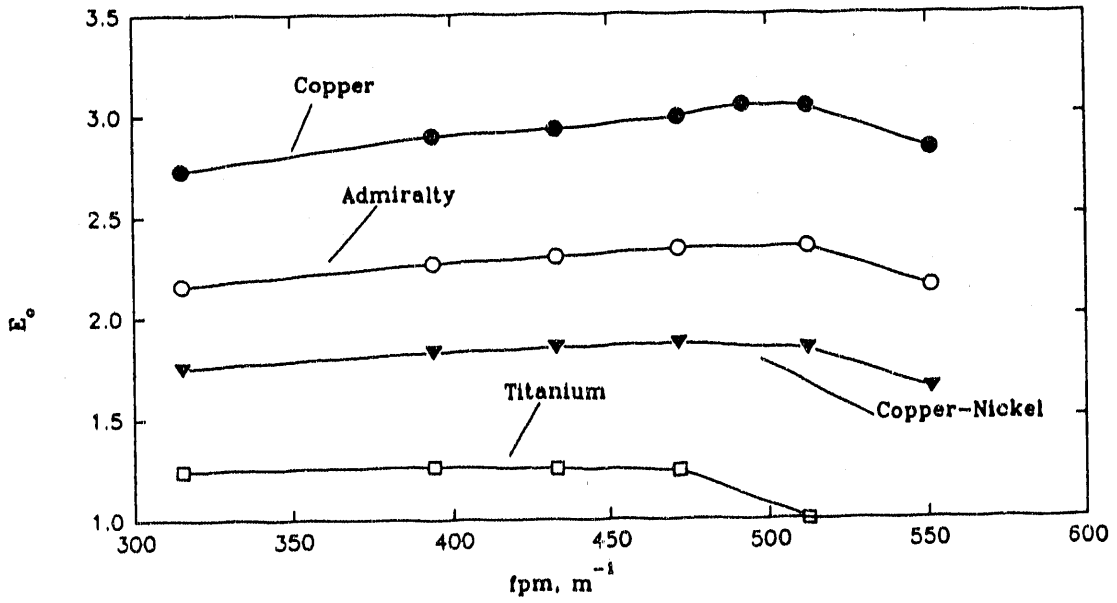

Figure 5.5. Enhancement level versus fpm, for e = 1.0 mm, t_b = 0.9 mm, t_t = 0.2 mm, D_o = 22.23 mm.

Several other important parameters, based on the predictions of Figure 5.5, have been tabulated in Tables 5.2, 5.3, 5.4, and 5.5. Tables 5.2, 5.3, 5.4, and 5.5, present the predicted values of c_b (fraction of tube flooded), η_u (fin efficiency in the unflooded region), η_f (fin efficiency in the flooded region), and the parameter hA/L. The results show that as the thermal conductivity decreases, the fin efficiency decreases. Table 5.6 summarizes the effect of thermal conductivity on the enhancement level and fin efficiency. The fin efficiencies in the unflooded region for copper, admiralty, copper-nickel, and titanium are 0.75, 0.55, 0.40, and 0.25, respectively. The calculations also show that the fin efficiency in the flooded region is higher than that in the unflooded region. Appendix E explains the reason for such a behavior.

5.3.3 Effect of Fin Height on the Enhancement Level

The same operating conditions and geometrical variables that were used in section 5.3.2 apply to the following predictions. The only variable that has been changed is the fin height which is 0.5 mm as compared to 1.0 mm in section 5.3.2. Figure 5.6 shows the enhancement level versus fins per meter for admiralty, copper-nickel, and titanium tubes with a fin height of 0.5 mm. The effect of thermal conductivity on the enhancement shows the same trend as obtained in Figure 5.5. However, by comparing Figures 5.5 and 5.6, it is seen that the enhancement levels for all three materials are higher for the 0.5 mm fins. This is mainly due to the

Table 5.2

Steam Condensation on Copper Tubes - Trapezoidal Fins

T_{sat} = 34 C (93 F), k = 350 W/m-K

[D_o = 22.23 mm, t_{wall} = 0.89 mm, E_i = 1.8, hA/L = W/m-K]

[e = 1.0 mm, t_b = 0.90 mm, t_t = 0.2 mm]

fpm	hA/L	E_o	c_b	η_u	η_f
315	2496	2.73	0.28	0.77	0.86
394	2699	2.90	0.32	0.75	0.87
433	2718	2.93	0.34	0.75	0.87
472	2797	3.00	0.37	0.75	0.86
492	2860	3.05	0.38	0.75	0.86
512	2858	3.04	0.39	0.74	0.86
551	2610	2.83	0.41	0.76	0.86

Table 5.3

Steam Condensation on Admiralty Tubes - Trapezoidal Fins

T_{sat} = 34 C (93 F), k = 121 W/m-K

[D_o = 22.23 mm, t_{wall} = 0.89 mm, E_i = 1.8, hA/L = W/m-K]

[e = 1.0 mm, t_b = 0.90 mm, t_t = 0.2 mm]

fpm	hA/L	E_o	c_b	η_u	η_f
315	1892	2.16	0.28	0.57	0.67
394	2013	2.27	0.32	0.55	0.67
433	2043	2.30	0.34	0.55	0.67
472	2086	2.34	0.37	0.55	0.66
512	2098	2.35	0.39	0.54	0.66
551	1875	2.15	0.41	0.56	0.65

Table 5.4

Steam Condensation on Copper-Nickel Tubes - Trapezoidal Fins

T_{sat} = 34 C (93 F), k = 52 W/m-K

[D_o = 22.23 mm, t_{wall} = 0.89 mm, E_i = 1.8, hA/L = W/m-K)]

[e = 1.0 mm, t_b = 0.90 mm, t_t = 0.2 mm]

fpm	hA/L	E_o	c_b	η_u	η_t
315	1502	1.75	0.28	0.41	0.51
394	1580	1.83	0.32	0.40	0.52
433	1601	1.85	0.34	0.40	0.52
472	1625	1.87	0.37	0.39	0.51
512	1594	1.84	0.39	0.39	0.50
551	1381	1.64	0.41	0.41	0.50

Table 5.5

Steam Condensation on Titanium Tubes - Trapezoidal Fins

T_{sat} = 34 C (93 F), k = 19 W/m-K

[D_o = 22.23 mm, t_{wall} = 0.89 mm, E_i = 1.8, hA/L = W/m-K]

[e = 1.0 mm, t_b = 0.90 mm, t_t = 0.2 mm]

fpm	hA/L	E_o	c_b	η_u	η_f
315	1054	1.24	0.28	0.26	0.27
394	1070	1.26	0.32	0.25	0.28
433	1063	1.25	0.34	0.25	0.28
472	1059	1.24	0.37	0.25	0.27
512	796	0.99	0.39	0.27	0.27

Table 5.6

Effect of Tube Thermal Conductivity on the Enhancement Level

T_{sat} = 34 C (93 F)

[D_o = 22.23 mm, t_{wall} = 0.89 mm, E_i = 1.8, k = W/m-K]

[12 FPI, e = 1.0 mm, t_b = 0.9 mm, t_t = 0.2 mm]

Material	k_m	E_o	$\eta_{f,u}$	$\eta_{f,f}$
Titanium	19	1.24	0.25	0.27
90/10 Cu/Ni	52	1.87	0.40	0.51
Admiralty	121	2.34	0.55	0.66
Copper	350	3.00	0.75	0.86

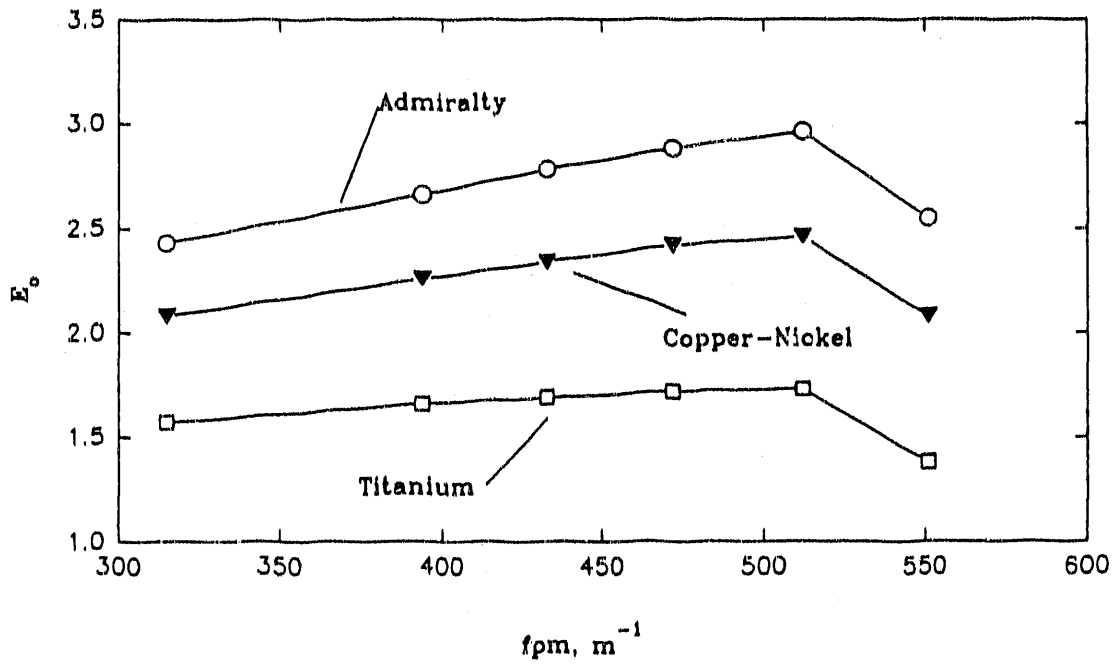

Figure 5.6. Enhancement level versus fpm, for e = 0.5 mm, t_b = 0.9 mm, t_t = 0.2 mm, D_o = 22.23 mm.

increase in the fin efficiency in both the flooded and unflooded regions. The increase in the enhancement level is also attributed to the decrease in flooding as shown in section 5.3.1. Tables 5.7, 5.8 and 5.9 present the predicted values of the other relevant parameters. The comparison between Tables 5.7, 5.8, and 5.9 and Tables 5.3, 5.4, and 5.5, show that the fin efficiency for the 0.5 mm fins is higher than that of the 1.0 mm fins. When the fin height was reduced from 1.0 mm to 0.5 mm the fin efficiency, in the unflooded region, increased by approximately 29%, 35%, and 44% for admiralty, copper-nickel, and titanium, respectively. For the flooded region, the increase in the fin efficiency was 20%, 29%, and 54% for admiralty, copper-nickel, and titanium respectively. For a fin height of 0.5 mm, the highest enhancement level is obtained at 512 fpm for admiralty, copper-nickel, and titanium. The maximum enhancement level is 2.96, 2.46, and 1.73 for admiralty, copper-nickel, and titanium, respectively.

5.3.4 Effect of Fin Base Thickness on the Enhancement Level

To determine the effect of the fin base thickness on the enhancement level, the fin density was fixed at 472 fpm and the tube diameter at 22.23 mm (7/8"). The fin height and tip thickness were set at 0.5 mm 0.2 mm, respectively. The water side enhancement level was set at E_i = 1.8. Figure 5.7 shows the enhancement level versus the fin base thickness for admiralty, copper-nickel, and titanium tubes, respectively. The results show that the enhancement level increases as the fin base

Table 5.7

Steam Condensation on Admiralty Tubes - Trapezoidal Fins

T_{sat} = 34 C (93 F), k = 121 W/m-K

[D_o = 22.23 mm, t_{wall} = 0.89 mm, E_i = 1.8, hA/L = W/m-K]

[e = 0.5 mm, t_b = 0.90 mm, t_t = 0.2 mm]

fpm	hA/L	E_o	c_b	η_u	η_f
315	2157	2.43	0.24	0.74	0.80
394	2422	2.66	0.27	0.72	0.80
433	2551	2.78	0.29	0.71	0.79
472	2673	2.88	0.31	0.71	0.79
512	2768	2.96	0.33	0.70	0.78
551	2295	2.55	0.35	0.73	0.79

Table 5.8

Steam Condensation on Copper-Nickel Tubes - Trapezoidal Fins

T_{sat} = 34 C (93 F), k = 52 W/m-K

[D_o = 22.23 mm, t_{wall} = 0.89 mm, E_i = 1.8, hA/L = W/m-K]

[e = 0.5 mm, t_b = 0.9 mm, t_t = 0.2 mm]

fpm	hA/L	E_o	c_b	η_u	η_f
315	1835	2.08	0.24	0.58	0.69
394	2029	2.26	0.27	0.56	0.69
433	2122	2.34	0.29	0.55	0.68
472	2212	2.42	0.31	0.54	0.67
512	2261	2.46	0.33	0.54	0.66
551	1835	2.08	0.35	0.57	0.67

Table 5.9

Steam Condensation on Titanium Tubes - Trapezoidal Fins

T_{sat} = 34 C (93 F), 19 W/m-K

[D_o = 22.23 mm, t_{wall} = 0.89 mm, E_i = 1.8, hA/L = W/m-K]

[e = 0.5 mm, t_b = 0.9 mm, t_t = 0.2 mm]

fpm	hA/L	E_o	c_b	η_u	η_f
315	1390	1.57	0.24	0.38	0.44
394	1482	1.66	0.27	0.37	0.44
433	1518	1.69	0.29	0.36	0.43
472	1553	1.72	0.31	0.36	0.42
512	1565	1.73	0.33	0.35	0.41
551	1186	1.38	0.35	0.38	0.42

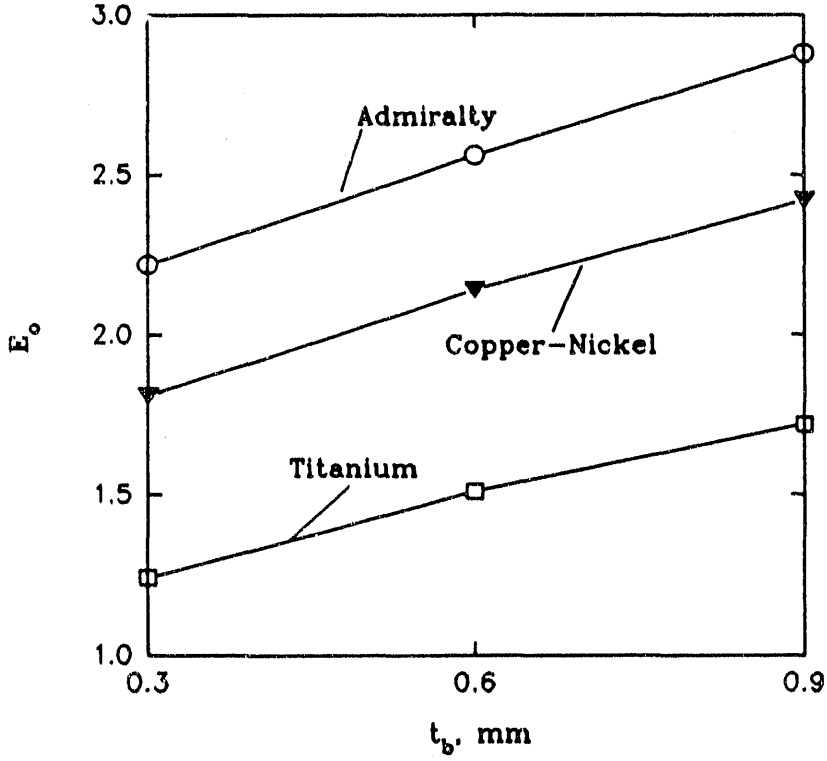

Figure 5.7. Enhancement level versus fin base thickness for 473 fpm, e = 0.5 mm, t_t = 0.2 mm, D_o = 22.23 mm..

thickness increases. This is due to the fact that by increasing the fin base thickness, the fin efficiency increases.

5.3.5 Effect of Tube Diameter on the Enhancement Level

The effect of tube diameter on the enhancement level is directly related to the fraction of tube flooded, c_b. The fin height, tip thickness, base thickness were set at 0.5 mm, 0.9 mm, 0.2 mm, respectively. The water side enhancement level was 1.8. Figure 5.8 shows the enhancement level versus fins per meter for a copper-nickel tube with 22.23 mm (7/8") and 25.4 mm (1.0") tube diameter. The enhancement level increases as the tube diameter increases. This is due to the decrease in flooding. For example, at 472 fpm (1.22 mm fin spacing) the enhancement increases by 6% when the tube diameter increases from 22.23 mm to 25.4 mm.

5.3.6 Effect of Saturation Temperature on the Enhancement Level

To determine the effect of saturation temperature on the enhancement level, all geometrical variables were fixed together with the water side operating conditions. A 22.23 mm (7/8") copper-nickel tube with e = 0.5 mm, t_b = 0.9 mm, t_t = 0.2 mm was considered. The water side enhancement is set at E_i = 1.8. The tube performance was determined at saturation temperatures of 34 C and 100 C. Figure 5.9 shows the enhancement level versus the fins per meter for both saturation

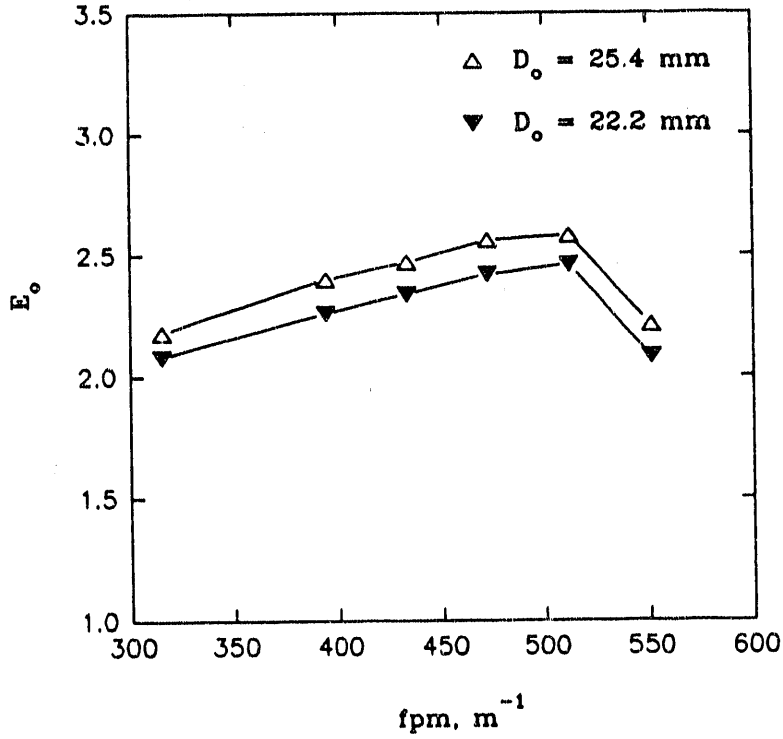

Figure 5.8. Enhancement level versus fpm , for e = 0.5 mm, t_b = 0.2 mm, t_t= 0.2 mm, copper–nickel.

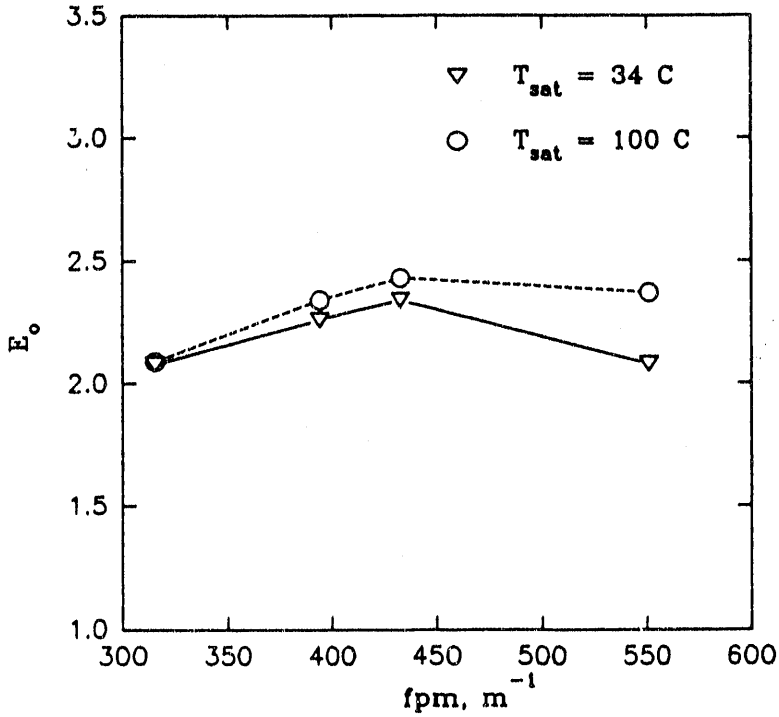

Figure 5.9. Enhancement level versus fin density for a 22.23 mm copper nickel tube e = 0.5 mm, t_t = 0.2 mm, t_b = 0.9 mm.

temperatures. The results show that the enhancement level increases as the saturation temperature is increased. The change in saturation temperature affects the condensate thermodynamic and transport properties. As the saturation temperature is increased from 34 C to 100 C, the surface tension decreases by 11 % while the condensate viscosity decreases by 92%. Such a decrease in the viscosity will result in a smaller drainage radius as determined by Equation [3.42]. Moreover, the decrease in the surface tension as T_{sat} increases results in a decreases in c_b, as shown by Equation [3.11].

5.4 Titanium Tubes/Wall Thickness

In conducting the above parametric study, the tube wall thickness was assumed to be 0.89 mm (0.035"). Although this is a typical wall thickness for admiralty and copper-nickel tubes, titanium tubes however, are made with a smaller wall thickness. A typical wall thickness for titanium tubes is 0.71 mm (0.028"). However, some titanium tubes are made with a wall thickness as small as 0.46 mm (0.018 mm), such as the two titanium tubes tested in this program. Sample calculations show that variation of the tube wall thickness from 0.89 mm to 0.46 mm has a negligible effect on the enhancement level. However, in a tube-for-tube replacement (the tube outside diameter remains constant), a smaller tube wall thickness is advantageous. Decreasing the tube wall thickness increases the inside diameter and hence reduces

the tubeside pressure drop. These remarks are based on the assumption that the plain and enhanced tube have the same wall thickness.

5.5 Conclusions

The parametric analysis shows that:

1. The fraction of tube flooded is affected by the tube diameter and the fin geometry. As the tube diameter increases the flooding decreases. Moreover, the flooding decreases as the fin height and tip thickness are decreased.

2. A fin height of 0.5 mm is desirable for admiralty, copper-nickel, and titanium tubes.

3. For a fixed tube and fin geometry, and operating conditions, an optimum fin density exists. The optimum fin density is defined as that which gives the highest enhancement level. The optimum fin density varies between 394 fpm and 512 fpm depending on fin height and tube material. For a fin height of 0.5 mm, the optimum fin density is 512 fpm for admiralty, copper-nickel, and titanium tubes.

4. The enhancement level decreases as the tube thermal conductivity decreases.

5. The enhancement level increases as the fin base thickness increases.

6. The enhancement level increases as the tube diameter increases.

7. The enhancement level increases as the saturation temperature increases.

CHAPTER 6

APPLICATION TO ELECTRIC UTILITY STEAM CONDENSERS

6.1 Potential for Doubly Enhanced Tubes

As mentioned in Chapter 1, candidate enhanced tubes for steam condensers should have enhancement on both the inside and outside of the tube (doubly enhanced). The UA value of candidate doubly enhanced tubes was calculated based on the experimental results in Chapter 4, and existing correlations for the tube side heat transfer coefficient. The value UA is evaluated using the following definition:

$$\frac{1}{UA} = \frac{1}{h_c A_i} + R_f + \frac{1}{h_o A} \qquad [6.1]$$

For the reference plain tube, the inside heat transfer coefficient, h_c, is calculated using the Petukhov (1970) equation. The outside heat transfer coefficient is calculated using the Nusselt analysis for condensation on a horizontal plain tube.

For the enhanced tubes, the inside heat transfer coefficient is evaluated from existing correlations that were provided by the tube manufacturers. The outside heat

transfer coefficient, h_o, is calculated as the product of the enhancement level and the Nusselt theory for condensation on a horizontal tube. The enhancement level is obtained from the experimental results of Chapter 4. The fouling resistance, R_f, is assumed to be zero.

The calculations are based on a 22.23 mm (0.875 in) tube outside diameter with 2.0 m/s (6.5 ft/s) tube side water velocity. The tube wall thickness is 0.89 mm for the copper-nickel tubes, and 0.41 mm for titanium tubes. The UA value was evaluated for T_{sat} = 54 C (130 F), and 23 C (73 F) cooling water temperature. Electric utility steam condensers operate at approximately 38 C (100 F) condensation temperature and 21 C (70 F) cooling water temperature.

Table 6.1 describes the tube side enhancements used with the four tubes chosen for overall performance evaluation. Figure 4.2c shows the wavy inside surface used in the actual C/N-11 tube having 433 fpm. A similar wavy surface (Wavy-2) exists inside the TiA-11 tube but with a smaller wave height as shown in Table 6.1. As mentioned in Chapter 4, the inside enhancement of the TiA-11 tube is estimated as 10% higher than that of a plain tube. The attached particle tube (A/P-50) is evaluated for a copper-nickel tube with the inside enhancement formed by a corrugated tube, with 45 degree corrugation helix angle. This inside tube geometry is described as "KORO-45" and is shown in Figure 6.1a. For the C/N-19 tube a three dimensional "dimpled" single start inside enhancement is used. This geometry is

Table 6.1

Description Of Tubeside Enhancement Geometries

Outside	Inside	D_i mm	e_i mm	p mm
C/N-19	3D-ss	19.5	0.25	5.5
C/N-11	Wavy-1	18.2	0.25	1.75
A/P-50	KORO-45	19.5	0.73	14.6
TiA-11	Wavy-2	20.5	0.11	1.75

a

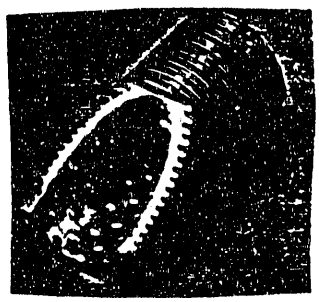

b

Figure 6.1. Photographs of tubes showing internal enhancement, (a) Hellicaly corrugated, KORO-45 (b) 3-Dimensional distributed roughness, 3D-ss

denoted as 3D-ss and is shown in Figure 6.1b. Table 6.2 shows the tube side heat transfer enhancement level for the four candidate tube side enhancement geometries, as a function of Reynolds number. Webb and Chamra (1991) provide additional description of the tube side geometries, and the friction factor characteristics. They give the measured fouling characteristics of these tubes, and show that the internal enhancements are cleanable with on-line ball or brush cleaning techniques.

At 2.0 m/sec (6.5 ft/sec) water velocity, the tube side enhancement level, E_i, is obtained from Table 6.2. The resulting UA values of the doubly enhanced tubes were then calculated for the different tube geometries. The calculated UA values were then compared to the plain tube UA value to establish the UA enhancement ratio. The UA enhancement ratios are shown in Table 6.3. The calculated UA values are based on the actual inside diameters that will exist for 22.23 mm outside diameter. The inside diameters (see Table 6.1) differ, because of the different fin heights and tube wall thicknesses. In calculating the enhancement in the UA value, it was assumed that the cooling water velocity is the same in both the plain and enhanced tubes. Table 6.3 shows that the greatest UA enhancement occurs for the copper-nickel tubes. The C/N-11, C/N-19, and A/P-50 tubes give UA enhancement ratios of 1.80, 1.61, and 1.68, respectively. The UA value of the C/N-19 tube is lower than that of C/N-11 primarily because it has a smaller water side heat transfer coefficient. It is not possible to make a wavy inside enhancement for the C/N-19 that will have the same E_i as the wavy inside enhancement used in the C/N-11 tube. This

Table 6.2

Internal Enhancement Levels, E_i

Enhancement Level, E_i

Re	Wavy-1 (Fig. 4.2c)	3D-ss (Fig. 6.1a)	KORO-45 (Fig. 6.1b)
10,000	1.31	1.63	1.72
20,000	1.54	1.63	1.71
30,000	1.72	1.62	1.70
40,000	1.88	1.61	1.70
50,000	2.03	1.60	1.69
60,000	2.17	1.59	1.68

Note: The enhancement level, E_i, is based on the same water velocity in the plain and enhanced tube.

Table 6.3

Overall Heat Transfer Coefficient

----- Outside	Tube ----- Inside	Material	E_o	E_i	$UA)_c/UA)_p$
C/N-11	Wavy-1	cu/ni	1.75	1.86	1.80
C/N-19	3D-ss	cu/ni	1.64	1.61	1.61
A/P-50	KORO-45	cu/ni	1.70	1.70	1.68
TiA-11	Wavy-2	Ti	1.34	1.20	1.23

is because the C/N-19 tube has a smaller wave pitch and a lower external fin height than those of the C/N-11 tube. For the titanium tube, the UA enhancement ratio is 1.21. The UA enhancement of the titanium tube is smaller than that of the copper-nickel tubes, because both the condensation and water side heat transfer coefficients are smaller.

The experimental enhancement level of the TiA-11 was scaled up to a 22.23 mm tube diameter. Based on the theoretical model developed in Chapter 3, it was determined that increasing the tube diameter from 18.29 mm to 22.23 mm (with all other dimensions unchanged) will increase the enhancement level of an integral finned tube by approximately 10%. The primary reason for this increase is the reduction of the condensate flooding angle, and hence an increase in the active (unflooded) region. The predictive model uses the analytical expression of Rudy and Webb (1985) for the calculation of the flooding angle. Hence, the enhancement level for the TiA-11 tube increases from 1.22 (18.29 mm diameter) to 1.34 for a 22.23 mm tube.

6.2 Discussion

Copper tubes are not acceptable for electric utility steam condensers, which use copper-nickel alloys, titanium, or stainless steel tubes. The acceptable alloys for steam condensers have much lower thermal conductivity than that of copper. For

example, the thermal conductivity of 90/10 copper-nickel and titanium are only 15% and 6% that of pure copper, respectively. Hence, lower fin efficiencies will result.

The attached particles on the A/P-50 tube create a surface tension induced pressure gradient, which drains the condensate film from the particles. The particles also create another surface tension induced pressure gradient on the tube surface between the particles. The resulting thin film enhance the condensation coefficient. Although the tested version used copper particles on a copper-nickel tube, the envisioned commercial tube would be made of titanium with aluminum particles.

The experimental results show modest condensation enhancement for the titanium tubes, with the TiA-11 tube providing higher enhancement than the TiB-11. Even with modest improvements on the steam side, the combined effect of internal and external enhancement will produce an appreciable increase in the UA value. It is possible that higher condensing coefficients can be obtained for the integral fin tubes, if the drainage channel is made with a flat, rather than a circular shape. The reason, as discussed in Chapter 3, is the existence of a surface tension induced pressure gradient in a flat channel. This region does not exist in a circular channel.

CHAPTER 7

CONCLUSIONS

1. The experimental results obtained in this program show that for a 22.23 mm diameter integral fin tube, the condensing coefficient can be enhanced by 280%, 75%, and 34% for copper, copper-nickel, and titanium tubes, respectively. The enhancement level is defined as the ratio of the condensing coefficient of the enhanced tube to that of a plain tube at the same vapor to wall temperature difference. The diameter over the fins, of the enhanced tube is equal to the outside diameter of the plain tube.

2. The experimental results also show that the enhancement level is strongly dependent on the tube thermal conductivity.

3. Combining the steam side enhancements obtained from the present experimental results and the correlations obtained by the tube manufacturer, the UA value for a set of selected tubes was determined and compared to that of a plain tube. The enhancement level in the UA value is 61 to 80% for copper-nickel tubes, and 23% for titanium tubes.

4. The proposed theoretical model can predict the performance of enhanced tubes with different fin/channel combinations. Data for 53 tubes and three fluids (obtained from the literature) were predicted. The model predicted the condensing coefficient of steam, refrigerant R-11, and refrigerant R-113, for 51 tubes, within ±15%. The five tubes tested in this program were also predicted. Four of the tubes were predicted within ±15% (except for one point). The titanium tube with a fin height of 0.28 mm was over predicted by 22% to 30%. Hence, a total of 73 data points were predicted and 90% of the data points were predicted within ±15%.

5. Results of the parametric study show that the fin geometry, thermal conductivity, and fin density affect the performance of the tube. For admiralty, copper-nickel, and titanium tubes, the preferred fin geometry is one with 0.5 mm fin height, 0.9 mm base thickness, and 0.2 mm tip thickness. The 'optimum' fin density that gives the maximum enhancement is 512 fins/meter for all three tube materials. The maximum enhancement obtained at this fin density is 2.96, 2.46, and 1.73 for admiralty, copper-nickel, and titanium tubes, respectively.

CHAPTER 8

MAJOR CONTRIBUTIONS OF THE PRESENT PROJECT

8.1 Experimental Program

The literature survey that was presented in Chapter 2, show the following trends:

1. Most authors used copper tubes which are characterized by high thermal conductivity.

2. The authors did not consider "optimum" fin shape and geometry suitable for low thermal conductivity materials, such as copper-nickel and titanium tubes.

3. Authors who did consider low thermal conductivity tubes used tubes with threaded fins. Such fins do not promote condensation on the tube surface between the fins.

Based on these findings, the present project is the first one directed towards identifying enhanced tubes of low thermal conductivity material. A special set of tubes have been made especially for this project and based on the author's

recommendations. These tubes were made by tube manufacturers in the U.S. and Europe.

8.2 Theoretical Model

The theoretical models that were discussed in section 2.3 were not general enough to predict existing data for different fluids and tube/fin geometries, within acceptable limits. The most recent models discussed in sections 2.3.2 and 2.3.3 were also had some deficiencies. The following observations can be made regarding these two models:

1. Honda and Nozu (1987, 1987a) model:

    a. Expressions for the heat transfer in different sub-regions contained constants that were derived from the numerical solution of a differential equation that was solved only for limiting cases.

    b. Fin efficiency in the flooded region does not apply for low thermal conductivity materials

c. Fin efficiency in the unflooded region for trapezoidal fins was approximated by that of a rectangular fin with an average fin thickness.

d. Model was not justified for low thermal conductivity materials

e. Model does not apply to circular drainage channels

f. Model assumes constant pressure gradients in all sub-regions were surface tension forces dominate

2. Adamek and Webb (1990) model:

a. same as *d* and *f* above

b. Model does not account for circumferential wall temperature variations

c. The conjugate heat transfer problem between the coolant and vapor was not solved.

d. The expression for the surface tension dominated sub-region, on the fin tip, does not apply for trapezoidal fins with an angle greater or equal to 45 degrees (the angle between the fin side and the vertical).

All of the above assumptions in both models have been relaxed in the present project. Moreover, all the deficiencies and/or discrepancies discussed above do not exist in the present model.

CHAPTER 9

RECOMMENDATIONS FOR FUTURE RESEARCH

8.1 Experimental Program

1. The experimental results obtained in this program show that the condensing coefficient can be increased by 75% for cu/ni tubes. This value was obtained for the C/N-11 tube which has a fin height of 1.12 mm and a circular drainage channel. Two improvements can be made:

a) A tube with a lower fin height such as 0.5 mm will produce a higher condensing coefficient due to an increase in the fin efficiency.

b) A flat drainage channel will produce a surface tension drained sub-region on the tube surface (between the fins). This tube will have a higher condensing coefficient. This sub-region will not exist in a circular channel. Therefore, it is possible that a tube such as the C/N-11 tube with a fin height of 0.5 mm and a flat drainage channel, can be a good candidate for future testing.

2. The attached particle tube (A/P-50), has resulted in an appreciable enhancement in the condensing coefficient. The data showed a strong dependence of the condensing coefficient on (T_{sat} - T_w). It is believed that at high values of (T_{sat} - T_w) (higher than 12 C) the particles and the tube surface area are flooded. It is possible that the particle distribution and particle size used in this project where not "optimum" values. Hence, a study of different particle size and distribution can result in performance improvement.

3. The titanium tubes tested in this program have produced little enhancement on the steam side. The low thermal conductivity of titanium results in a low fin efficiency. The TiA-11 tube resulted in an average enhancement level of 32% (for a 7/8" O.D. tube). It is possible to increase this enhancement level by making a tube with a flat drainage channel. It should be possible to increase the enhancement level, by manufacturing a tube with a higher wave height on the tube side (around 0.25 mm). If the TiA-11 tube can be made with higher wave heights, the inside enhancement will be as high as 80% (as discussed in Chapter 6).

Another possible alternative to increase the condensation coefficient on titanium tubes is to make use of the attached particle concept (such as the A/P-50). The A/P-50 tube is made by sintering copper particles on a copper-nickel tube with smooth inside enhancement. A corrugated titanium tube (such as the KORO-45 tube) has an average inside enhancement of 60%. By sintering aluminum particles

on such a titanium tube, it should be possible to obtain a condensation enhancement of approximately 70%. The combination of both of these enhancements can produce an enhancement level of approximately 63%.

Finally, it is recommended to install several tubes in an electric utility condenser. Such instrumented tubes would be placed in different locations in the condenser and monitored for a period time. A total assessment of the enhanced tubes should include shell side enhancement, tube side enhancement, pressure drop, fouling, corrosion, tube vibration, and economic feasibility.

8.2 Theoretical Model

1. The expressions for the heat transfer coefficient in the surface tension subregions,*bc* and *cd*, at the fin tip are based on the assumption that the film thickness at s = 0 is zero. In reality this is not true and this assumption will lead to an overestimation of the heat transfer coefficient in these sub-regions. Future modification of the model should take this fact into account.

2. The present model assumed one dimensional radial conduction through the fin. This is a safe assumption for fins of high thermal conductivity such as copper. However, for low thermal conductivity titanium fins, this assumption might not be good. A two dimensional temperature distribution in the fin can improve the

accuracy of the model. This implies that each sub-region along the fin side and fin top will have its own characteristic wall temperature and hence (T_{sat} - T_w).

3. The model assumes that the condensing vapor is stationary and hence no shear forces exist at the vapor-condensate interface. In actual condensers, the vapor velocity can be very high, particularly at the condenser inlet. Hence, it is desirable to include vapor velocity effects in the model.

4. The predictions and parametric study were also based on single tube performance. To account for the row effect that exists in condensers, it is necessary to modify the model to account for this phenomenon.

REFERENCES

Adamek, T., 1981, "Bestimmung der Kondensation-grossen auf feingewellten oberflachen zur Auslegun aptimaler Wanprofile," Warme-und Stoffuberstrangung, Vol. 15, pp. 255 -270.

Adamek, T., Webb, R. L., 1990, "Prediction of Film Condensation on Horizontal Integral Fin Tubes," to be published in Int. J. Heat Mass Transfer.

Batchelor, G. K., 1967, An Introduction to Fluid Dynamics, pp. 63-66, Cambridge University Press, London.

Beaty, K. O., Katz, D. L., 1948, "Condensation of Vapors on Outside of Finned Tubes, "Chemical Eng. Progress, Vol. 44, No. 1, pp. 55 - 70.

Bergles, A. E., Nirmalan, V., Junkhan, G. H., Webb, R. L., 1983, "Bibliography on Augmentation of Convective Heat and Mass Transfer - II," Engineering Research Institute, Iowa State University, Ames, Iowa 50011.

Bergles, A. E., Webb, R. L., 1985, "A Guide to the Literature on Convective Heat Transfer Augmentation, "ASME-HTD, Vol. 43, pp. 81 - 89.

Boyd, L. W., Hammon, J. C., Littrel, J. J., Withers, J. G., 1983, "Efficiency Improvement at Gallatin Unit 1 with Corrugated Condenser Tubing, "ASME, 83-JPGC-PWR-4.

Edwards, D. K., Gier, K. D., Ayyaswamy, P.S., Catton, I., 1973, "Evaporation and Condensation in Circumferential Grooves on Horizontal Tubes," ASME, No. 73-Ht-25, Atlanta, Georgia.

Fenner, G. W., Ragi, E., 1979, "Enhanced Tube Inner Surface Heat Transfer Device and Method," U.S. Patent 4,154,293.

Fujii, T, 1987, "Importance of Vapor Flow in Condensers, "ASME-JSME Thermal Eng. Joint Conference, Honolulu, Hawai.

Gregorig,, R., 1954, "Film Condensation on Finely Rippled Surfaces with Consideration of Surface Tension," Z. Angew. Math. Phys., Vol. 5, pp. 36 - 49.

Handbook of Heat Transfer, Rohsenow, W. M., Hartnett, J. P., 1973, McGraw-Hill Co., New York.

Hirasawa, S., Hijikata, K., Mori, Y., Nakayama, W., 1980, "Effect of Surface Tension on Condensate Motion in Laminar Film Condensation (Study of Liquid Film in a Small Trough)," Int. J. Heat Mass Transfer, Vol. 23, pp. 1471 - 1478.

Honda, H., Nozu, S., Mitsumori, K., 1983, "Augmentation of Condensation on Horizontal Finned Tubes by Attaching a Porous Drainage Plate," Proceedings, ASME-JSME Thermal Engineering Joint Conference, Y. Mori and W.J. Wang eds., Vol. 3, pp. 289 - 296.

Honda, H. Nozu, S., 1985, "Effect of Drainage Strips on the Condensation Heat Transfer Performance of Horizontal Finned Tubes," Proc. Int. Symp. on Heat Transfer, Vol. 2, 85-ISHT-II-32.

Honda, H., Nozu, S.,1987a, "A Prediction Method For Heat Transfer During Film Condensation on Horizontal Low Integral Fin Tubes," J. of Heat Transfer, Vol. 109, pp. 218 - 225.

Honda, H., Nozu, S., Uchima, B., 1987, "A Generalized Prediction Method For Heat Transfer During Film Condensation on a Horizontal Low Finned Tube," Proc. 2nd ASME-JSME Thermal Eng. Joint Conference, P.J. Marto and I. Tanasawa eds., JSME, Vol. 4, pp. 385 - 392.

Honda, H. S., Nozu, S., 1987, "Effect Of Drainage Strips On The Condensation Heat Transfer Performance Of Horizontal Finned Tubes," in Heat Transfer Science And Technology, ed. B. X. Wang, pp. 455-462, Hemisphere, Washington, D.C.

Jacob, M., 1949, Heat Transfer, Vol. I, pp. 668-669, John Wiley & Sons Inc.

Karkhu, V. A., Borovkov, V. P., 1971, "Film Condensation of Vapor at Finely Finned Horizontal Tubes," Heat Transfer Soviet Reaserch., Vol. 3, No. 2, pp. 183 - 191.

Katz, D. L., Hope, R. C., Datsko, S. C., 1946, "Liquid Retension On Integral-Finned Tubes," Department of Engineering Research, University of Michigan, Project No. M592.

Katz, D. L., Beaty, K. O., Foust, A. S., 1945, "Heat Transfer Through Tubes with Integral Spiral Fins," Trans. ASME, Vol. 70, pp. 907 - 914.

Kern, D. Q., Kraus, A. D., 1972, Extended Surface Heat Transfer, McGraw-Hil Co., New York.

Kedzierski, M. A., 1987, "A Theoretical and Experimental Study of Surface Tension Drainage Condensation," PhD Thesis, Pennsylvania State University.

Kedzierski, M. A., Webb, R. L., 1989, "Practical Fin Shapes for Surface-Tension-Drained Condensation," Journal of Heat Transfer, Vol. 112, pp. 479-485.

Marto, P. J., Mitrou, E., Wanniarachchi, A. S., Rose, J. W., 1986, "Film Condensation of Steam on Horizontal Finned Tubes: Effect of Fin Shape," Proc. IJHT, pp. 1695 - 1700.

Marto, P. J., Wanniarachchi, A. S., Cakan, O., Rose, J. W., 1988, "Enhancement of Steam Condensation on a Horizontal Finned Tube Using Drainage Strips," Proc. 2nd U.K. National Heat Transfer Conference, Glasgow, Scotland, pp. 603 - 616.

Marto, P. J., Zebrowski, A. S., Wanniarachchi, A. S., Rose, J. W., 1988, "An Experimental Study Of Condensation Of Refrigerant R-113 On Low Integral-Fin Tubes," ASME-HTD-96, Vol. 2, pp. 583-592,

Masuda, H., Rose, J. W., 1987, "An Experimental Study Of Condensation Of Refrigerant R-113 On Low Integral-Fin Tubes," in Heat Transfer Science and Technology, ed. B. X. Wang, pp. 480-487, Hemisphere, Washington, D.C.

Mehta, M. H., Rao, R., 1979, "Analysis and Correlation of Turbulent Flow Heat Transfer and Friction Factor in Spirally Corrugated Tubes for Steam Condenser Applications," 1979, Advances in Enhanced Heat Transfer, San Diego, pp. 11 - 22.

Michel, J. W., 1981, "Enhancement on Vertical Fluted Surfaces", Power Condenser Heat Transfer Technology, eds. P. J. Marto and R. H. Nunn, pp. 325 - 344, Hemisphere Publishing Co. .

Mills, A. F., Hubbard, G. L., James, R. K., Tan, C., 1975, "Experimental Study of Film Condensation on Horizontal Grooved Tubes," Desalination, Vol. 16, pp. 121 - 133.

Minkowycz, W. J., Sparrow, E. M., 1966, "Condensation Heat Transfer In The Presence Of Non-condensibles, Interfacial Resistance, Superheating, Variable Properties, And Diffusion," Int. J. Heat Mass Transfer, Vol. 9, pp. 1125-1144.

Mitrou, E., 1986, "Film Condensation Heat Transfer on Horizontal Finned Tubes," M. S. Thesis, Naval Postgraduate School, Monterey, California.

Notaro, F., 1979, "Enhanced Condensation Heat Transfer Device and Method," U.S. Patent 4,154,294.

Owen, R. G., Sardesai, R. G., Smith R. A., Lee, W. C., 1983, "Gravity Controlled Condensation on Low Integral Fin Tubes," Proc. Symp. on Condensers : Theory and Practice, I.Chem.E Symp. Ser., No. 75, pp. 415 - 428.

Perry's Chemical Engineers' Handbook, 1984, eds. Perry, R. H., Green, D. W., Maloney, J. O., McGraw-Hill Co., New York.

Rabas, T. J., 1987, "Data and Correlation Review of the Enhancement for Steam Condensation on Spirally Indented Tubes," ASME-HTD, Vol. 85, pp. 97 - 106.

Reilly, D. J.,1978, "An Experimental Investigation of Enhanced Heat Transfer on Horizontal Condenser Tubes," Thesis in Mechanical Engineering, Naval Postgraduate School, Monterey, CA.

Rifert, V. G., Barabash, P. A., Golubev, A. B., Leont'yev, G. G., Chaplinsky, S. I., 1977, "Investigation of Film Condensation Enhanced by Surface Forces," Heat Transfer Soviet Research, Vol. 9, No. 2, pp. 23 - 27.

Rifert, V. G., 1980, "A New Method for Calculating Rates of Condensation on Finned Tubes," Heat Transfer Soviet Research, Vol. 12, No. 3, pp. 142 - 147.

Rifert, V. G., Barabash, P. A., Vizel, Y. F., Trokoz, Y. Y., 1985, "Effect of Surface Tension on the Hydrodynamics and Heat Transfer in Condensation of Vapor on Finned or Corrugated Surfaces," Heat Transfer Soviet Research, Vol. 17, No. 1, pp. 18 -27.

Rudy, T. M., 1982, "A Theoretical and Experimental Study of Condensation on Single, Integral-Fin Tubes," PhD. thesis, The Pennsylvania State University.

Rudy, T. M., Webb, R. L., 1981, "Condensate Retention on Horizontal Integral-Fin Tubing," Advances in Heat Transfer, ASME HTD, Vol. 18, pp. 35 - 41.

Rudy, T. M., Webb, R. L., 1983, "Theoretical Model for Condensation on Horizontal Integral Fin Tubes," Heat Transfer Seattle, AICHE Symp. Ser., No. 225, Vol. 79, pp. 11 - 18.

Rudy, T. M., Webb, R. L., 1985, "An Analytical Model to Predict Condensate Retention on Horizontal Integral-Fin Tubes," J. of Heat Transfer, Vol. 107, pp. 361 - 366.

Shekriladze, I. G., Rusishvili, D. G., 1980, "Heat Transfer in Condensation on Capillary Surfaces," Heat Transfer Soviet Reaserch, Vol. 12, No. 4, pp. 48 - 49.

Shklover, G. G., Mil'man, O. O., Baskov, V. S., Ankudinov, G. A., 1981, "Heat Transfer in Condensation of Steam on Finely Finned Horizontal Tubes," Heat Transfer Soviet Reaserch, Vol. 13, No. 2, pp. 1-8 - 114.

Straub, L. G., Silberman, E., Nelson, H. C., 1958, "Open-Channel Flow At Small Reynolds Number," Trans. Am. Soc. Civ. Eng., Vol 123, pp. 685-714.

Tapproge, 1986, "Cleaning Test with Enhanced Heat Transfer Tubes of Wieland Werke AG," Tapproge report C-301.

Thomas, D. G., 1968, "Enhancement of Film Condensation Rate on Vertical Tubes by Longitudinal Fins," AIChE Journal, Vol. 14, No. 4, pp. 644-649.

Van Dromme, M. A., Hellinckx, L. J., 1973, "Dependence of Friction Factor Upon Liquid Level in Two-Phase One-Component Stratified Flow," J. of Heat Transfer, Vol. 95, pp. 427-429.

Wanniarachchi, A. S., Marto, P. J., Rose, J. W., 1984, "Filmwise Condensation of Steam on Externally Finned Horizontal Tubes," Fundamentals of Phase Change : Boiling and Condensation ASME-HTD, Vol. 38, pp. 133 - 141.

Wanniarachchi, A. S., Marto, P. J., Rose, J. W., 1985, "Film Condensation of Steam on Horizontal Finned Tubes : Effect of Fin Spacing, Thickness, and Height," Multiphase Flow and Heat Transfer, ASME HTD, Vol. 47, pp. 93 - 99.

Wanniarachchi, A. S., Marto, P. J., Rose, J. W., 1986, "Film Condensation of Steam on Horizontal Finned Tubes : Effect of Fin Spacing," J. of Heat Transfer, Vol. 108, pp. 960 - 966.

Webb, R. L., 1988, "Enhancement of Film Condensation,"International Communications in Heat and Mass Transfer, Vol. 15, No. 4, pp. 475 - 508.

Webb, R. L., 1986, "Performnace Evaluation Criteria for Enhanced Tube Geometries Used in Two-Phase Heat Exchangers," in Heat Transfer Equipment, ed. R. K. Shah, Hemisphere Pub. Corp., Washington, D. C.

Webb, R. L., Haman, L. L., Hui, T. S., 1984, "Enhanced Tubes in Electric Utility Steam Condensers," Heat Transfer in Heat Rejection Systems, ASME-HTD, Vol. 37, eds. S. Sengupta and Y. S. Mussalli, pp. 17 - 25.

Webb, R. L., Keswani, S. T., Rudy, T. M., 1982, "Investigation of Surface Tension and Gravity Effects in Film Condensation," Proc. 7th Int. Heat Transfer Conference, U. Grigull, et al. eds., Hemisphere Publishing Corp., Washington, D. C., Vol. 5, pp 175 -180.

Webb, R. L., Rudy, T. M., Kezierski, M.A, 1985, "Prediction of the Condensation Coefficient on Horizontal Integral Fin Tubes," J. of Heat Transfer, Vol. 107, pp. 369 - 376.

Yau, K. K., Cooper, J. R., and Rose, J. W., 1984, "Effects of Drainage Strips and Fin Spacing on Heat Transfer and Condensate Retention for Horizontal Finned and Plain Condenser Tubes," Fundamentals of Phase Change : Boiling and Condensation, ASME HTD, Vol. 38, pp. 151 - 156.

Yau, K. K., Cooper, J. R., Rose, J. W., 1985, "Effect of Fin Spacing on the Performance of Horizontal Integral Fin Condenser Tubes," J. of Heat Transfer, Vol. 102, pp. 20 - 25.

Yau, K. K., Cooper, J. R., Rose, J. W., 1986, "Horizontal Plain and Low-Finned Condenser Tubes-Effect of Fin Spacing and Drainage Strips on Heat Transfer and Condensate Retention," J. of Heat Transfer, Vol. 108, pp. 946 - 950.

Yorkshire Imperial Metals Ltd., 1973, Technical Bulletin No. 17, Leeds, England.

Yorkshire Imperial Metals Ltd., 1988, private communication.

Zener, C., Lavi, A., 1974, "Drainage Systems for Condensation," J. of Engineering for Power, Vol. 96, pp. 209 - 215.

Zozulya, N. V., Karkhu, V. A., Borovkov, V. P., 1977, "An Analytic and Experimental Study of Heat Transfer in Condensation of Vapor on Finned Surfaces," Heat Transfer Soviet Reaserch, Vol. 9, No. 2, pp 18 - 22.

APPENDIX A

DERIVATION OF THE EXPRESSION FOR THE FIN EFFICIENCY IN THE FLOODED REGION

In the flooded region, the fin sides are assumed to offer negligible contribution to the heat transfer process. Hence, the sides are considered insulated with heat transfer occurring only at the fin top. The convective heat transfer is given by:

$$Q_{conv} = h_t A_t (T_s - T_t) \qquad [A1]$$

where T_t is the temperature of the fin top and $A_t = \pi D_o t_t$. The heat transfer through the fin is assumed to be conducted in the radial direction only and is expressed by:

$$Q_{cond} = \frac{T_t - T_b}{R_c} \qquad [A2]$$

where R_c is the conduction resistance through the fin and is a function of the fin shape. T_b is the temperature of the fin at the base. A heat balance requires that:

$$Q_{cond} = Q_{conv} = Q \qquad [A3]$$

From Equations [A1] and [A2] we can write:

$$T_s - T_t = \frac{Q_{conv}}{h_t A_t} \qquad [A4]$$

and

$$T_t - T_b = Q_{cond} R_c \qquad [A5]$$

Adding Equations [A5] and [A6] we obtain:

$$T_s - T_b = Q\left[R_c + \frac{1}{h_t A_t}\right] \qquad [A6]$$

The maximum possible heat transfer is expressed as:

$$Q_{max} = h_\infty A_t (T_s - T_b) \qquad [A7]$$

From the definition of fin efficiency:

$$\eta_f = Q/Q_{max} \qquad [A8]$$

and using Equations [A7] - [A9] we obtain:

$$\eta_f = \frac{1}{R_c h_\infty A_t + \frac{h_\infty}{h_t}} \qquad [A9]$$

Note that h_t is based on the fin top temperature hence, an iterative solution is required.

APPENDIX B

DERIVATION OF THE CONDUCTION RESISTANCE IN THE FLOODED REGION

In the flooded region, the fin sides are blanketed by condensate and hence rendered inactive. The only active heat transfer area is the fin top, hence the thermal boundary condition on the sides is an adiabatic one. Three different shapes are analyzed.

The one dimensional heat conduction equation, written in integral form, is expressed in terms of radial coordinates as follows:

$$Q_r \int_{r_r}^{r_o} \frac{dr}{A(r)} = k \int_{T_b}^{T_t} dt \qquad [B1]$$

The problem is to determine the functional form of the cross sectional area, A(r), and then perform the integration. The functional form of the area is, in general written as:

$$A(r) = 2\pi r D(r) \qquad [B2]$$

Rectangular Fin. The area is given as D(r) = t and the integration of Equation [B1] yields:

$$R_c = \frac{\ln(r_o/r_i)}{2\pi tk} \qquad [B3]$$

Trapezoidal Fin. The equation for the side is that of a straight line and has the general form:

$$D(r) = -ar + b \qquad [B4]$$

The values of a and b are determined from the geometric boundary conditions. Substitution of equation (B4) into (B1) yields:

$$R_c = \frac{-\log\left[\frac{t_t}{t_b}\frac{r_o}{r_b}\right]}{2\pi bk} \qquad [B5]$$

Parabolic Fin. The equation for D(r) is expressed as:

$$D(r) = \left[\frac{r - c}{-a}\right]^{0.5} \qquad [B6]$$

The values of a and c are determined from the geometric boundary conditions. Substituting into equation (B1) yields:

$$R_c = \frac{1}{2\pi k\sqrt{c/a}}\frac{N_o}{N_r} \qquad [B7]$$

where

$$N = \frac{\sqrt{c/a - Hx/a} - \sqrt{c/a}}{\sqrt{c/a - r/a} + \sqrt{c/a}} \qquad [B8]$$

The values of N_o and N_r are obtained from Equation [B8] by substituting $r = r_o$ and $r = r_r$, respectively. The parameters a and c/a are given by the following expressions:

$$a = \frac{r_o - r_r}{t_b^2 - t_t^2} \qquad [B9]$$

and

$$c/a = \frac{(\frac{t_b}{t_t})^2 \frac{r_o}{a} - \frac{r_r}{a}}{\left[(\frac{t_b}{t_t})^2 - 1\right]} \qquad \text{[B10]}$$

APPENDIX C

TABULATED DATA OF THE MEASURED

CONDENSING AND OVERALL COEFFICIENTS

Table C.1

Measured Condensing Coefficient

Smooth, T_{sat} = 54 C, L = 0.305

T_{sat} - $T_{w,av}$, C	h, W/m^{2}K	T_1, T_2, T_3, C
10.57	11237	44.8, -, 43.3
11.56	10959	44.5, -, 41.7
12.80	10459	43.2, -, 40.4
13.05	10833	44.0, -, 39.2
14.21	10311	43.0, -, 37.9
15.00	9914	41.2, -, 38.2

Smooth, T_{sat} = 69 C, L = 0.305 m

T_{sat} - $T_{w,av}$, C	h, W/m^{2}K	T_1, T_2, T_3
18.57	9840	53.0, -, 49.1
20.76	9255	51.1, -, 46.6
21.94	9170	50.0, -, 45.4

CU-11, T_{sat} = 54 C, L = 0.305 m

T_{sat} - $T_{w,av}$, C	h, W/m^2-K	T_1, T_2, T_3
	Set # 1	
2.52	44226	52.9, 53.0, 49.6
3.10	41847	52.5, 52.6, 48.3
2.93	44572	52.8, 52.8, 48.4
3.58	40649	52.3, 52.4, 47.3
4.51	37571	51.5, 51.8, 45.5
	Set # 2	
3.46	43647	52.5, 52.4, 47.4
3.79	43488	52.2, 46.6, 46.8
4.88	38860	51.4, 51.4, 44.9
4.26	41217	51.9, 51.9, 45.8

C/N-11, T_{sat} = 54 C, L = 0.305 m

T_{sat} - $T_{w,av}$, C	h, W/m^2-K	T_1, T_2, T_3
	Set # 1	
6.86	20424	51.2, 49.5, 40.9
7.40	20844	51.0, 49.0, 39.8
8.06	20168	50.7, 48.5, 38.6
8.48	19975	50.5, 48.0, 38.1
10.07	18544	49.7, 46.5, 35.5

o

Set # 2

5.92	21923	51.9, 49.8, 43.4
7.14	20373	51.6, 49.0, 40.5
8.07	19918	51.1, 48.3, 38.6
10.51	18226	50.1, 46.3, 33.8
11.30	17994	49.7, 45.3, 33.1

C/N-19, T_{sat} = 54 C, L = 0.305 m

T_{sat} - $T_{w,av}$, C	h, W/m^2-K	T_1, T_2, T_3

Set # 1

4.55	21991	53.3, 51.9, 43.3
5.49	21003	52.8, 51.2, 41.3
6.09	20537	52.4, 50.9, 40.0
6.64	20696	52.0, 50.4, 39.2
7.32	20764	51.3, 50.0, 38.8
7.44	19589	51.5, 49.7, 37.8

Set # 2

3.24	24540	53.9, 52.8, 46.1
3.81	24989	53.5, 52.3, 45.1
8.37	20759	50.6, 48.8, 36.9

Set # 3

4.72	22093	52.8, 51.5, 43.7
5.36	21258	52.3, 50.9, 43.0
7.73	18885	51.1, 49.1, 38.2
8.71	18357	50.4, 48.4, 36.6

A/P-50, T_{sat} = 54 C, L = 0.305 m

T_{sat} - $T_{w,av}$, C	h, W/m^2-K	T_1, T_2, T_3

Set # 1

2.45	29537	50.8, 48.6, 42.6
3.12	25403	50.6, 47.9, 41.5
3.64	23672	50.4, 47.7, 40.1
4.36	21497	50.2, 47.2, 38.4
4.32	22939	50.2, 47.0, 39.0
4.89	21219	50.2, 46.7, 37.3
4.99	22218	50.3, 46.6, 37.0

Set # 2

2.53	28464	50.7, 49.2, 41.3
3.34	24398	50.6, 48.7, 38.8
4.12	22275	50.8, 48.3, 36.7
5.49	20344	50.6, 47.2, 33.5
6.56	18368	50.5, 46.3, 31.1

Set # 3

4.28	21327	50.7, 48.0, 36.7
5.50	18692	50.3, 47.1, 33.9
6.49	17216	50.1, 46.3, 31.9
6.96	18028	50.4, 45.8, 30.6

TiA-11, T_{sat} = 54 C, L = 0.305 m

T_{sat} - $T_{w,av}$, C	h, W/m^2-K	T_1, T_2, T_3
11.59	13474	45.7, 43.8, 38.9
12.34	13548	44.8, 43.1, 38.2
12.90	13258	44.4, 42.4, 37.8
13.40	13275	44.1, 41.8, 37.3
13.43	13525	43.8, 41.3, 38.4
10.35	13599	46.2, 45.1, 40.7
8.93	14172	47.2, 46.2, 43.2

Set # 2

11.51	14070	45.3, 44.0, 39.3
11.64	13917	45.0, 43.9, 39.2
10.94	13922	45.7, 44.6, 39.9
11.04	13218	45.7, 44.5, 39.6
10.22	13798	46.4, 45.6, 40.0

TiB-11, T_{sat} = 54 C, L = 0.305

T_{sat} - $T_{w,av}$, C	h, W/m^2-K	T_1, T_2, T_3
9.11	12310	49.1, 46.3, 40.4
10.56	11782	46.2, 45.3, 39.5
11.58	11526	47.0, 43.2, 38.8
10.63	12429	47.9, 44.4, 39.4
10.94	12304	47.6, 43.8, 39.6

Table C.2

Measured Overall Coefficient

T_{sat} = 42 C

u_c, m/sec	UA, W/K
C/N-11 Tube	
0.97	4798
1.21	5366
1.45	5871
1.69	6234
1.99	6808
TiA-11 Tube	
1.46	2152
1.75	2436
2.04	2674
2.33	2901
2.48	2970

APPENDIX D

STATISTICAL ANALYSIS

D.1 Uncertainty Analysis: Theory

The following is a presentation of basic equations in error analysis and its application to one data point to determine the uncertainty in the measured condensung coefficient.

From the theory of error analysis, if a quanity F is determined by a set of independent parametrs, x_n, it can be expressed, in general, as follows:

$$F = f(x_1, x_2, ..., x_n) \qquad [D1]$$

where the x_n's are the actual measurements used to determine the quantity F. If each x_i has an error of $\pm\Delta x_i$, and each Δx_i is assumed to be three standard deviations of the corresponding x_i,then the root mean square error is expressed as:

$$E_{rms} = \left[\left(\frac{\partial F}{\partial x_1}\Delta x_1\right)^2 + \left(\frac{\partial F}{\partial x_2}\Delta x_2\right)^2 + ... + \left(\frac{\partial F}{\partial x_n}\Delta x_n\right)^2\right]^{\frac{1}{2}} \qquad [D2]$$

The uncertainty in the calculation of F, is:

$$\%error = (1-(F-E_{rms})/F)*100 \qquad [D3]$$

A sample data point will be analysed. This point will be at the lowest (T_{sat} - T_w) where the uncertainty is expected to be the highest. The data point constitutes of the following readings: Q = 8049 Btu/hr, ΔT_w = 13.42, * = 1.20 GPM, (T_{sat} - T_w) = 5.28, T_{sat} = 130.34 F, L = 1 ft, D_o = 7/8".

D.2 Error in the Heat Load

The heat load, Q, is calculated from the measurements of the cooling water temperature rise and its flow rate. It is expressed as:

$$Q = \dot{m}_w c_p \Delta T_w \qquad [D4]$$

The flow rate was measured with a rotameter (Dwyer-Type C,) and the temperature rise was measured with thermistors. The error in the flow rate is ±2% of maximum range (which is for this case ±0.044 gpm). The error in the thermistor reading is ±0.15 C. The error in the specific heat is assumed to be negligible. The partial derivatives of Q with respect to ΔT_w, c_p, and $\dot{m}_w$ are:

$$\frac{\partial Q}{\partial m_w} = c_p \Delta T_w \qquad [D5]$$

and

$$\frac{\partial Q}{\partial c_p} = m_w \Delta T_w \qquad [D6]$$

$$\frac{\partial Q}{\partial \Delta T_w} = c_p m_w \qquad [D7]$$

By applying Equations [D3] and [D4], the uncertainty in the heat load calculation is found to be 3.8%.

D.3 Error in the Temperature Difference

The temperature difference is written as:

$$\Delta T = T_{sat} - T_w \qquad [D8]$$

The saturation pressure was measured by a mercury manometer and then the saturation temperature was obtained from the Steam Tables. The error in the saturation temperature is ±0.09 F and the error in the thermocouple is ±0.36 F.

The partial derivatives of ΔT with respect to T_w and T_{sat} are:

$$\frac{\partial \Delta T}{\partial T_{sat}} = 1 \qquad [D9]$$

and

$$\frac{\partial \Delta T}{\partial T_w} = -1 \qquad [D10]$$

By applying Equations [D3] and [D4] the uncertainty in ΔT is found to be 7%.

D.4 Error in the Heat Transfer Coefficient

The condensing coefficient is calculatyed as follows:

$$h = \frac{Q}{A\Delta T} \qquad [D11]$$

where A is the projected area and it is equal to $\pi D_o L$. The error in the calculation of the area is negligible. The error in ΔT is found to be ±7% from the above analysis.

The partial derivatives of h with respect to ΔT and Q are:

$$\frac{\partial h}{\partial \Delta T} = -\frac{Q}{A\Delta T^2} \qquad [D12]$$

and

$$\frac{\partial h}{\partial Q} = \frac{1}{A\Delta T} \qquad [D13]$$

Applying Equations [D3] and [D4] results in an uncertainty of ±8%. It should be noted that the uncertainty in the condensing coefficient is mainly due to the error associated with the measurement of the temperature difference between the saturation temperature and the wall temperature. From Equation [D13] it can be

seen that the uncertainty in the condensing coefficient will decrease as (T_{sat} - T_w) increases.

APPENDIX E

COMPARISON BETWEEN FIN EFFICIENCY IN THE UNFLOODED AND FLOODED REGIONS

As shown in the results obtained in Chapter 5, the fin efficiency in the flooded region is higher than that in the unflooded region. This result can be explained by a sample calculation.

An integral finned titanium tube (k = 19 W/m-K, 315 fpm) of 22.23 mm diameter (over the fins) will be considered. The fin height, tip thickness, and base thickness are 0.5 mm, 0.2 mm, and 0.9 mm, respectively. Hence, the angle between the fin side and the vertical is 35 degrees. At a steam saturation temperature of 34 C, average coolant, temperature coolant velocity, and internal enhancement level of 22 C, 2.0 m/sec, and 1.8 respectively, the model predicts an average fin heat transfer coefficient in the unflooded region is 100600 W/m^2-K. The parameters K^2 and μ are evaluated using Equations [3.60] and [3.61] while the values of the modified Bessel functions are evaluated from curve fits of tabulated values. Then from Equation [3.59], the fin efficiency is found to be 0.38. This is the same value that appears in Table 5.9.

The predicted average heat transfer coefficients in the flooded region are h_{∞} = 124568 W/m^2-K (based on the fin base temperature) and h_t = 161667 W/m^2-K

(based on the fin tip temperature). The conduction resistance, R_c, is evaluated using Equation [B5] and was found to have the value of 0.527 C/W. Using Equation [3.63], the fin efficiency in the flooded region is found to be 0.44. This is also the value found in Table 5.9. Thus, the fin efficiency in the flooded region is higher than that in the unflooded region.

VITA

Mohamad Hassib Jaber was born in Freetown, Sierra Leone, on July 9, 1961. He obtained his high school degree from Rawdah High School in Beirut, Lebanon. He graduated with the degree of Bachelor of Engineering in Mechanical Engineering, from the American University of Beirut, Beirut, Lebanon. He obtained his Master's in Mechanical Engineering from The Pennsylvania State University in August of 1987. He completed a doctoral degree in Mechanical Engineering from The Pennsylvania State University and is currently employed by UOP of Tonawanda, New York. He is a member of the American Society of Mechanical Engineering.

END

DATE FILMED

9/1/92